Reconstruction of contact metamorphism of the Uitkomst Complex, near Badplaas, Mpumalanga Province, South Africa, based on mineralogical and petrological investigations of the contact aureole

Thesis submitted in fulfillment of the requirements for the degree of

Master of Science

handed in by
Jens Kirste

In the Department of Geology
Faculty of Agricultural and Natural Sciences
University of the Free State
Bloemfontein, South Africa

Supervisor: Prof. Christoph Gauert
Co-supervisor: Prof. Willem van der Westhuizen

May 2009

DECLARATION

Herewith I, Jens Kirste, declare that this thesis is my own, unaided work. It is being submitted for the Degree of Master of Science at the University of the Free State, Bloemfontein, South Africa. This thesis has not been submitted before for any degree or examination at any other University.

Leipzig, 14 May, 2009.

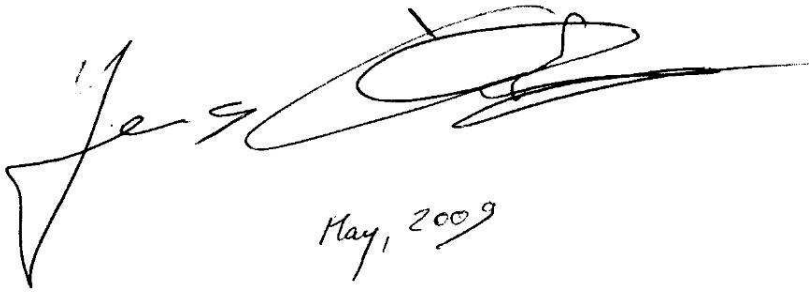

Jens Kirste

ABSTRACT

This study presents petrological, mineralogical and geochemical data from the country rocks surrounding the basic to ultrabasic Uitkomst Complex in the Mpumalanga Province, South Africa. The investigations resulted in a isograde map based on the determination of critical mineral reactions for different lithotypes, i.e. the Timeball Hill Shale, Bevets Conglomerate and the Malmani Dolomite. Several minerals occurring in the metamorphic aureole, for example almandine in the Timeball Hill Shales, allow to determine temperatures and to a lesser degree pressure prevailing in the country rocks during the emplacement of the Complex. Geochemical profiles perpendicular to the contact into the country rocks indicate moderate enrichment of Mg, Fe, Cr and Ni close to the contact, levelling out to threshold values within 50 m distance from the contact.

Additionally to the thermometric aspects of this thesis, an appraisal of the possible applications of corundum is given. The Uitkomst corundum shows, in parts, gem quality. Sapphire has been found in the Timeball Hill Shales south of the Complex.

The corundum-bearing hornfelses are found in a distance of approximately 240 – 270 m from the contact in north-easterly and south-westerly direction. The rocks in this zone are characterized by a under-saturation of SiO_2 and an elevated Al_2O_3-activity; the required temperature of corundum formation lies above 400 °C on average.

ZUSAMMENFASSUNG

Die vorliegende Studie präsentiert petrologische, mineralogische und geochemische Daten der Nebengesteine des Uitkomst Komplexes in der Mpumalanga Provinz, Südafrika. Die Untersuchungen resultieren in einer Darstellung von Isograden. Diese beruht auf die Untersuchung markanter Mineralreaktionen für jeden Lithotyp, genauer für die Timeball Hill Shales, das Bevets Conglomerate und den Malmani Dolomite. Es gibt einige Minerale die die Temperaturen in den Nebengesteinen während der Platznahme des Komplexes sehr gut repräsentieren. So zum Beispiel die Almandine in den Timeball Hill Shales.

Zusätzlich war es ein Bestreben der Arbeit die Verwendungsmöglichkeiten des Korunds in den „Shales“ zu beurteilen. In diesem Zuge wurde die Eignung als Edelstein dargelegt. Denn teilweise zeigen sich neben den braunen, gewöhnlichen Korunden auch Saphire.
Die Bildung des Korundes ist auf einen Bereich beschränkt, der sich durch eine SiO_2-Untersättigung und die benötigten Temperaturen von ca. 400 – 410°C auszeichnet.

CONTENTS

FIGURES

page

TABLES

page

ABBREVIATIONS

Minerals

Act	Actinolite
Ab	Albite
Alm	Almandine
An	Anorthite
An.-cl.	Anorthoclase
And	Andalusite
Andr	Andradite
Arg	Aragonit
Bt	Biotit
Cal	Calcite
Chl	Chlorite
Cpx	Clinopyroxene
Crd	Cordierite
Crn	Corundum
Czo	Clinozoisite
Di	Diopside
Dol	Dolomite
En	Enstatite
Ep	Epidote
Fo	Forsterite
Grt	Garnet
Hbl	Hornblende

Ilm	Ilmenite
Kfs	K-feldspar
Ky	Kyanite
Ms	Muscovite
Ol	Olivine
Opx	Orthopyroxene
Pl	Plagioclase
Qtz	Quartz
Rt	Rutile
Sa	Sapphirine
Sil	Sillimanite
St	Staurolite
Tlc	Talc
Tr	Tremolite
Wo	Wollastonite
Zo	Zoisite

Other abbreviations

BGAB	Basal Gabbro Unit
BMZ	Basal mineralized zone
BSE	Backscatter Electron (Image)
BRQ	Black Reef Quartzite
CH	Corundum hornfelse
EMPA	Electron Microprobe Analysis
f_{O2}	oxygen fugacity

f_{H2}	hydrogen fugacity
GAB	Gabbro
GN	Gabbronorite Unit
LHZBG	Lower Harzburgite Unit
LrPXZ	Lower Pyroxenite Unit
MAL	Malmani Subgroup
MALM	Malmani Subgroup
MCHR	Massive Chromite
MHZBG	Main Harzburgite Unit
MMZ	Main Mineralized Zone
MSB	Massive Sulphide Body
PCMZ	Chromitiferous Mineralized Zone
PCR	Chromitiferous Harzburgite Unit
PRD	Peridotite
PRDMZ	Peridotite Mineralized
PXT	Pyroxenite Unit
RHF	Rooihogte Formation
SHZO	Sheared Zone
TBH	Timeball Hill Formation
THS	Timeball Hill Shale
WDS	Wavelength Dispersive Spectroscopy
XRD	X-ray Diffraction
XRF	X-ray fluorescence spectroscopy

1. Introduction

1.1 Geography and geological setting

The Uitkomst Complex, situated north of Badplaas in the Mpumalanga Province approximately 300 km east of Johannesburg (Fig.1.1) is a layered ultramafic to mafic intrusion with a U-Pb SHRIMP age of 2044 ± 8Ma (DE WAAL et al., 2001). It extends over the farms Vaalkop 608 JT, Uitkomst 541 JT, Slaaihoek 540 JT and Little Mamre 538 JT (Fig. 1.2). The Complex describes an elongated trough-shaped body that concordantly intruded the sediments of the Lower Transvaal Group. The intrusion dips with a shallow angle (4-5°) towards north-west and is exposed over a total distance of almost 9 km. At its south-east end on the farms Uitkomst 541 JT and Vaalkop 608 JT, the Complex is eroded to a thin gossaniferous cover of intrusive rocks on a floor of the Lowermost Malmani Subgroup and the Black Reef Group of the Transvaal Supergroup. The thickness of the Complex increases from 370 m on the Uitkomst/Slaaihoek boundary to the full thickness of approximately 750 m on the farm Slaaihoek 540 JT, due to various levels of erosion.

In the north-west the Complex is covered by quarzite and shales of the lower Timeball Hill Formation (Fig. 1.3), forming a part of an escarpment. It can be traced about another 3 km to the north-west as far as the farm Little Mamre. Due to a lack of borehole data, the depth extension of the Complex is unknown beyond this point.

At the contact the intrusive rocks have transformed the surrounding country rocks as well as country rock xenoliths within the intrusion into contact metamorphic rocks of variable metamorphic degree and variable spatial extent from the contact. The mineralogy of the contact rocks and the p-T – conditions of their formation are the object of this study.

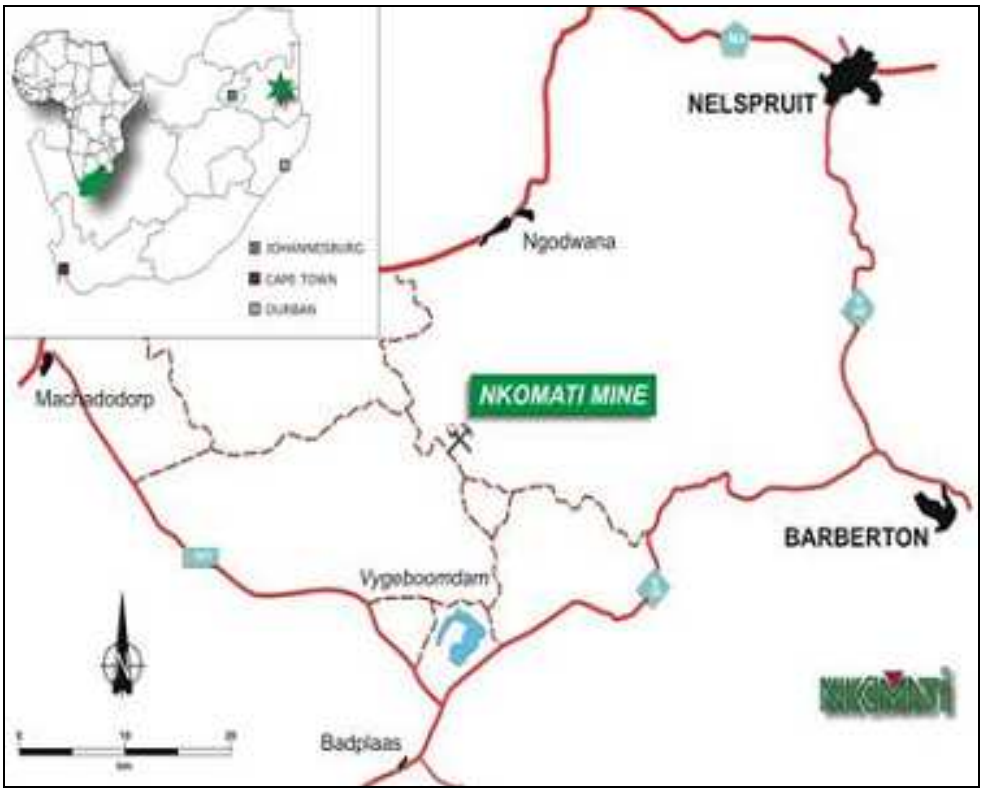

Fig.1.1: Geographical situation of the Uitkomst Complex and the Nkomati Mine near Badplaas, Mpumalanga Province South Africa; ARM African Rainbow Minerals; Norilsk Nickel 2007

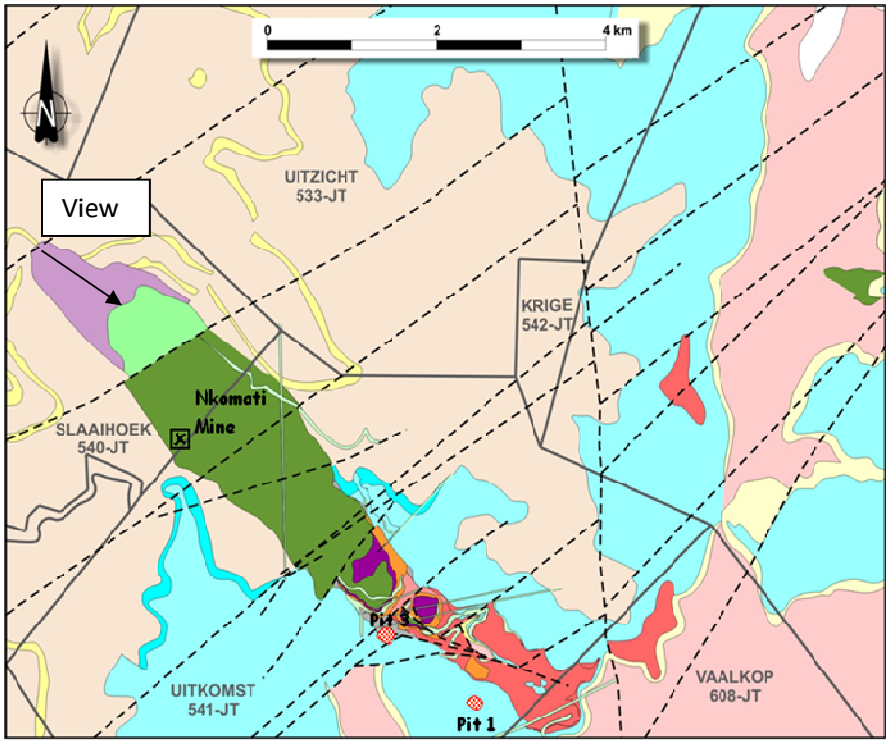

Fig. 1.2: Overview of the extent of the Uitkomst Complex; WOOLFE 2006

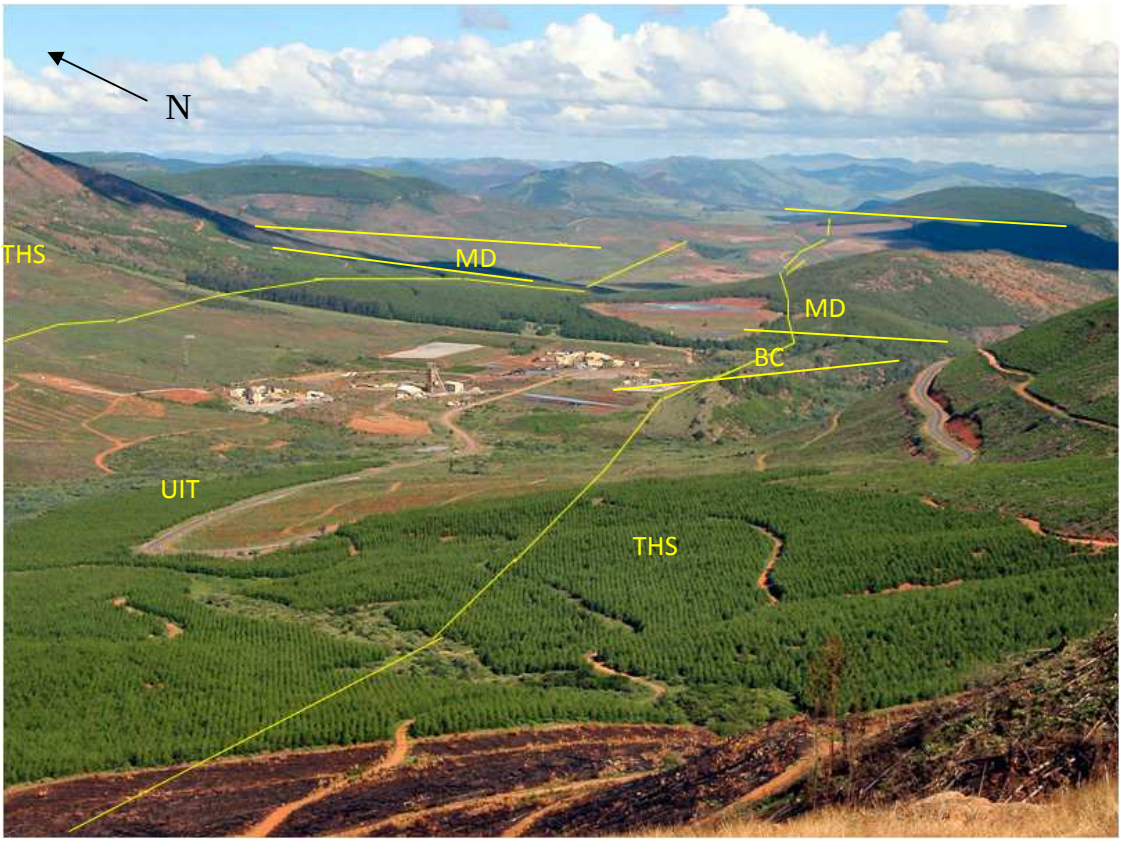

Fig.1.3: Estimated position of the contact Complex – country rocks; WOOLFE 2006, modified by KIRSTE 2007; THS = Timeball Hill Shale, MD = Malmani Dolomite, BC = Bevets Conglomerate, UIT = Uitkomst Complex

1.2 Exploration and mining history

The occurrence of Ni-Cu and PGE-sulphides in the ultramafic rocks of Uitkomst is known since Wagner (1929) and several mining houses undertook exploration since 1972 until it became a mine early in 2006 as a AAC and AVMIN Ltd. (NICO) joint venture.

The deposit gave rise to a low–tonnage high grade operation from and changes since 2005 to a large tonnage but is the biggest primary Ni deposit in South Africa with an annual production of approximately 36,000 t of Ni concentrate (WOOLFE 2006).

The reason for economic interest and repeating exploration work is a complex Ni-Cu-Co-PGE metal sulphide mineralisation which hosts South Africa`s first primary nickel mine.

Lately for an expansion project of the sulphide orebody has been conducted. The ARM – Norilsk Nickel Joint Venture has started an interim Expansion Project and continues to mine the Main Mineralized Zone (MMZ) to close the gap between the depletion of the MSB and the proposed Exploration Project, planned for 2010.

Additional, the exploitation of the chromite mineralization has temporally enhanced the economic value of the Nkomati orebody, as oxidized massive chrome resource overlie the nickel mineralization. The full chrome production started in 2007, aiming at a high grade pelletised chrome product for local consumption and for export.

From 2006 ongoing parts of massive Chromites (MCHR) and chromitiferous Harzburgite (PCR) in two open pits. A third and largest pit of 5 km length has been started.

The Mine`s resources are shown in Table 1.1. The resources are combinations of indicated and measured categories at different cut off grades.

Table 1.1: Original and current resources of the sulphide (nickel) and chromite mineralized zones. (WOOLFE, 2006; oral presentatiom) (UG = underground, OP = open pit)

UNIT	NICKEL	CHROMITE	RESSOURCE (UG+OP)
PRD	PRDMZ	-	not quoted
PCR		MCHR	6.2 Mt @ 33.5 % Cr_2O_3 (current oxidized MCHR only)
	PCMZ	PCMZ	142.6 Mt @ 0.25 % Ni, 0.08 % Cu, 0.72 g/t 4E. 12.25 Cr_2O_3
LrPXT	MMZ	-	133.7 Mt @ 0.45 % Ni, 0.19 % Cu. 1.02 g/t PGE
GAB	BMZ	-	274,000 t @ 0.49 % Ni, 0.34 % Cu, 1.26 g/t PGE (measured: UG only)
	MSB	-	originally 3 Mt @ 2.63 % Ni, 1.44 % Cu and 8.28 g/t PGE

(GAB=Basal Gabro, LrPXT=Lower Pyroxenite, BMZ=Basal Mineralized Zone, MSB=Massive Sulphide Body, MMZ=Main Mineralized Zone, MCHR=Massive Chromite, PRD=Peridodite , PRDMZ=Peridotite Mineralized Zone, PCR=Chromitiferous Harzburgite Unit ,PCMZ=Chromitiferous Mineralized Zone)

1.3 Contact metamorphism

Contact metamorphism is processed in country rocks adjacent to igneous intrusions and is generally a static thermal event of local extent (EHLERS & BLATT, 1982). The maximal width differs, depending of the heat capacity of the intrusion, from several meters to a maximum extension of a few kilometres. Beside that the extent of the aureole is also a function of the thickness of the intrusion. So called “baled” rocks occur in the surrounding of small intrusions. They show a higher hardness than the other country rocks and are often characterized by a reddish colour due to oxidation processes. Intrusions with a higher thickness generate a broad thermal aureole, resulting in a wide zone of country rock. Within the aureole there may be different zones of mineralogy which can be related to the distance from the contact intrusion – country rocks (EHLERS & BLATT, 1982). The major parts of magmatic intrusions are of granitic composition (WINKLER, 1965).

Accompanying with the generation of a thermal aureole by intrusions processes of compositional changes occur abstracted as “metasomatism”. The change of the composition of the country rocks are mainly induced by fluids emanating from an igneous intrusion, or from a fluid migration activated within the country rock by the presence of intrusion. Those metasomatic effects are greatest in rocks of carbonatic nature next to silicic intrusions. Rocks whose compositions have been altered by fluids caused by the named reasons are called skarns or tactites (EHLERS & BLATT, 1982).

Influenced by contact metamorphic events the mineralogy of limestones is characterized by the presence of calcium-rich silicates, and commonly include grossulartite, andradite, epidote, wollastonite or tremolite. The temperature of the country rocks depends on the temperature of the magma. In table 1.2 temperatures of different magma are given based on the investigation of Winkler (1962).

Table 1.2: Temperatures for different types of magma

MAGMA	TEMPERATURE
granitic	700 – 800 °C
Syenitic	about 900 °C
Gabbroic	about 1200°C

The character of the Uitkomst magma is nearly gabbroic with a tendency to an ultrabasic character. That means that the temperatures of the Complex were approximately at 1,000 – 1,200 °C.

The mineral assemblages resulting from the contact metamorphism and generated in the country rocks are differently dependent on the lithotype they formed in. At this thesis there will be a division in three different types of country rocks:

1) Timeball Hill Shales (including the Hornfelses, as part of the Timeball Hill Formation)
2) Bevets Conglomerate (Rooihoghte Formation)
3) Malmani Dolomite

Close to the contact there are minerals expected like andalusite in the Timbehall Hill Shales or wollastonite in the Malmani Dolomite. Generally it is a fact that in closer distance to the contact there are the metamorphic minerals which are originated under high temperature but low pressure depending on depth of intrusion. With increasing distance to the contact the conditions of mineralmetamorphosis due to a decrease in temperatue, not necessary if recrystallization or blastesis of new minerals are changing (e.g. LIKHANOV et al., 2000)..

That is the basis for the analysis of the contact aureole. With the aim of the mineralogical and chemical zoning in the end of the investigation it is possible to construct or to show different areas with individual textures and metamorphic parageneses. Those are corresponding to different temperatures. Following the monitoring of the mineral assemblages it should be possible to produce isograde in the country rocks.

The Bevets Conglomerate rocks are mainly constituted by quartz and therefore not influenced in the same way as the more reactive shales or the dolomites. This is the reason why the Bevets Conglomerate unit was not investigated in such a copious way as the calc-silicates of the Malmani Group or the shales and the hornfelses of the Timeball Hill Formation.

1.4 Review of corundum genesis

The corundum (Al_2O_3) is a constituent of the contact hornfelses in a certain distance to the contact. It is i.e. in a distance of 200 – 250 m to the contact. A chapter of this thesis is dedicated to find out the reasons for the spatial limitation of the corundum occurence.

Corundum is a mineral with a great hardness. With a Mohs-hardness of 9.5, corundum is the second hardest natural mineral after diamond. Additionally to that there are varies which are suitable as gemstones. The variants are the sapphire (blue, coloured by Fe & Ti) and ruby (coloured by Cr).

Concerning the genesis of the natural corundum there are two possibilities. There is the primary and the secondary forming of corundum. The primary accumulation of corundum includes the magmatic forming in Al-rich lithotypes like syenites, granites and its pegmatites, peridotites and anorthosites. Corundum is also generated primarily through metamorphism of Al-rich educts. So corundum can also be found in crystalline schists, dolomites and marble.

Secondary corundum is developed under sedimentary conditions. Because of its high chemical and physical resistibility corundum is enriched in placers. (RÖSLER, 1991)

After WINKLER (1965) corundum is forming through the transformation of gibbsite (γ-$Al(OH)_3$ to diaspore (α-AlO(OH). With the achievement of temperatures of approximately 400 – 410°C and at an assumed pressure of 1 kbar diaspore converts to corundum (Al_2O_3) and water (WINKLER 1965). The precondition for these reactions is an Al-rich educt.

1.5 Methods used for investigation

To reconstruct the conditions of metamorphism surface grab samples were taken in the most parts of the area. They were taken in a size of ca. a cigarette box by sampling traverses over different litho- and geological units.

But the bulk of the investigated samples came from drillcores which were taken over several years during the exploration work at the uitkomst Complex.

Additionally, underground samples have been taken from the Country rock and xenolithe sidewalls in different distances from the contact. The aim of the underground sampling was to understand the metamorphism of the dolomites xenolithes in the Main Mineralization Zone (MMZ) in contact with massive sulphide massive ores.

1.6 Objectives and scientific methods

The aim of this study is to investigate the physical and chemical different mineral paragenesis and the grade of metamorphism in the country rocks of the contact aureole caused by the thermal overprint of the Uitkomst intrusive rocks. This depends on the mineralogical composition of the country rocks and is a function of their distance to the contact, due to a prevailing thermal gradient.

The study should produce data to reconstruct temperature gradients in the country rock in various distances to the contact present during and after the emplacement of the Uitkomst Complex.

Finally, the genesis of corundum porphyroblasts in the hornfels especially their mode of occurence resulting from the chemical conditions in the aureole of the meta-pelites should be investigated. Furthermore their extractability and benefit should be characterized resulting from their physical, chemical and mineralogical qualities.

2. Methods of investigation

2.1 Sampling

Grab samples were taken for getting a statistical variation of the grain sizes. Over all nearly 25 grab samples were taken over all lithologies. But not all of them were used for completing the mineralogical parageneses around the Complex, because in the majority of cases unweathered samples from boreholes were used for the investigations.

Traverse sampling of lithotypes was important for the investigation and the reconstruction of the metamorphic conditions; this refers especially to the p-T – conditions prevailing in the country rocks, during the emplacement of the Uitkomst Complex. The disadvantage of the surface samples is their state of weathering and the following negative influence on the quality of the measurements. For this reason the focus of the sampling was shifted to samples from boreholes. These holes were drilled during the last 30 years for realizing the exploration and for estimating the extent and the properties of the ore bodies. The samples are not weathered by surface weathering but influenced by metasomatic processes caused by the emplacement of the Complex.

At all there are 20 locations on the northern and the southern side (Fig. 2.1) of the Complex. 34 samples are the outcome of the examination of the drill cores. The result of the additional analyses is an overview about the mineralogy and the chemistry from samples of different lithologies and conclusions on the p-T – conditions during contact metamorphism.

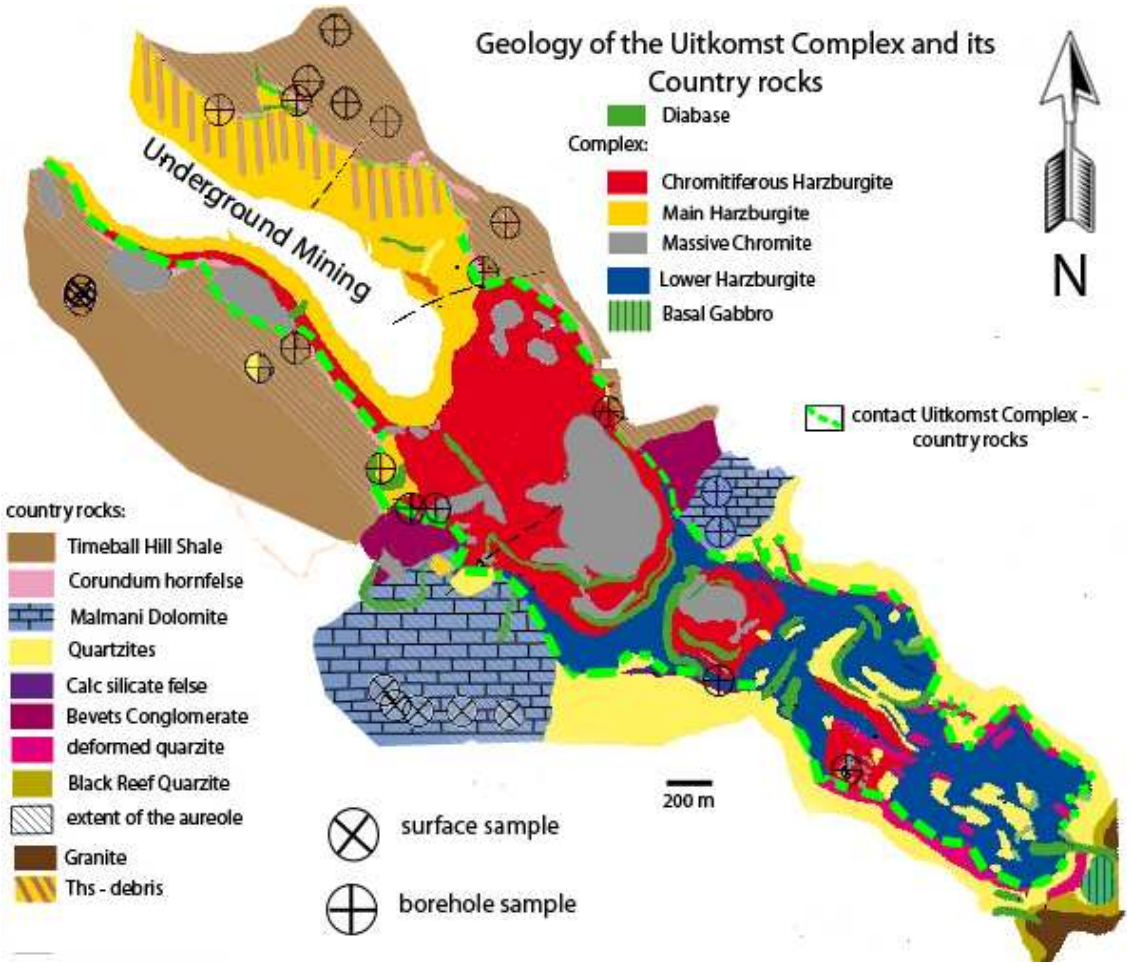

Fig. 2.1: Sampling area with marked sampling localities; (GAUERT, 1995)

2.2 Microscopy

A good method for getting a first impression of the mineralogy is to make thin sections out of the sample material and investigate them under a microscope. To prepare the samples for analyzing them under the microscope in transmitted light it is indispensable to produce thin sections with a thickness of 30 µm. The size of the slide is 2.5 cm in width and 4.5 cm in length. These are standard measures for slides. So it is possible to place and arrest the slides under the microscope.

The slides were observed under four different magnifications, 2.5 x, 10 x, 20 x and 40 x magnification. The analyses were made in transmitted light and with and without crossed Nichols.

Altogether 76 thin sections were investigated as a preliminary method. Dependent on their condition and their quality it was to decide which analyzes are made on them in the progress of the study. But during the observations with the microscope the minerals were determined and described in detail. Attendant to the mineral appraisal it was important to identify and to describe metamorphic textures as accurately as possible. The investigations via microscope are a great part of this project and the record follows later in this paper. The investigations were processed with a microscope named EM 2 from Nikon.

2.3 Electron Microprobe Analysis (EMPA)

Mineral chemistry determined by microprobe was of an eminent importance for this study. The microprobe which was used for the studies is a CAMECA SX100 (Fig. 2.2). The aim of the investigation with this technique was to find out the composition of petrogenetically important minerals such as pyroxene, amphibole, garnet and mica. Furthermore it should be possible to proof metasomatic processes while the metamorphism takes place. The knowledge about the chemical composition of those minerals is significant for the reconstruction of metamorphic processes and conditions. The measurements were executed with the microprobe of the “Institut für Mineralogie und Materialwissenschaften” at the University of Leipzig in Germany. All in all eight thin sections with were investigated.

Fig. 2.2: CAMECA SX 100 Universal EMPA; www.cameca.fr

The measurements were executed with 5 spectrometers at once. The detector crystals itself are of an artificial character named, PET, LIF and TAP. The following elements were measured: Si, Mg, Fe, Ca, Mn, Ti, Al, Cr, Na and K. The content of oxygen was calculated afterwards.

Additional to that quality measurements by creating WDS-spectra were created in cases when the mineral could not be indicated by measuring the mentioned elements. The quality measurements were executed with a static beam with a diameter of 1 µm or if needed also with a scan.

The following table 2.1 shows the standards, used for calibration and their compostion.

Table 2.1: composition of the standards used for electron microprobe analyses

Name of the standard	**Composition (atomic-%)**	**Elements used for calibration in this std.**
Albite ($NaAlSi_3O_8$)	O: 48.76 %, Na: 8.71 %, Al: 10.32%, Si: 32.1 %, K: 0.11 %	Na, Al
Diopside ($CaMg[Si_2O_6]$)	O: 44.33 %, Mg: 11.22 %, Si: 25.94 %, Ca: 18.51 %	Mg, Si & Ca
Orthoclase ($K[AlSi_3O_8]$)	O: 46.47 %, Na: 1.01 %, Al: 9.81 %, Si: 30.4 %, K: 12.18 %, Ba: 0.13 %	K
Rutile (TiO_2)	O: 40.05 %, Ti: 59.95 %	Ti
Cr_2O_3	O: 31.5805 %, Cr: 68.4195 %	Cr
Rhodonite ($CaMn_4Si_5O_{15}$)	O: 37.72 %, Mg: 0.98 %, Si: 21.63 %, Ca: 5.20 %, Mn: 33.68 %, Fe: 0.79 %	Mn
Andradite glass ($Ca_3Fe_2Si_3O_{12}$)	O: 37.781%, Ca: 23.6055 %, Fe: 21.9788 %, Si: 16.5797 %,	Fe

The measuring was done by a scan of 10 µm on the surface of the thin section after the metallization of the surface with carbon. That was necessary for the avoidance of charging on the sample surface. Because of the roughness of the thin section it was essential to do the metallization two times with a resulting layer of carbon about 6 µm thick. The measurements were processed with a voltage of 15 kV and a sample electricity of 20 nA.

2.4 XRF-analyses

The X-ray fluorescence spectroscopy is a suitable method for determining chemistry in samples of unknown composition. The result of such an investigation is the knowledge of the whole rock chemistry.

2.4.1 Sample preparation

The first step was to crush the samples using a Retsch KG 5657 Haan BB 100 jaw crusher. This crusher is equipped with breaking jaws and plates of tungsten carbide. The crushed samples were milled in a Giebtechnik Labor-Scheibenschwingmühle (Type T400). The milled powder was weighed, dried for 24 hours at 110°C and weighed again for determination of amount of adhesive water. Subsequently the specimen is roasted for another 4 hours at 1000°C.

The roasted powder is the basis for the production of pellets and fusion disks. The pellets are made out of 8 g sample material and 3 g Hoechst Wax and are used for trace element analyses. For analysing the major elements fusion disks were produced consisting of 0,28 g material and 1,52 g of Li-meta- and Li-tetraborate.

The major and trace element analyses were arranged at the Department of Geology, UFS, by the PANanalytical WDXRF Axios spectrometer.

The spectrometer worked with SuperQ Version 4 Software with two analytical options: IQ+ and Pro-Trace. Pro-Trace is necessary for making spectral overlap corrections for tube lines including tube contamination, e.g. Mo, Zn, Ni, Cu and Cr.

The anode is operating with following working parameters:

- Accelerator voltage: 60 kV
- Current: 160 mA
- Power level: 4 kW

The following standards were used for the XRF-investigations (Tab. 2.2):

Table 2.2: standards used for XRF-investigations for main- and trace elements; please find the compositions of the standards in the appendix

Elements	**Standard names**
Major elements	G-1, W-1, AGV-1, BCR-1, DTS-1, G-2, GSP-1, PCC-1, BHVO-1, MAG-1, SY-2, SY-3, MRG-1, ASK-1, ASK-2, GR,GA, GH, BR, MICA-FE, MICA-MG, DR-N, UB-N, BX-N, DT-N, VS-N, GS-N, FK-N, GL-O, AN-G, BE-N, MA-N, AL-I, IF-G, AC-E, JG-1, JG-1A, JG-2, JG-3, JB-1, JB-1A, JB-2, JB-3,JR-1, JR-2, JA-1, JA-2, JA-3, JF-1, JF-2, JP-1, JGB-1, JCH-1, JDO-1, JLK-1, JLS-1, JSD-1, JSD-2, JSD-3, JSI-1, JSI-2, JR-3, JGB-2, JH-1, NIM-D, NIM-G, NIM-L, NIM-N, NIM-P, NIM-S, SARM-39, SARM-40, SARM-41, SARM-42, SARM-43, SARM-44, SARM-45, SARM-46, SARM-47, SARM-48, SARM-49, SARM-50, SARM-51, SARM-52
Trace elements	AC-E, AGV-1, AL-I, AN-G, ASK-1, ASK-2, BCR-1, BE-N, BHVO-1, BR, BX-N, DR-N, DT-N, DTS-1, FK-N, G1, G2, GA, GH, GL-O, GR, GS-N, GSP-1,IF-G, JA-1, JA-2, JA-3, JB-1. JB-1A. JB-2. JB-3, JCH-1, JDO-1, JF-1, JF-2, JG-1, JG-1A, JG-2, JG-3, JGB-1, JGB-2, JH-1, JLK-1, JLS-1, JP-1, JR-1, JR-2, JR-3, JSD-1, JSD-2, JSD-3, JSI-1, JSI-2, MAG-1, MA-N, MICA-FE, MICA-MG, MRG-1, NIM-D, NIM-G, NIM-L, NIM-N, NIM-P, NIM-S, PCC-1, SARM-39, SARM-40, SARM-41, SARM-42, SARM-43, SARM-44, SARM-45, SARM-46, SARM-47, SARM-48, SARM-49, SARM-50, SARM-51, SARM-52, SY-2, SY-3, UB-N, VS-N, W-1

2.5 XRD-analyses

The X-ray Diffraction (XRD) is a very good tool to get information about the mineral phases in a specimen of unknown composition. The advantage of this method is the easy and fast way of sample preparation.

2.5.1 Sample preparation

The way of sample preparation is the same like the sample preparation for the XRF-analyses. The powder, as outcome of the crushing and the milling-processes is pressed in sample carriers with a circular depression of ca. 2.5 cm of diameter. The powder is pressed in this circular depression and was putted in a vertical framework which can grab 20 samples. Such samples can be measured at once. The limit of detection is ca. 2 %. (BEUKES, oral communication 2007)

2.5.2 Sample analysis

The analysis with the Siemens D 5000 State can be done qualitative or semiquantitative. For this reason the specimen is irradiated by high-energetic monochromatic X-rays. Those rays are produced in a special X-ray tube. The X-rays are refracted on the crystal lattices of the minerals which existing in the sample. A detector describes a semicircle and is recording the whole of the reflexes. These reflexes are plotted in diffractograms afterwards. The reflexes can be converted, after the Braggs Law ($n\lambda = 2d*\sin\theta$) in distances between the crystal lattices, which are special for each mineral. That's why the XRD-analyses are a practical method for determining minerals. The measurements are running under the following working parameters:

- Voltage: 45 – 55 kV; - Current: 40 – 50 mA

The evaluation of the results was processed with the software EVA 3.0.

2.6 Thermodynamic modelling and phase relation calculation with TWQ

Depending on their suitability samples were analyzed as thin sections or powders by using them for several analytical investigations including EMPA, XRF and XRD etc.
Based on the petrographic data TWQ was used for calculating phase equilibria. The interactive program TWQ (**T**hermobarometry **W**ith **E**stimation of **Eq**uibrilation State) is a tool for mineral-fluid equilibria. Developed and maintained by Rob Berman (Geological Survey of Canada; 1988, 1991, 2007) it can calculate many types of phase diagrams. But its primary application is geothermobarometry using internally consistent thermodynamic data for endmembers and solid solutions that have been derived simultaneously from relevant experimental constraints. (http://gsc.nrcan.gc.ca/sw/twq_e.php; 2008)

3. Previous work

The major part of the scientific investigation of the Uitkomst Complex is due to the economic potential of the Ni-Co-Cu-PGE-bearing Complex itself.

The attention of the mining companies was attracted by the work of WAGNER (1929). He described the Complex as an ultrabasic sill consisting of platiniferous amphibolitized pyroxenitic rocks with considerable value of Ni. In the consequence there have been feasibility studies since 1970. The economic potential of the Uitkomst Complex was re-evaluated in the mid-1990s. KENYON et al. (1986) concentrated their studies on the interpretation of the lower rock units of the Complex on the farm Uitkomst 541JT. Kenyon advanced the idea of the chemical inverse layering of the Complex.

The geology and the geochemistry of the Basal Gabbro Unit (BGAB) and the Chromitiferous Harzburgite (PCR) were described by ALLEN (1990) amongst others. The entire magmatic stratigraphy was described by GAUERT et al. (1995, 1998 & 2001). VON SCHEIBLER (1991) described the genesis of the Uitkomst Complex and published a geological map of the Complex. ERIKSSON, HATTINGH & ALTERMANN (1995) and ERIKSSON & ALTERMANN (1998) also mentioned the tectonic setting in their work about the geology of the Lower Transvaal.

GAUERT et al. (1995) suggested that the elongated Uitkomst body represents a magma conduit in which open and closed system conditions dominated different parts of a magma chamber. Currently there are two dominant petrogenetic models. Firstly the already mentioned model of the "inverted layering" by KENYON et al. (1986) proven to be not the case and furthermore secondly the "multiple intrusion model" of VON SCHEIBLER (1991). GAUERT et al. (1995) supported the latter. This is the momentary accepted theory for the genesis of the Uitkomst Complex. Also LI et al. (2002) are of the opinion that the Complex was build up by multiple magma emplacements. Evidence for this statement of LI et al. is the investigation of "Olivine and sulphur isotopic compositions of the Uitkomst Ni-Cu sulphide ore-bearing complex". This assumption is also supported by the work of SARKAR et al. (2008) who made investigations concerning the stable isotopes of the magmatic lithology, especially sulphur and oxygen, and the analysis of the fluid inclusions with the aim to clarify the origin of the fluid phase. They suggested a sulphur transfer via a fluid associated with dehydration reactions in the Country rocks. Furthermore they determined strongly elevated $\delta^{18}O$ of quartz and albite in the Upper

portion of the Uitkomst Compkex show that minerals like quartz, albite, actinolite, chlorite and epidote are generated with the influence of meteoric water. The temperature of those alteration processes is indicated with 500°C proved by investigation of fluid inclusions (SARKAR et al., 2008).

The country rocks of the Uitkomst Complex are less investigated so far. The metamorphosed country rocks are in the focus of this thesis A classification of the mineral parageneses like developed for other thermal aureoles in the same way like for example LIKHANOV et al. (2001) describing the different zones of mineralization in Fe- and Al – rich graphitic metapelites in the Transangarian region of the Yenisei Ridge in eastern Siberia.

The contactmetamorphic induced aureole surrounding the Uitkomst Complex was not in the focus of scientific interest so far. But contact aureoles are in the spot of scientific efforts in other regions and geological settings in the world. The scientific approach of SYMNES & FERRY (1995) was the metamorphism of pelitic rocks from the Onawa Contact Aureole in Central Maine, USA. SYMNES and FERRY mapped and characterized metapeltic rocks based on mineral assemblages. But in contrast to the aureole of the Uitkomst Complex, partial melting was of an eminent important role at the Onawa aureole. Nevertheless their observations are also important for the understanding of the thermal aureole of the Uitkomst Complex. The contact metamorphism of carbonatic and calc-silicate rocks has been a main interest of metamorphic petrology for the last decades. POVODEN, HORACEK and ABART (2002) dealt with the contact metamorphism of siliceous dolomite and impure limestones in the eastern Monzoni contact aureole in the Western Dolomites. They underlined the different extent of the contact aureole in marly limestones and dolomitic lithologies due to the control of whole rock chemical composition on mineral parageneses on the one hand and the different “openness” of the lithologies for external fluids on the other hand. Of course those observations can also be made in other lithologies but this shows parallels regarding the metamorphism and the lithotypes of the country rocks surrounding the Uitkomst Complex.

The studies of the thermal aureole were influenced by the works of ENGELBRECHT (1988) in the Marico district of the Bushveld Complex and BRÖCKER & FRANZ (2000). They did research on the Contact aureole on Tinos (Cyclades, Greece). The named scientific papers are just a small number of researches which dealt with contact aureole and their influence on the country rocks.

But they reflect the aims of this thesis, more precisely to understand the generation of the aureole investigate the whole rock and the mineral chemistry and construct zones different zones of different mineral assemblages. Based on all the gained knowledge it should be possible to estimate the position of isogrades and isothermes around the Uitkomst body.

4. Local Geology and stratigraphy

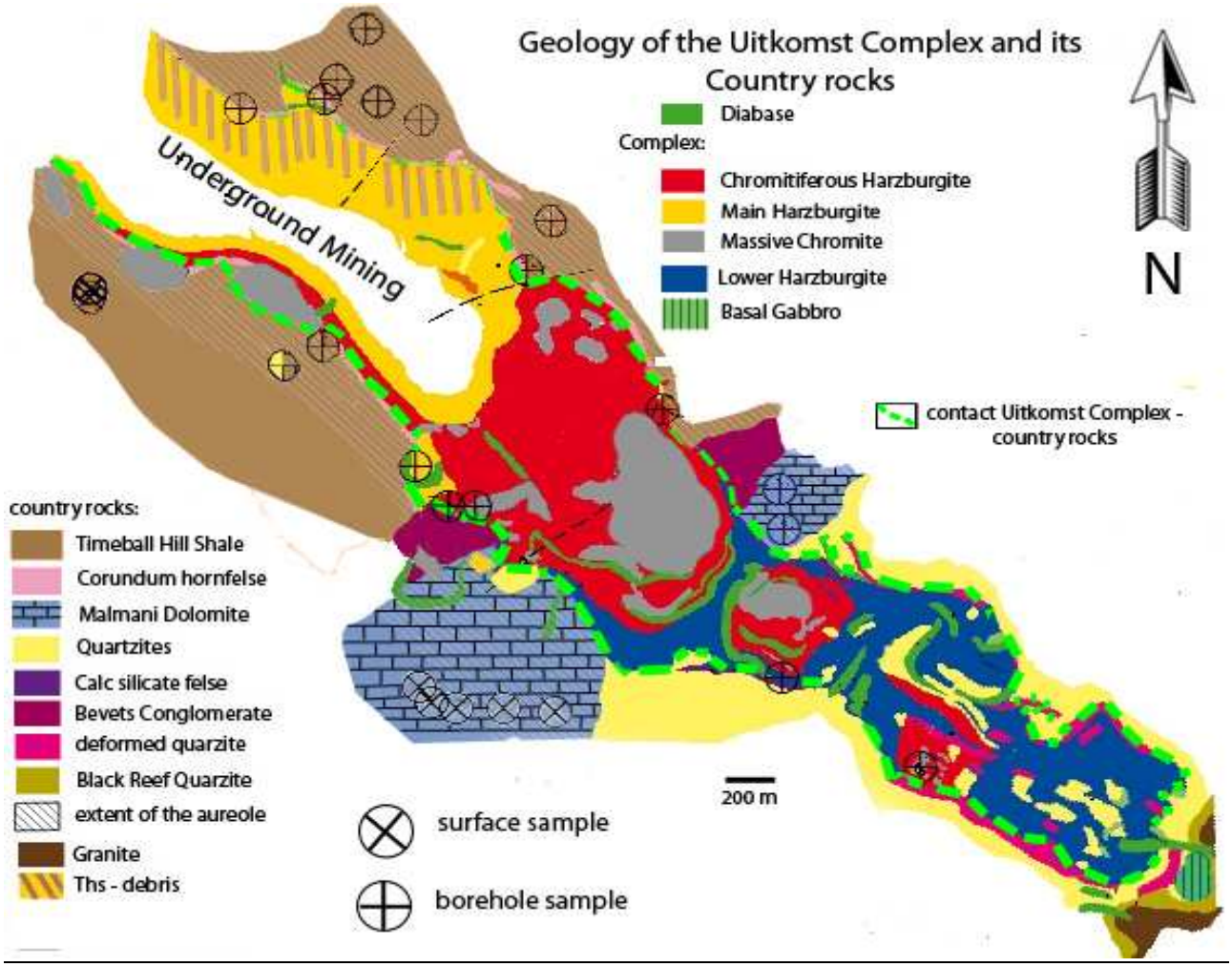

Fig. 4.1: Geological map of the Uitkomst Complex and its country rocks; (GAUERT, 1995)

4.1 General

The Uitkomst Complex is related to the Bushveld Intrusion but intruded 10 km below the current level of the Base of the Bushveld Complex (MAIER et al., 2004). In the area of the Uitkomst Complex the Nelshoogte granite of Archean age (~ 3220 Ma, ANHAEUSSER, 2001) is overlain places by the Gondwan Formation of the Ventersdorp Supergroup (Fig. 4.2). The Gondwan Group is built up by basaltic lavas, polymict quartzites and shales (HORNSEY, 1999). The

Archaean basement in the footwall of the Complex is overlain by the quartzite of the Black Reef Formation. Also the dolomite and quartzite of the Malmani Subgroup (2449.9 ± 2.6 Ma; WALRAVEN & MARTINI, 1995), the Bevets Conglomerate member of the Rooihogte Formation and the Timeball Hill Formation overlie the basement. The upper dolomite of the Malmani Subgroup contains layers of chert and sulphides of sedimentary and hydrothermal origin which are associated with organic matter. The Timeball Hill Shale Formation is composed of ~ 1200 m of graphitic, locally suphidic shale with irregularly distributed layers of quartzite and ironstone.

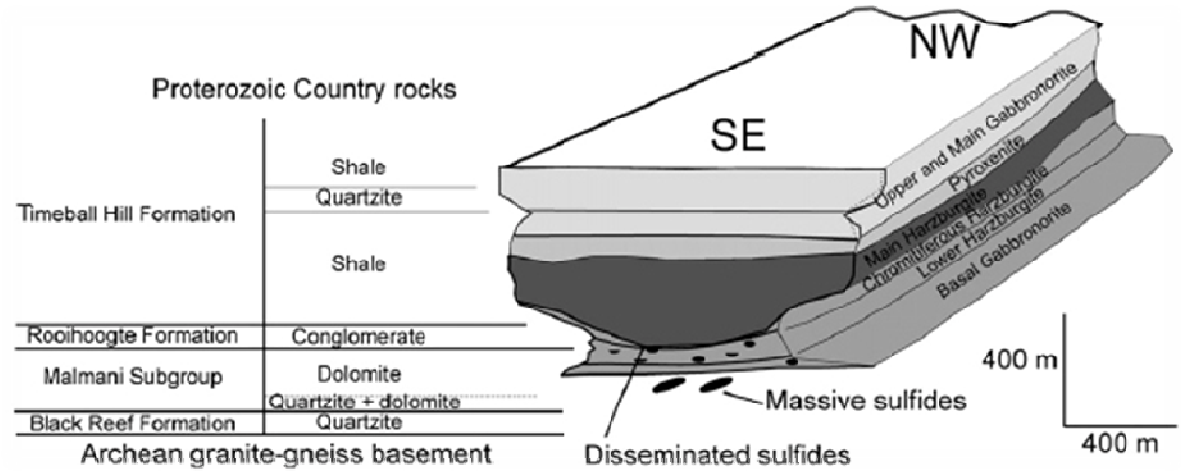

Fig. 4.2: Simplified cross-section sketch of the Uitkomst Complex (after Maier et al., 2004)

4.2 The Complex

The Uitkomst Intrusion is a body of tabular shape with an exposing area measuring ~ 0,8 km in width and ~ 8 km in length. Supported by geophysical investigation it can be suggested that the Complex may extend several kilometres at depth (GAUERT, 1998). The Intrusion penetrated the gently-dipping (5° - 10°) Late Archaean Transvaal Supergroup near the contact with the Archaean basement, stratigraphically ~ 10 km below the base of the coeval Bushveld Complex (MAIER et al., 2004).

Seven lithological units are building up the Uitkomst Complex (Fig. 4.1 & Fig. 4.2). More precisely that are, from bottom to top: the Basal Gabbronorite, Lower Harzburgite, Chromitiferous Harzburgite, Main Harzburgite, Pyroxenite, Main Gabbronorite and Upper Gabbronorite units. Following the litholgical units should be described separately.

4.2.1 Basal Gabbrornorite (BGAB)

The contact of the BGAB with the Black Reef Quartzite Formation is defined by a strongly sheared talc-chlorite-carbonate rock. Those are locally exposed. For example on the southeastern end of the Complex of the farm Uitkomst 541 JT. The Basal Gabbro Unit has an average thickness of 5.6 m ranging between 0 and 15 m (GAUERT et al. 1995). In some places the BGAB extends tens of metres laterally under the country rocks. The contact of the Basal Gabbro Unit with the overlying Lower Harzburgite Unit is gradational (GAUERT et al., 1995). The gabbroic rocks which constitute the BGAB show intense saussuritization and uralitization. In some places they show carbonate veining. The BGAB outcrops on the southeastern end of the Complex (Fig. 4.1) Borehole information indicates that the unit is not constantly developed at the base of the Complex and is completely absent in some places (GAUERT et al., 1995).

4.2.2 Lower Harzburgite (LHZBG)

The Lower Harzburgite Unit has an average thickness of 50 m (max. 90 m). Those rocks are highly altered and are mineralized with abundant xenoliths of country rock. The xenoliths are of quartzitic and carbonatic character and form rafts that are orientated parallel to the igneous layering. The harzburgite is dominantly poikilitic but includes variations of local variations of feldspar-bearing lherzolite, grading into sulphide-rich feldspathic olivine-wehrlite and amphibolites. (GAUERT et al., 1995)

Especially in the vicinity of inclusions of country rock, a pegmatoidal pyroxenite is developed. The pyroxenite comprises coarse-grained clinopyroxene, orthopyroxene, amphibole, and plagioclase crystals with interstitial pyrrhotite, pentlandite, chalcopyrite and magnetite. Although the primary magmatic minerals are intensely altered through serpentinization, sausseritization and uralitization. Outcrops of the Lower Harzburgite are located in the southeastern end and in the middle of the Complex.

4.2.3 Chromitiferous Harzburgite Unit (PCR)

This layer shows an average thickness of 60 m and follows the LHZBG with a gradational contact. In contrast to the LHZBG where chromite is just content in trace quantities it is now a major component. The PCR consists of sheared chromitite lensoids with a distinct “schlieren”-

type structure embedded in highly altered harzburgite (GAUERT et al., 1995). Towards the top of the PCR-unit the chromitite becomes more and more massive in character showing well-preserved igneous layering on a decimetre scale. The top of this unit is the 3 – 4 m thick massive chromitite layer.

The original magmatic minerals were nearly completely replaced by talc, carbonate, phlogopite, chlorite and serpentine (GAUERT et al., 1995). Momentary the PCR-unit is in quarrying in two opencasts, there third opencast is planned in the moment.

4.2.4 Main Harzburgite Unit (MHZBG)

This unit is in the average 330 m thick and constitutes more than one third of the Complex. The Main Harzburgite is represented by a rather monotonous sequence of harzburgitic rock grading locally into dunite, visibly lacking mineralization except for the lowermost 10 m. Locally there are plagioclase bearing sections. From boreholes it is obvious that the MHZBG-unit shows a distinct macro-layering caused by modal and grain size variations. The thickness of the layers varies from cm to m. The unit differs from the unit below in its alteration type. Serpentinization is the dominating form of alteration. The talc-carbonate alteration is rare (GAUERT et al., 1995). The best outcrops of the unit are located in the north-western part of the farm Uitkomst 541 JT and in the southeastern part of the farm Slaaihoek 540 JT.

4.2.5 Pyroxenite Unit (PXT)

The PXT-unit follows the MHZBG-unit with a sharp transitional contact. The average thickness of this unit is approximately 60 m. It seems to be more laterally distributed than the MHZBG-unit. The PXT can be divided into the following sub-units.

A lower olivine-orthopyroxenite, followed by pure orthopyroxenite with only minor accessory chromite and sulphide in the middle and an upper norite to gabbronorite showing increasing plagioclase, clinopyroxene and minor quartz to the top. The sequence represents the transition between the ultrabasic lower units and the basic Gabbronorite Unit in which olivine is no longer visible and plagioclase enters the mineral assemblage.

The Pyroxenite-Unit is unaffected by secondary alteration. The PXT-unit is exposed in the middle to the western parts of the farm Slaaihoek 540 JT. It forms a distinct marker horizon in the

boreholes (GAUERT et al., 1995)

4.2.6 Gabbronorite Unit (GN)

This unit is approximately 250 m thick and forms the uppermost sequence of the intrusion. The contact to PXT below is gradational. The Gabbronorite Unit forms a sill-like body that extends 1.4 km laterally (VON SCHEIBLER, 1991). Xenoliths of quartzitic and argillaceous rocks are found in places (GAUERT et al., 1995)

4.3 Country rocks

The Uitkomst Complex is placed in sedimentary rocks of the Lower Transvaal Supergroup (Fig. 4.3). The base of the LTS lies on average only five meters about the Archaean basement.

4.3.1 Archaean basement

To the southeast of the Complex, the basement is built up by biotite trondhjemite gneiss of the Nelshooghte Pluton, with an estimated age of 3.2 – 3.5 Ga (ANHAEUSSER et. al., 1981). The genesis of these rocks is explained with the derivation from a basaltic precursor by partial melting (ARTH & HANSON, 1979; CONDIE & HUNTER, 1976; TARNEY et al., 1979).

The gneisses vary concerning their composition from grey feldspar- and quartzrich varieties to darker, more biotite and hornblende rich subtypes. They show a high grade of sericitization and silification in places, and are frequently cut by chlorite and quartz veins. Occasionally it is possible to see stringers of chalcopyrite and pyrite. In some boreholes on the farms Uitkomst 541JT and Slaaihoek 540JT (e.g. AH 15), large xenoliths (up to 30 m in intersection) of silificied dark green meta-sedimentary and metavolcanic rock occur within the gneisses. The xenoliths are altered to a secondary rock consisting mainly of antophyllite (GAUERT, 1998). They are supposed to be the remnants of the older green stone belts (ROBB & ANHAEUSSER, 1983) or as metamorphosed sediments (hornfels) of the pre- Transvaal Gondwan Formation (GAUERT, 1998), which is mainly situated in the north-eastern part of the Uitkomst Complex (in the Ngodwana after which the Gondwan formation was named).

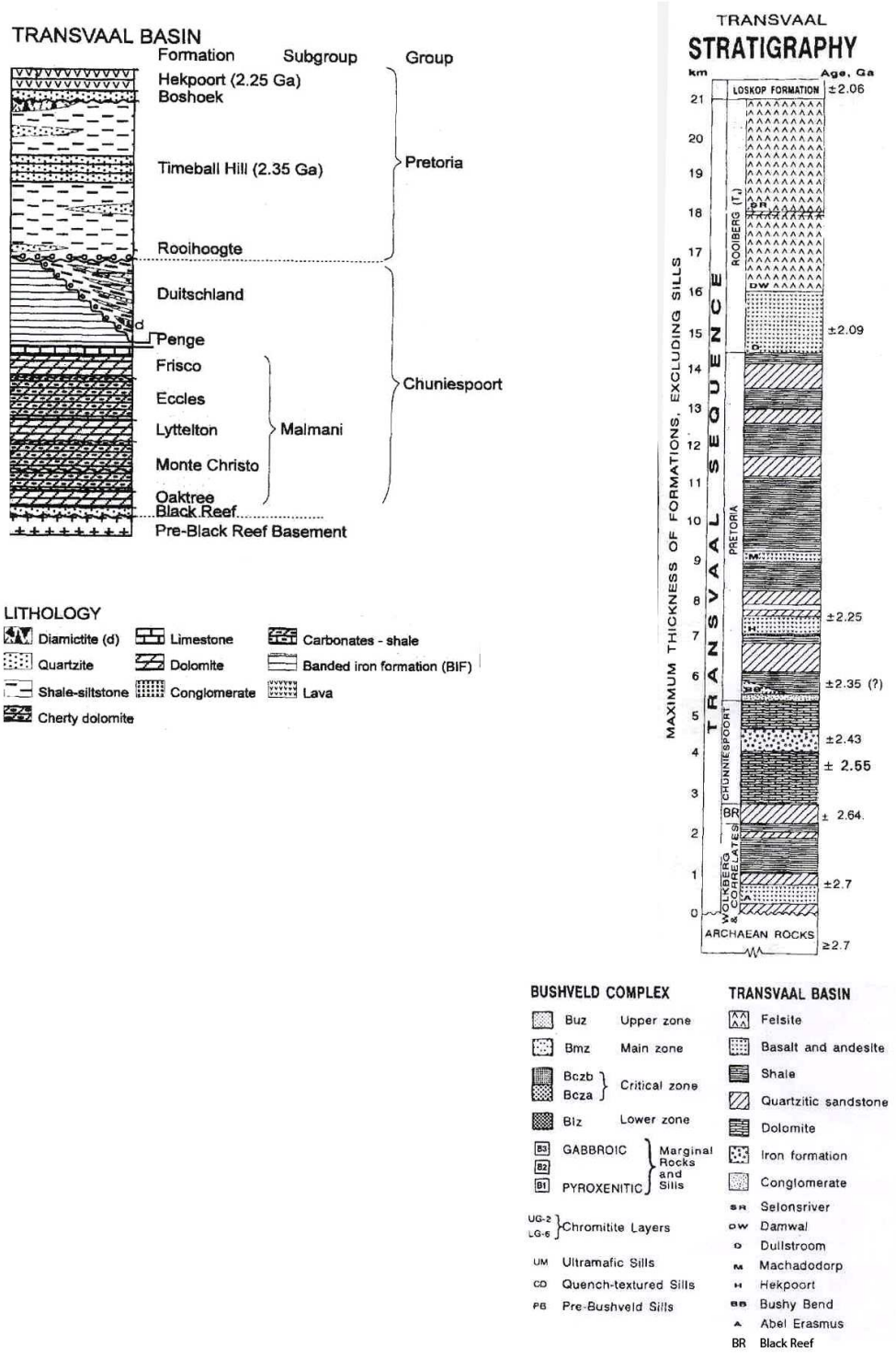

Fig. 4.3 Stratigraphy of the Transvaal Basin and Transvaal Stratigraphy (Eriksson et al., 1995)

4.3.2 Lower Transvaal Supergroup

Fig. 4.3 describes the lithostratigraphy and the geochronology of the Transvaal/Bushveld basin after ERIKSSON et al. (1995). Referring to those authors and based on the data from BUTTON (1986), are the Transvaal sediments in the Bushveld basin are nearly 15,000 m thick. They consist of relatively undeformed and low grade metamorphosed mud rocks, sandstones, volcanic rocks, dolomites and iron formations. The base of this sequence is formed by clastic rocks of the Black Reef Formation overlain by chemical sediments of the Chuniespoort Group. The overlying volcano-sedimentary unit of the Pretoria Group is followed by the volcanic Rooiberg Group.

In the region north of Badplaas the Lower Transvaal Supergroup is incomplete. Also the Chuniespoort Group is only represented by the Oaktree and Lower Monte Christo Formation of the Malmani Subgroup, predominately consisting of chert-rich dolomites, instead undeveloped are the Penge iron formation and the carbonates and clastic sediments of the Duitschland Formation. In contrast, the Pretoria Group is fully developed.

The Uitkomst Complex itself is hosted by the Black Reef Formation, the reduced Malmani Subgroup and the Rooihoogte and Lower Timeball Hill Formation of the lower Pretoria Group.

4.3.2.1 Black Reef Formation

The Black Reef Formation forms a prominent escarpment in the area and describes the base of the Transvaal Supergroup. It is built up by a transgressive conglomerate and quartzite and extends over an average thickness of 10 m in the Transvaal Basin. In the area north of Badplaas the Formation is very poorly developed (CLENDENIN et al., 1991; HENRY et al., 1990; ERIKSSON et al., 1993), ranging from a few tens centimetres to a maximum thickness of 5 m. It is placed unconformably on the Archaean basement with the undulating basal contact being sharp. At the farm Uitkomst 541JT it shows a creamy to light greenish grey, is medium grained and hosts locally cross-bedded quartzite. In some places a basal conglomerate of several tens of centimetres in the thickness may be developed. The quartzite is mature in its nature with only minor Fe-oxide, chlorite and muscovite. The quartz grains are clear (glassy), suggesting an aqueous depositional environment (CLENDENIN et al., 1991). The size of the grains ranges from fine at the top to coarse at the base.

4.3.2.2 Chuniespoort Group

This group overlies the Black Reef Formation. At the Uitkomst exists only a 145 m thick portion of the basal Malmani Subgroup of the Chuniespoort Group consisting of the Oaktree and the Monte Cristo Formations (Fig. 4.3). These are composed of compact, medium grained, laminated carbonate rock, interbedded with minor chert, fine-grained quartzite (in its lower portion) and mudrock. In its upper part, stromatolitic carbonates are observed (e.g. borehole UD 106) Close to the basal units of the Oaktree Formation a 2 – 4 m thick quartzite layer is an important marker horizon. Generally this quartzite layer constitutes the floor of the Uitkomst Intrusion. The layer is fractured and includes stringer mineralization of pyrite and chalcopyrite which most probably derive from the Complex. The upper contact is sheared and shows a hydrothermally alteration. A dolomite layer of variable thickness (0.10 - 10 m) is underlying the Oaktree quartzite and is referred to as the Basal Shear Zone (GAUERT, 1998).

4.3.2.3 Pretoria Group

The units of this group overlie the chemical sedimentary rocks of the Chuniespoort Group with an angular conformity, which is also a strong weathered palaeokarst surface (BUTTON, 1973). The Pretoria Group is built up by an alternation of mudrock and sandstone units. The latter commonly recrystallized to quartzites, with subordinate conglomerates, diamictites and carbonate beds (ERIKSSON et al., 1991). Throughout the succession occur interbedded volcanic rocks and make up a significant portion of the stratigraphy.

The strong volcanic component of the Pretoria Group in combination with the alluvial-fan and fan-delta sediments inferred for many sandstone formations, suggest the possibility of fault-controlled or graben basins (ERIKSSON et al. 1991, 1993; SCHREIBER 1990; SCHREIBER et al. 1992)

Table 4.2 shows the lithology of the Timeball Hill Formation in the eastern Transvaal, South Africa (ERIKSSON et al. 1991, 1993).

Table 4.2: Lithology of the Timeball Hill Formation in the eastern Transvaal, South Africa

Upper mudrocks, diamictite/conglomerate lens	Upper mudrocks ± 400 – 500 m, arkose wedge in north, thin diamictites, deformed mudrocks
Klapperkopp Quartzite Member	Quartzite 0 – 15 – 100 m, thins to south
Lower Mudrocks, Bushy Bend Lava Member	Lower mudrocks, 400 – 700 m, thins southwards

The Timeball Hill Shales, are exposed in the northwestern and the southeastern region of the Complex and are partly high-metamorphosed. In a particular distance to the contact the shales show corundum in their mineral assemblage. Next to the contact with the Complex the shales are changed into hornfelses and houses sillimanite in places.

The Bevets Conglomerate is a member of the Rooihoogte Formation at the base of the Pretoria Group and is located in the north and the south of the Complex. Locally the Conglomerate is up to 30 m thick. One can find quartzites in this formation in some places. The Malmani Dolomite is placed in NNE and the SSW of the Complex.

4.4 The intrusion and the composition of the initial magma

4.4.1 Emplacement of the magma

Observations and borehole data give a hint that the emplacement of the first magma took place at the base of the Malmani Subgroup in the Transvaal Supergroup and probably flowed from southeast to northwest.

The Malmani dolomite and the Bevets conglomerate of the Rooihoogte Formation build up a kind of barrier which avoids the lateral extension of the lower part of the conduit, whereas the shales above these formations allowed lateral extension of the magma chamber (GAUERT et al., 1995). The reason may be the massive character of the dolomite and the conglomerate in opposite to the shale which is more prone to slabbing. The major volume of the country rocks in the chamber must have been removed towards the southeast since no obvious doming of the roof rocks are in evidence. Furthermore, minor sagging of the floor rocks may have occurred, causing

the slight trough-like depression along the major axis of the intrusion, and thinning of the quartzite floor may be related to thermal and chemical erosion by the magma (GAUERT et al. 1995).

4.4.2 Composition of the initial magma

Most information about the earliest magma pulses of the Complex are given in the chilled margin of the Basal Gabbro Unit. Unfortunately, as proven by relatively high Sr isotope ratios, the Basal Gabbro Unit shows definite signs of contamination so that these rocks can hardly be seen as pristine initial magma. It is notable that the average Basal Gabbro (with the exception of Ni, Cu and Ti) has a distinct similarity with the B1-micropyroxenite liquid which is possibly the primary magma of the Bushveld Complex. (HATTON & SHARPE, 1989). The comparable ages of the Bushveld and the Uitkomst Complex and their similarity in terms of initial Sr (R_0) ratios and last but not least their geographical proximity, clearly suggest a genetic link.

5. Petrography and mineralogy

5.1 Timeball Hill Shale

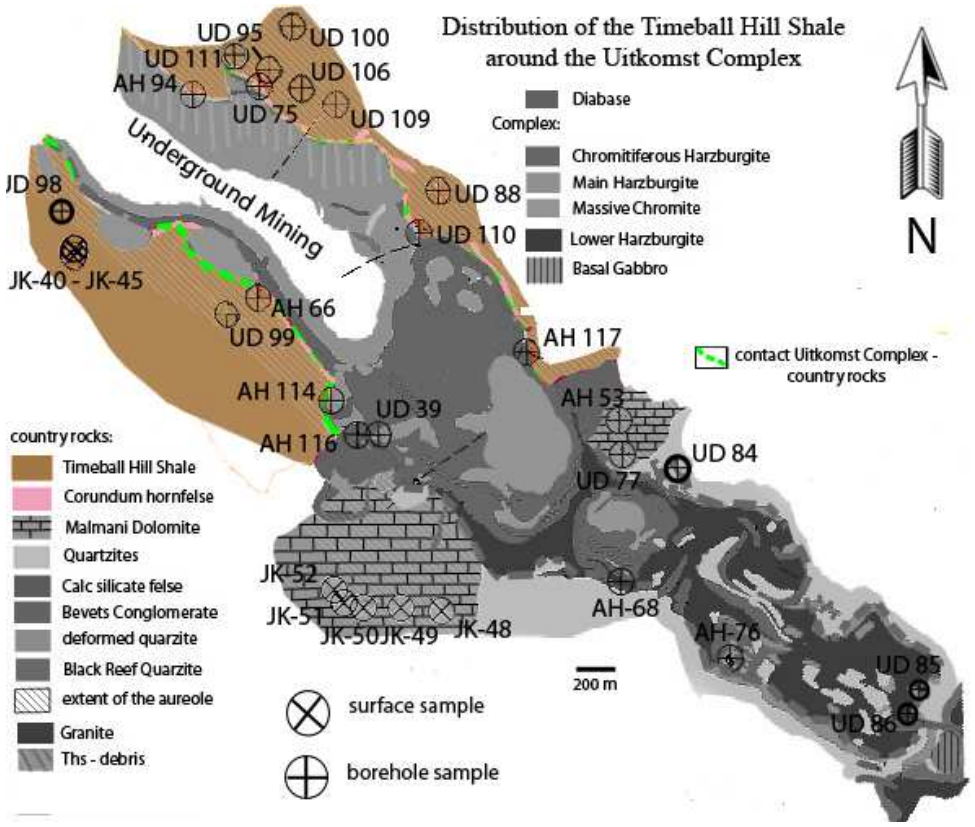

Fig. 5.A: Distribution of the Timeball Hill Shale and the Corundum Hornfelse in the area of the Uitkomst Complex

5.1.1 Macroscopic description

The map in figure 5.A displays the distribution of the Timeball Hill Shale and the Corundum Hornfelse in the area of the Uitkomst Complex.

It is necessary to divide between specimens of Timeball Hill shale were taken from the surface and those taken out of the boreholes. Beside that the so called Hornfelses are an important part of the Timeball Hill Shales. The term “hornfels” describes a fine grained rock which is generated by contact metamorphism.

The samples from the surface show traces of intense weathering, whereas the samples from the boreholes are not weathered in this scale. That is the reason why the Timeball Hill Shale will be

described as “fresh” sample out of the drillcores and as samples from the surface. It is natural that those samples out of one lithotype are different in special characteristics. These characteristics will be divided in the microscopic investigations.
Macroscopic visible is the resistance of the Shale and the hornfelses towards weathering. The Shale generates ridges in the morphology in the landscape around the Uitkomst Complex. This is mainly obvious in the southern part of the Complex.

5.1.1.1 Timeball Hill Shale – surface samples

The samples of the Timeball Hill Shale were taken in traverses with increasing distance to the contact with the Uitkomst Complex. Fig. 5.1 shows a specimen gained in the field.

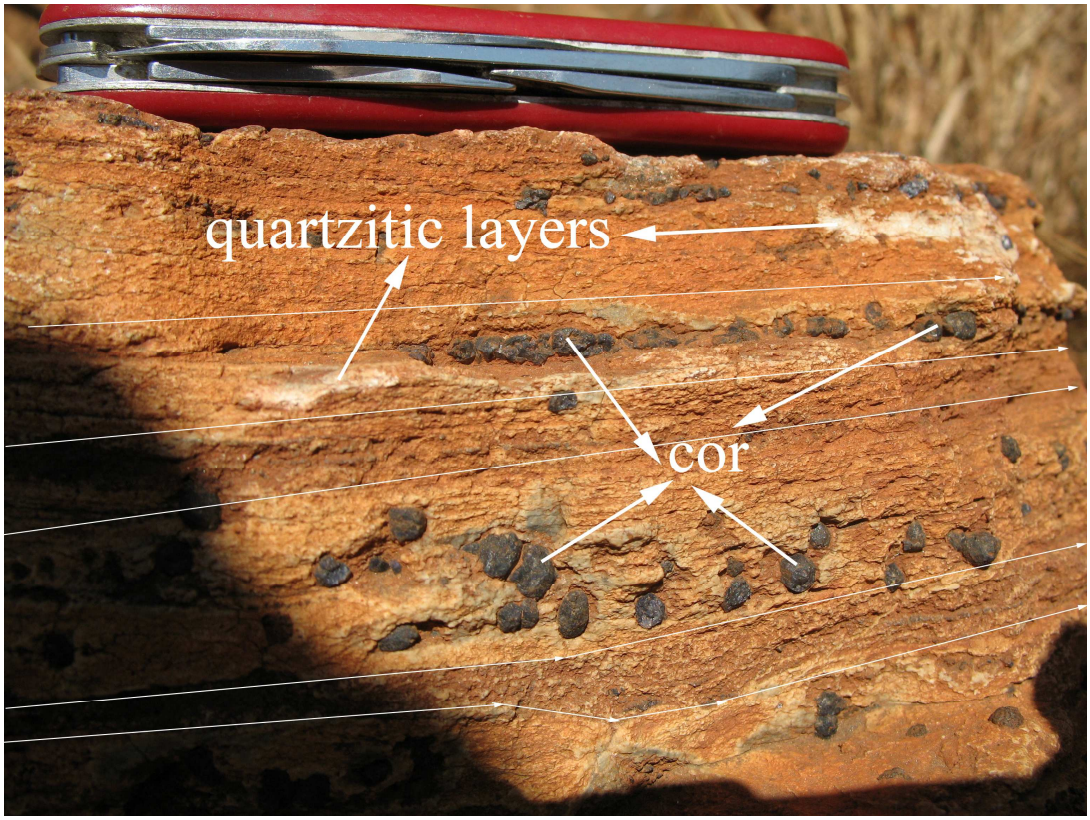

Fig. 5.1: Surface sample of hornfelsic Timeball Hill Shale with visible crystals of corundum (cor) and quartzitic layers; south of the Complex

The Timeball Hill Shale in grab samples has an intense reddish-brownish colour coat caused by Fe-hydration. In fresh condition they tend to be black to grey in colour. It shows a rest of a visible lamination. In spite of the weathered condition it is relatively hard and not easy to split up. The

reason for this phenomenon is the partly quartzitic character of the shales. The shales itself are silficified in various extent. The spectrum is from less quartztic shales to shales with quartzitic lamellae to nearly complete silicified shales. The grade is, next to a higher hardness with increasing quartz content, also remarkable by a certain level of gleam. It is conspicuous that in a certain distance to the contact many hand specimens of the Timeball Hill Shales show corundum (Fig. 5.1) as dark brownish blasts. In some cases those corundum blasts are removed by weathering and cavities are left. Additionally there are superficial concretions of iron and manganese. It was observed that those concretions are not simultaneous constituent with corundum in the Timeball Hill Shales.

The Timeball Hill Shale can be found in outcrops and in debris. Debris of shale is located especially in the northwest of the Complex.

In outcrops the Timeball Hill Shale is massive, layered and show a system of regular splits.

Fig. 5.2: Outcrop of Timeball Hill Shale above Bevets Conglomerate; south of the Complex

Figure 5.2 shows that the Timeball Hill Shale is developed in massive layers of five to thirty cm thickness. The well formed system of vertical and lateral joints is obvious. The formation is folded from time to time, also visible in Figure 5.2.
The reason is syn-emplacement collisional tectonics which caused a thrust component in the country rocks (GAUERT, personal communication, 2007). Additionally to those phenomena there is deformation caused by intruding post-Uitkomst diabase dykes and sills.

5.1.1.2 Hornfelses

At the contact of the Timeball Hill Shales with the Uitkomst Complex one can find hornfelses. Those rocks are recognizably caused by their quartzitic composition, their very great hardness and their black greyish colour. If one can ascertain make sure that they are not a part of debris, they normally mark the direct contact between the country rocks and the igneous rocks of the Uitkomst Complex.
Within the Hornfelses quartzitic layers are changing with layers of corundum. It is conspicuous that layers which contain corundum are also containing quartz and are lighter in colour than the darker reddish layers next to the corundum-quartz layers (Fig. 5.1).

5.1.1.3 Timeball Hill Shales – samples from boreholes

The samples of the shales gained from the boreholes are taken because they are nearly unweathered.
The major part of the specimens is coloured dark grey to black and shows veins of pyrite and calcite. That is a hint for the metamorphic and metasomatic processes which have taken place during the emplacement.
In Figure 5.3 one can see a typical Timeball Hill Shale with the black colour and hints of calcitic veins. The sample is out of a depth of 34.98 m below the earth surface. In Fig. 5.4 one can see a piece of Timeball Hill Shale with typical concretions and mineralization of pyrite.

Fig. 5.3: Specimens of Timeball Hill Shale; borehole UD 77

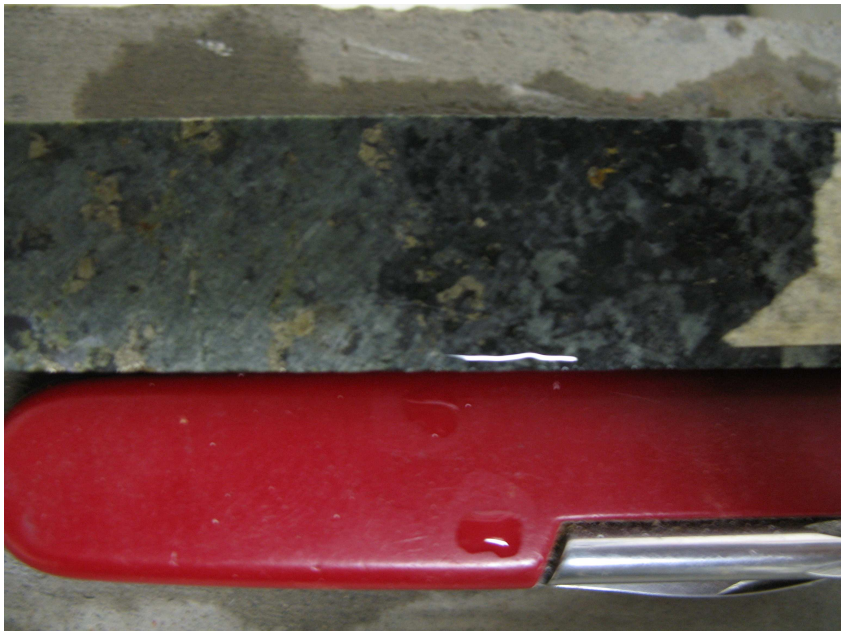

Fig. 5.4: Timeball Hill Shale with mineralization of pyrite

5.1.2 Textures – Timeball Hill Shale

Visible textures can be divided into two types. The first type can be described as laminated and is present in the surface samples of the Timeball Hill Shales. An example is given in Fig. 5.5 and 5.6. The picture shows the lamination which can be observed in the thin section of the samples JK – 43 and JK – 41. Corundum is visible as blue minerals in both slides.

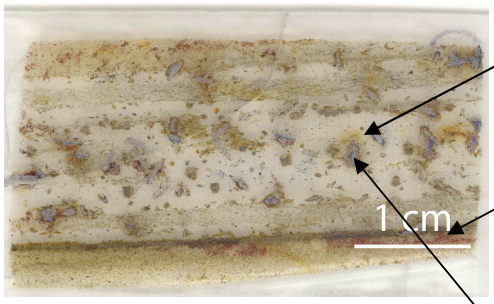

Fig. 5.5: Laminated structure of JK – 43

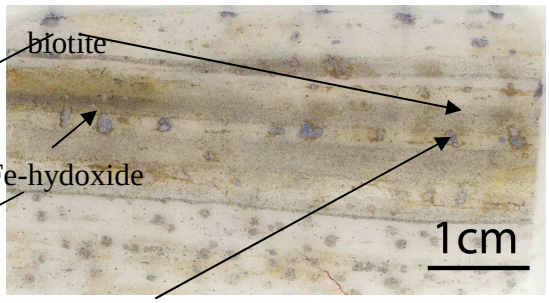

Fig. 5.6: Laminated structure of JK – 41

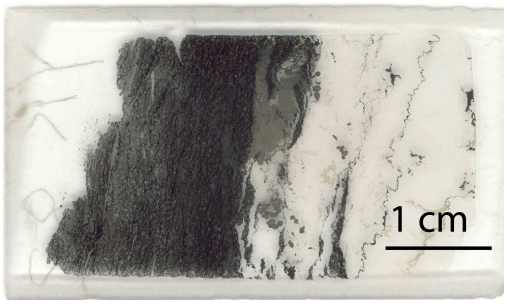

Fig. 5.7: “Flow-structure” of JK – 82

The second type is a structure which is dominated by veins and looks and can be named as “flow-structure”. Fig. 5.7 shows an example for this kind of structure which is also often associated with ore minerals like chalcopyrite ore pyrite (e.g. in the middle of Fig. 5.7).

5.1.3 Microscopic description

The unweathered samples of the Timeball Hill Shales synonymous with the shales from the boreholes are the basis for thin sections. Additionally to that further thin sections were made from surface samples if their constitution and shape was of suitable character. In the following the results, referenced to the mineralogy and petrological processes, of the microscopic analyses are presented. To examine the circumstances of the formation of the minerals in the rocks and the petrology a sequence of stratigraphy is given to every slide produced out of the samples from the boreholes.

5.1.3.1 Microscopic description – surface samples

The following table gives the minerals assemblages of the investigated specimen of the Timeball Hill Shales, including the hornfelses, taken as grab samples in south of the Complex. This is a first insight in the mineralogy of the surface samples of the Timeball Hill Shales.

The distances to the contact are measured on the ArcGIS map which was build based on the field observations. The position of the Contact is estimated and constructed with the knowledge of the petrogenesis in this area.

Tab. 5.1: Overview of the mineralogy of the surface samples of the Timeball Hill Shale (including hornfelses)

coordinates	distance to contact [m]	thin section no.	lithotype	minerals (recognizable with microscope)	text/remarks
S 25 43.934 E 30 35.966 altitude: 1401 m (above sea level)	241	JK-40	hornfels	tremolite, biotite, corundum	dense matrix, granoblastic structure, corundum (crn)surrounded by biotite, crn is altered – shows reaction rims with biotite,
S 25 43.934 E 30 35.966 altitude: 1404 m (above sea level)	248	JK-41	cor- undum hornfels	corundum, biotite	slide shows a lamination, layering built up by lamellae of light grey and grey colour, dark layers are coloured olive to dark green; crn is associated with the lighter layers and are located at the border to the darker layers; again rims of biotite around corundum
S 25 43.938 E 30 35.959 altitude: 1402 m (above sea level)	254	JK-42	silicified hornfels	biotite an bright mica	matrix is very dense and quartzitic; mica minerals are cloudy and blurred
S 25 43.953 E 30 35.956 altitude: 1397 m	283	JK-43	cor- undum hornfels	corundum and biotite	layered structure, crn in each lamella but different in shape dependent on the layer they are in; slide shows crn of ideal shape and with a clear cleavage at its rim; embedded in the brighter zones in the middle of the thin section – smaller and mostly strip-like crn-minerals; crn is surrounded by biotie (bt), bt is greenish to dirty brown and of cloudy shape
S 25 43.953 E 30 35.956 altitude: 1397 m	283	JK-44	quartzitic shale	quartz and mica	content of mica is proportionally high; occasionally there are phenomena of alteration; qtz at the rim of the slide
S 25 43.953 E 30 35.956 altitude: 1417 m	283	JK-45	hornfels	biotite, muscovite, corundum	dense matrix, crn surrounded by rims of biotite, muscovite – colourless, strip-like mineral

Below one can see images of thin sections (Fig. 5.8) from some samples in the table above. Conspicious are the mineralisations of corundum and the tremolite in JK-40.

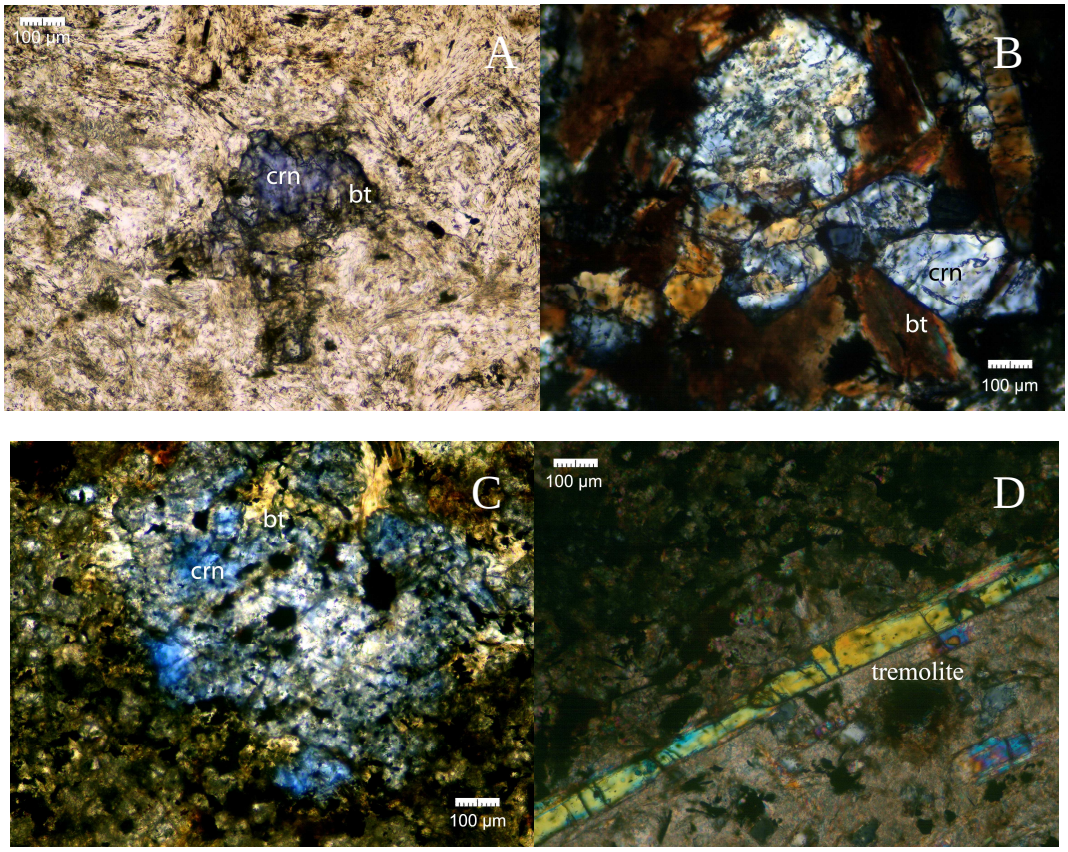

Fig. 5.8: Microscopic images of chosen grab samples of shales and hornfelses; A: Corundum with a rim of biotite; JK – 40; transmitted light; B: Corundum with biotite; JK – 41; crossed nichols; C: Altered corundum together with biotite; JK – 45; crossed nichols; D: Tremolite in strip-like shape; JK – 45; crossed nichols

5.1.3.2 Microscopic description – borehole samples

The positions of the boreholes are given in the map which is part of the Appendix and an extra part of the thesis. Furthermore, like mentioned before, the stratigraphy is partly given to illustrate the geological setting the sample is taken from. At the end of this chapter a table with the whole mineral assemblage of each specimen will be given, then combined with the results of the XRD-analyses. But before, the specimens are described in detail and are related with their stratigraphical position.

JK – 64 (UD 100) - hornfelse

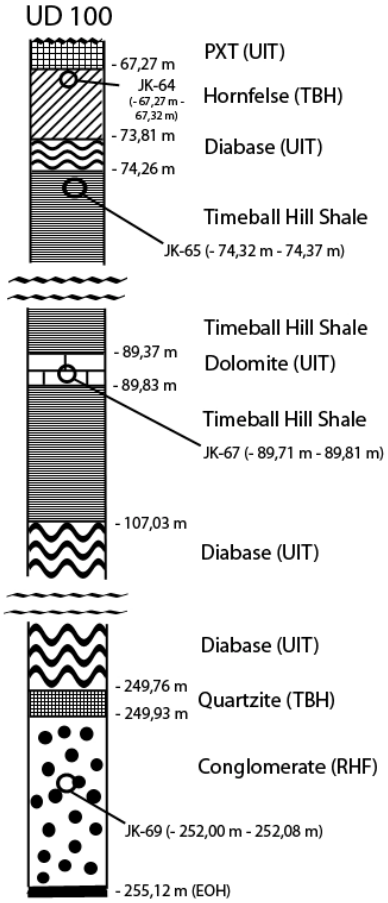

Fig. 5.9: position of the samples JK – 64, JK – 65, JK – 67 and JK – 69 in the stratigraphy of UD 100; not to scale.

Distance to contact: 346 m

Figure 5.9 shows the sample position at a depth of 67.27 m. The register of the boreholes name this particular layer as hornfels.

The main constituent of this rock is the quartz, which is building up the major part of the thin section.

The thin section shows pale green chlorites which are probably Fe/Mg-chlorites because of their colour and their optical properties in transmitted light.

Beside the chlorite hematite is visible. The hematite is showing strong red reflexes within the grain. Additionally a development of several zones with hematite crystals is recognizable. They are noticeable because of their dark-red colour.

There are very small contents of clinozoisite coloured typically “Prussian”-blue.

The mineral assemblage suggests prograde metamorphism in these rocks during and after the intrusion. For example the presence of clinozoisite is a hint for prograde metamorphism.

JK – 65 (UD 100) – shale

Distance to the contact: 346 m

The sample is postioned of a depth of 74.32 m below the earth surface (Fig. 5.9). After a first look at the thin section of this rock one can see a large number of different minerals. Because of the dense matrix and structure it is not possible to identify each of them with the microscope. The optical analysis is leading to a mineral assemblage with different pyroxenes, maybe enstatite or

augite next to minerals like sillimanite and epidote. The sillimanite grains and all the different pyroxene grains are very small. The enstatite was identified by the colourless occurrence, the straight extinction and the colour of interference (Orange I).
One likely possibility for the source of the augites and the enstatites are ultramafic magmatic rocks, but more probable are reactions from primary mineralisations to pyroxenes induced by metamorphic, especially temperature-controlled, processes in some cases in the presence and the operation of fluids.
The diopside is normally a mineral of the metamorphic rock. Because of a widespread compositional mixing gap there is the possibility for the co-existence of Mg-rich pyroxenes like the enstatite and a Ca-rich pyroxene like the diopside in one rock (MATTHES & OKRUSCH, 2005). In all one can say that prograde metamorphism, combined with metasomatism has taken place in this rock.

JK – 67 (UD 100) dolomitic xenolithes in Timeball Hill Shale

Distance to contact: 346 m

This specimen is taken out of a dolomitic xenolithe (GAUERT, 1995) in the Timeball Hill Shale (Fig. 5.9). The matrix is dense and "felted". Dark, opaque, little (diameter 0.1 – 2 mm), isotrope blasts are visible. In parts the matrix is transformed to chlorite. Again nearly the complete number of visible mineral grains is developed in small sizes (up to some mm). The small mineral sizes particulary hinder the optical analyses. But it is sure that there is chlorite in the mineral assemblage. Next to chlorite muscovite can be found. Indicated by their typical colour of interference (second order) it is possible to identify augite next to the chlorite. The augites are xenomorph and very small in size.

JK – 68 (UD 75) – silicified - shale

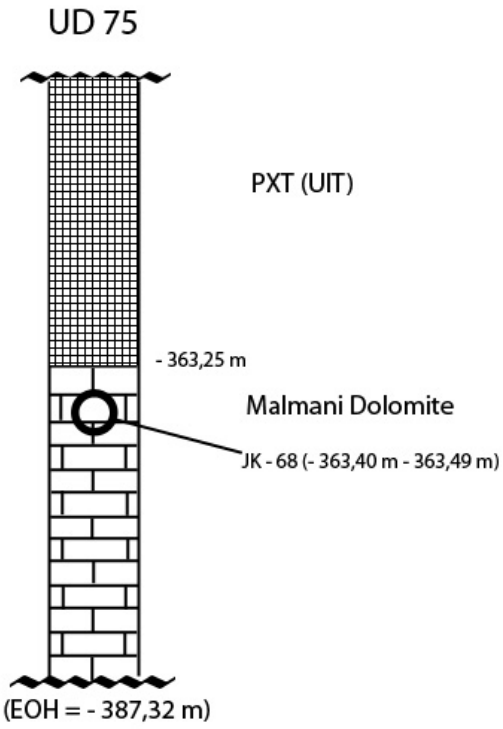

Fig. 5.10: position of the samples JK – 68 in the stratigraphy of UD 75; not to scale

Distance to contact: 10 m

The image on the left hand side shows a part of the stratigraphy of UD – 75.Out of this borehole the sample JK – 68 was gained.

The mineral assemblage shows a high diversity. The thin section is divided by a quartz vein, which also shows contents of plagioclases and diopsides. The diopside is associated with wollastonite (Fig. 5.12) sometimes which also is present in single minerals (Fig. 5.11). There is also clinopyroxene which can not be identified exactly because of the altered shape (Fig. 5.15). Twinning is showed by the plagioclases (Fig. 5.14) like albite (Fig. 5.13).

Except this vein, the structure of the slide is homogeneous and dense. There are no opaque phases in the slide at all. Conspicuous are the phases of prismatic colours. Those minerals were identified as epidote (Fig. 5.16). The epidote and clinozoisite develop pseudomorphoses to plagioclases as so called“filled plagioclases” which are visible in the slide.

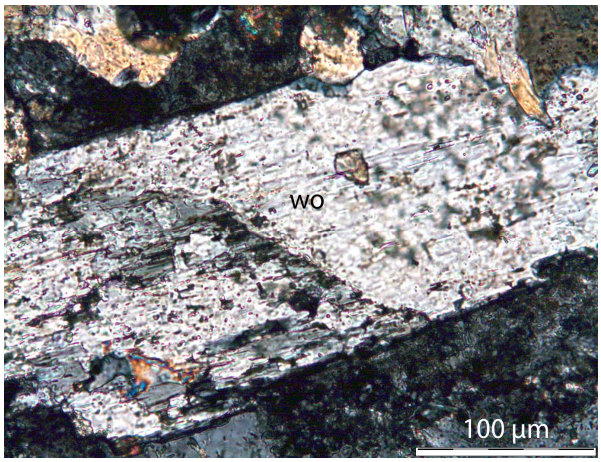

Fig. 5.11: Wollastonite in JK – 68; UD 75; crossed nichols

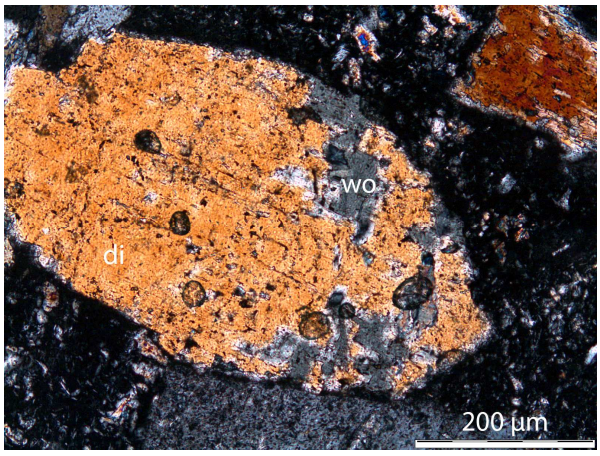

Fig. 5.12: Diopside associated with wollastonite in JK – 68; UD 75; crossed nichols

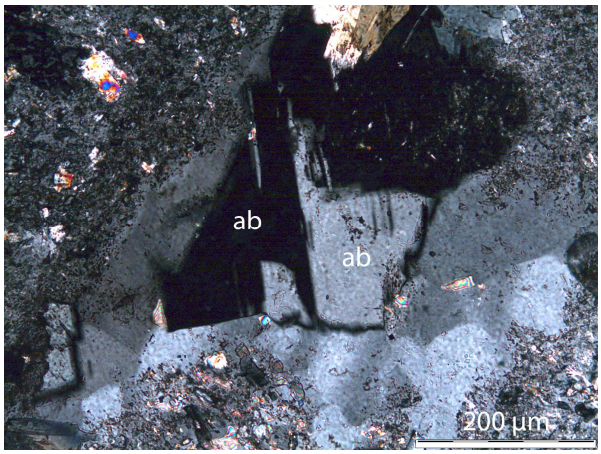

Fig. 5.13: Albite in JK – 68; UD 75; crossed nichols

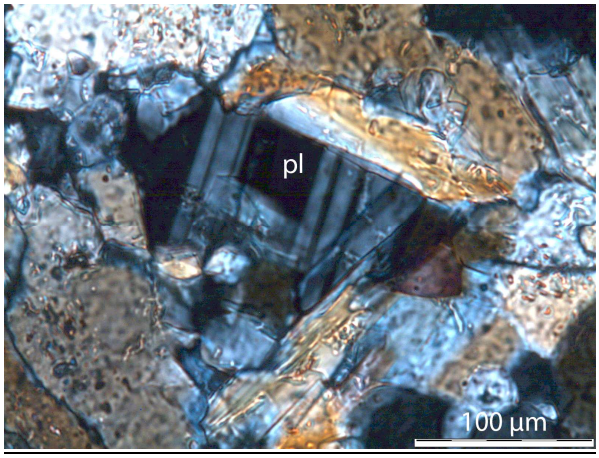

Fig. 5.14: Plagioclase in JK – 68; UD 75; crossed nichols

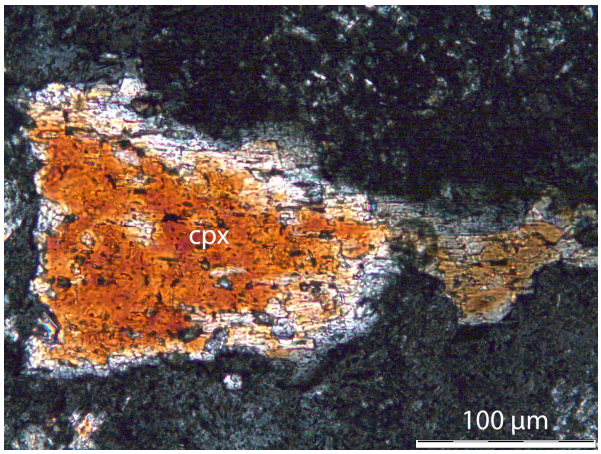

Fig. 5.15: Clinopyroxene in JK – 68; UD 75; crossed nichols

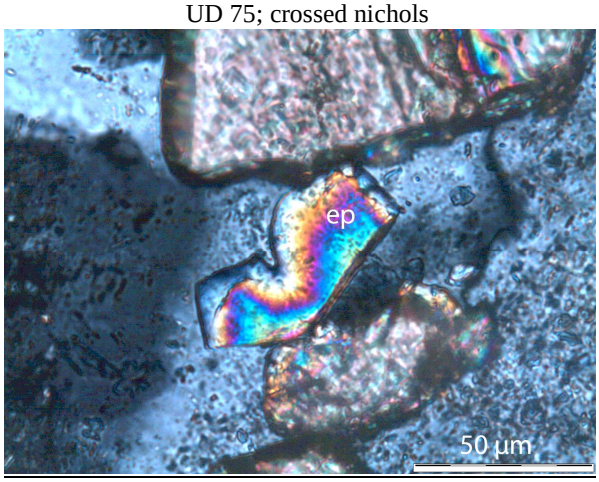

Fig. 5.16: Epidote in JK – 68; UD 75; crossed nichols

JK – 72 (UD 106) shale

Distance to the contact: 197 m

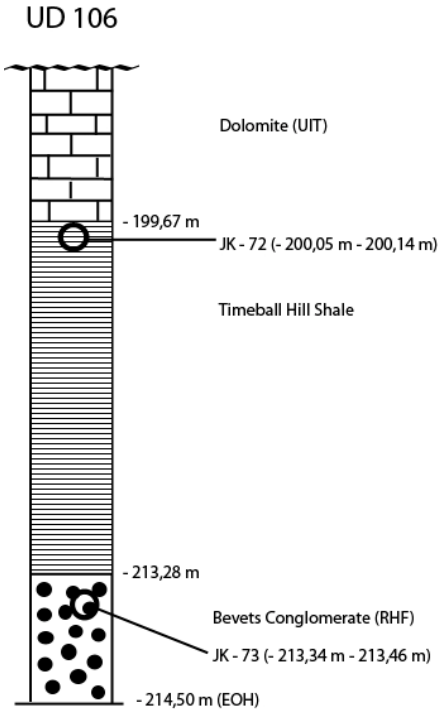

The position of the sample JK – 72 in the stratigraphy of UD – 106 is given in Fig. 5.17. A first look at the thin section exposes the content of goethite showing a cloudy shape. With goethite an opaque mineral is existent. The opaque phase is probably pyrite. This conclusion is supported by observations with reflected light. The main constituent of the matrix is a chlorite. But to make a certain statement concerning the type of the chlorites only based on optical observation is difficult because they are too small in size. Additional to the chlorites diopsides can be found in this slide.

Fig. 5.17: position of the samples JK – 72 and -73
in the stratigraphy of UD 106; not to scale

JK – 74 (UD 88) - shale

Distance to the contact: 190 m

Fig. 5.18 shows the position of the sample JK – 74 in the stratigraphy of the borehole UD 88. The thin section exposes a mineral assemblage with a high complexity. First of all there is one noticeable mineral. It is colourless shows a high relief and owns a nearly kelyphytic rim. The first assumption concerning the mineral was a pyrope. But later investigations using a electron microprobe will lead to the fact that this mineral is almandine.
Those garnets are outstanding in a dense matrix where no minerals can be divided surely because they are too small. But it is a fact that chlorite is again a major component of the matrix. It is coloured green to darkish green.

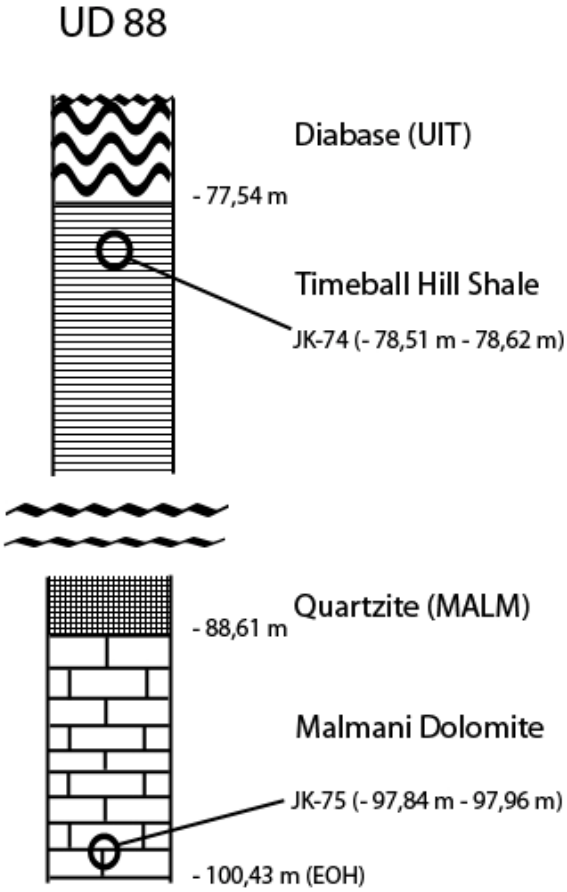

In direct neighbourhood of the almandine hornblende can be found. Fig. 5.19 is showing a almandine. The almandines are an important
Component of the sample JK – 74.

Fig. 5.18: position of the samples JK – 74 and -75 in the stratigraphy of UD 88; not to scale

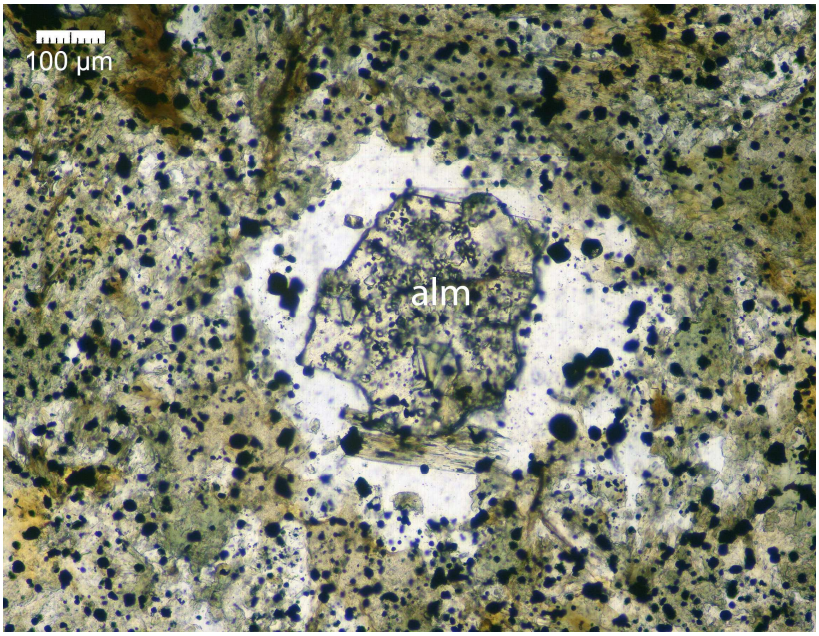

Fig. 5.19.: Almandine in JK -74 (UD 88); transmitted light

JK – 79 (UD 77) – “hornfels-like” shale

Distance to contact: 98 m

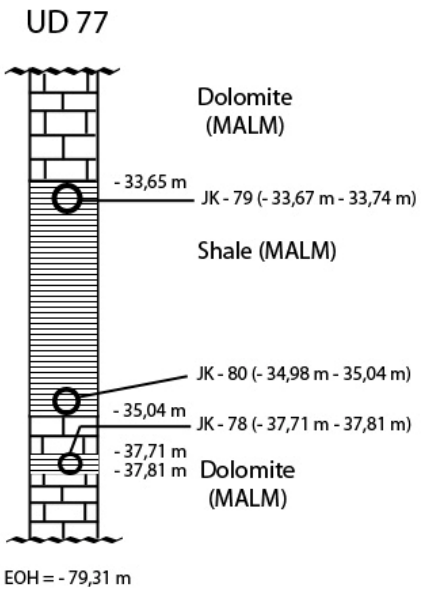

Fig. 5.20: stratigraphical position of JK – 78, JK – 79 & JK – 80 in UD 77; not to scale

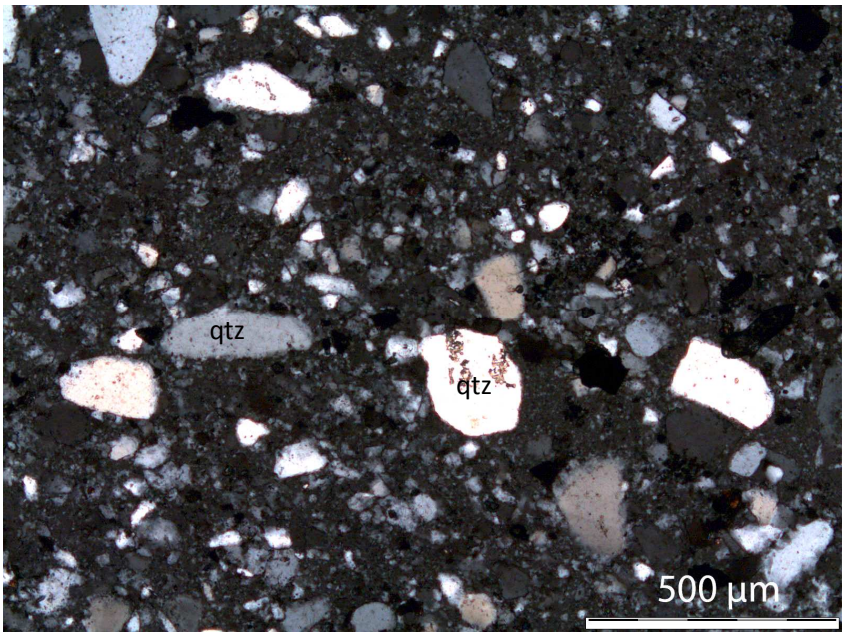

Fig. 5.21: Overview of the structure in JK – 79, crossed nichols

The matrix of JK – 79 is very dense and the grains show a wide spectrum of sizes, typical for a hornfels the size vary from ≤ 5 µm to 300 µm (Fig. 5.21).

The matrix is mainly constituted by quartz. The clasts are surrounded by veins. The veins and the lower part of the thin section is mainly composed by chlorite. The grains which are embedded between the veins are of hyidiomorphe and idiomorphe shape. First of all the grains are quartzes.

The chlorite shows the typical blue to blue grey colour.

Also significant is the high content of mica together with chlorite at the rim of the slide. A sign for prograde metamorphic processes is the generation of epidote which is recognizable in the section.

Opaque phases in the thin section are identified as magnetite.

JK – 80 (UD 77) - shale

Distance to the contact: 98 m

The position of this sample in the stratigraphy is given in Fig. 5.20. It is possible that this section is contaminated by the intrusion which is visible in the matrix.
First of all there are several opaque minerals which can be determined as hematite in ideal shape. In one part of the thin section there is an assemblage of mica and quartz. The quartz is showing a pavement-structure. This is a sign for the influence of pressure while forming this rock (PICHLER & SCHMITT-RIEGRAF, 1993).
With the help of the optical investigations it was possible to identify augites in JK-80 (Fig. 5.22). It is probable, supported by the optical behaviour of the mineral, that those augites are diopsides.

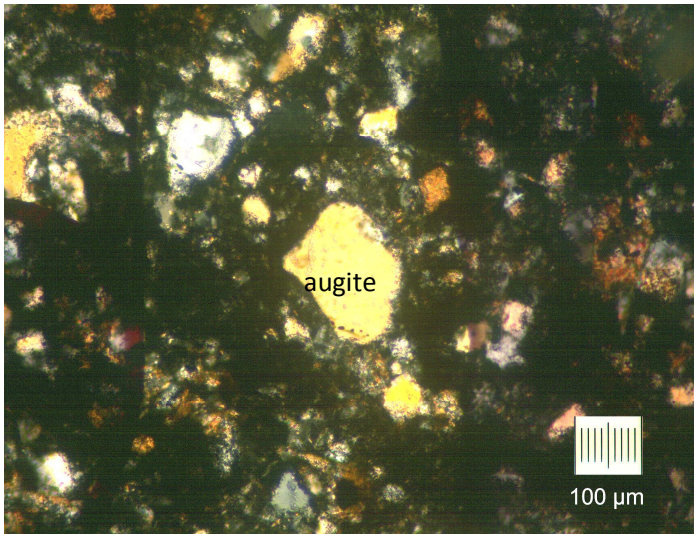

Fig. 5.22: Augite (middle of the picture in JK – 80; crossed nichols

JK – 82 (UD 98) – partly metasomatised shale

Distance to contact: 175 m

The position of the sample in the stratigraphy of UD 98 is given in Fig. 5.51. The section is divided by a vein of pyrite and chalcopyrite. This was identified using reflected light microscopy.

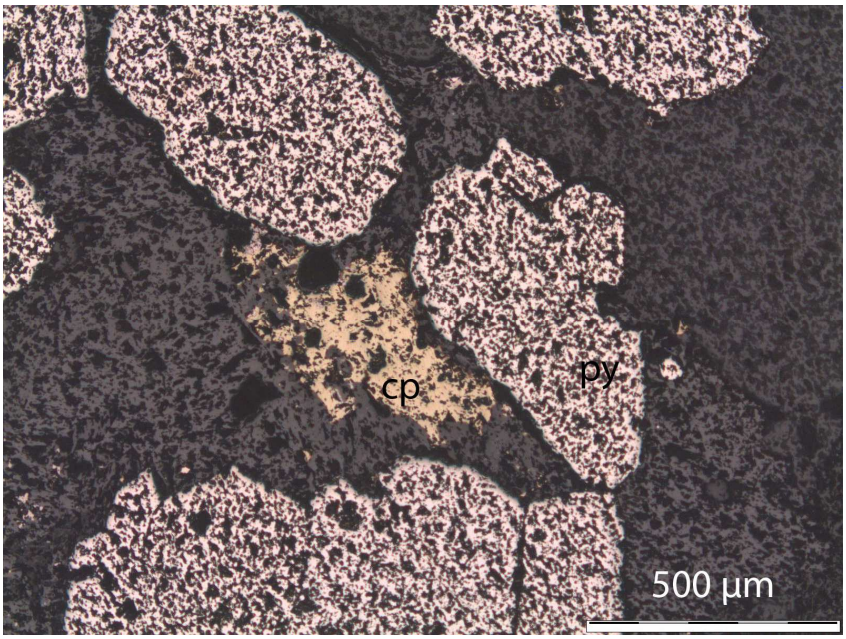

Fig. 5.23: Detail of the chalcopyrite (cp) – pyrite (py) – vein in JK – 82; reflected light

Divided by the vein (Fig 5.23) the section is built up of a dark and a lighter part. The chalcopyrite and the pyrite seem to be a kind of border between two different chemical facies. More explicit one can say that possibly a hydrothermal reaction rim is marked by this vein. The other variant is that the vein is a hint for metasomatic processes.

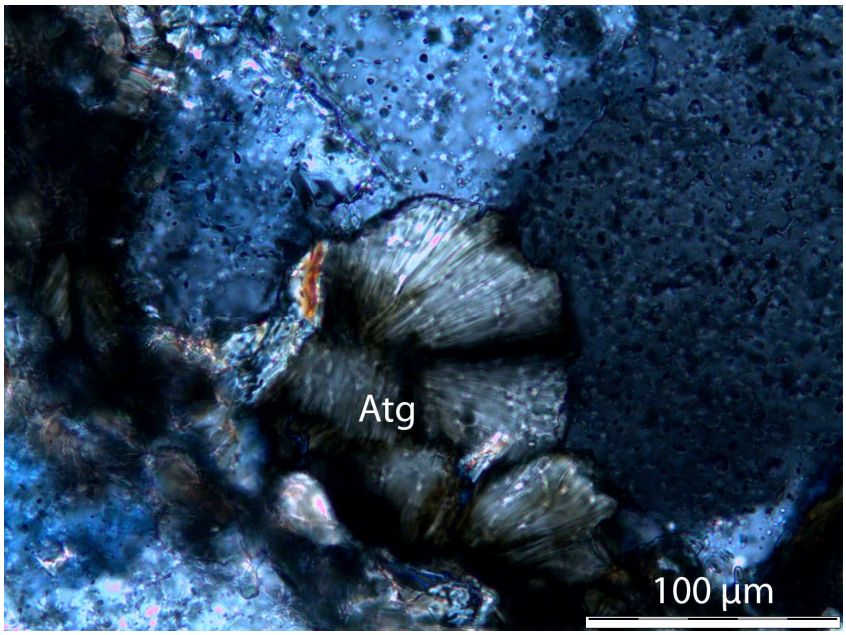

Fig. 5.24: Antigorite in typical fansJK – 82, crossed nichols

The major part of the dark part of the matrix is intersected by opaque veins. Epidote can be found between those veins. Those veins, but in a smaller scale, are also visible in the lighter part of the observed thin section.

Additional to that, there is a rest of a quartzitic vein visible in the opaque part of the sample. The vein is sometimes interrupted.

A third kind of vein in the sytem seems to be made up by antigorite. In some places those veins are opaque but this is caused by overlying extinctions of small crystals of antigorite. In addition very small aggregates of clino- and orthopyroxenens and also augites are existent.
The antigorite was crystallized in typical fans (Fig. 5.24).
The entire rock can be named as “metasomatised shale”.

JK – 87 (UD 109) – serpentinized shale

Distance to the contact: 196 m

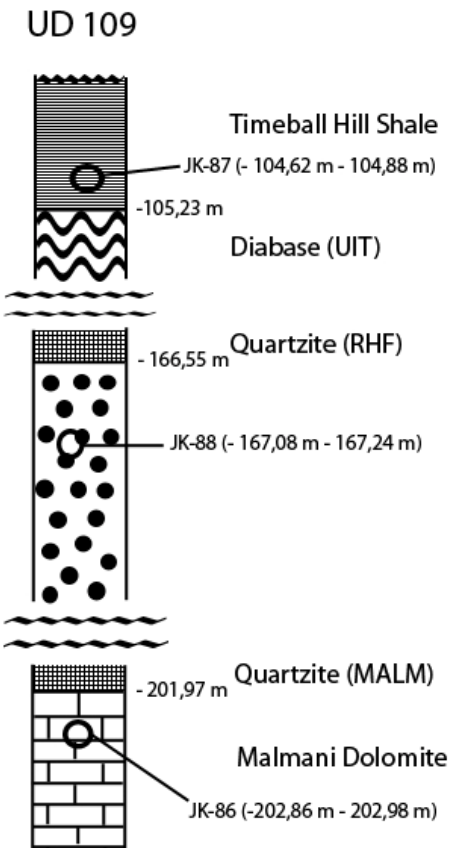

Fig. 5.25: Stratigraphical position of JK -86, JK – 87 and JK – 88 in UD 109; not to scale

On the left hand side the position of the sample JK – 87 is visible (Fig. 5.25). The sample has a matrix composed of quartz, talc in a small content, chlorite and epidote. These grains are equal concerning their small size.
As ore minerals magnetite, chalcopyrite and chromite are constituents in the section. The aggregates of chalcopyrite are distributed in a disperse way. The chromites are of grey to brown colour and slightly transmissive for light.
The bulk of the silicate minerals are chloritized. The chlorites are blue greenish in colour, fibrous or they show a leaf-like shape.
One mineral with light yellow colours of interference was identified as andalusite. Andalusite is a product of temperature dominated metamorphic processes. It was probably developed during prograde metamorphism whereas the chlorites are produced by a retrograde metamorphism.
A special phenomenon is serpentinized olivine (Fig. 5.26). This fact and the occurrence of quartz is a sign for a geological background which is characterised by intense contact-metasomatic conditions.

Residual orthoclase is also a component of the mineral assemblage of JK – 87.

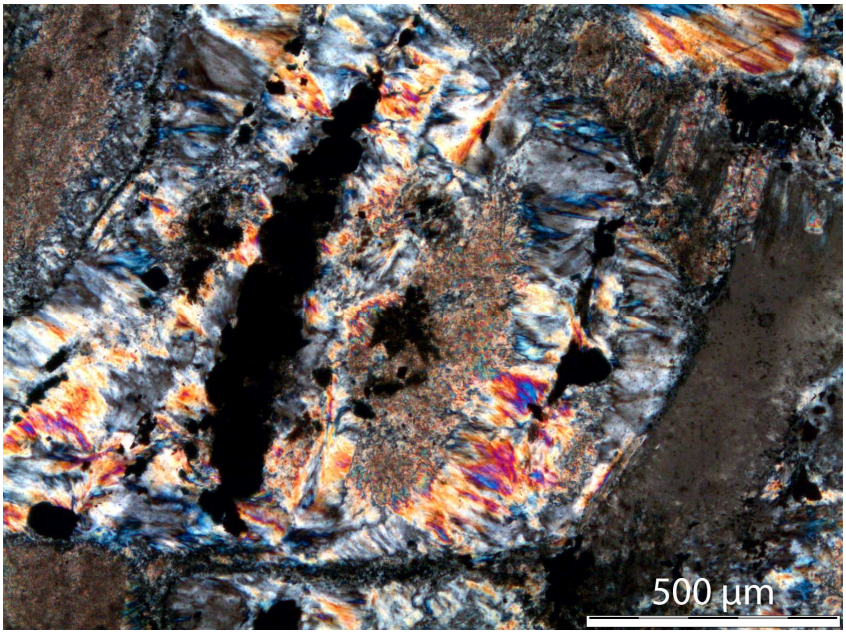

Fig. 5.26: Serpentinized olivine in JK – 87; crossed nichols

5.2 Bevets Conglomerate

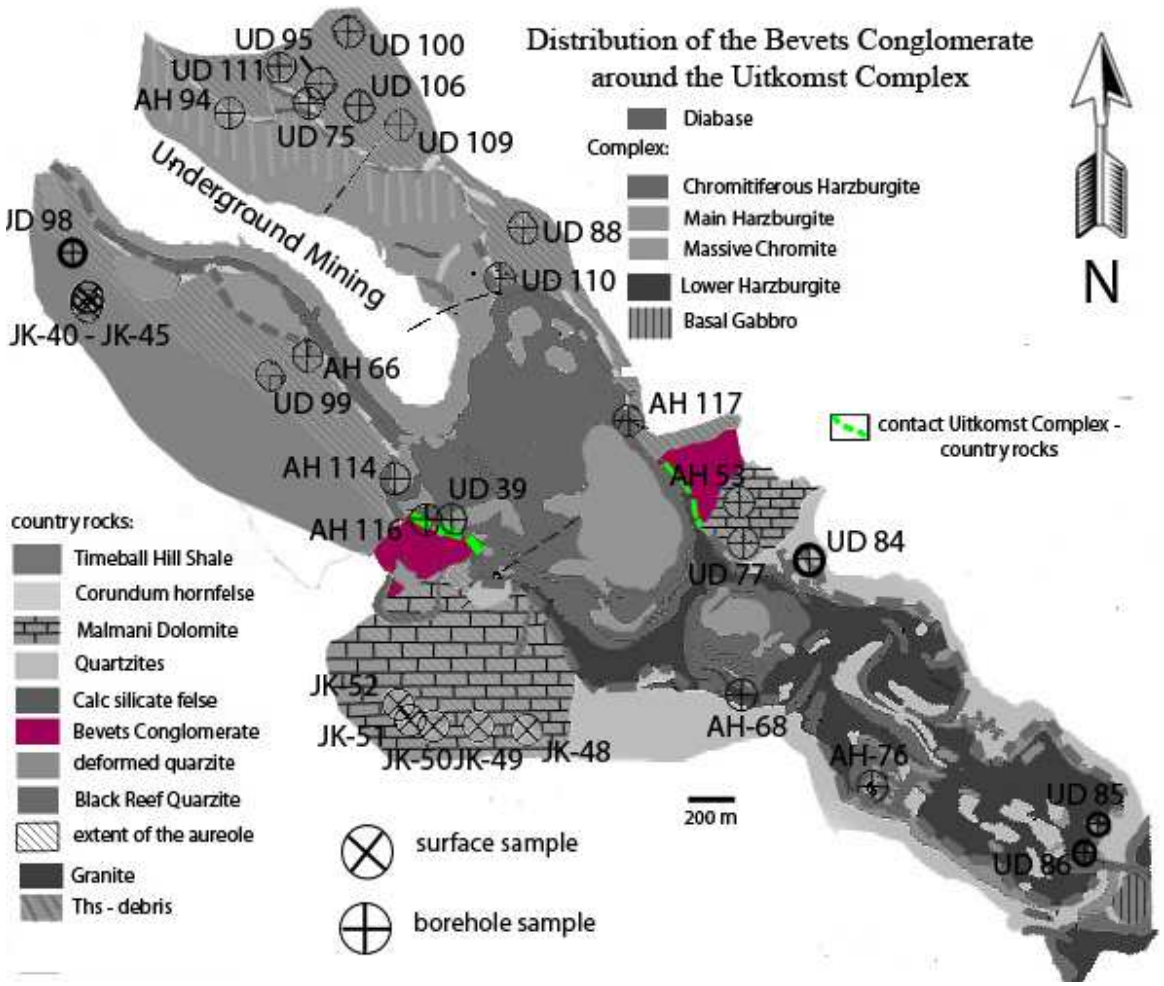

Fig. 5.B: Distribution of the Bevets Conglomerate around the Uitkomst Complex

Figure 5.B shows the distribution of the Bevets Conglomerate around the Uitkomst Complex. In the same fashion as for Timeball Hill Shale and Malmani Dolomite the samples of Bevets Conglomerate are gained from boreholes.

A physicochemical change of the mineral assemblage in a scale of the metamorphic minerals in the shales or Dolomites is not expected. That is the reason for a smaller number of samples.

5.2.1 Bevets Conglomerate – Structures

The Conglomerate shows one type of structure. The name itself explains the structure. The conglomerate is very easy to recognize. In the thin section the most outstanding and most common structure is built uo by pavement-like quartz grains. Apart from this phenomenon veins are conspicuous which are mostly built up by chlorite or epidote.
Also angular shaped cherts fragments are visible.

5.2.2 Macroscopic description

The conglomerate exhibits quartz grains or clast fragments of sizes from 0.5 cm to several cm. The matrix is siliceous in major parts. Additionally some samples show chlorite or other minerals of low-metamorphic grades in the matrix. Fig. 5.30 shows a specimen of the Bevets Conglomerate from the north of the Complex while Fig. 5.31 shows a piece of Bevets Conglomerate from the south of the Complex.

Fig. 5.27: Bevets Conglomerate; north of the Complex; Fig. 5.28: Bevets Conglomerate; south of the Complex

The fragments of chert (X) in the left picture are of a strip-like shape, but also grains which are more of angular shape are common. The best outcrop of Bevets Conglomerate is situated in the south of the Complex and is a large river located in a chasm which is produced by the Gaeddespruit River. Fig. 5.28 displays the clasts in the southern conglomerate are more spheric than their correspondents in the north of the Complex. The lower grade of sphericity is an indication of shorter routes of transport in the former fluvial regime.

5.2.3 Bevets Conglomerate borehole samples

JK – 69 (UD 100) - conglomerate

Distance to the contact: 346 m

The sample position in the stratigraphy can be seen in Fig. 5.9. An insight in the mineralogy of JK – 69 is given in Fig. 5.29.

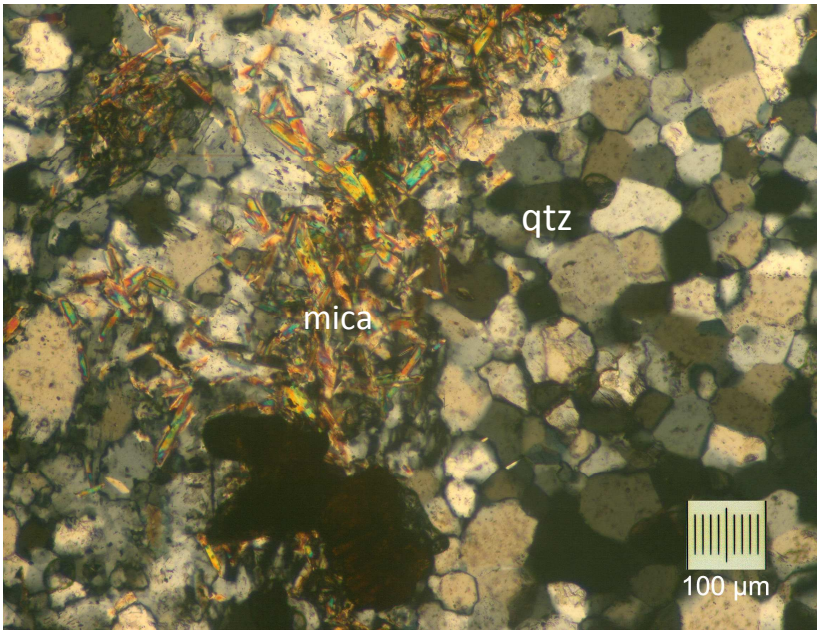

Fig. 5.29: Overview over the mineral assemblage in JK – 69, crossed nichols

In this slide the pavement-structure of the quartz grains is noticeable. This can be interpreted as a sign for the exposure to pressure (PICHLER & SCHMITT-RIEGRAF, 1993). A further hint of an exposure to pressure is the undulatory extinction of the quartz grains (PICHLER & SCHMITT-RIEGRAF, 1993).

A conspicuous mineral is the interstitial mica. Not visible in the picture above, but existent in JK – 69, are chlorites also concentrated in veins between the grains of quartz.

Also a content of this sample are minerals with a clear and well developed cleavage and a strip-like shape. The mineral is muscovite because tremolite has a bright yellow colour of interference.

The structure of this slide shows the described quartz-pavement crossed by veins which are constituted by mica and chlorites indicating a fluid overprint. The minerals of the actinolite series occur with hypidiomorphic shape between quartz minerals. But those mineralisations are always connected with the veins.

JK – 70 (UD 95) - conglomerate

Distance to the contact: 108 m

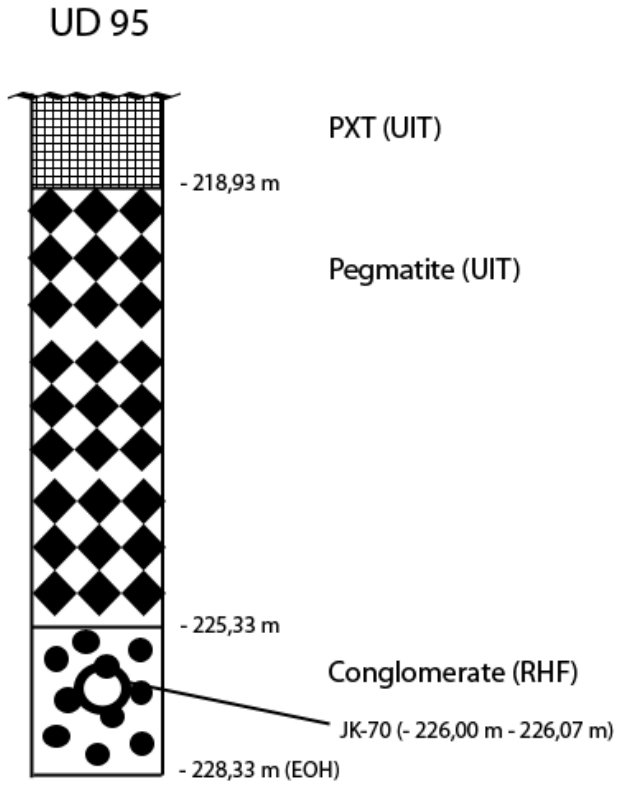

Fig. 5.30: Position of JK – 70

in the stratigraphy of UD 95; not to scale

With a view to the sequence of the stratigraphy and the position of the sample in it (Fig. 5.30) the assumption is probable that the slide shows significant metamorphic structures and minerals. But against all a priori assumptions the section shows almost no metamorphic mineral assemblage or metamorphic structures.

The thin section is built up by pavement-like quartz up to 90 % at all. So it shows again that the rock was exposed to pressure (PICHLER & SCHMITT-RIEGRAF, 1993). A little amount of chlorite is recognized in this thin section. But they are too small to assume the chemical composition.

JK – 73 (UD 106) - conglomerate

Distance to the contact: 197 m

The position in the stratigraphy of UD 106 is given in Fig. 5.17. The rock shows a polygonal structure interspersed with mineralisations of mica. Beside the transparent mica, which is probably muscovite, a kind of oxybiotite can be observed. The rare oxybiotite is of leaf-like shape, shows the typical colours of interference and the common light-brown colour. At all the rock has no trace of metamorphic processes.

JK – 84 (UD 99) – ep – atg - conglomerate

Distance to contact: 255 m

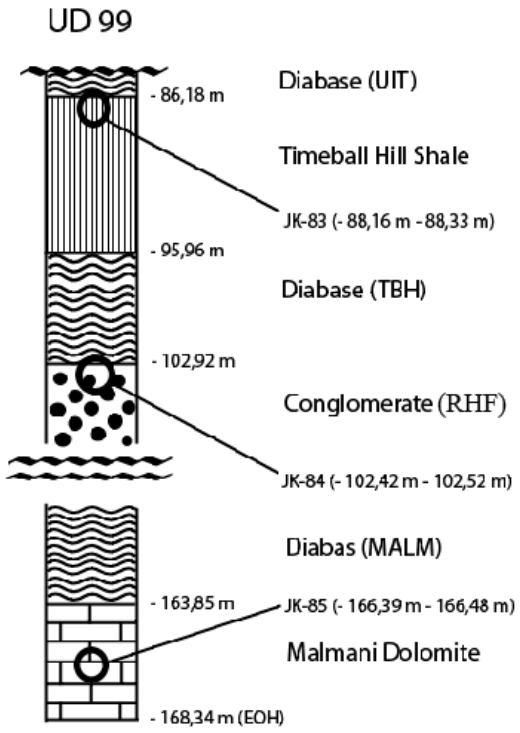

Fig. 5.31: Position of JK – 83, JK – 84 and JK – 85 in the stratigraphy of UD 99; not to scale

In Fig. 5.31 one can see the lithological and stratigraphical classification of JK – 84. The main constituent of this section is quartz.

In the silicatic matrix epidote is visible. Unusual for this type of rock there is clinopyroxene and orthopyroxene observed. Furthermore, there are antigorite and diopside. The antigorite is accumulated as a product of the alteration of orthopyroxene. It is in strip-like shape and not crystallized in a fan like in other samples. The diopside was identified based on the observation of the angle of extinction with almost 40° and its typical colours of interference. But the Ca-pyroxenes are hard to see.

The epidote is developed xenomorph and interstitially.

Under reflected light opaque phases respectively ore minerals like chalcopyrite are contained in low amounts.

Figures 5.32 and 5.33 show a part of the mineral assemblage. In Fig. 5.32 the antigorite is visible but, as said before, in a strip-like shape and not mineralized as a fan. Fig. 5.33 shows interstitial epidote surrounded by quartz grains.

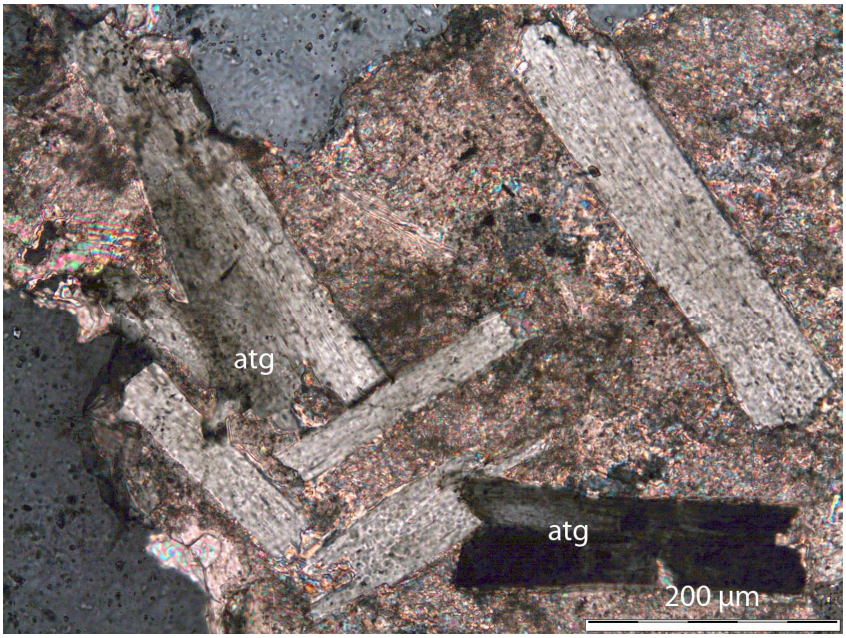

Fig. 5.32: Strip-like Antigorite in JK -84; crossed nichols

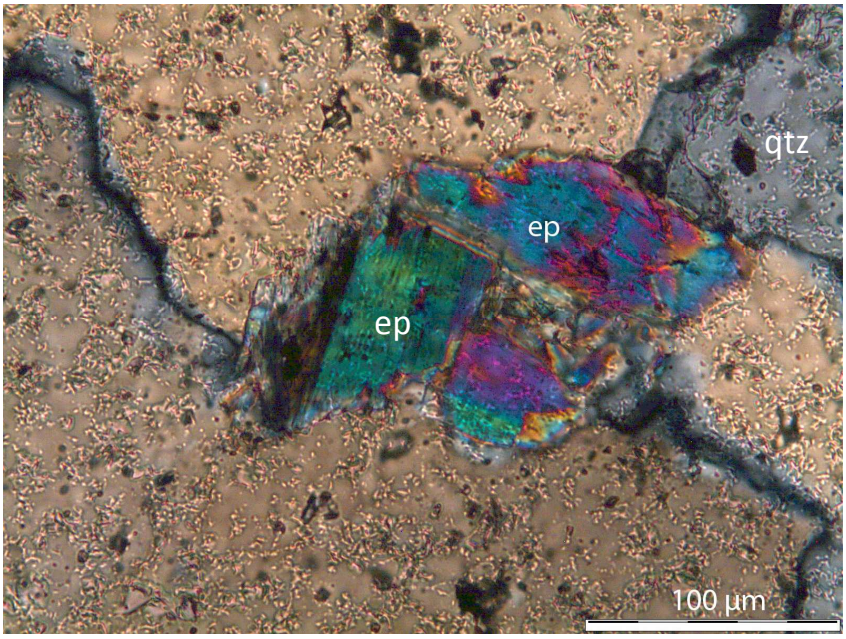

Fig. 5.33: Interstitial epidote in JK – 84; crossed nichols

JK – 88 (UD 109) - conglomerate

Distance to the contact: 196 m

The place of the sample in the stratigraphy is to be seen in Fig. 5.25. This section is relatively equable. The major part is made up by quartz. There are no metamorphic structures or minerals visible. The sample seems to be completely unaffected by metamorphism.

5.3 Malmani Dolomite

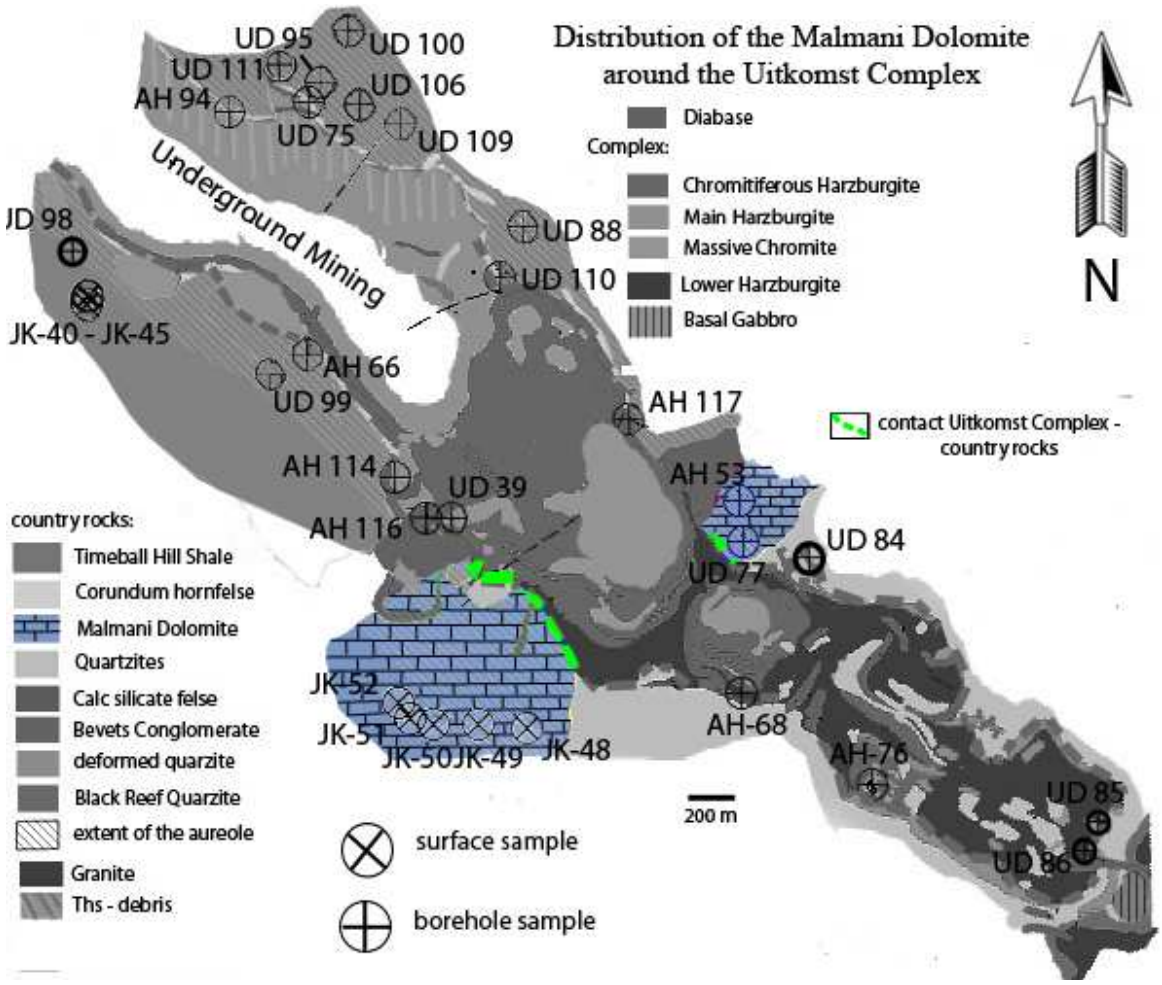

Fig. 5.C: Distribution of the Malmani Dolomite around the Uitkomst Complex

The map in Fig. 5.C displays the distribution of the Malmani Dolomite around the Uitkomst Complex.

The dolomite of the Malmani subgroup is of eminent importance for the understanding of the metamorphic processes in the thermal aureole of the Uitkomst Complex.

The chert-rich dolomite shows a wide spectrum of different minerals. As a whole, the mineralogy of the dolomite is manifold. The investigation of the thermal aureole combined with the classification of different mineral zones, respectively several isogrades is very practicable in the Malmani dolomite because of the physical properties of this unit which are prone to change through metamorphic and metasomatic processes. First of all the dolomite is characterized by a well developed system of fissures which are ideal pathways for volatiles, both fluids and gases, which were generated and distributed during the emplacement and the linked metamorphism. Additional to that the rock-specific properties concerning the heat conductivity are important.

Also in this section there will be samples from the named and shown boreholes which were investigated.

Surface grab samples, in the south of the Complex, are also investigated but are restricted to a small number. The major part of the samples was gained from boreholes. Following the macroscopic and the microscopic appearance of the Dolomite should be described.

5.3.1 Macroscopic description

The Malmani Dolomite, underlying the Bevets Conglomerate, is located in the north and the south of the Complex. Especially in the south of the Complex outcrops of Dolomite can be found. The rocks of the northern part occur as loose rocks.

The dolomite is easy to identify by its “elephant-skin”. This is a special surface texture of these rocks and it shows scratches in a certain pattern that reminds the observer of an “elephant skin”. Fig. 5.34 shows an example of that structure for better understanding.

Fig. 5.34: Surface structure of the Malmani Dolomite – weathering cracks ("elephant-skin"); south of the Complex

Several samples show, also macroscopically, talc and tremolite. Tremolite is developed in radial aggregates and the talc overlays the surface of the samples. Especially the tremolite is common in the dolomites.

Talc is a metamorphic product of Mg-Si-minerals such as amphiboles or pyroxenes. Beside the corundum in the Timeball Hill Shale it is the best macroscopic sign for contact metamorphic processes in the country rocks of the Uitkomst Complex.

5.3.2 Microscopic description

5.3.2.1 Microscopic description – surface samples

JK – 48 – garnet bearing dolomite

Position:	S 25 44.976 E 30 37.123	Altitude:	1312 m	Distance to contact:	320 m

The section is very unclear at first glance. Nearly all of the minerals are dark green and marginal transparent.

But quartz is visible in finely spread aggregates all over the matrix. The quartz occurs kryptocrystalline. Already with optical methods it is possible to see garnets in the thin section. But to identify the type and the composition of the garnet other methods have to be used. The results of those investigations are discussed later in this thesis.
Muscovite is also visible and is identified by the low relief, the well developed cleavage and the pink violet colours of interference.

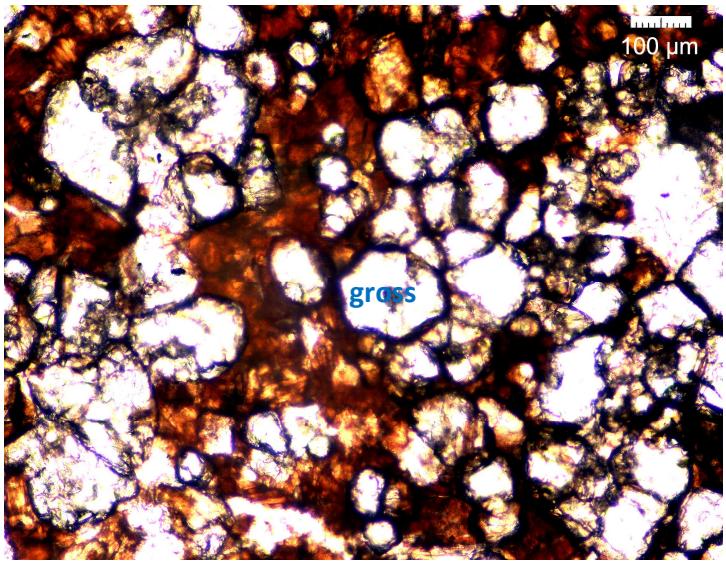

Fig. 5.35: Detail of JK – 48 with grossular (gross); transmitted light

In the left hand picture (Fig. 5.35) one can see a detail of JK – 48 in transmitted light. The brighter grains were determined as grossular. They partly show ideal shape (e.g. the grain in the centre of the image). Probably the dark cloud-like mineralisations between the garnets are a mixture of different mica-minerals. But it is not possible to determine the composition of this "mineral-mix" just trough the microscope.

JK – 49 – wo – px - dolomite

Position:	S 25 44.962	Altitude:	1339 m	Distance to contact:	500 m
	E 30 36.991				

The structure of this rock is typically metamorphic with a high number of strip-like aggregates of several metamorphic minerals. The centre of the slide shows a brown colour but the disperse distributed mineral which causes the colouration cannot be identified with the microscope. It can be assumed that a constituent of this mass is biotite. Nevertheless, a large and significant mineral assemblage is existent. First of all there are wollastonites which were determined by the low

birefringence (Grey I) and the straight extinction in the longitudinal section of the wollastonites. In the same assemblage tremolite is included.

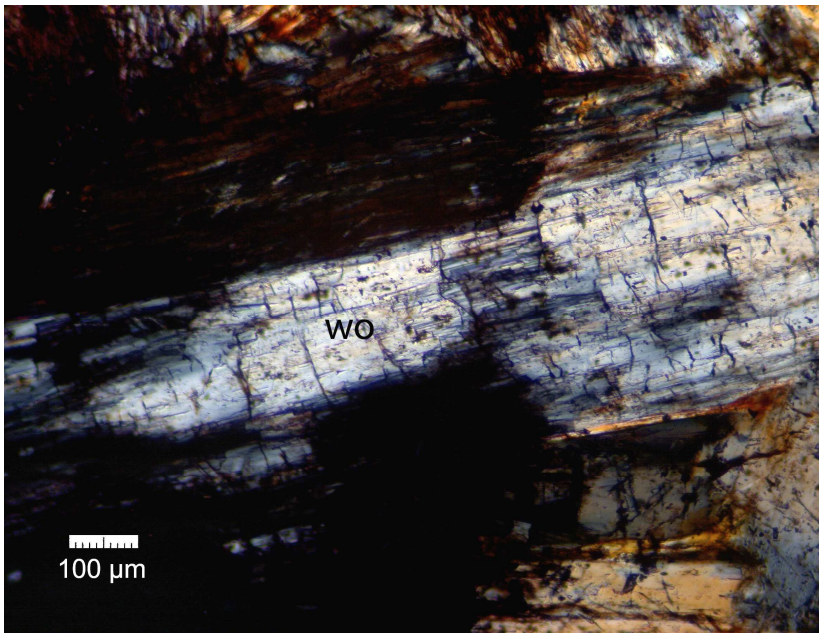

Fig. 5.36: Wollastonite (wo) in JK – 49; crossed nichols

The Fig. 5.36 shows a wollastonite in its longitudinal section. The mineral is altered and broken. This fact can be interpreted as a sign for chemical and stress for the rock and the mineral assemblage. One possibility is recrystallisation or a conversion induced by metamorphic processes. Surely it can be clarified by the comparison with other samples and the classification in the complete system of the metamorphism induced by the emplacement of the Uitkomst Complex. The occurrence of such different minerals, concerning especially the circumstances of their accumulation is a hint for different metamorphic processes. It is imaginable that pro- and retrograde metamorphism influenced the minerals alternately combined with a last retrograde metamorphism.

The wollastonite is also observed in direct neighbourhood with tremolites and other amphiboles.

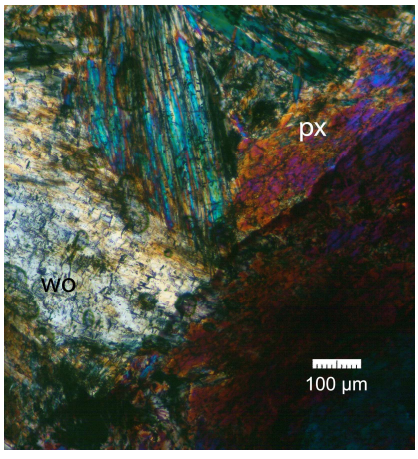

Fig. 5.37: Wollastonite next to pyroxene in JK – 49; crossed nichols

But next to the wollastonite there are also other types of pyroxenes, amongst others enstatite. This might be an important hint for the metamorphic processes and conditions and intergranular chemical reactions.

Fig. 5.37 shows the variety of pyroxenes in JK -49. The brighter lightgrey grain on the left hand side of the image is a wollastonite (wo). On the right hand side of this thin section, signed with px, is a pyroxene of unknown composition. There are different types of pyroxenes investigated. More explicit the enstatite, but other pyroxenes can't be excluded. That is why

the pyroxene in the picture is signed with “px” for representing the whole spectrum of pyroxenes because all of them can be found in the neighbourhood of wollastonite. The colour of birefringence is partly not typical for pyroxenes. But other optical methods lead to the assumption that the identification as pyroxene is right and in cases the section is to mighty in thickness.

JK – 50 – calcitic dolomite

Position:	S 25 44.965 E 30 36.874	Altitude:	1351 m	Distance to contact:	715 m

The major part of the matrix of JK – 50 is built up by calcite. There seem to be mica at the rim of the slides but the occurrence of the typical colours of interference is due to the properties of the slide in some places. More exactly the cuneiform rims of the section cause resultant colour shift. Tremolite is a component of the mineral assemblage and shows the known strip-like shape and is colourless in transmitted light.

JK – 52 - calcitic dolomite

Position:	S 25 44.918	Altitude:	1336 m	Distance to contact:	590 m
	E 30 36.783				

The main minerals which set up the matrix are quartz and calcite. The sizes of the minerals are homogenous. The slide is crossed by a vein which is made up by quartz combined with calcite. The calcite is significant. This mineral shows traces of exposure to pressure.

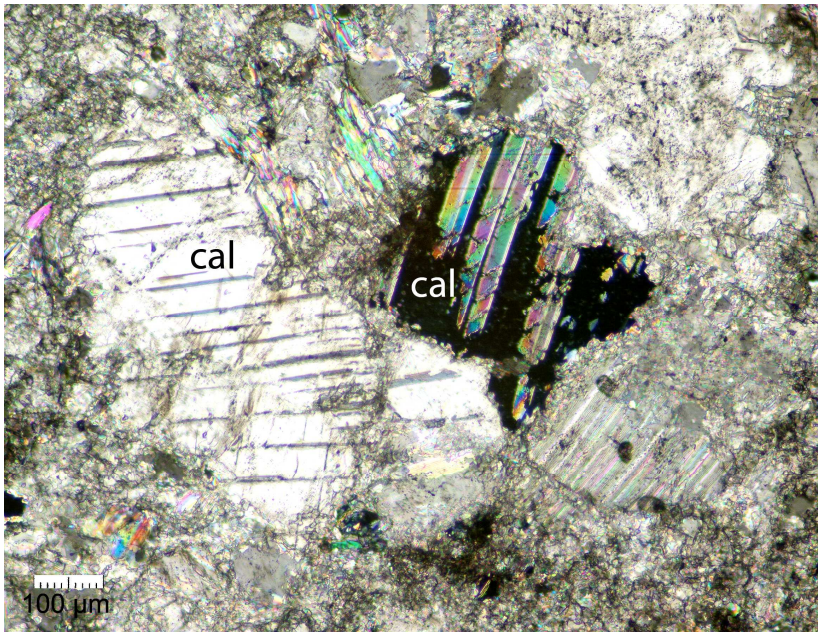

Fig. 5.38: Calcite (cal) with typical signs of compressive stress; JK – 52; crossed nichols

Fig. 5.38 shows calcite observed with transmitted light and with crossed Nichols. The varicoloured stripes which are visible in the calcite minerals are a sign for compressive stress (PICHLER & SCHMITT – RIEGRAF, 1993). The left calcite is in another position and the typical rhomboedrical pattern can be divined.

In addition to the mentioned minerals also tremolite and plagioclase can be determined in little contents.

5.3.3 Microscopic description – borehole samples

JK – 63 (UD 111) - dolomite

Distance to contact: 50 m

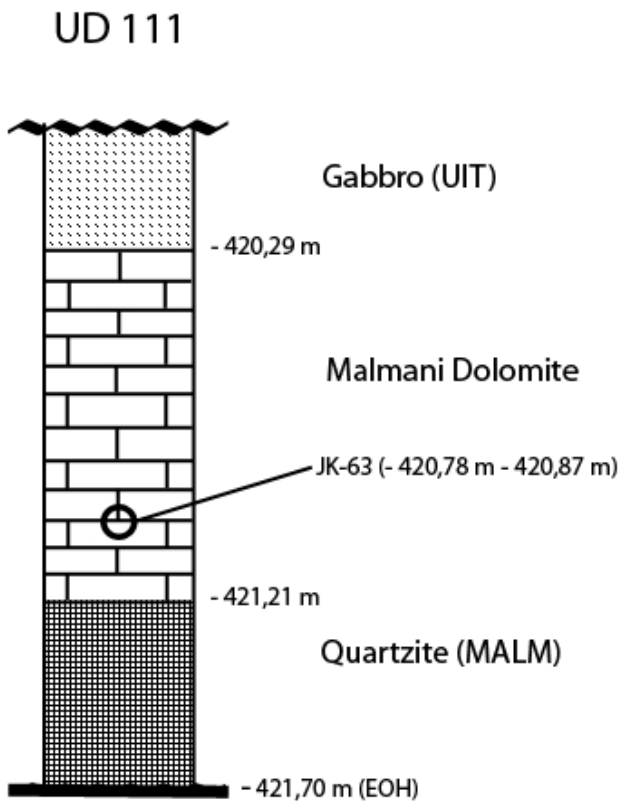

Fig. 5.39: Position of the sample JK – 63 in the stratigraphy of UD 111; not to scale

The detail of the stratigraphy which is given on the left hand (Fig. 5.39) shows the position of the sample in the lithological sequence of UD 111.

Unfortunately, the thin section is not significantly caused by a bad quality of the slide.

It can be assumed that the sample shows the following minerals: quartz, diopside and actinolite (Fig. 5.40).

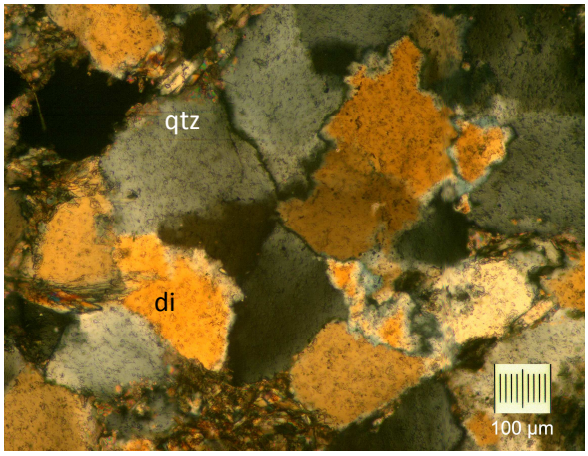

Fig. 5.40: Overview of the mineral assemblage of JK – 63; quartz (qtz) & diopside (di) crossed nichols

As viewable at Figure 5.43 the rock is build up by minerals with nearly the same size. The grains size is 250 – 300 µm in average. The structure can be described as granoblastic.

JK – 71 (UD 110) – calc – silicate fels

Distance to contact: 30 m

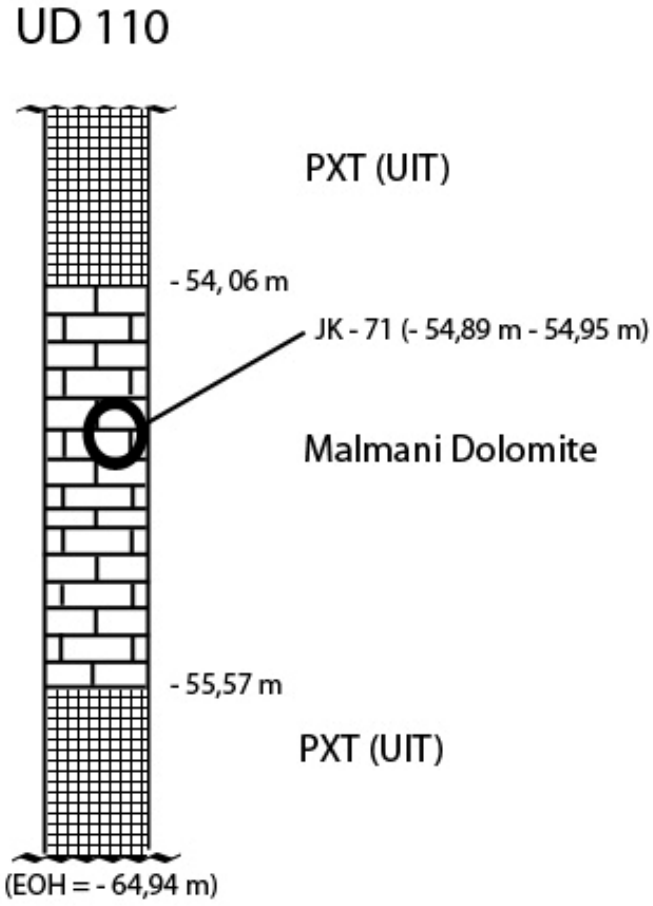

Fig. 5.41: Position of JK – 71 in a sequence of the stratigraphy of UD 110; not to scale

On the left hand side the Fig. 5.41 shows a sequence of the stratigraphy of borehole UD 110. Concordantly it shows the position of the sample in the lithology of borehole UD 110.

First of all, talc and epidote are conspicuous as components of the matrix. In reflected light one can see pyrite and chalcopyrite as ore minerals, which occur as opaque phases in transmitted light. Additionally magnetite builds up a major part of the opaque phases.

Altered minerals are common in this tin section. On the one hand there is a kind of "epidosation" visible, also the protolithes which can't be determined.

But it is probably that a part of the proto-lithes are plagioclases (Fig. 5.42).

The talc is generated by the transformation of antigorite to talc induced by the supply of SiO_2. At last it should be mentioned that the epidote varies in grain size and shape. It is developed xenomorph to hypidiomorph all over the thin section. The following image (Fig. 5.42) shows the epidotes in the matrix of JK – 71.

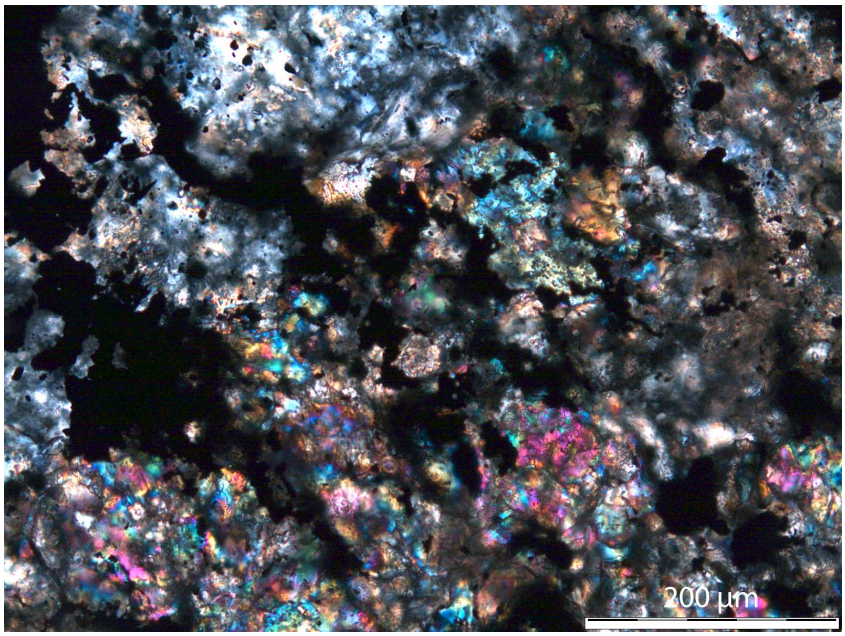

Fig. 5.42: Epidotes (varicoloured minerals) in the matrix of JK – 71; UD 110

JK – 75 (UD 88) – Calc – silicate fels

Distance to contact: 190 m

The sample is derived from the borehole UD 88, north of the Complex. The stratigraphy is given in Fig. 5.18. The rock includes a manifold mineral assemblage.

First of all, there is chlorite and muscovite which build up a great part of this slide. The chlorites show an undulatory extinction and a fan-like shape. Contained amphiboles are colourless and of strip-like shape and because of that and their behaviour under crossed nichols are determined as tremolite (Fig. 5.44).

Next to tremolites there are minerals which show a high relief, an oblique extinction of ca. 38° and orange colours of interference (Orange I). That supports the assumption that those minerals are diopsides.

Also calcites can be observed and are recognizeable because of their prominent rhomboedric cleavage structure (Fig. 5.43).

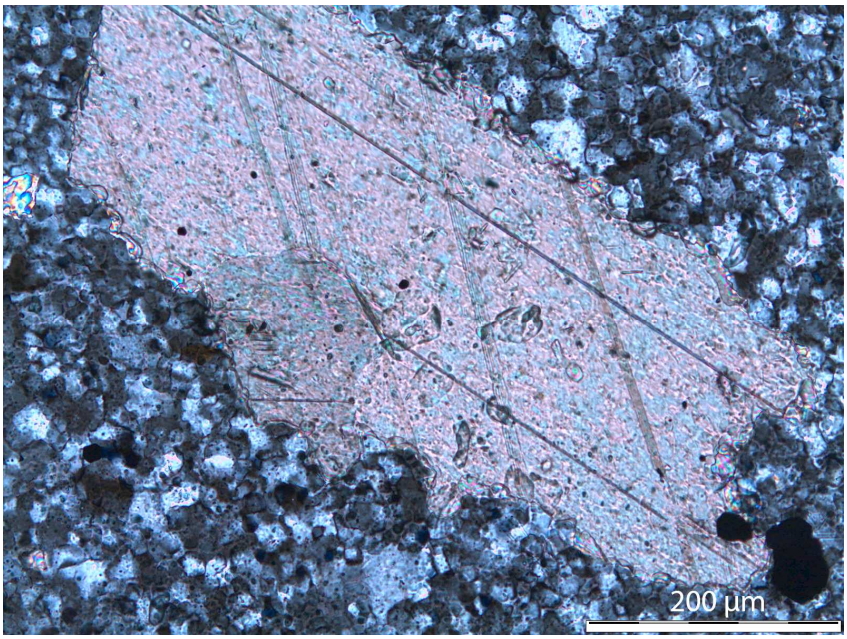

Fig. 5.43: Calcite with the typical rhomboedric cleavage structure in JK – 75; UD 88

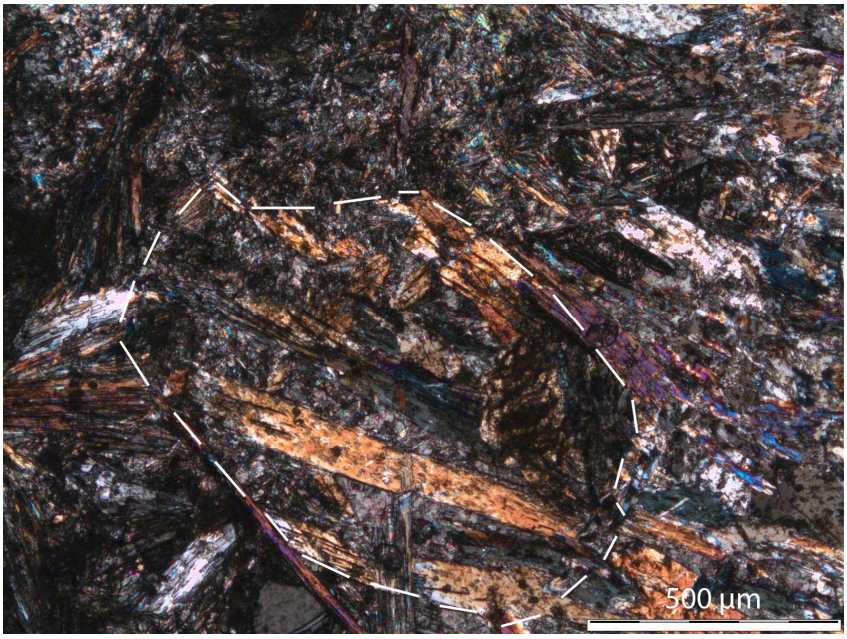

Fig. 5.44: Pseudomorphism of tremolite; JK – 75; crossed nichols

JK – 76 (UD 39) - dolomite

Distance to contact: 20 m

On the left-hand side, in Fig. 5.45, a sequence of the stratigraphy of UD 39 is given. UD 39 is located in the south of the Complex.

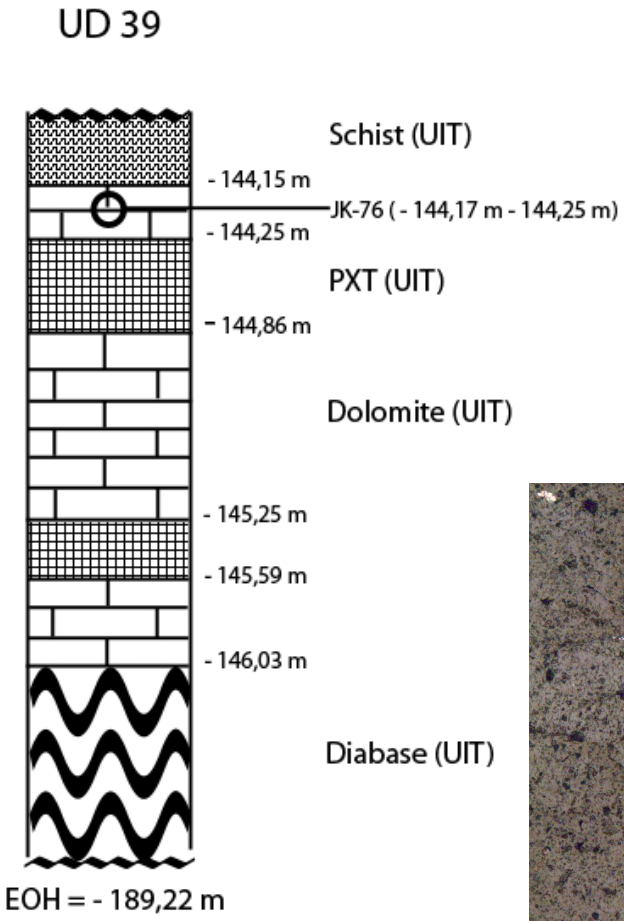

Fig. 5.45: Position of JK – 76 in a sequence of the stratigraphy of UD 39; not to scale

The thin section shows a matrix which is built up mainly by calcite, again easy to identify by its typical rhomboedric cleavage structure. Next to epidote as developed grains there is epidote in veins. This mineral is associated with actinolithe in some places. In reflected light one can see pyrite and chalcopyrite.

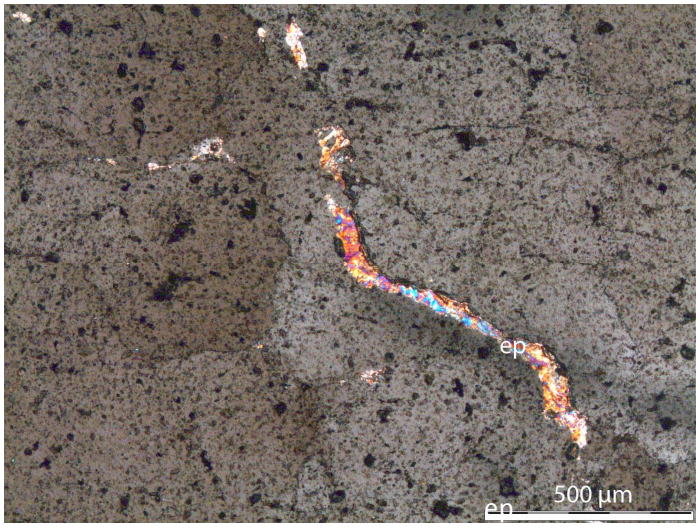

Fig. 5.46: Epidote in a crack in JK – 76; UD 39

JK – 77 (UD 72) - dolomite

Distance to contact: 0 m

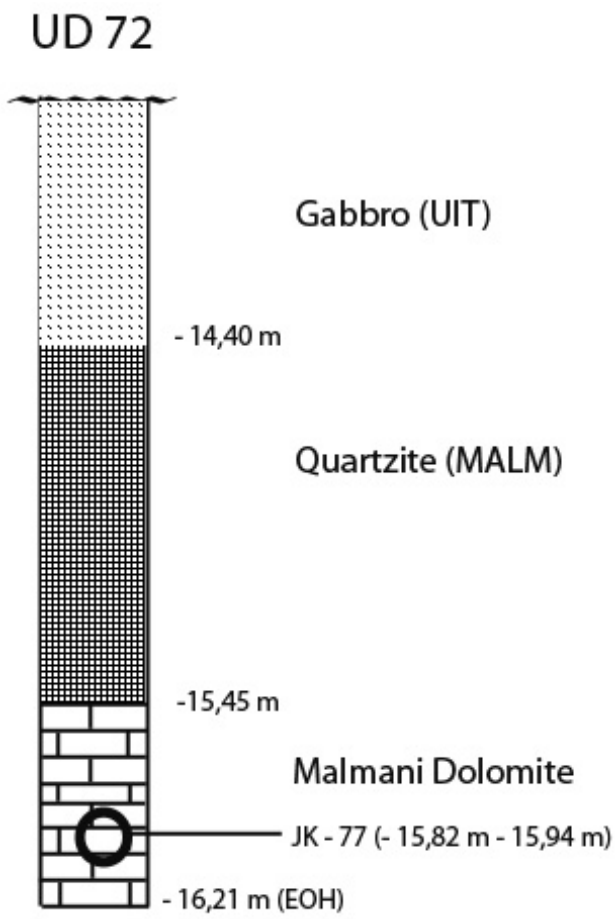

Fig. 5.47: Position of JK – 77 in a sequence of the stratigraphy of UD 72; not to scale

The image on the left hand side (Fig. 5.47) shows the position of the sample JK – 77 in a sequence of the stratigraphy of UD 77. The slide shows a matrix which is homegene concerning the sizes of the grains. In contrast to the expectation there are no specific metamorph minerals visible in this section. But there are veins which contain plagioclase and quartz.

Wedge-shaped minerals are conspicuous within the thin section. These minerals are identified as titanite in other slides. So, especially after the observation of the mineral ahape, it is to assume that this mineral is also titanite.

Veins of pyrite and chalcopyrite are crossing the samples in some places.

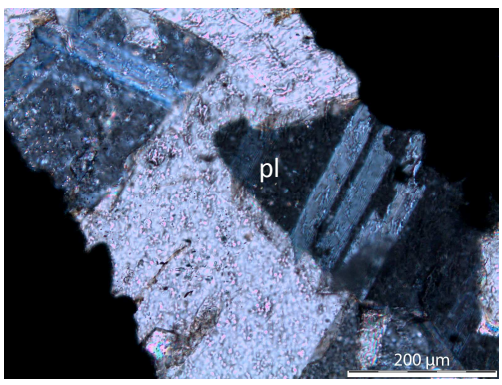

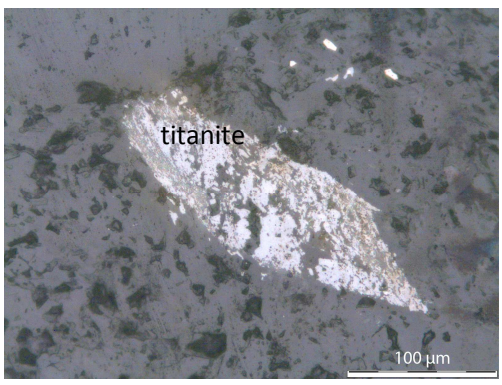

Left: Fig. 5.48: Plagioclase in quartz matrix JK – 77; crossed nichols

Right: Fig. 5.49: Titanite in JK -77; crossed nichols

JK – 78 (UD 77) – calcitic quartzite

Distance to contact: 98 m

The position of this sample is given in the Fig. 5.20. The minerals in the slide are of nearly the same size. The mineral assemblage is very many-sided. But it has to be recognized that the thin section varies concerning its mineral assemblage from the results of the XRD-analyzes which are presented later in this thesis. This phenomenon can be explained with the heterogeneous composition of the rock and the different position of the sample material in the stratigraphical sequence.

The matrix consists of quartz with content up to 90 %. In this slide also small, red minerals occur. After a more explicit observation of their optical properties the minerals can be determined as hematite. Partially the hematite shows signs of a transformation to goethite. The quartz minerals show extinction at certain angles. This is a hint for the former exposure of the rock to pressure. Also the existence of mica is a sign for a metamorphism of medium grade.

Remarkable in this thin section are the small minerals (≤ 100 µm) of diopside (Fig. 5.50). Some grains of the diopside show traces of transformation to tremolites. The amphiboles are existent in veins at the whole sample but they are also common in nests around the aggregates of diopside.

Additionally there are the clinopyroxene and augite as components of the mineral assemblage visible.

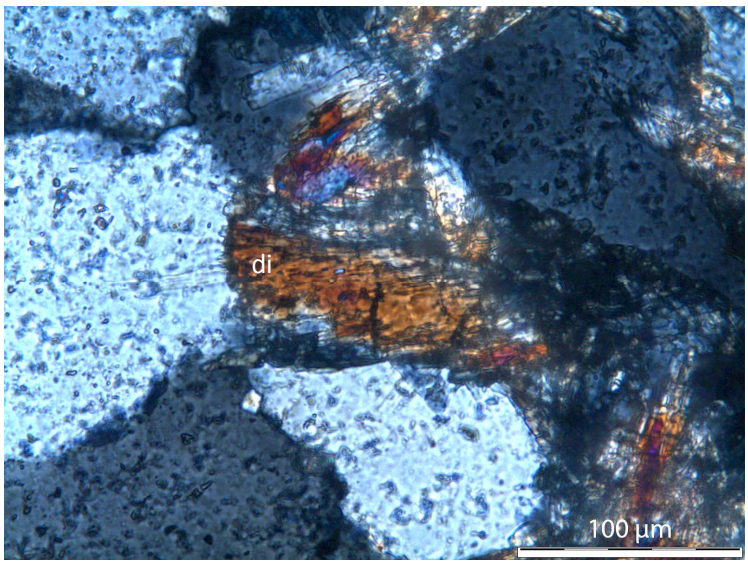

Fig. 5.50: Diopside in JK – 78; UD 77

JK – 81 (UD 98) - dolomite

Distance to contact: 175 m

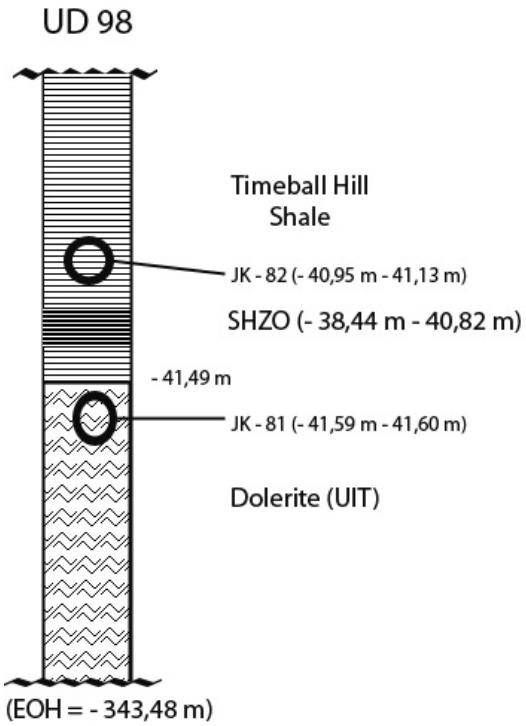

Fig. 5.51: Position of JK – 81 in a sequence of the stratigraphy of UD 98; not to scale

On the left hand side (Fig. 5.51) the position of the sample JK – 81 in a sequence of the stratigraphy of UD 98 is given.

There are no metamorphic minerals obvious. But the calcite, which is building up the matrix, shows a different extinction and different colours of interference in the same grain at a certain position of the sample carrier. This is a sign for metamorphic effect on this sample (PICHLER & SCHMITT-RIEGRAF 1993). Beside the calcite is just quartz visible.

JK – 85 (UD 99) – diopside – tremolite fels

Distance to contact: 255 m

The origin of the sample out of the stratigraphy of UD 99 can be seen in Fig. 5.31. At first view it is obvious that nearly the whole of the thin section is built up by amphiboles. The educts are pyroxenes in the majority of cases. After a closer look one can say that the major part of amphiboles can be determined as “tschermaktic hornblendes”. The minerals are a part of the solid-solution of the tschermakite.

Another hint for the influence of fluids during metamorphic and metasomatic processes is the existence of fluid inclusions in these hornblendes. They trace the fissures in the amphiboles (Fig. 5.52).

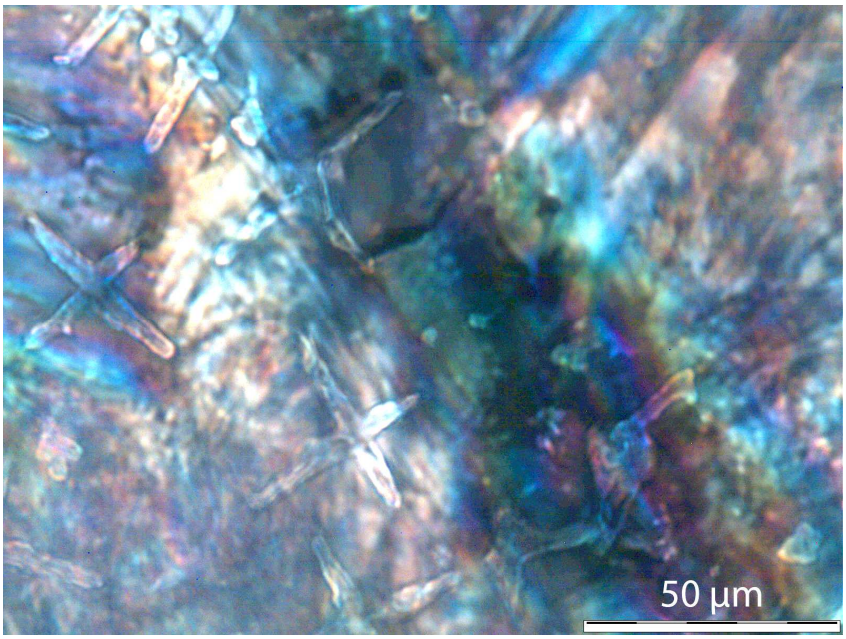

Fig. 5.52: Fluid inclusions in JK – 85; UD 99

But the compound of amphibole solid solution is not only including minerals of the tschermakite solid solution system but also tremolite, actinolite and green hornblende. The tremolite is embedded in altered calcite (Fig. 5.53).

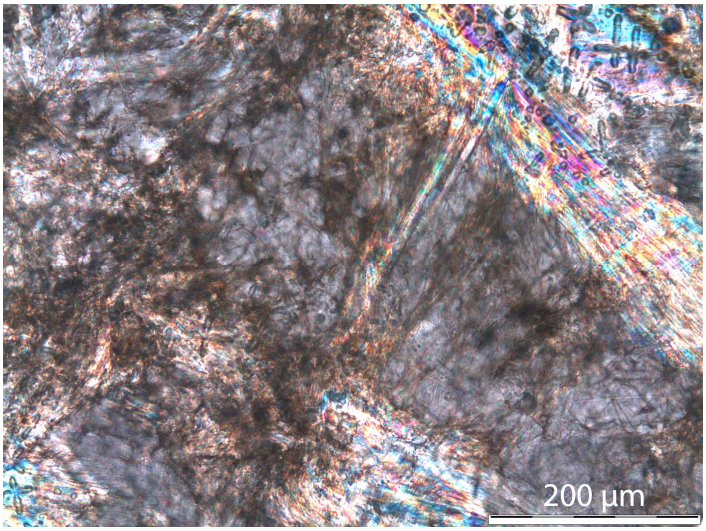

Fig. 5.53: Tremolite (varicoloured) in calcite; JK – 85; UD 99; crossed nichols; not to scale

The transformation of pyroxenes to different amphiboles in such a scale is an evidence for metamorphic and metasomatic processes. A better characterization is possible to get by the observation of the associated occurrence of epidote and clinozoisites. These minerals are in parts pseudomorphoses of plagioclase. Those minerals show the lamellae which are typical of plagioclases and the variocoloured colours of interference which are typical of epidote. The former plagioclases are so-called “filled plagioclases” (PICHLER & SCHMITT-RIEGRAF, 1993). They are generated by saussuritization, which means the decrease of the anorthite-component during retrograde metamorphic processes.

The adjoining image shows the filled plagioclases in JK – 85 with the resulting variocoloured appearance.

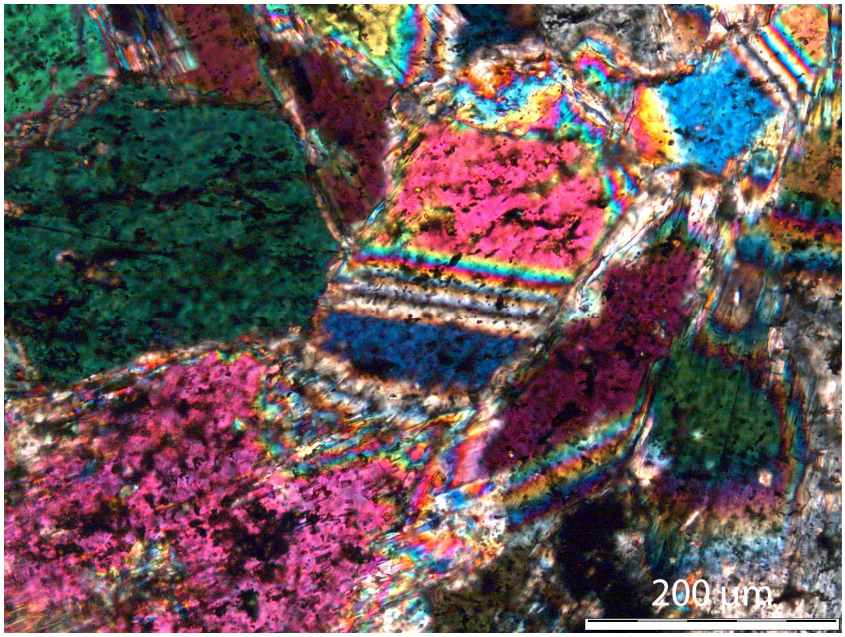

Fig. 5.54: Filled plagioclases in JK – 85; crossed nichols; UD 99; not to scale

JK – 89 (AH 117) – tremolite fels

The sample derived directly from the contact zone. Figure 5.55 shows the position of the sample in the stratigraphy of AH 117. The dolomite shows a compact matrix of very small (several µm) grains. The majority of the thin section is made up by tremolites.

The second most abundant mineral which is a content of this piece of sample is plagioclase. The plagioclases are partly transformed to epidote (Fig. 5.57). The calcite which is the main constituent of the matrix is hard to prove but the result is confirmed with XRD-analyzes.

Next to the transformation to epidote the plagioclase fades to tremolite (Fig. 5.56). Minerals like diopside or wollastonite are no constituents of the slide.

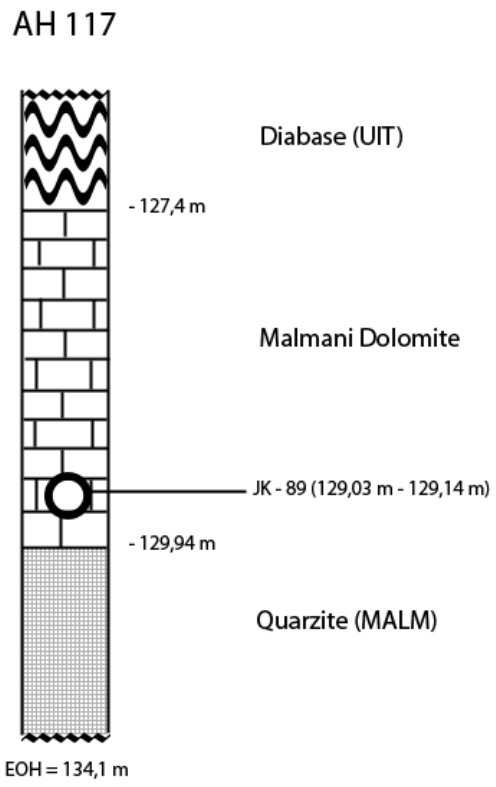

Fig. 5.55: Position of the sample in a sequence of stratigraphy in JK – 89; AH 117; not to scale

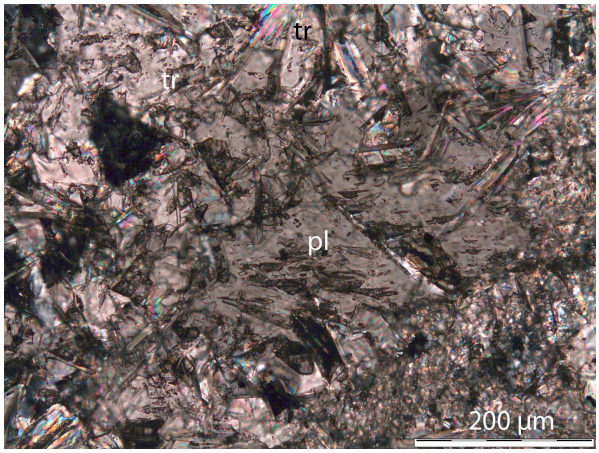

Fig. 5.56: Plagioclase, associated with tremolite; UD 99

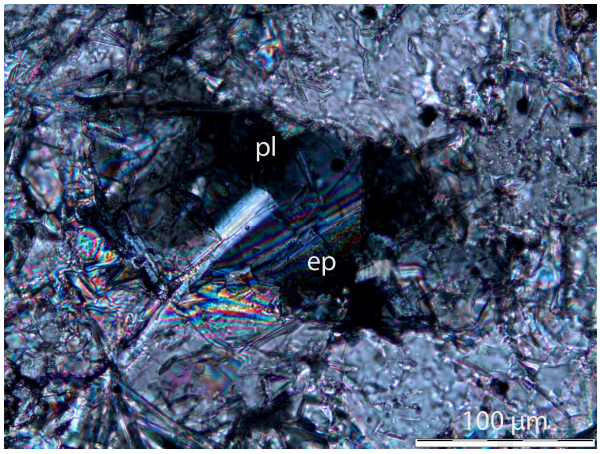

Fig. 5.57: Plagioclase with epidote (variocoloured); JK – 89; UD 99; crossed nichols

JK – 90 (AH 114) - chloritic dolomite

Distance to contact: 0 m

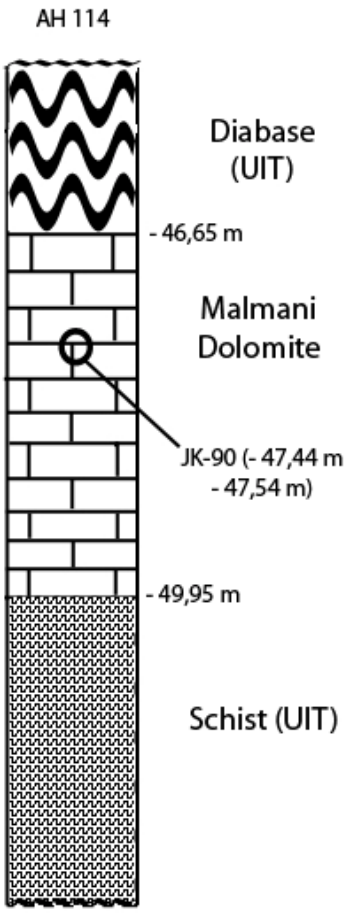

Fig. 5.58: Position of JK – 90 in a sequence of the stratigraphy of AH 117; not to scale

The image to the left of the text (Fig. 5.58) shows a sequence of the stratigraphy of AH 114. The borehole is located in the north-western area of the Complex and is drilled directly at the contact of the Complex with the country rocks. This fact makes a high metamorph mineral assemblage assumable.

But if one takes a look at the thin sections chlorites are flamboyant. After a closer look the chlorites can be identified as Fe-Mg-chlorites. Partly there is muscovite. There are no amphiboles and augites detectable.

The matrix is often crossed by plagioclases. The plagioclases are associated with epidotes again and some aggregates show twinning (Fig. 5.59).

In the slide pyrites and chalcopyrites can be determined as opaque phases. It is conspicuous that the majority of the opaque phases are detectable in the neighbourhood of the muscovites.

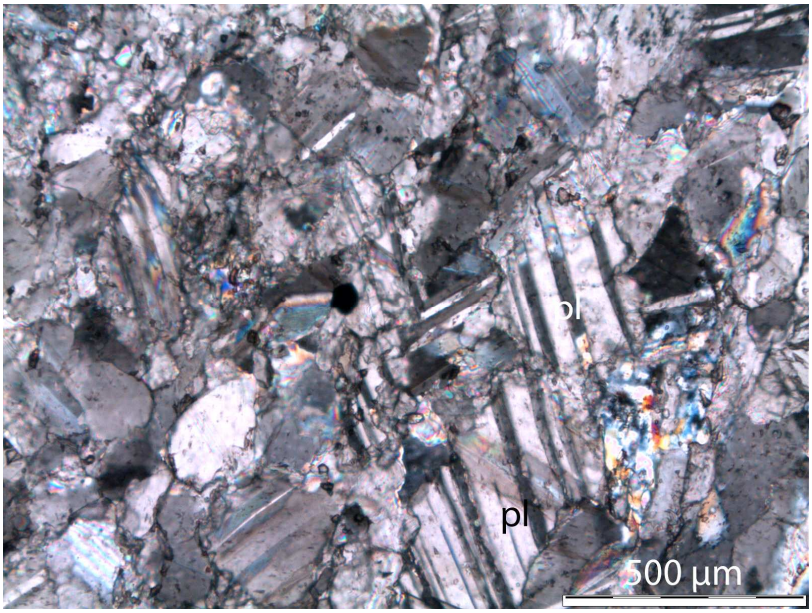

Fig. 5.59: Plagioclase (pl) twins in JK – 90; AH 114; crossed nichols

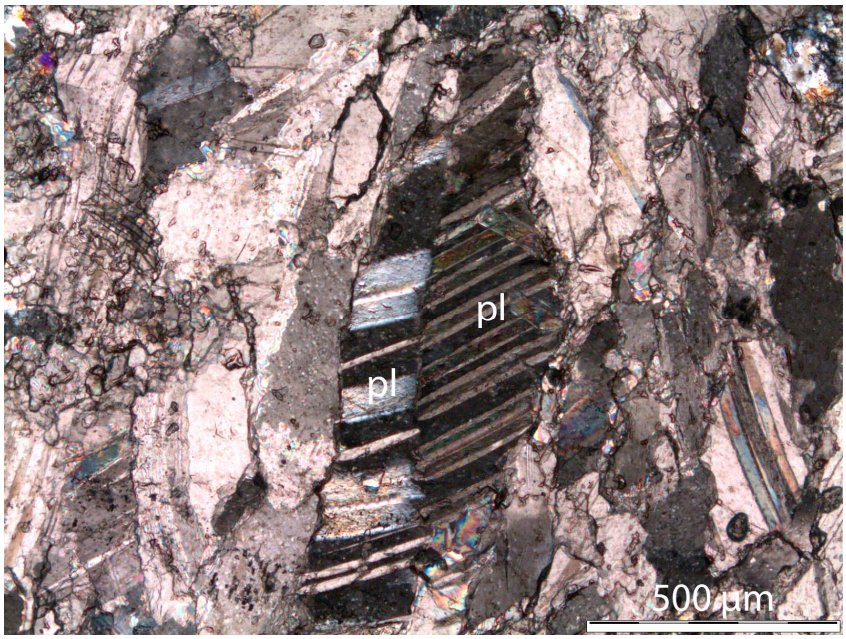

Fig. 5.60: Plagioclases (pl) in JK – 90; AH 117

The left hand picture (Fig. 5.60) shows plagioclase with the typical lamination which represents a twinning within the grains. The lower picture (Fig. 5.61) shows pyrite as one of two opaque phases in the slide. It is notably that the pyrite is developed in veins (Fig. 5.61).

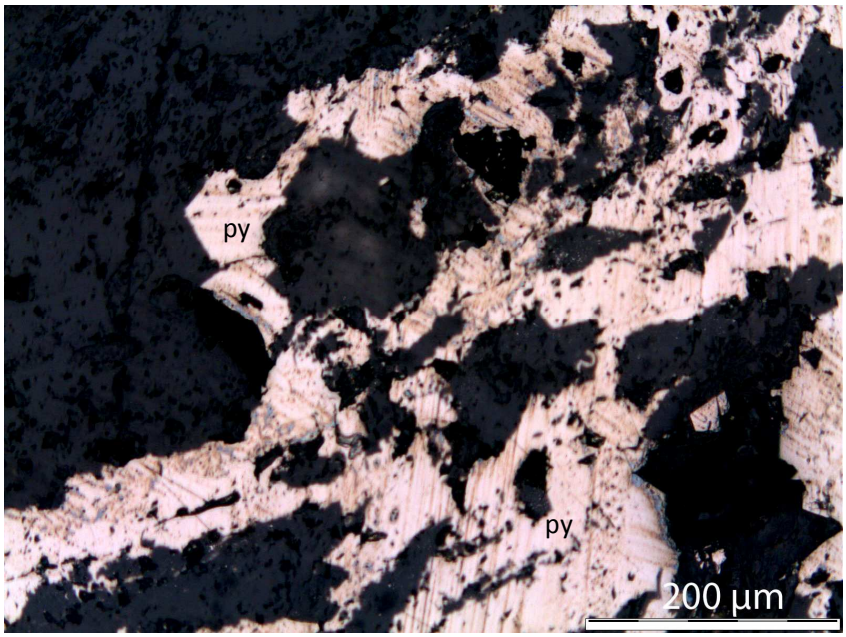

Fig. 5.61: Pyrite vein in JK – 90; AH 117; reflected light

JK – 91 (AH 94) – dolomitic clasts

Distance to contact: 4 m

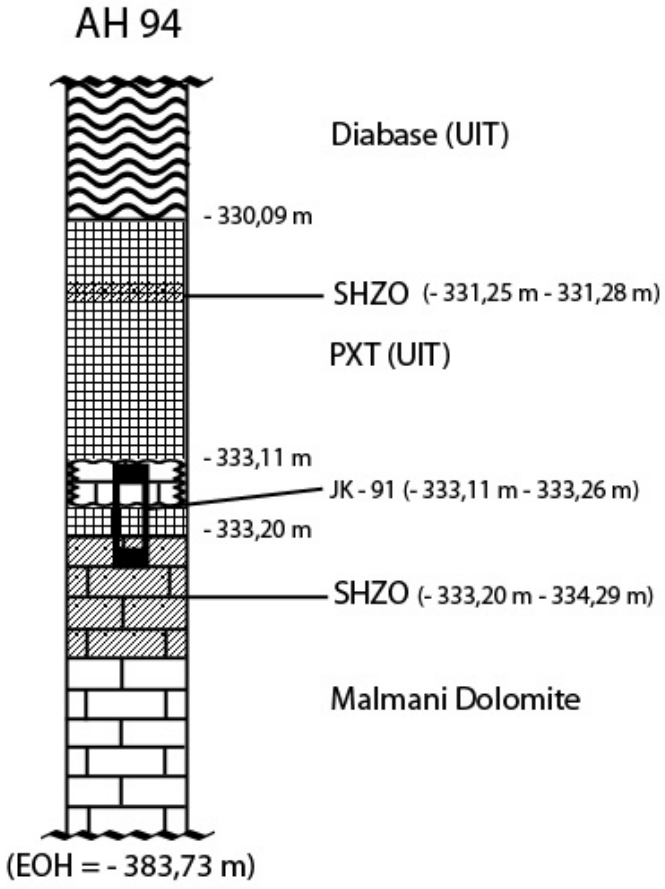

Fig. 5.62: Position of JK – 91 in a sequence of the stratigraphy of AH 94; not to scale

The image on the left-hand side shows the position of the sample JK – 91 in a sequence of the stratigraphy of the borehole AH 94. This borehole is located in the northwestern area of the Complex. The point is located in short distance to the contact of ca. 4 m.

The sample itself is made up by dolomitic clasts in pyroxenite (PXT).

The majority of the thin section is made up by calcite and dolomite which are hardly distinguishable with optical methods (Fig. 5.64).

In the calcitic matrix xenomorph, pale yellow greenish minerals are visible. The yellow greenish minerals are situated in veins. The mentioned properties and the form of the minerals lead to the result that the observed minerals are amphiboles. After a closer look into the optical properties it can be said that those amphiboles are of tschermakitic character. The amphibolites are transformed to epidote at their rims. Also remarkable are opaque minerals like chalcopyrite and pyrite. Pyrite and chalcopyrite are forming veins (Fig. 5.65). There is only one generation of veins detectable so it is assumable that there was a single event of mineralisation of the opaque minerals maybe due to sulphidebearing fluids which came from the Complex through metasomatic processes.

Remarkable within the plagioclase are the typical stripes which show a transformation to clinozoisite (Fig. 5.63). Last but not least one can say that the aggregates are of relatively big size, a major part of them is bigger than 500 µm. In the following one can see images out of the section which show the phenomena described in the text above.

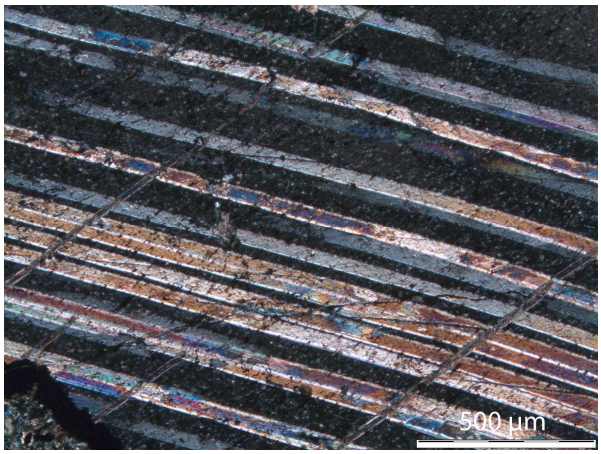

Fig. 5.63: Stripes in plagioclase which are transformed to epidote; JK – 91; AH 94; crossed nichols

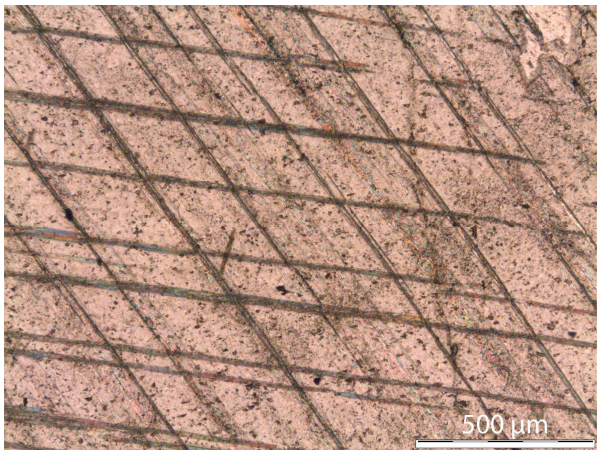

Fig. 5.64: Typical rhomboedric cleavage structure of calcite; JK – 91; AH 94; transmitted light

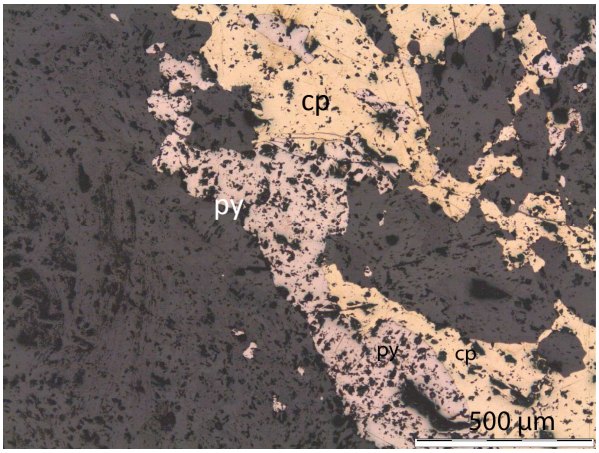

Fig. 5.65: Vein of Pyrite (py) and chalcopyrite (cp) in JK – 91; AH 94; reflected light

JK – 92 (AH 66) shale in Malmani dolomite

Distance to contact: 0 m

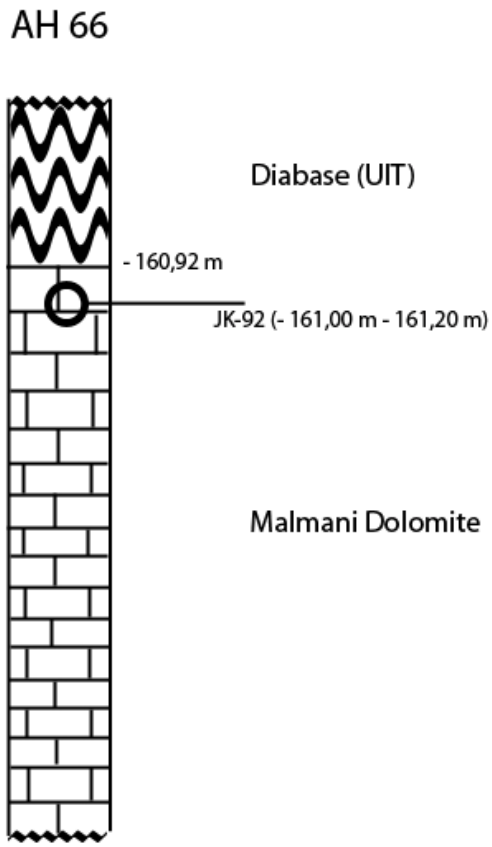

Fig. 5.66: Position of JK – 92 in a sequence of the stratigraphy of AH 66; not to scale

The sequence of stratigraphy to the left of the text clarifies the position of the sample in the lithology of the Complex (Fig. 5.66).

Primarily it is conspicuous that the sample is altered in the whole field the thin section is showing. As a product of alteration there are Fe-Mg-chlorites visible cognizable because of their colours of interference. Again there is epidote in the thin section producing veins crossing the slide.

Next to the chlorite, there are amphibolites in the slide.

Very interesting is the collective appearance of amphibole, more explicit tremolite and wollastonite in this sample.

The calcite, the major mineral in the matrix, occurs in grains of small size and shows a pavement-like shape.

Opaque phases are limited to pyrite basically.

JK – 93 (AH 53) – tremolite calcite

Distance to contact: 200 m

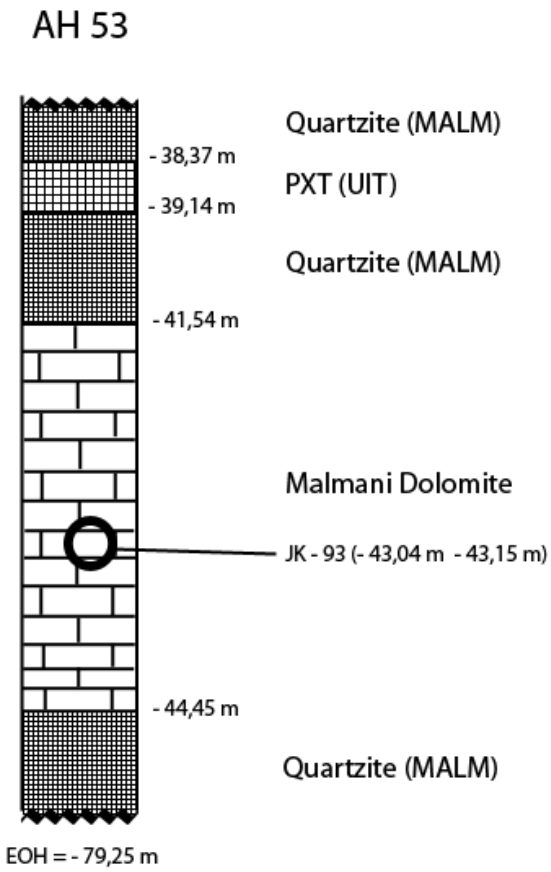

Fig. 5.67: Position of JK – 93 in a sequence of the stratigraphy of AH 53; not to scale

The minerals which are building up the matrix are too small to be identified only with the help of optical methods. Major part of the matrix is built up by calcite (Fig. 5.68) and tremolite (Fig. 5.69).

Important is the high amount of tremolite in the section. All over the section are quartz-veins.

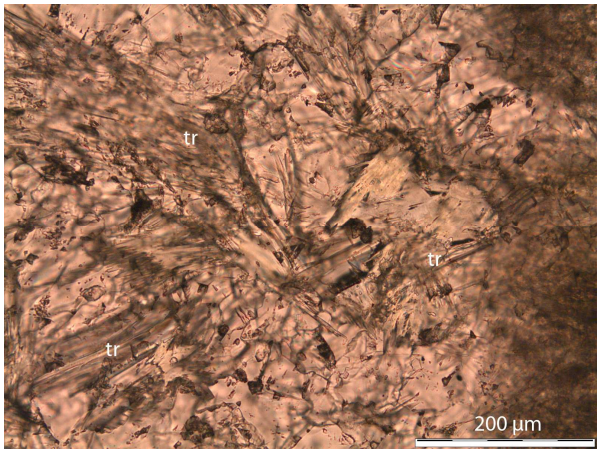

Fig. 5.68: Tremolites (tr) in JK – 93; AH 53; transmitted light

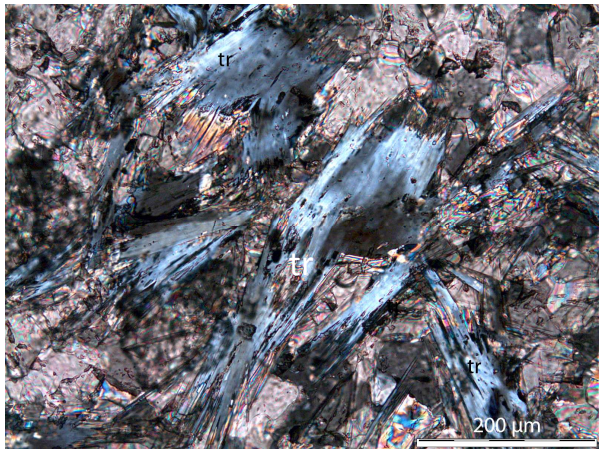

Fig. 5.69: Tremolites in JK – 93; AH 53; crossed nichols

JK – 94 (AH 116) – amphibole – calcite – plagioclase felse

Distance to contact: 0 m

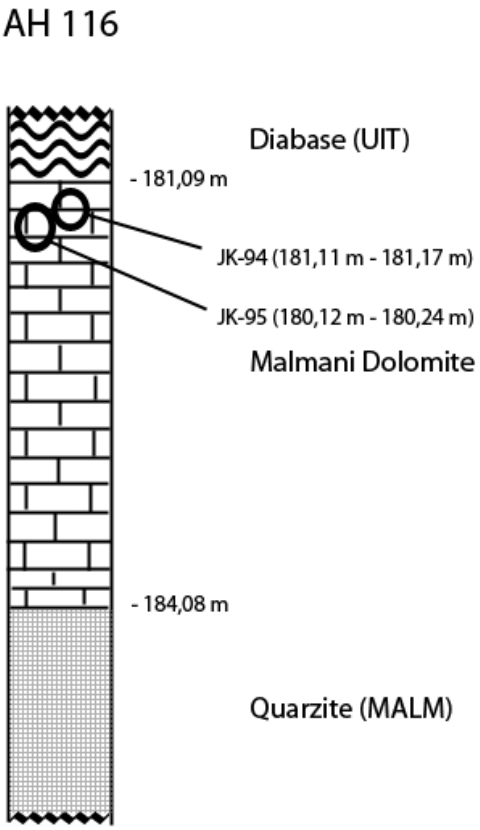

Fig. 5.70: Position of JK – 94 in a sequence of the stratigraphy of AH 116; not to scale

This thin section shows a manifold mineral assemblage. The matrix is calcitic and penetrated by plagioclases. With the exception of some veins the whole of the thin section seems to be transformed into amphibolites. In the thin section one can find actinolite which can easily be mixed up with uralite, a product of the transformation from diopside to tremolite. The actinolite appears pale greenish. But the process of the uralisation cannot be excluded.

The product of the transformation form augite to hornblende is associated with plagioclases. Between some plagioclase stripes one can find altered wollastonite.

Furthermore green hornblende, goethite, orthopyroxene and antigorite can be observed in this sample.

Also biotite is visible in this sample which forms so called “kink bands” in places (Fig. 5.71-5.74).

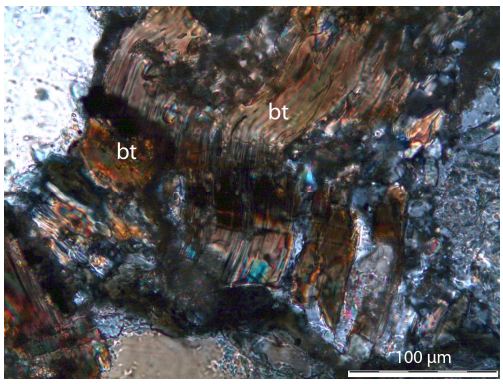

Fig. 5.71: Kink bands of biotite (bt) in JK – 94; AH 116; crossed nichols

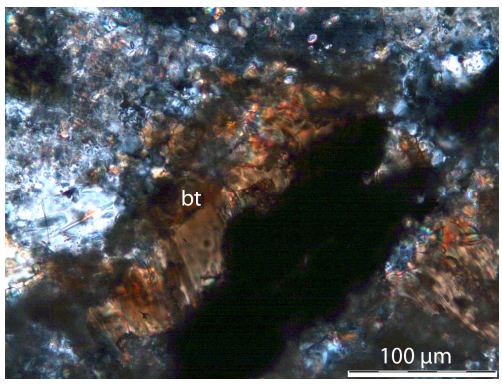

Fig. 5.72: Biotite (bt) JK – 94; AH 116; crossed nichols

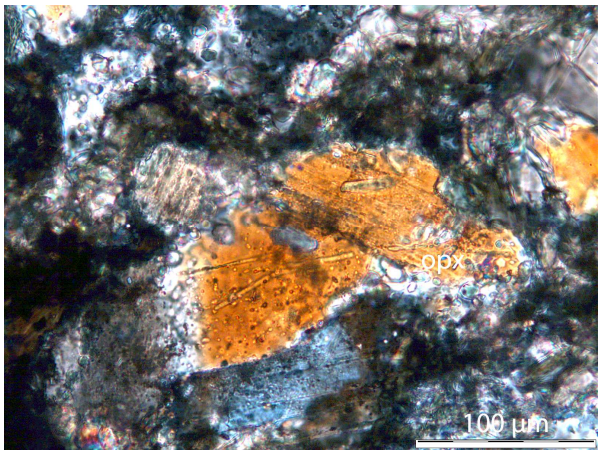

Fig. 5.73: Broken Orthopyroxene in JK – 94; AH 116; crossed nichols

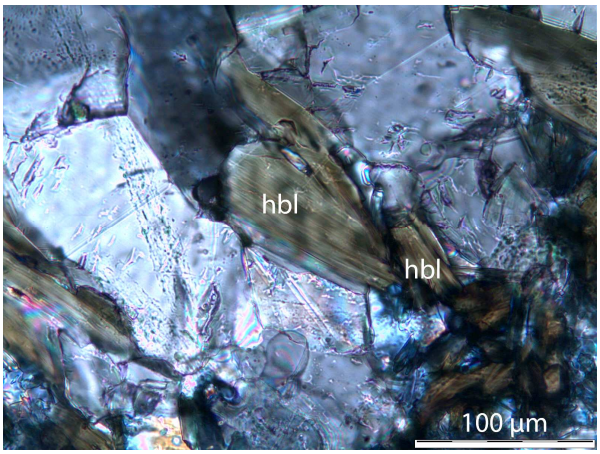

Fig. 5.74: Green Hornblende (hbl) in JK – 94; AH 116; crossed nichols

JK – 95 (AH 116) – cpx – tremolite – calcite fels

Distance to contact: 0 m

The position of the sample JK – 95 is given in Fig.5.70. Conspicuous is that the rock is transformed to chlorite and amphiboles. A further major part of the matrix is biotite. It is visible that the texture is of metamorphic character, more explicit radial foliated. A special mineral, observed the first time during the investigation, is chrysotile (Fig. 5.75). This mineral is fibrous, corrugated and dense and associated with mica. Also in the thin section one can find diopsides which are altered to a great extent. The diopsides are identified by the mineral-typic colours of interference and the particular angle of extinction.

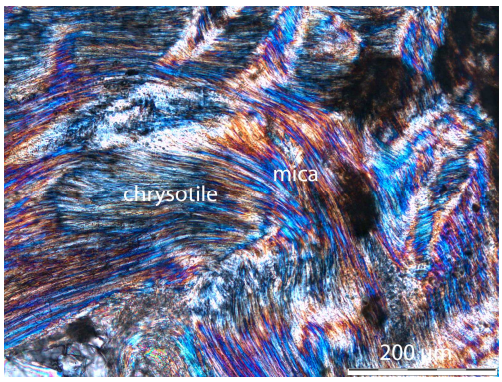

Fig. 5.75: Chrysotile associated with mica in JK – 95; AH 116; crossed nichols

Another important observation is that there is a high amount of amphibolites. With their strip-like shape and the pale-yellowish colours of interference it must be tremolite. But the minerals examined in transmitted light are of bluish colour.

Besides, the “tremolite-like” amphiboles, actinolites and tremolites (Fig. 5.76), which show the typical optical properties can be observed.

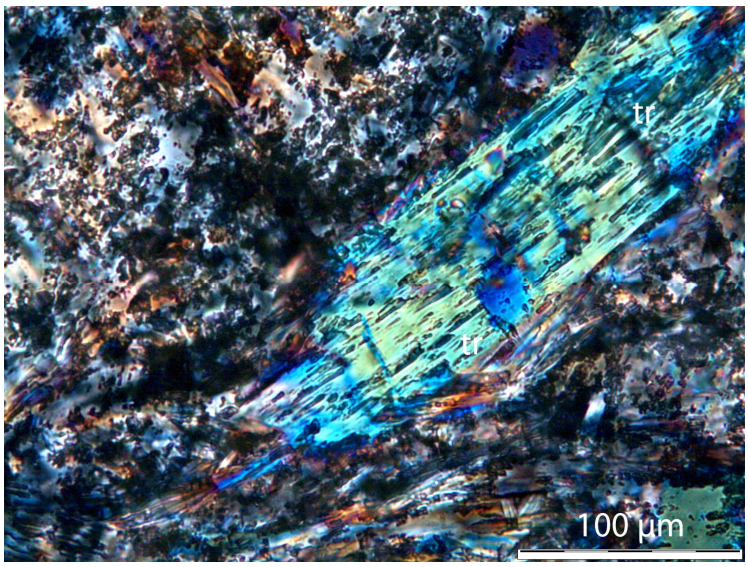

Fig. 5.76: Tremolite (tr) in JK – 95; AH 116; crossed nichols

JK – 96 (AH 76) calcite – tremolite - fels

Distance to contact: 0 m

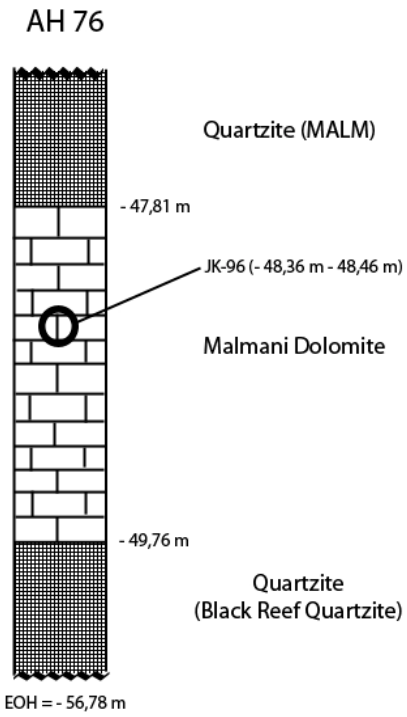

Fig. 5.77: Position of JK – 96 in a sequence of the stratigraphy of AH 76; not to scale

In the image (Fig. 5.77) the position of sample JK – 96 is visible. The sample is taken from the base of the Malmani Group and it is not assumed to show high-grade metamorphic structures and minerals.

The complete thin section shows a dentritic alteration partly visible in the overview (Fig. 5.78). Next to and between the dentritic alteration one can find chlorites and mica. The quartz in the matrix is of small size and broken. The opaque phases are mainly restricted to hematite, pyrite is also visible, but in low contents.

Another important mineral which was observed is the diopside. Its aggregates are also of altered and broken shape.

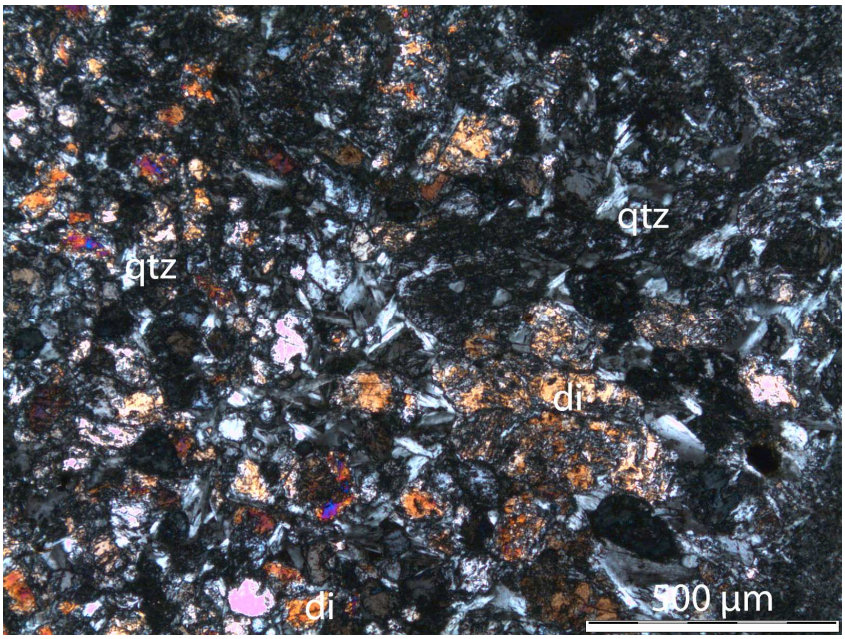

Fig. 5.78: Overview of the mineral assemblage; quartz (qtz), diopside (di) of JK – 96; AH 76; crossed nichols

Additional samples

In the following two thin sections are observed which were taken from a former unfinished project. The samples were taken from CR in the contact aureole of the Uitkomst Complex in 1993. Unfortunately there is no record concerning the depths they are coming from. But the boreholes are named and given in this thesis.
Those samples are especially used for the later microprobe analyses.

JK – 101 (UD 86) – calc - silicatic rock

Distance to contact: 0 m

The minerals in this slide are well developed, nearly idiomorphic and of moderate size. The spectrum of the minerals is wide. The aggregates are embedded in a fine-grained matrix. The matrix consists of quartz and calcite in great parts. The rock can be determined as a calc-silicate rock.

In detail, the minerals which can be detected with optical methods are actinolite, tremolite, plagioclase and augite (Figs. 5.79 and 5.80). It is conspicuous that the plagioclases are often adjectent by augites.

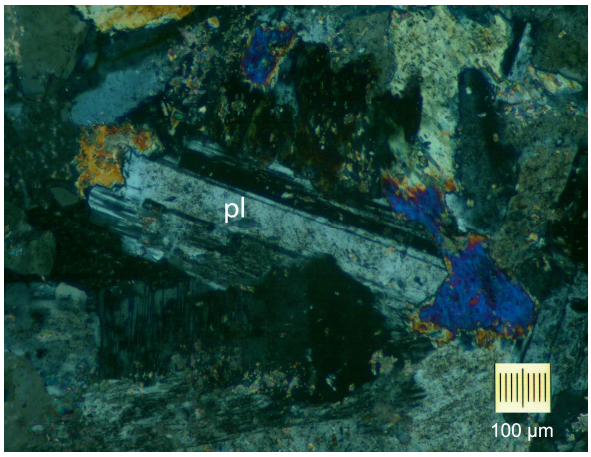

Fig. 5.79: Plagioclase in association with sugite in JK – 101; UD 86; crossed nichols

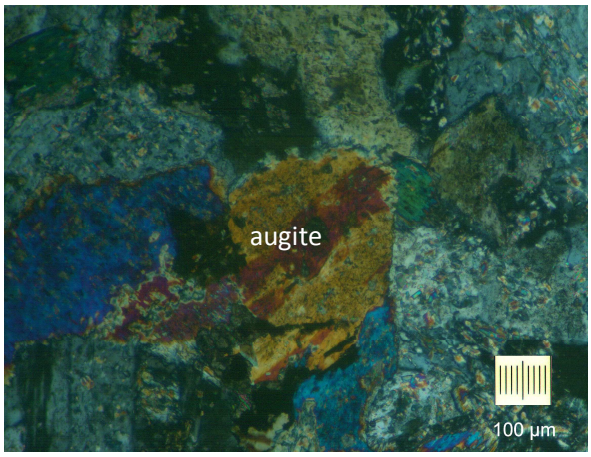

Fig. 5.80: Augite in JK – 101; DU 86; crossed nichols

JK – 105 (UD 64) – Cpx – Ep - calcic rock

Distance to contact: 0 m

The matrix of the thin section is built up by quartz and calcite which shows exposure to pressure. The matrix is crossed by veins but there are only few signs for alteration. The districts in the thin sections with minerals of small size are diffuse. In those areas there are no several minerals detectable. The grain size varies all over the thin section (Figs. 5.81-5.83) but nearly all of the aggregate are idiomorph. Most of the minerals are of big size (several 100 µm). That makes the section ideal for further investigations. The whole mineral assemblage extends over calcite, quartz, orthopyroxene and augite.

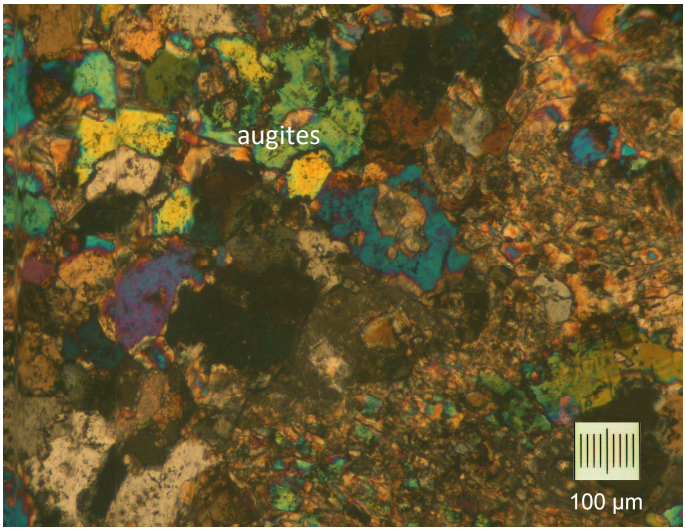

Fig. 5.81: Survey of JK – 105; UD 64; crossed nichols

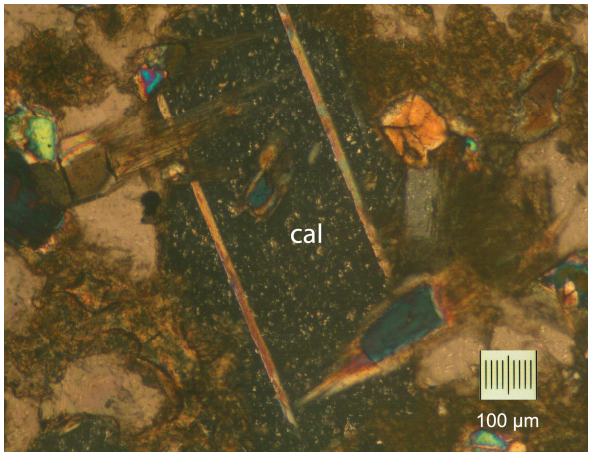

Fig. 5.82: Calcite in JK – 101; UD 64; crossed nichols

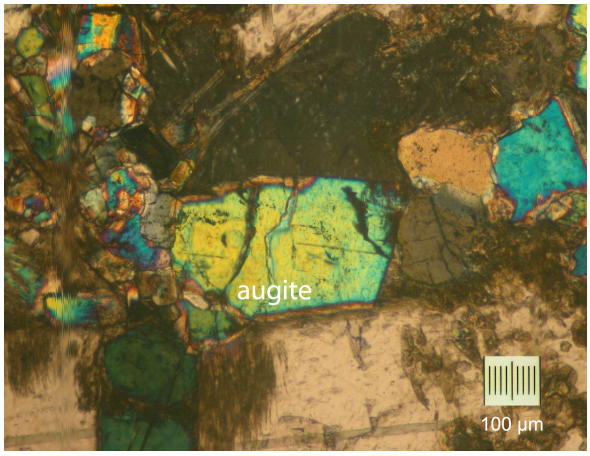

Fig. 5.83: Augite in JK – 101; UD 64; crossed nichols

5.3.4 Textures of Malmani Dolomite

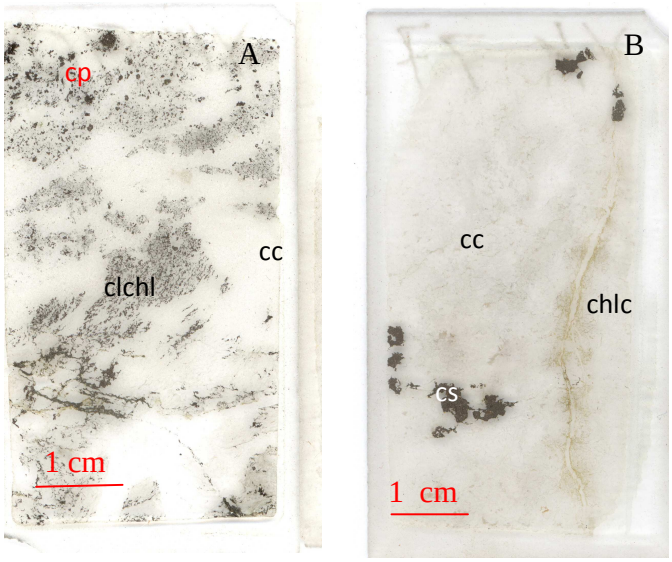

Fig. 5.84: Texture of Malmani Dolomite; A) calcitic (cc) to Mg-calcitic matrix with dessiminated chalcopyrite (cp) and clinochlorite (clchl) in JK-90; B) chloritinated calcite (chlc), Mg-calcite (cc) and chlorite serpentine (cs) matrix in JK-77

The image A in Fig. 5.84 shows a dessimination of chalcopyrite and clinochlore in a calcitic matrix. The calcite grains are equal in size and shape. The picture B in Fig. 5.87 shows a mineralization of clinochlore and chlorite along a vein crossing the section. Also chalcopyrite is developed in this sample and visible in the upper right corner of the thin section.

5.4 Mineral assemblages

The following table 5.2 displays the mineral assemblages in dependency of the distance from the contact resulting from investigations with the microscope and analyzes with the XRD.

sample name	distance to contact [m]	borehole no.	lithology	mineral assemblage
		surface		
JK-40	241		THS-surface	microcline,albite, orthoclase, sanidine
JK-41	248		THS-surface	sillimanite, muscovite, chlorite serpentine, clinochlore
JK-42	254		THS-surface	chlorite serpentine, corundum, quartz, sillimanite
JK-43	283		THS-surface	quartz, talc [$Mg_3Si_4O_{10}(OH)_2$]

JK-44	283		THS-surface	chlorite serpentine, vermiculite, clinochlore, paragonite, anorthite, corundum chromian [$Al_{1.54}O_3Cr_{0.46}$]
JK-45	283		THS-surface	chlorite serpentine, vermiculite, clinochlore, sillimanite
JK-48	320		dolomite-surface	quartz, zinnwaldite, muscovite
JK-49	500		dolomite-surface	diopside (Al-Na), augite,
JK-50	715		dolomite-surface	cummingtonite, magnesiohornblende, clinochlore, chlorite serpentine, tremolite, actinolite
JK-51	760		dolomite-surface	talc
JK-52	590		dolomite-surface	quartz
	boreholes			
JK-77	0	UD 72	dolomite	qtz, cc, dol, ank, chlorite serpentine, calcite magnesian [$(Mg_{0.064}Ca_{0.936})(CO_3)$], clinochlore, wollastonite
JK-89	0	AH 117	dolomite	cc, calcite-magnesian, chlorite serpentine, chalcopyrite, plagioclase, tremolite, epdiote
JK-90	0	AH 114	dolomite	cc, chalcopyrite, Mg-calcite [$Mg_{0.03}Ca_{0.97}(CO_3)$], calcite, muscovite, plagioclase, epidote
JK-94	0	AH 116	dolomite	qtz, cc, an, chlorite serpentine, albite, clinochlore, chlorite chromian, biotite, green hbl, actinolite, antigorite, anorthite, wollastonite, opx, goethite
JK-95	0	AH 116	dolomite	qtz, cc, hbl (Mg,Fe), trem (Na), graphite, qtz, calcite, Mg-calcite, Mg-hbl, biotite, crysotil, diopside, tremolite, actinolite
JK-96	0	AH 76	dolomite	qtz, cc, hbl (Mg,Fe), trem (Na), clinochlore, chlorite chromian, cpx ,chlorite serpentine, diopside, hematite
JK-91	5	AH 94	dol. Clasts	cc, chalcopyrite, Mg-calcite, tschermakitic amphibole, clinozoisite, pyrite, chalcopyrite
JK-66	17	UD 75	dolomite	dol, augite (alumnian), cpx (Ti, Al), di (alumnian), diopside sodian, diospide subalcalic, diopside chromian – sodian [$(Na_{0.45}Ca_{0.55})(Cr_{0.45}Mg_{0.55})(Si_2O_6)$]
JK-68	17	UD 75	pyroxen & dol.xenos	qtz, augite (alumnian), cpx (Ti,Al), ab (calcian), di, trem, albite, albite low, albite high, diopside ferroan, anorthite, wollastonite, clinozoisite, epdiote
JK-76	20	UD 39	dolomite	qtz, dolomite, clinochlore
JK-71	31	UD 110	dolomite	cc, dol, augite (alumnian), wo, chlorite serpentine, hematite, andradite, chlinochlore, diopside sodian, diopside subalcalic, diopside alumnian, dioside chromian, calcite magnesian [$Mg_{0.064}Ca_{0.936}CO_3$], talc, epidote. magnetite, pyrite, chalcopyrite

JK-63	50	UD 111	dolomite	qtz
JK-64	50	UD 111	hornfelse	qtz, chlorite serpentine, chlinochlore (Cr-bearing, dehydrated), clinochlor ferroan [$(Mg,Fe)_6(Si,Al)_4O_{10}(OH)_8$], augite
JK-65	50	UD 111	shale	qtz, muscovite, sillimanite, zinnwaldite, chlorite serpentine, augite, epidote
JK-81	65	UD 98	dolomite	qtz, dol (ferroan), uvsp. chlorite serpentine, chlinochlore, vermiculite, zinnwalditte, muscovite [$KAl(Si_3Al)O_{10}(OH,F)_2$], qtz
JK-82	65	UD 98	shale	qtz, muscovite, zinnwaldite, augite, cpx, opx, antigorite, epidote,
JK-92	80	AH 66	dolomite	cc, ank, hbl (Mg), trem, magnesioriebeckite, magnesio-arfvedsonite, actinolite, wollastonite, chlorite, clinozoisite, epidote
JK-78	108	UD 77	dolomite	dol, ank, augite (alumnian), hbl (Mg, Fe), cpx (Ti,Al), di (alumnian), trem (Na), qtz, tremolite
JK-79	108	UD 77	shale	qtz, orthoclase, graphite, epidote, magnetite,
JK-80	108	UD 77	shale	qtz, orthoclase & anorthoclase, sanidine [$K_{0.65}Na_{0.35}AlSi_3O_8$], orthoclase [$K(AlSi_3O_8)$], microcline intermediate [$K_{0.94}Na_{0.06}AlSi_3O_8$]
JK-70	113	UD 95	conglomerate	qtz
JK-72	200	UD 106	shale	quartz low, zinnwaldite
JK-73	200	UD 106	conglomerate	qtz
JK-86	202	UD 109	dolomite	qtz, ank, augite, augite (alumnian), di, di (alumnian), trem (Na), actinolite, hematite, tephrite, diopside subalcalic, diopside ferroan
JK-87	202	UD 109	shale	qtz, hbl (Mg), cummingtonite manganoan, tremolite, magnesiohornblende, magnesio-arfvedsonite, magnesio-riebeckite, actinolite, chlorite chromian, epdiote
JK-88	202	UD 109	conglomerate	qtz, cpx
JK-93	205	AH 53	dolomite	cc, hbl (Mg), wo, trem (Na), Mg-calcite, qtz, epidote, pyrite, chalcopyrite
JK-74	212	UD 88	shale	qtz, zinnwaldite, chlorite serpentine, almandine [$Mg_{0.6}Fe_{2.4}Al_2(SiO_4)_3$]
JK-75	212	UD 88	dolomite	qtz, cummingtonite manganoan, magnesiohornblende, calcite, muscovite, augite, tremolite, chlorite
JK-83	258	UD 99	shale	qtz
JK-84	258	UD 99	conglomerate	qtz, diopside, antigorite, epidote,opx
JK-85	258	UD 99	dolomite	cc, hbl (Mg,Fe), trem (Na), actinolite, magnesiohornblende, pargasite potassian, tremolite, green hornblende, tschermakite, clinozoiste
JK-67	346	UD 100	dol. Xenos in Ths	qtz, zinnwaldite, laumontite [$CaAl_2Si_4O_{12}(H_2O)_2$], clinochlore (Cr-bearing, dehydrated
JK-69	346	UD 100	conglomerate	qtz

Based on these results it is possible to create mineralization zones. The generation of those zones is done separately for the Malmani Dolomite and the Timeball Hill Shale because of their different physicochemical properties and the consequent diverse susceptibility for metamorphic and metasomatic processes.

5.4.1 Mineral assemblages in the Malmani Dolomite in certain distances from the contact

Table 5.3: Zones of mineralization in the Malmani Dolomite around the Uitkomst Complex

distance to contact	**mineral assemblage**	**name of the mineralization zone**
0 – 50 m	qtz, cc, dol, ank, chlorite serpentine, calcite magnesian [$(Mg_{0.064}Ca_{0.936})(CO_3)$], clinochlore, wollastonite, chalcopyrite, plagioclase, tremolite, epdiote, Mg-calcite [$Mg_{0.03}Ca_{0.97}(CO_3)$], muscovite, albite, chlorite chromian, biotite, green hbl, actinolite, antigorite, anorthite, opx, goethite, hbl (Mg,Fe), trem (Na), graphite, Mg-hbl, biotite, crysotil, diopside, cpx, hematite, Mg-calcite, tschermakitic amphibole, clinozoisite, pyrite, augite (alumnian), cpx (Ti, Al), di (alumnian), diopside sodian, diospide subalcalic, diopside chromian – sodian [(Na0.45Ca0.55)(Cr0.45Mg0.55)(Si2O6)], andradite,. magnetite, clinochlor ferroan [(Mg,Fe)6(Si,Al)4O10(OH)8], sillimanite, zinnwaldite	wollastonite zone [wo]
50 – 150 m	qtz, dol (ferroan), uvsp. chlorite serpentine, chlinochlore, vermiculite, zinnwalditte, muscovite [$KAl(Si_3Al)O_{10}(OH,F)_2$], cc, ank, hbl (Mg), magnesioriebeckite, magnesio-arfvedsonite, actinolite, wollastonite, chlorite, clinozoisite, epidote ,augite (alumnian), hbl (Mg, Fe), cpx (Ti,Al), di (alumnian), trem (Na), qtz, tremolite	diopside - serpentine – hornblende zone [di-serp-hbl]
150 – 300 m	qtz, ank, augite, augite (alumnian), di, di (alumnian), trem (Na), actinolite, hematite, tephrite, diopside subalcalic, diopside ferroan, cc, hbl (Mg), wo, trem (Na), Mg-calcite, qtz, epidote, pyrite, chalcopyrite, cummingtonite manganoan, magnesiohornblende, calcite, muscovite, augite, tremolite, chlorite. hbl (Mg,Fe), trem (Na), actinolite, magnesiohornblende, pargasite potassian, tremolite, green hornblende, tschermakite, clinozoiste	hornblende zone [hbl]
300 – 500 m	quartz, zinnwaldite, muscovite, diopside (Al-Na), augite	quartz-diopside-

		mica zone [qtz-di-mic]
500 – 800 m	cummingtonite, magnesiohornblende, clinochlore, chlorite serpentine, tremolite, actinolite, talc, quartz	quartz-hbl-mica [qtz-hbl-mic]

5.4.2 Mineral assemblages in the Timeball Hill Shale in certain distances from the contact

Table 5.4: Zones of mineralization in the Timeball Hill Shale around the Uitkomst Complex

distance to contact	**mineral assemblage**	**name of the mineralization zone**
0 – 50 m	qtz, chlorite serpentine, chlinochlore (Cr-bearing, dehydrated), clinochlor ferroan [$(Mg,Fe)_6(Si,Al)_4O_{10}(OH)_8$], muscovite, sillimanite, zinnwaldite, chlorite serpentine, augite, epidote	sillimanite zone [sil]
50 – 100 m	qtz, muscovite, zinnwaldite, augite, cpx, opx, antigorite, epidote	augite – antigorite zone [aug-atg]
100 – 200 m	qtz, orthoclase, graphite, epidote, magnetite, orthoclase & anorthoclase, sanidine [$K_{0.65}Na_{0.35}AlSi_3O_8$], orthoclase [$K(AlSi_3O_8)$], microcline intermediate [$K_{0.94}Na_{0.06}AlSi_3O_8$]	sanidine zone [san]
200 – 250 m	qtz, zinnwaldite, chlorite serpentine, almandine [$Mg_{0.6}Fe_{2.4}Al_2(SiO_4)_3$] muscovite, zinnwaldite, augite, cpx, opx, antigorite, epidote, microcline,albite, orthoclase, sanidine, sillimanite, muscovite, chlorite serpentine, clinochlore	almandine zone [alm]
250 – 300 m	chlorite serpentine, corundum, quartz, sillimanite, quartz, talc [$Mg_3Si_4O_{10}(OH)_2$], chlorite serpentine, vermiculite, clinochlore, paragonite, anorthite, corundum chromian [$Al_{1.54}O_3Cr_{0.46}$]	corundum zone [cor]

The zones were named after the minerals which are the major constituents of the observed samples.

6. Whole rock chemistry and geochemical trends from contact

The whole rock chemistry was investigated by processing XRF-analyses. In the following chapter the chemistry will be described separately for every lithotype. It is intended to establish to establish elemental interrelationships with the mineralogy of every special kind of country rock. Also the major and trace element variation within the contact aureole should be displayed and be interpreted in terms of metamorphic and metasomatic processes.

6.1 General

In every degree of metamorphism, no matter which kind of metamorphism is investigated, are special characteristics existent, for example special minerals or mineral assemblages or significant p-T conditions. That has to be mentioned and proved.
The information about the mineralogy is useful for understanding the chemistry of the rocks.
The procedure is to show an interelement correlation after Pearson and afterwards the demonstration of the chemical composition in different chosen ternary systems like ACF-diagrams dependent on the kind of specimen.
By combining these methods it should be possible to indicate changes in the chemistry of the samples and maybe construct relations to metamorphic and metasomatic processes. The observations are limited to the major elements (Fe, Al, Ti, Na, Ca, K, Mg, Mn, P, Cr) which are significant for the whole rock chemistry and which, if they vary strongly they can be an indicator for changes in mineralogy and chemistry due to the contact metamorphism. Additionally the whole rock chemistry gives us information about the educts of the metamorphic lithotypes.
The whole rock chemistry will be presented in different ternary diagrams which are appropriate to every lithology. The characteristic criteria of every diagram will be explained in subchapters 6.2 to 6.4.
The mineralogy of all samples is displayed in Table 5.2 in chapter 5. Keeping the mineralogy in mind the understanding of the whole rock chemistry will be much easier.
It is possible that a marginal part of the mineral assemblage was not identified during the investigation. This is due to the metamorphic structures, the small sizes of the mineral grains and the lack of an adequate norm calculation.

If possible some reactions and intersections will be shown in diagrams. The diagrams are generated with TWQ (BERMAN, 2006) with the last database from 2006.
If possible and necessary, EMPA analyses will be presented for improving the knowledge about the mineral assemblage.

6.1.1 The Pearson Correlation

At first, for a better understanding of the correlations which are following in this chapter the Pearson Correlation has to be defined and explained concerning its information.

The formula for the Pearson Correlation is (HARTUNG, 1999):

$$r = \frac{\sum (x - \bar{x})(y - \bar{y})}{\sqrt{\sum (x - \bar{x})^2 \sum (y - \bar{y})^2}}$$

X and y are the averages of the random samples. The correlation is "1" if there is an increasing linear relationship between the variables. If the correlation is "-1" there is a decreasing linear relationship between the variables. Every value in between this interval represents a grade of relationship of variables.
More exactly there is a positive correlation if $r \geq 0.5$ and a negative correlation if $r \leq 0.5$. That means that elements which correlate positive ($r \geq 0.5$) are part of the same chemical and maybe mineralogical environment. In the opposite, if the correlation is negative ($r \leq 0.5$) one can say that elements exclude each other concerning their chemical and mineralogical environment at the time of their generation.
All coefficients in the interval [-0.5;0.5] show neither positive nor negative correlation. Correlations with this result for some variables stand for an absence of any relation of the variables. They are independent from each other.
It is logical that the reliability of the correlations increases with the number of variables (samples) the correlation is calculated with.
It is necessary to mention that the Pearson Correlation is an additive method which is not able to substitute a systematic investigation of the geological and mineralogical conditions.

6.2 Timeball Hill Shale

6.2.1 Chemical Composition

Table 6.1: average concentration of the main elements in the Timeball Hill Shale

	THS - boreholes			
	av. content [wt-%]	Max	Min	standard deviation
SiO_2	62.64	78.05	51.70	9.08
Al_2O_3	16.49	32.57	3.96	8.44
Fe_2O_3	7.63	14.71	0.66	4.91
MnO	0.22	1.28	0.01	0.41
MgO	4.86	19.93	0.90	5.90
CaO	2.61	10.96	0.11	4.00
Na_2O	0.80	2.24	0.15	0.69
K_2O	4.57	12.22	0.31	3.97
TiO_2	0.92	2.27	0.09	0.75
P_2O_5	0.14	0.39	0.02	0.12
	THS-surface			
	av. content [wt-%]	Max	Min	standard deviation
SiO_2	50.39	85.90	38.34	18.45
Al_2O_3	35.57	49.30	0.16	18.66
Fe_2O_3	5.80	10.54	1.41	3.39
MnO	0.02	0.04	0.01	0.01
MgO	3.75	12.97	0.35	4.61
CaO	1.02	1.84	0.21	0.76
Na_2O	2.26	4.76	0.00	1.59
K_2O	2.45	4.30	0.00	1.43
TiO_2	0.48	0.94	0.02	0.30
P_2O_5	0.06	0.15	0.00	0.05

The data given in Table 6.1 shows the average contents of the main elements. The concentrations are given in wt-% of the elementoxides. At first one closer look to the Timeball Hill Shale borehole samples.

The maximum value of SiO_2 is due to the specimen JK-79 which is described as shale but is identified as a quartzite now based on the geochemical analyzes. JK-79 shows also the lowest concentration in MgO. The lowest content of quartz is detectable in the specimen JK-65 which

also shows the highest concentration in Al_2O_3. Nevertheless the both elements are associated with each other which are especially shown by the presence of sillimanite in this special specimen.
A maximum of Fe is concentrated in the sample JK-74, which contains Fe-bearing minerals like goethite, Fe-hornblende and almandine.
Maximal values of Mg-content are noticeable in JK-64. This sample is a hornfels.
Also the surface samples show great variation in the element concentrations. This is displayed in Table 6.1 also. With a content of quartz of 85.90 wt-% JK-42 is mainly build up by SiO_2. The highest concentration of MgO is also noticeable in JK-42 the lowest in JK-45. The values for Fe_2O_3 vary from 10.54 wt-% in JK-44 and 1.41 in JK-42.

6.2.2 Pearson Correlation

By investigating the Correlation a certain number of positive and negative correlations can be determined. The Pearson Correlation for the surface samples of the Timeball Hill Shale are visible in Table 6.1.
It is conspicuous that Al and Si show a nearly perfect correlation. This is caused by the association of both elements in the minerals sillimanite, muscovite and biotite. Beside that mentioned association, probably with less consequence for the correlation, Al is placed in the included different siliceous minerals like biotite, muscovite and anortholclase.
Interesting is the negative correlation between Si and Fe. That would be meaning that there are no siliceous minerals which contain Fe in high contents but one can find biotite in several specimens. This recognition is very important because the consequence is that the amphiboles in the sample which are identified as tremolites are tremolites. This assumption is supported by the values for r for the relation of Mg and Si and Fe and Si which are > 0.5 in both cases.
Despite that negative correlation of Fe and Si the occurrence of Fe-bearing garnets like almandine is proven.
Furthermore it is possible to say that no garnet is a constituent of these samples because Al shows a negative relation to Mg and no relation to Ca. This means that Ca- and Mg-bearing garnets like grossulare in the Timeball Hill Shales are improbably.
If there is a negative correlation of Si and Fe it is assumable that the biotite in this sample is poor in Fe and relatively enriched in Al because there also a negative coefficient for the correlation of Si and Ti.

Ti shows a value for r ≤ 0.5 for the correlation with Si and Ca but it is correlating positively (r = 0.623) with Fe. That fact makes it probable that the samples include ilmenite which is proven by microscopy. A correlation not shown by the Pearson correlation but observed by analytical methods is existing between Fe and Mn. Goethite substitutes Mn for Fe in surface near localities. The negative values for Si – Na and Si – K define the "anorthoclase" as an anorthite.
Other correlations are probably due to weathering processes or constituents of other minerals which have no eminent importance for the study of the sample.

Table 6.2: Pearson correlation – surface samples (n = 6) Timeball Hill shale; green: r ≥ 0.5; red: r ≤ -0.5

		SiO2	Al2O3	Fe2O3	MnO	MgO	CaO	Na2O	K2O	TiO2	P2O5
SiO_2	Pearson Correlation	1	-.994(**)	-0.523	0.629	.867(*)	0.202	-0.796	-0.641	-0.517	-0.364
Al_2O_3	Pearson Correlation	-.994(**)	1	0.436	-0.668	-.859(*)	-0.137	0.790	0.651	0.496	0.354
Fe_2O_3	Pearson Correlation	-0.523	0.436	1	-0.189	-0.593	-.819(*)	0.391	0.411	0.623	0.408
MnO	Pearson Correlation	0.629	-0.668	-0.189	1	.844(*)	0.308	-0.510	-.926(**)	-.814(*)	-0.721
MgO	Pearson Correlation	.867(*)	-.859(*)	-0.593	.844(*)	1	0.461	-0.640	-.929(**)	-.850(*)	-0.664
CaO	Pearson Correlation	0.202	-0.137	-.819(*)	0.308	0.461	1	-0.043	-0.451	-0.712	-0.443
Na_2O	Pearson Correlation	-0.796	0.790	0.391	-0.510	-0.640	-0.043	1	0.450	0.446	0.586
K_2O	Pearson Correlation	-0.641	0.651	0.411	-.926(**)	-.929(**)	-0.451	0.450	1	.916(*)	0.768
TiO_2	Pearson Correlation	-0.517	0.496	0.623	-.814(*)	-.850(*)	-0.712	0.446	.916(*)	1	.879(*)
P_2O_5	Pearson Correlation	-0.364	0.354	0.408	-0.721	-0.664	-0.443	0.586	0.768	.879(*)	1

Table 6.3: Pearson correlation – surface samples (n = 8) Timeball Hill shale; green: r ≥ 0.5; red: r ≤ -0.5

		SiO2	Al2O3	Fe2O3	MnO	MgO	CaO	Na2O	K2O	TiO2	P2O5
SiO_2	Pearson Correlation	1	-0.566	-.866(**)	-0.414	-0.227	0.122	-0.486	0.406	-.690(*)	-.708(*)
Al_2O_3	Pearson Correlation	-0.566	1	0.227	0.076	-0.454	-0.549	0.274	0.190	0.303	0.359
Fe_2O_3	Pearson Correlation	-.866(**)	0.227	1	0.597	0.412	0.061	0.317	-.684(*)	0.651	0.552
MnO	Pearson Correlation	-0.414	0.076	0.597	1	-0.092	0.012	-0.115	-0.130	0.628	0.005
MgO	Pearson Correlation	-0.227	-0.454	0.412	-0.092	1	0.000	0.003	-0.513	-0.058	0.160
CaO	Pearson Correlation	0.122	-0.549	0.061	0.012	0.000	1	0.310	-0.487	0.057	0.157
Na_2O	Pearson Correlation	-0.486	0.274	0.317	-0.115	0.003	0.310	1	-0.422	0.562	.837(**)
K_2O	Pearson Correlation	0.406	0.190	-.684(*)	-0.130	-0.513	-0.487	-0.422	1	-0.182	-0.410
TiO_2	Pearson Correlation	-.690(*)	0.303	0.651	0.628	-0.058	0.057	0.562	-0.182	1	.690(*)
P_2O_5	Pearson Correlation	-.708(*)	0.359	0.552	0.005	0.160	0.157	.837(**)	-0.410	.690(*)	1

Table 6.3 shows the Pearson correlation coefficients for the borehole samples of the Timeball Hill Shales. The Correlation is difficult and should be interpreted carefully. The mineral assemblages in all the samples differ from specimen to specimen. The result is a wide spectrum of different mineral collectivisations. Different possible reactions will be the result of the wide mineral spectrum. But in the Correlation it is visible that, in contrast to the surface samples, sillimanite could be seldom mineral in the Timeball Hill Shale borehole samples. This is proven by a negative correlation coefficient from SiO_2 and Al_2O_3. This investigation is supported by the chemical and optical analyses. Without the support of these methods it is not reputable to interpret this Correlation combined with the determination of minerals. But the positive relation of TiO_2 and Fe_2O_3 are a sign for the existence of Ti-Fe-minerals like ilmenite which can be found in the samples.

6.2.3 Geochemical trends and relations in the Timeball Hill Shale

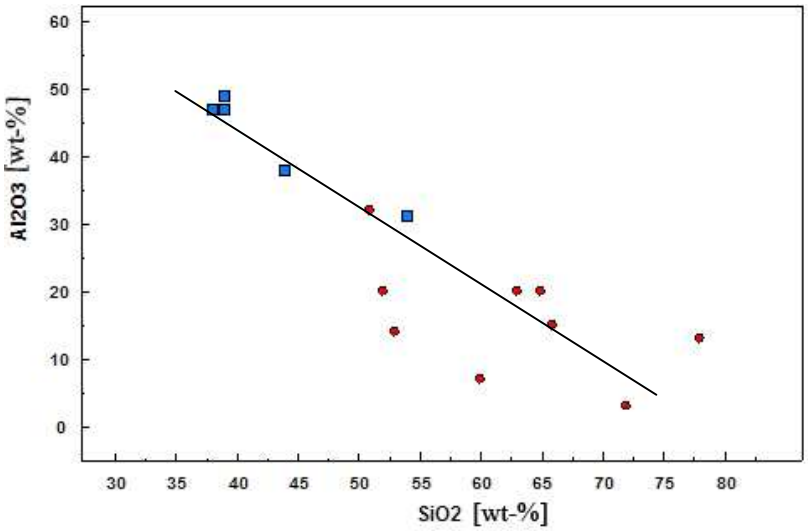

Fig. 6.1: Harker-diagram Al_2O_3 vs. SiO_2; THS – samples; quadrats = surface samples, spots = borehole samples

The diagram on the left hand side (Fig. 6.1) shows a trend which indicates a decreasing content of Al_2O_3 in the samples of the THS from the surface and the boreholes by increasing content of SiO_2. The reason for the phenomenon is based on the 2 possible coordinations of the Si - atom (MASON & MOORE, 1985). Si appears 4x coordinated and 6x coordinated. The atom is coordinated 4x in cases of high-temperature environments. The pressure has no eminent impact on the coordination of Al, although the Al(6) is the more compact variation and would be expected under the impact of high pressure. If the Al is coordinated 6x it is very similar to Fe^{2+}, Fe^{3+} and Mg^{2+} concerning the structure and its chemical behaviour. If Al is coordinated 4x it shows the same chemical behaviour and structure like Si. During high-temperature metamorphic processes Al substitutes Si in the minerals, especially in minerals like pyroxenes, amphiboles and mica. The grade of the substitution increases with increasing temperature. The Al(4) is typical for contact metamorphism. . The negative trend of Al – Si suggests a decreasing insertion of Al in silicate-minerals. The grade of Al - insertion is proportional to the temperature. The replacement of Si by 4x coordinated Al for Si is combined with a high temperature environment (MASON & MOORE, 1985). With decreasing temperature the insertion of Al for Si shrinks too. In addition to this reason it is assumable that non - silica minerals like corundum are concentrated in a part of the samples. The accumulation of sillimanite is restricted to a zone in the country rocks controlled by chemical composition and temperature. A depletion of Si can also be caused by fluids which are produced by dehydration- and decarbonatization reactions during the metamorphism. The result is a relative enrichment in Al_2O_3.

But there is a second statement which is based on the Al_2O_3/SiO_2 – ratio which is of importance in surface near weathering environments. In such environments much more SiO_2 relative to Al_2O_3 is leached and mobilised. The result is the generation of AlOOH minerals by weathering, e.g. gibbsite, boehmite and diaspore in the surface samples.

The abundance of corundum in the surface samples of the Timeball Hill Shale shows a SiO_2-undersaturation in some samples.

If there is SiO_2-saturation or over-saturation, sillimanite is instead developed.

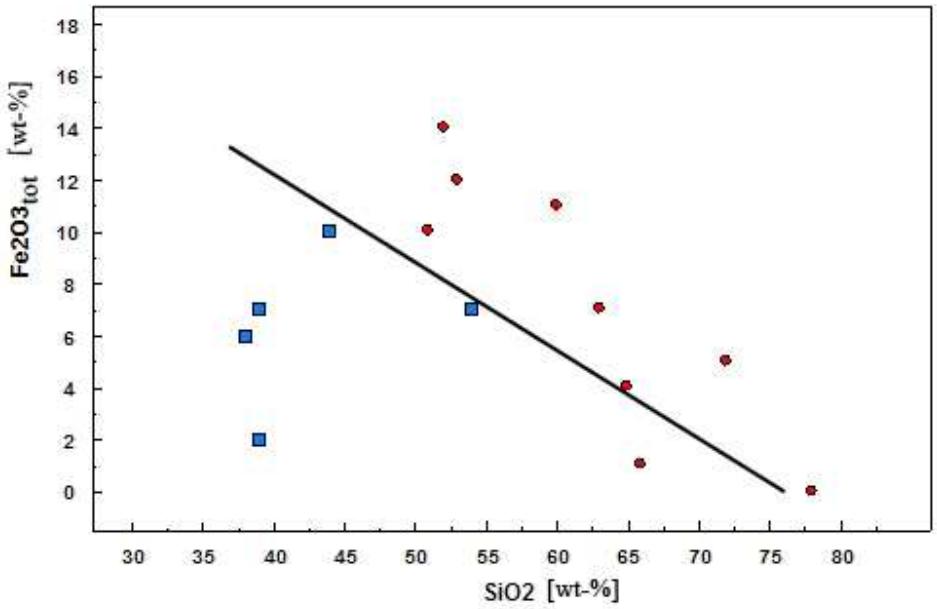

Fig. 6.2: Harker-diagram $Fe_2O_3tot(Fe_2O_3+ FeO)$ vs. SiO_2; THS – samples; (given in [wt-%]) quadrats = surface samples, spots = borehole samples

Fig. 6.2 shows that the relation of SiO_2 and Fe_2O_3tot.

There is a negative trend detected. That means when the concentration of SiO_2 is increasing the content of Fe decreases. Despite of the shown trend it is a fact that in some samples goethite and hematite are common. The mineralisation of goethite or hematite is a result of the oversaturation in Fe (MATTHES & OKRUSCH, 2005). Goethite and hematite is evidenced in the surface samples of the Shale. The macroscopic sign for those processes is the red colour of the rock in the outcrop.

The mineralisation of the Fe-minerals is also dependent on the fugacity of the oxygen (f_{O2}). Under surface and surface weathering conditions the partial oxygen pressure in the atmosphere is about 0.21 bar. During metamorphic processes the f_{O2} is much lower. In dependency of the

fugacity different Fe-minerals can be generated. More explicit hematite, magnetite and ilmenite are generated. If there is hematite as opaque phase in the samples it is clear that the O_2 is the result of the dissociation $H_2O \leftrightarrow H_2 + 0.5\ O_2$. The curves of this reaction are placed, nearly completely, in the stability field of hematite (Fig. 6.4) (MATTHES & OKRUSCH, 2005).
But there are also ilmenite and magnetite as opaque phases in the samples. That means a lower f_{O2} or a higher content of H_2, as given in the dissociation reaction of water. One possibility for those conditions is the occurrence of organic material in the lithology or, in higher metamorphosed rocks, graphite.
A first interpretation is given with the equation:

1) $CO_2 \leftrightarrow C + O_2$

The presented reaction is processed mainly in the stability fields of magnetite and wuestite with a fluid pressure in the interval of 10 bar to 10 kbar (Fig. 6.3).
Beside this the following reactions can influence f_{O2} and f_{H2}:

2) $CO_2 \leftrightarrow CO + 0{,}5\ O_2$ and
3) $C + 2H_2 \leftrightarrow CH_4$

CH_4, an indicator for reducing conditions, is determined in fluid inclusions of metamorphic minerals in other places (MATTHES & OKRUSCH, 2005). In graphite bearing metasediments CH_4 can build up a major part of the fluid phase.
Rocks which show anenrichment in Fe are the first places where garnet is developed (YARDLEY, 1997). While heating, the transformation is advanced and the field of possible chlorite composition is restricted more and more. Furthermore the garnet is generated in appreciably Mg-richer lithologies. If the given ratio is higher than 0.5 it is a hint that not the whole bulk of Fe-Mg-chlorites was changed by the following reaction:

4) $Na_{0,5}(Al,Mg)_6(Si,Al)_8O_{18}(OH)_{12}\cdot 5(H_2O) + (KAl_2[(OH,F)_2/AlSi_3O_{10}]) \rightarrow X^{II}{}_3Y^{III}{}_2(SiO_4)_3 + K(MgFe^{2+},Mn^{2+})_3[(OH,F)_2/(Al,Fe^{3+}.Ti^{3+})Si_3O_{10} + SiO_2 + H_2O$

(chlorite + muscovite → garnet + biotite + quartz + water) (YARDLEY 1997)

The chlorite on the left side of the reaction prefers the Mg more than Fe. The result is depletion in Fe in the chlorites during the progression of the reaction. So the Mg-content, visible in Fig. 6.4, is another hint for the dimension the reaction (4) was in progress.
Next to this one can say that Fe-rich chlorites get more and more unstable for rising temperatures, so the content of Fe-chlorites is also a clue for the temperature which was caused by metamorphism in this sample.

Specimens from the boreholes instead show no goethite and seldom hematite in their mineral assemblage but magnetite. Fig. 6.3 displays the correlation of T and f_{O2} and the stability fields of hematite, wuestite, magnetite and elementary iron.

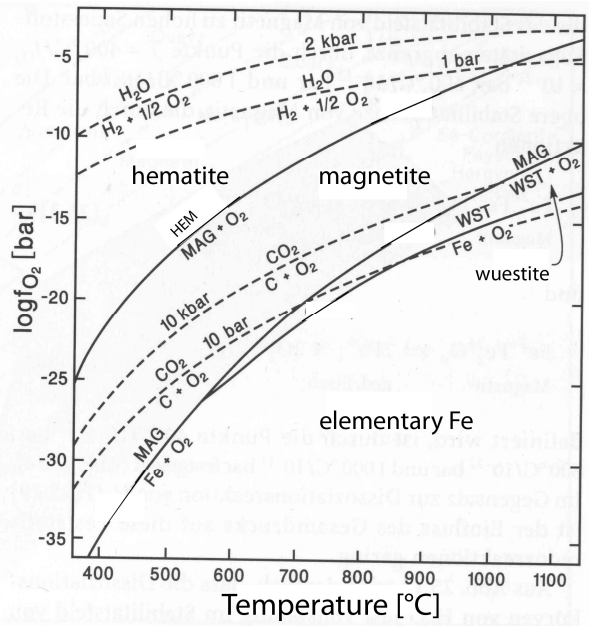

Fig. 6.3: T-f_{O2}-diagram with univariant equilibrium lines and fields of stability of hematite, magnetite, wuestite and elementary iron; the influence of pressure and the solid phases can be neglected (after MIYASHIRO 1973)

The discussed facts were mentioned to demonstrate the conclusions which can be made based on the knowledge about the mineralogy and the chemistry of the samples. So, the occurrence of hematite, magnetite or wuestite suggests certain properties of the fluids. A statement about a temperature can be made if the mineral building reaction is determined.

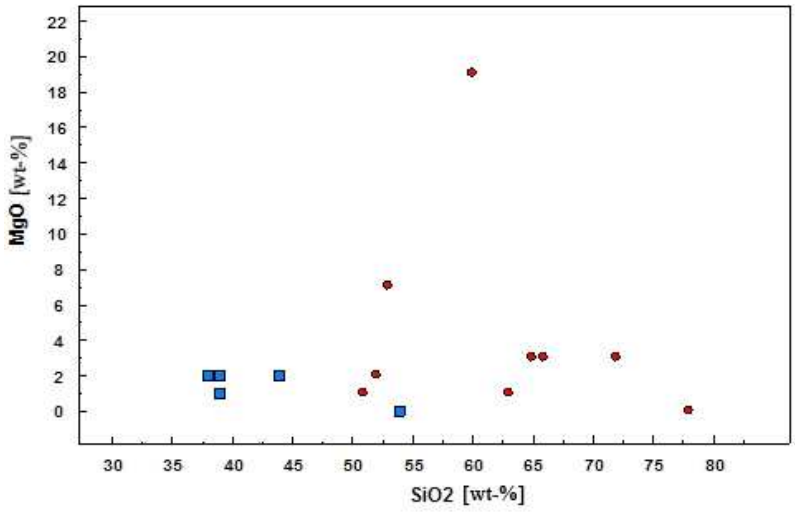

Fig. 6.4: Harker-diagram MgO vs. SiO_2; THS – samples; quadrats = surface samples, spots = borehole samples

The diagram (Fig. 6.4) shows the content of MgO in the sample in dependence on the SiO_2-content in the observed samples from the surface and all boreholes.

Except one sample with a high content in MgO there is trend visible which describes depletion in MgO if the SiO_2 content is rising.

But the content of MgO varies in very low scales so that it is assumable that the content of MgO is not dependent on metamorphic processes in these samples and is controlled mainly by weathering processes, especially in the surface samples. But it is comprehensible that minerals like biotite or tremolite influence the Mg-content dependent on their abundance in the shale. But after a look at the XRF-data (Appendix I) it can be seen that those minerals are not the reason for the MgO-contents.

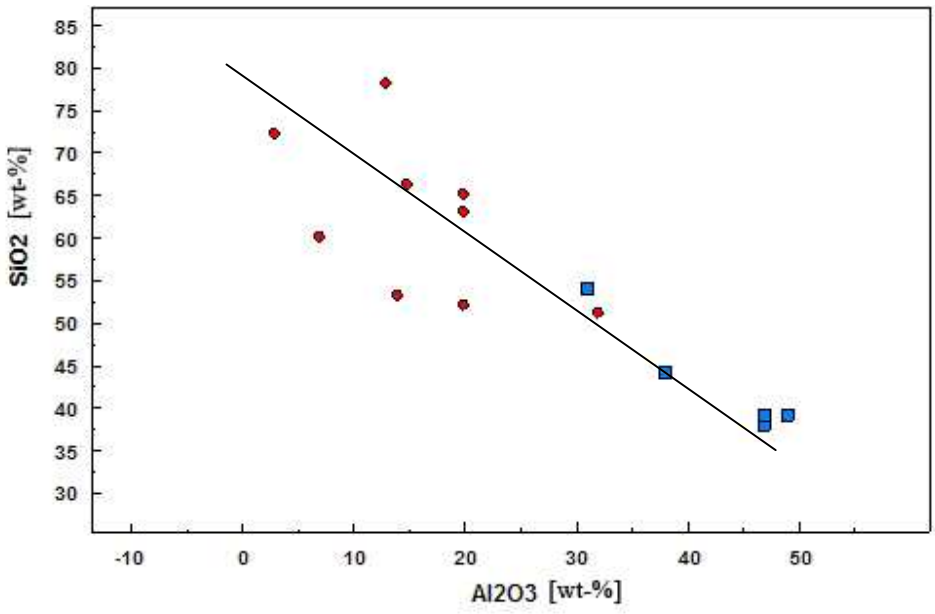

Fig. 6.5: Binary plot Al_2O_3 vs. SiO_2; THS-samples; quadrats = surface samples, spots = borehole samples

The plot above (Fig. 6.5) shows the relation of Al_2O_3 and SiO_2. Both elementoxides are given in wt-%. Obviously there is a negative trend between the both concentrations of Al_2O_3 and SiO_2. Especially the surface samples of the THS are rich in Al_2O_3 and show low contents of SiO_2. The chemistry is also reflected in the mineral assemblage. The surface samples with their high content of Al_2O_3 and low SiO_2 – concentrations host corundum whereas the samples of the boreholes, in the right of the plot, are relatively enriched in SiO_2 and have a lower content in SiO_2. The alumian phases are restricted to sillimanite in major parts. The occurrence of the different Al-minerals is steered by the offer of aluminium on the one hand and of the saturation of SiO_2 or the undersaturation in SiO_2 on the other hand. In systems with an undersaturation in the SiO_2 – phase corundum is generated as Al – mineral. Appropriated for the presentation of the whole rock chemistry are different ternary diagrams. On the one hand ACF – diagrams are used for SiO_2 – saturated systems with the consequence that minerals which were generated in SiO_2 – poor or SiO_2 – free systems, like corundum, cannot be displayed in such diagrams (MATTHES & OKRUSCH, 2005). The possibility of a "corundum + quartz" assemblage was discussed by MOURI et al. (2004). The assemblage is limited to a small number of places in the world which show ultra-high grade metamorphic terrains ($T \geq 1000°C$) with an intermediate pressure of 12 kbar. For that reason the system $CaO – SiO_2 – Al_2O_3$ is used additionally. Former studies (ARAMAKI & ROY, 1963; KROGH, 1977; GUIRAUD et al., 1996; SHAW & ARIMA, 1998) advance the view that a thermodynamic equilibrium of this assemblage is possible. But new thermodynamic datasets suggest that the "corundum + quartz" assemblage is metastable over all geological conditions (HARLOV & MILKE, 2002). Such assemblages are existent in surface samples of the Timeball Hill Shale.

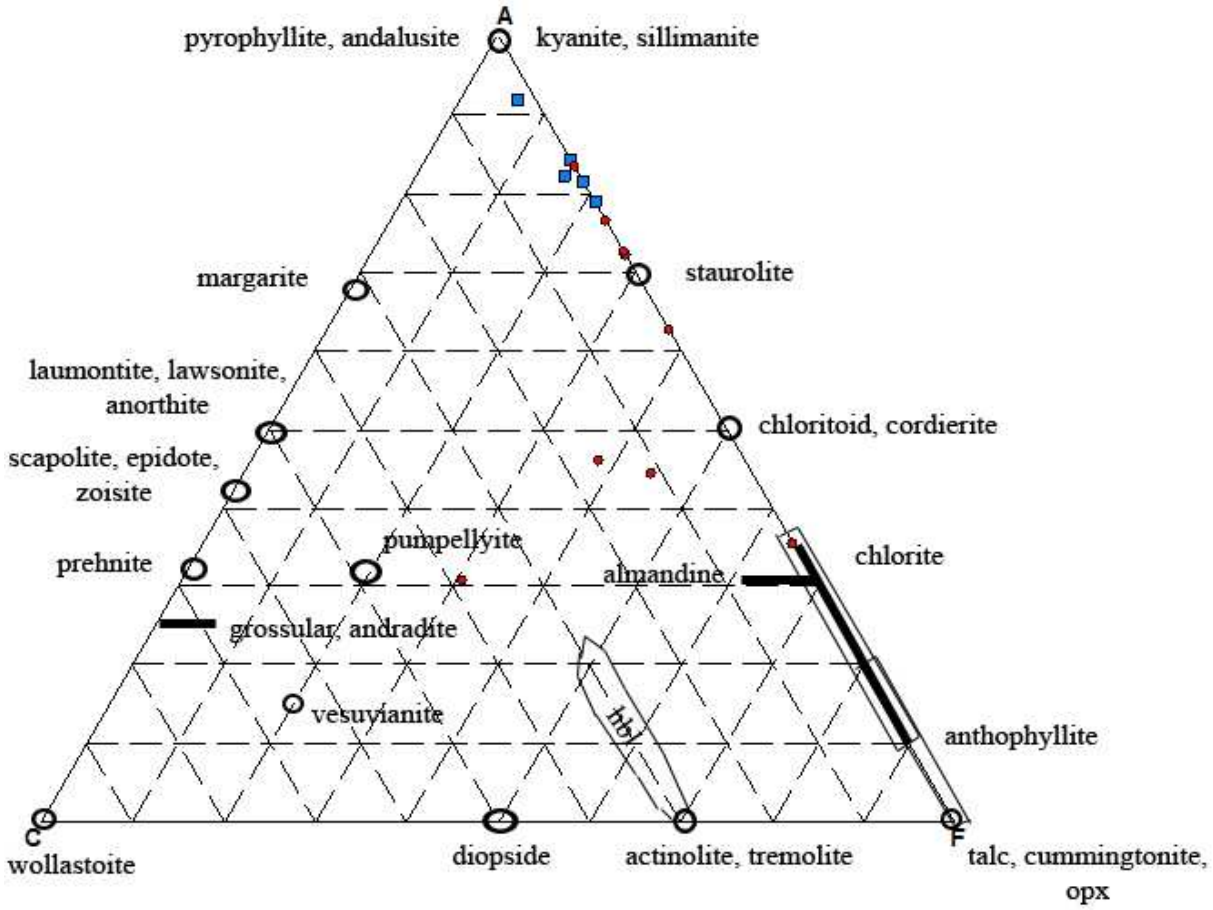

Fig. 6.6: AFC – diagram (after WINKLER 1979) for THS – samples with mineralogy; quadrats = surface samples, spots = borehole samples

The plot above (Fig. 6.6) illustrates the chemistry and the resulting mineral assemblages for all samples of the Timeball Hill Shale in an ACF – diagram with 3 vertices. Each of the vertices is a sum of the content of different elementoxides. Corner "A" is calculated by the following equation: $A = [Al_2O_3] + [Fe_2O_3] – ([Na_2O] + [K_2O])$. Vertex "C" conforms to [CaO]. The corner "F" is the sum of [MgO], [FeO] and [MnO]. The system is valid for parageneses which show saturation in SiO_2.

The samples presented by the quadratic symbols are the surface samples of the Timeball Hill Shale whereas the spots stand for the borehole samples of the Timeball Hill Shale. In the near of the A-vertex the plot show the sample from the surface. The placement in this area of the ternary diagram means a high Si-Al phase. Especially JK-40 shows high contents in Al_2O_3. The

sillimanite-bearing sample of JK-41 is also located in the top of the plot near the A-vertex. The disadvantage of the plot is that Si-free minerals like corundum can not be displayed. For that reason and completing the discussion and the analyses of the geochemistry a new triangular plot is implemented now, the system Al_2O_3 – CaO – SiO_2.

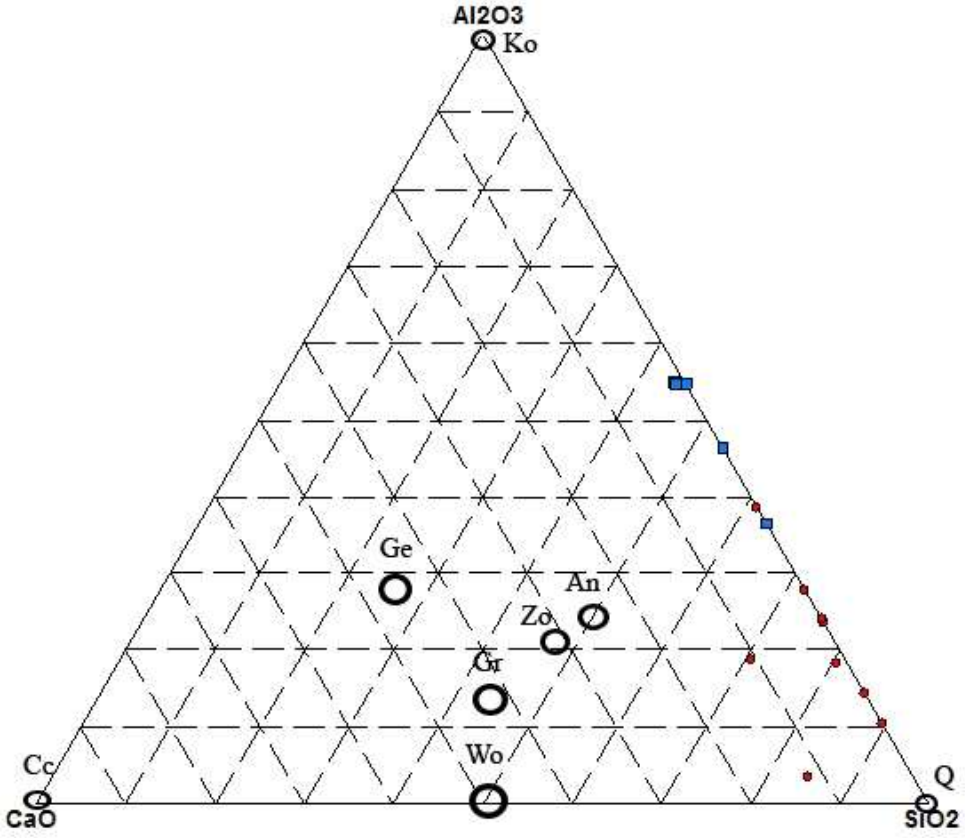

Fig. 6.7: Triangular plot of the system CaO – Al_2O_3 – SiO_2 with THS – samples with mineralogy; quadrats = surface samples, spots = borehole samples; Cc = calcite, Wo = wollastonite, Q = quartz, Gr = grossular, Zo = zoisite, An = anorthite, Ge = gehlenite, Ko = corundum after STORRE (1970)

At the line SiO_2 – Al_2O_3 the majority of the samples are located in the plot (Fig. 6.7). That is caused by the existence of Si-Al minerals, like sillimanite, in the specimens and also by the presence of corundum a SiO_2 – free phase in the mineral assemblage of the surface samples. In the samples of the boreholes no corundum is observed but sillimanite is common. The both projections (Fig. 6.6 & Fig. 6.7) show confirming results to the XRD and microscopy observation. The following triangular plot (Fig. 6.8) shows the educts which are the chemical

source for the different parageneses. But they are just showing the lithotype of the educt based on the chemistry of the samples.

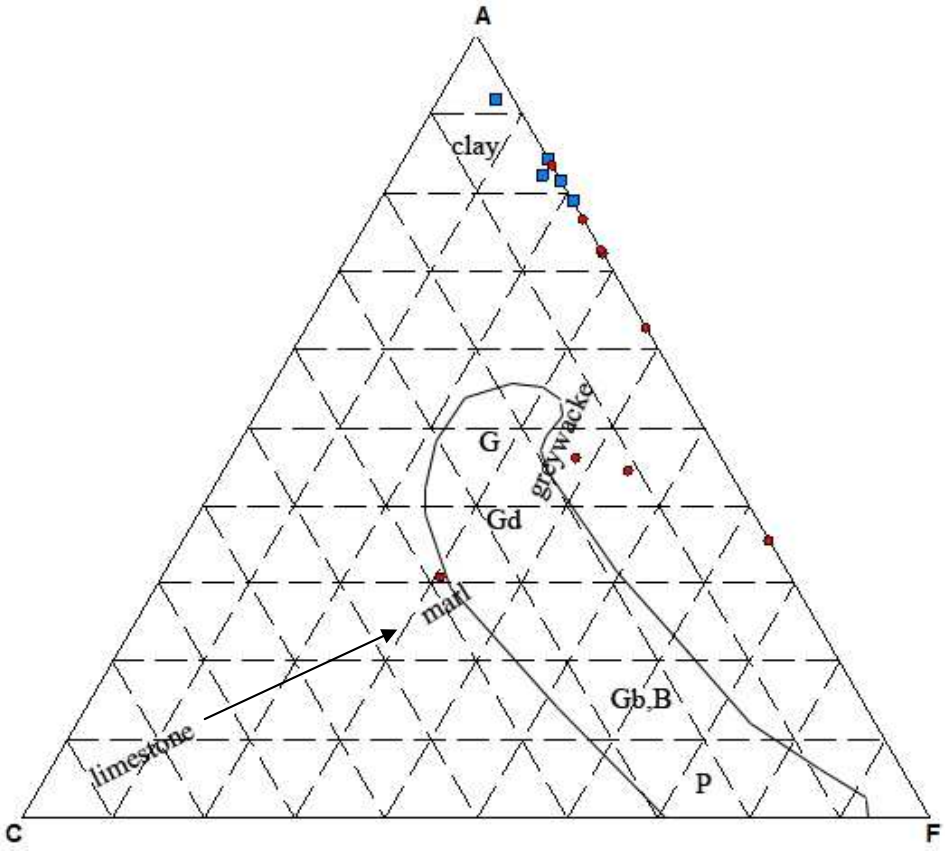

Fig. 6.8: ACF – diagram displaying the educts of important sedimentary and magmatic lithotypes after MATTHES & OKRUSCH (2005); G = granite, Gd = Granodiorite, Gb = gabbro, B = basalt, P = peridotite

Figure 6.8 shows that the educts of the Timeball Hill Shale samples are generated of clay in major parts and in exceptions out of greywackes (arkoses). An arkose is characterized by a content of feldspars of 25 % in minimum (FÜCHTBAUER, 1988).The feldspars are decomposed to clay. Arkoses contain calcite, sometimes silicate and Fe-oxides. Because of the isochemistry of metamorphism the original chemistry is directly detectable in the geochemistry of the metapelites.

6.2.3.1 Distance dependent geochemistry

Subsequent the chemical data is presented in different distances from the contact with the aim to recognize geochemical trends. The zones can but don't have to correspond to the mineralogical zones which were introduced in chapter 5 of this thesis. Of course the transitions between the different chemistries are more smoothly but the bars show the variation in a more obvious way.

The following table 6.4 exposes the different composition in major elements in different distances from the contact

.Table 6.4: Chemical composition of the Timeball Hill Shale samples in several distances from the contact

	0 - 50 m	**50 - 100 m**	**100 - 150 m**	**150 - 200 m**	**200 - 250 m**	**250 - 300 m**
SiO_2	55.92	63.39	72.11	65.05	46.16	59.39
Al_2O_3	19.98	20.84	14.16	20.27	32.87	24.19
Fe_2O_3	11.15	7.02	1.13	4.69	8.87	6.34
MnO	0.06	0.04	0.02	0.06	0.39	0.07
MgO	10.93	1.81	1.96	3.21	3.51	4.28
CaO	0.61	0.39	0.87	0.55	3.01	2.73
Na_2O	1.02	0.28	0.29	1.39	2.34	1.36
K_2O	1.61	6.50	10.21	4.89	2.65	2.04
TiO_2	0.61	0.81	0.57	0.64	1.31	0.42
P_2O_5	0.20	0.09	0.09	0.08	0.16	0.05

Variations in the major elements are due to the different mineral assemblages in the different zones and to the diverse influence of metasomatic and metamorphic processes at the mineral assemblage.

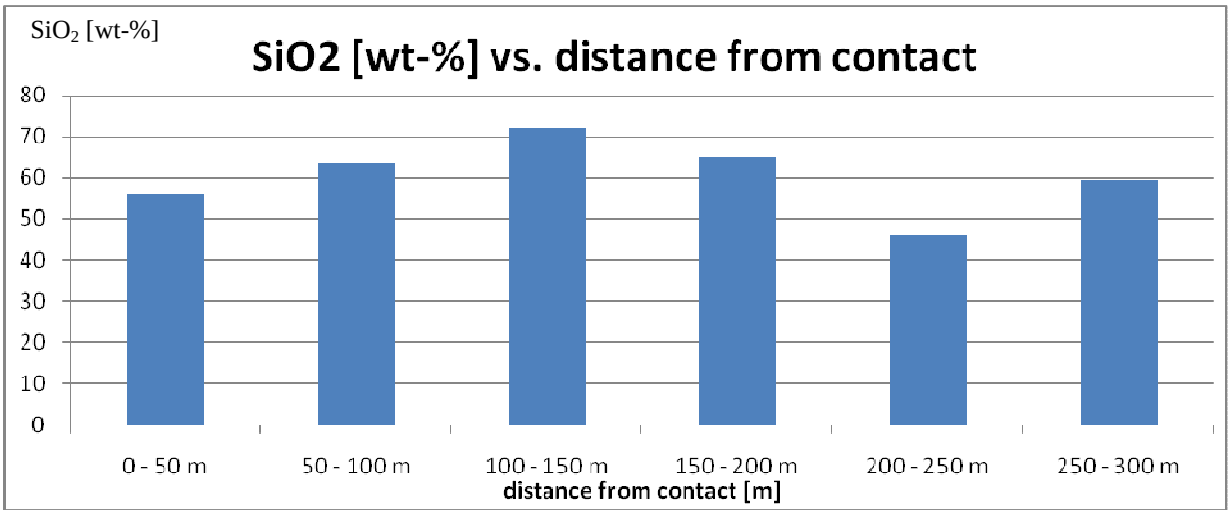

Fig. 6.9: Contents of SiO_2 in the THS-samples in wt-% in several distances from the contact

As visible in Fig. 6.9 the content of the SiO_2-phase shows a maximum in a distance from 100 to 150 m. Away from the contact zone to the named distance of 100 m the value for SiO_2 increases. The area with the minimum in the SiO_2-content is from 200-250 m, the zone where only corundum and no sillimanite is developed and the system is undersaturated in SiO_2. A different geochemical background results in a varying mineralogy next to this zone in a distance from 250 m also cliinochlore, sillimanite and chlorite serpentine are common.

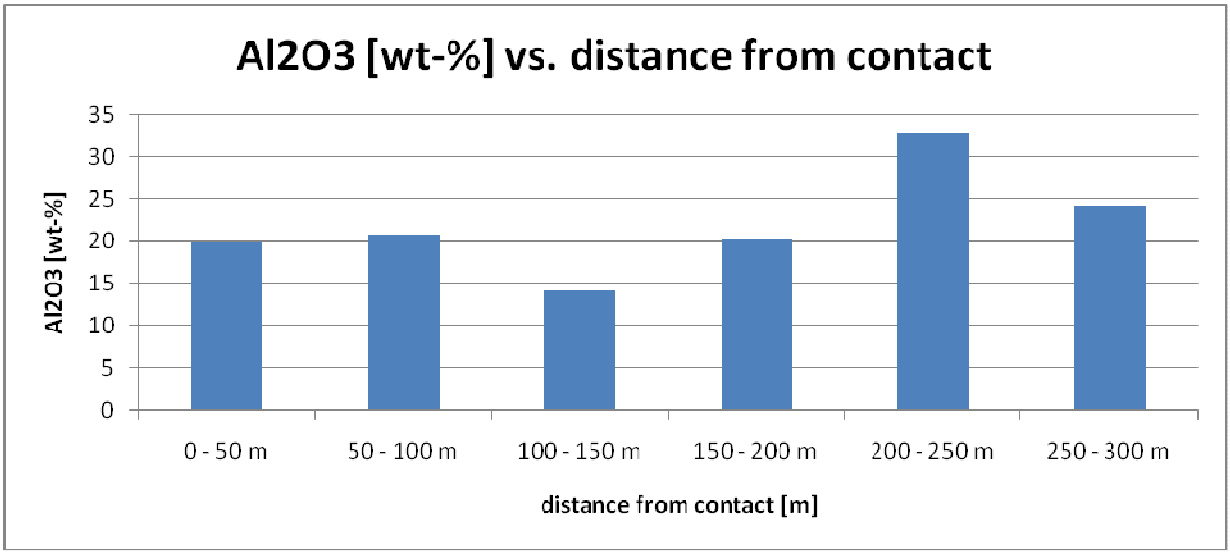

Fig. 6.10: Contents in Al_2O_3 in wt-% in several distances from the contact (THS)

The bars diagram in Fig. 6.10 shows the content in Al_2O_3 in wt-% for the samples of the Timeball Hill Shale in the known certain distances from the contact. The high content of Al_2O_3 up to 100 m away from the contact is due to the mentioned increasing insertion of Al for Si in silica-minerals in high-temperature environments. But the high contents of Al in the zones more far from the contact (over 150 m) are due to the probably high contents in Al_2O_3 in the educts of the metapelites. Nevertheless also the relatively enrichment in Al_2O_3 at an expense of other elementoxides like SiO_2 is common especially in the surface near samples which were gained in distances from the contact of 240 – 300 m. Remarkable again is the maximum of Al_2O_3 in the corundum-rich zone.

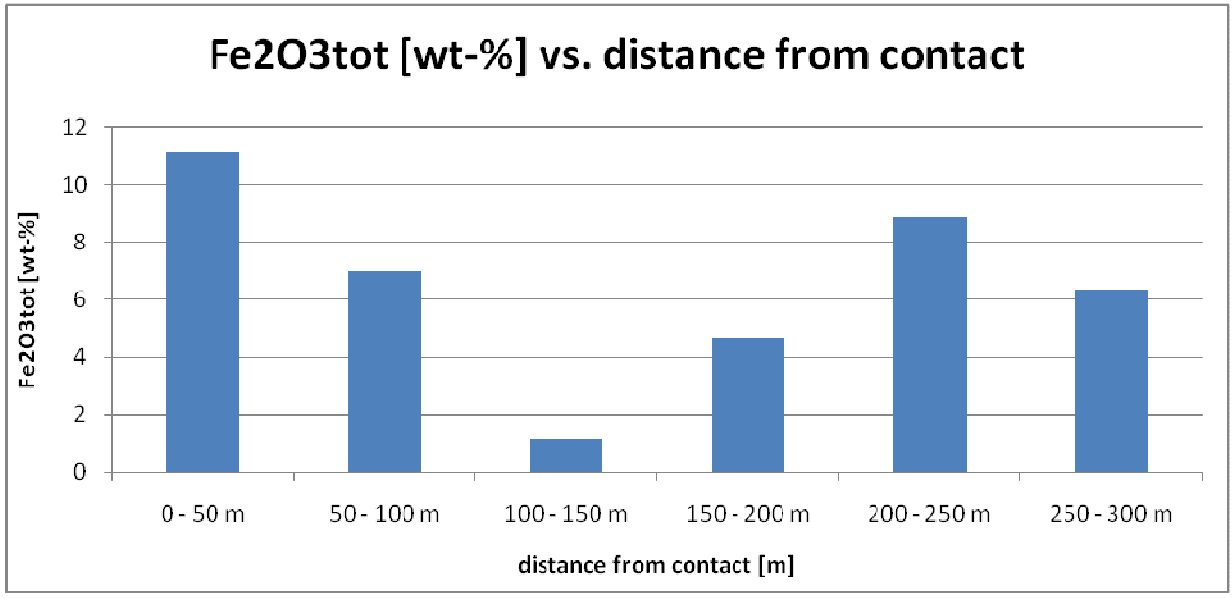

Fig. 6.11: Contents in Fe_2O_{3tot} in wt-% in several distances from the contact (THS)

The contact zone, as visible in Fig. 6.11, is enriched in Fe_2O_{3tot}, a sign for a metasomatism which delivers Fe in a great extent. In the area from 100 – 150 m away from the contact Fe is relatively depleted because of the high values in SiO_2.

The plot below 6.12 displays the content of MgO in relation to the distance from the contact zone. As it is expectable MgO shows a nearly similar geochemical behaviour like Fe_2O_{3tot}. First of all MgO shows also an enrichment in the contact near zone. So it is detectable that there was not only a Fe-metasomatism but rather a Fe-Mg-metasomatism.

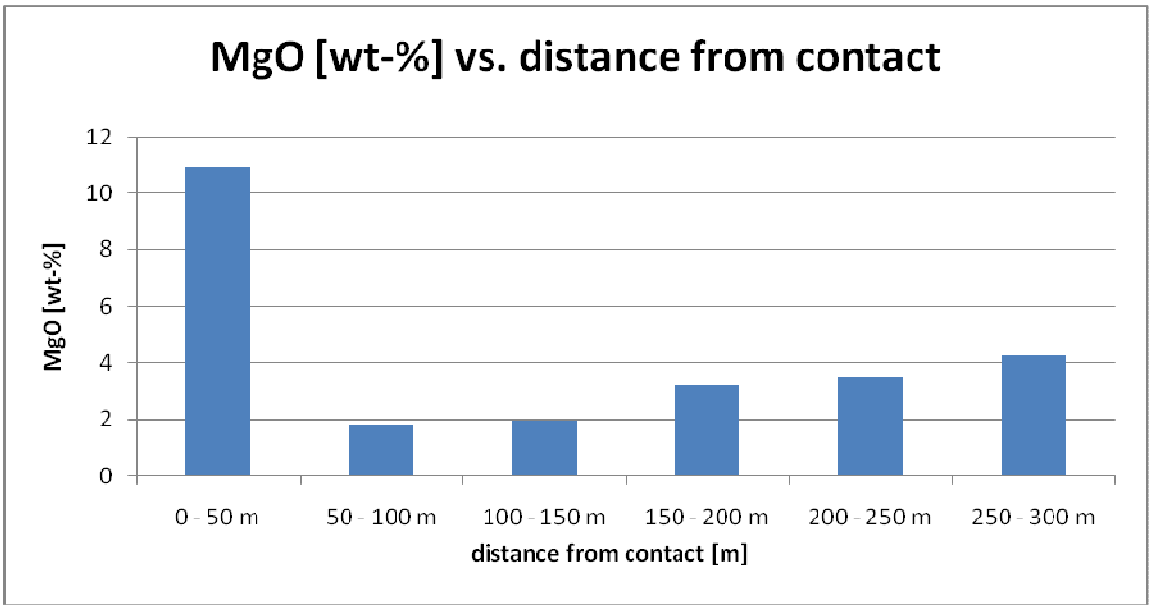

Fig. 6.12: Contents in MgO in wt-% in several distances from the contact (THS)

Investigations with the XRD suggest the existence of Cr-bearing minerals like Cr-bearing chlorite for example. That is the reason for the presentation of the different values of Cr in the several ranges. So Fig. 6.13 exposes this correlation.

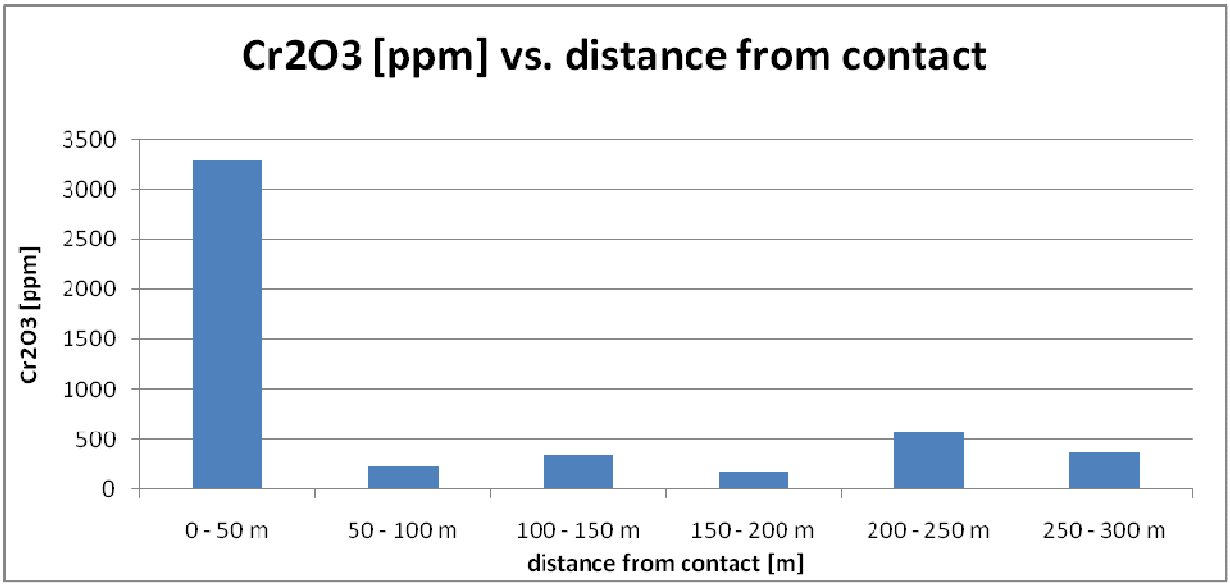

Fig. 6.13: Contents in Cr_2O_3 in wt-% in several distances from the contact (THS)

The bars in Fig. 6.13 support the assumption that there is also an enrichment of Cr in the contact-close area. The rest of the values are varying in a small way which can be neglected.

6.2.4 Phase relations in the Timeball Hill Shale

Based on field observations, XRD-analyzes and the chemical analyze of the specimens a reconstruction of the most important mineral reactions and transitions was processed. In the contact-area (0 – 50 m) sillimanite and muscovite is developed next to minerals of the serpentine group like antigorite or chlorinated serpentine. The common occurrence of K-feldspar and sillimanite, like in the samples of this area, is an indicator for a high-grade metamorphic environment (MATTHES & OKRUSCH, 2005). Because of the presence of serpentine phases, especially antigorite and a direct neighbourhood to the contact suggest the following reaction which is shown in Fig. 6.14. The pressures in the near of the contact can be estimated with $p \leq 1.5$ kbar. The pressure is 0.7 kbar in minimum because of the generation of epidote in this area of the Complex. The generation of epidote is combined with a pressure of 0.7 kbar (PICHLER & SCHMITT-RIEGRAF, 1993).

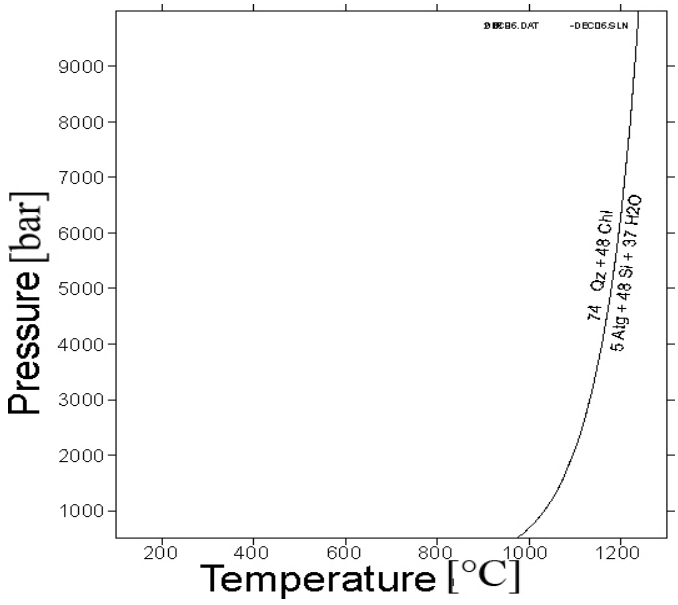

Fig. 6.14: Reaction of quartz (qz) and chlorite (chl) to antigorite (atg), sillimanite (si) and water (H_2O) calculated with TWQ (BERMAN 2006)

In consideration of a pressure of 1.5 kbar, typical for contact-metamorphic environments (WINKLER, 1979) the maximal temperature in this area can be estimated with approximately 1100 °C.
The occurrence of sillimanite in regions which are more distant from the contact can be explained corresponding to the mineral assemblage with the following reactions:

5) Muscovite ($KAl_2[(OH,F)_2/AlSi_3O_{10}]$) + Quartz ($SiO_2$) →K-feldspar ($KAlSi_3O_8$) + Sillimanite ($Al_2SiO_5$)

After KERRICK (1972) the reaction predicts temperature of ca. 600°C and pressures of nearly 2kbar. The accumulation of sillimanite by the reaction of corundum with quartz is improbable because the reaction is processed at pressures ≥ 6 kbar (BERMAN, 2006).
For the crystallization of the common tremolites is the following reaction the most probable one. But the reaction could not be evidenced because of the lack of epidote in the samples.
For the creation of tremolite the following equation is assumable.

6) Mg-Al-pumpellyite ($Ca_2MgAl_2(SiO_4)(Si_2O_7)(OH)_2\cdot(H_2O)$ + chlorite ($Na_{0,5}(Al,Mg)_6(Si,Al)_8O_{18}(OH)_{12}\cdot 5(H_2O)$) + quartz ($SiO_2$) → epidote ($Ca_2(Fe^{3+},Al)_3(SiO_4)_3(OH)$) + tremolite ($Ca_2Mg_5Si_8O_{22}(OH)_2$) + water ($H_2O$)

This reaction is independent of pressure to 6 kbar and takes places at a temperature of ca. 310°C (BUCHER & FREY 2002).

The [aug-atg]-zone is a kind of transisition zone with diospide as predominating mineral and a temperature between the temperatures of the [sil]-zone and the [san]-zone.

The next zone where a modelling concerning the temperature is possible is the “sanidine-zone” [san]. Under consideration of the mineral assemblage following reaction was determined (Fig. 6.15).

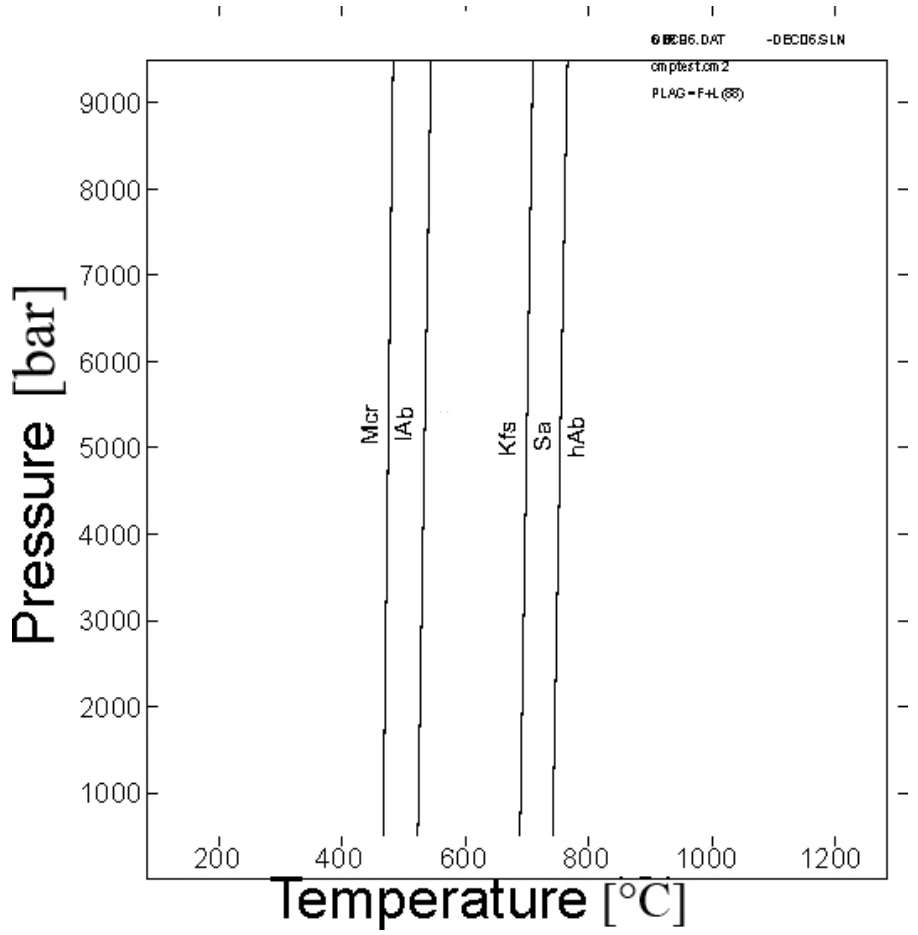

Fig. 6.15: Stability fields of microcline (mcr), low albite (lAb), kalifeldspar (kfs), sanidine (sa) and high albite (hAb) calculated with TWQ (BERMAN 2006)

The occurrence of sanidine leads to the assumption that the temperature in this area was about 700°C. The presence of high albite, detectable with XRD, in the area between the [sil]-zone and the [san]-zone means temperatures of ca. 750 °C in minimum. The reaction is relatively independent from pressure.

In the area between 200 and 250 m away from the contact almandine is the most characteristic mineral. Almandine was investigated in JK-74 with the microprobe (Fig. 6.16 and 6.20).

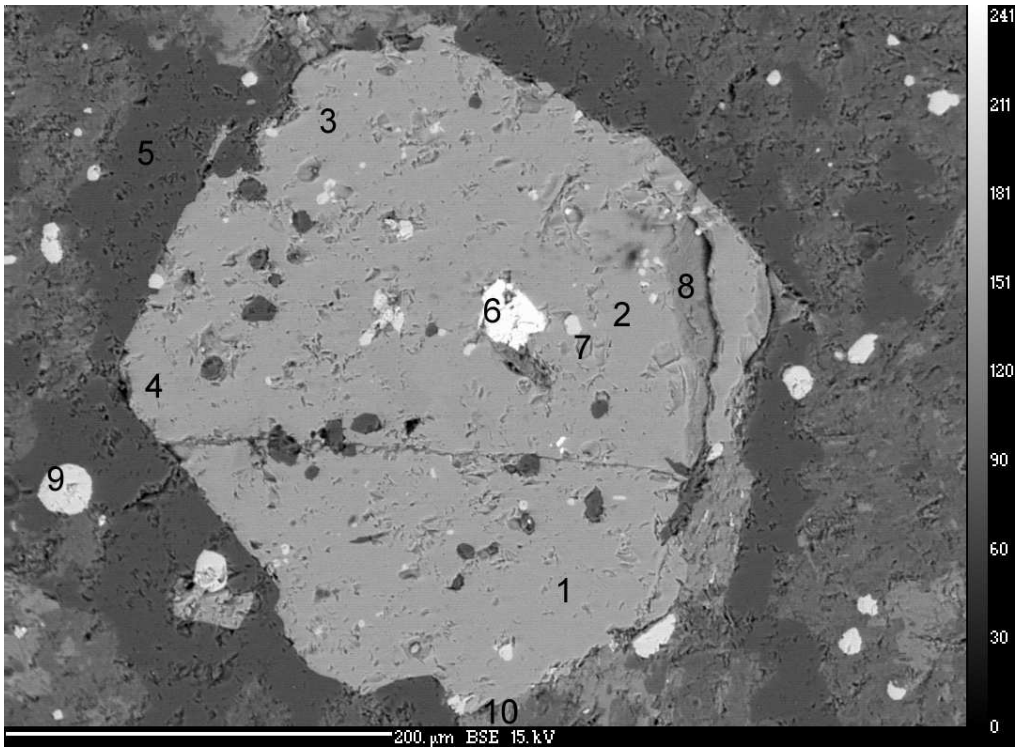

Fig. 6.16: BSE – image of an almandine in JK – 74; points: 1,2,3,4 almandine; 5: quartz; 6: chalcopyrite; 7: ilmenite (Mn-bearing; WDS-spectra in Fig.6.23); 8: chlorite; 9: ilmenite; 10: muscovite

The composition of the almandine measured in the points 1 – 4 is given in the following table 6.5.

Table 6.5: Chemical compositions of almandine (JK-74)

oxide	Oxide (wt-%)	Oxide (wt-%)	Oxide (wt-%)	Oxide (wt-%)
	point 1	point 2	point 3	point 4
SiO_2	36.33	36.41	36.48	36.80
TiO_2	0.20	0.27	0.27	0.20
Al_2O_3	19.05	18.97	19.08	19.80
Fe_2O_3tot	32.03	32.03	31.59	33.42
MnO	7.22	7.10	7.42	6.64
MgO	1.69	1.69	1.59	1.79
CaO	1.27	1.44	1.48	1.22
Na_2O	0.12	0.05	0.09	0.50
K_2O	0.00	0.00	0.00	0.00
Cr_2O_3	0.29	0.32	0.23	0.32
Sum	98.20	98.29	98.25	100.69

Table 6.6: Explicit formulae of the almandine in JK-74

Point no.	**Formula**
1	$Fe_{1.885}(Mg_{0.20},Mn_{0.48})Al_{1.76}[Si_{2.845}O_{12}]$
2	$Fe_{1.885}(Mg_{0.19},Mn_{0.47})Al_{1.75}[Si_{2.845}O_{12}]$
3	$Fe_{1.86}(Mg_{0.185},Mn_{0.49})Al_{1.76}[Si_{2.855}O_{12}]$
4	$Fe_{1.92}(Mg_{0.30},Mn_{0.43})Al_{1.785}[Si_{2.81}O_{12}]$

As visible in JK-74 the almandine in JK-74 shows also a spessartine and a pyrope-component. That means that the almandine contents Mg and Mn. The vacant space in the structure is probably owned by Cr, but the content of Cr is so low that the system error of the EMPA prohibits an implementation of Cr in the formula.

As visible in Fig. 6.16 chalcopyrite (WDS-spectra in Fig. 6.17) is building up a kind of seed crystal. The occurrence of chalcopyrite can be interpreted as a sign for the organic component in the educt of the Timeball Hill Shales. The observation of chalcopyrite is supported by microscopic investigations.

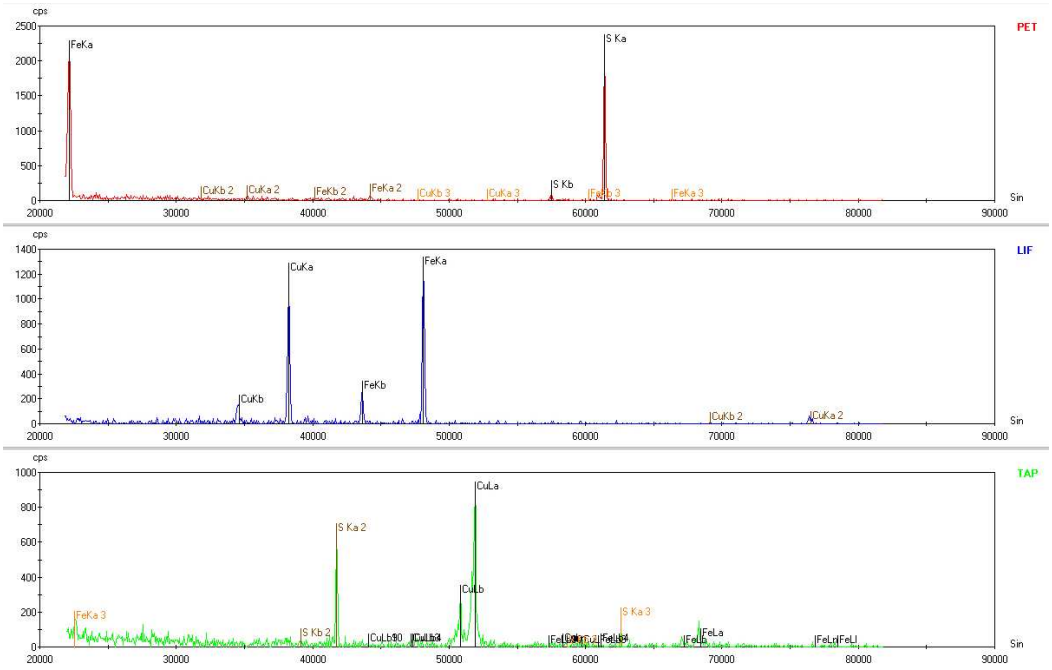

Fig. 6.17: WDS-spectra of the chalcopyrite (point 6) in JK-74; Fig. 6.16

The presence of muscovite means that the almandine was generated in medium-grade metamorphic conditions. The border of the medium to the high-grade metamorphism is marked by the breakdown of muscovite in the presence of quartz and plagioclase (WINKLER, 1979). Following reaction is responsible for the creation of almandine:

7) $Na_{0.5}Al_4Mg_2Si_7AlO_{18}(OH)_{12}\cdot 5(H_2O) + Fe^{2+}{}_{1.2}Mg_{0.6}Mn^{2+}{}_{0.2}Al_4Si_2O_{10}(OH)_4 + SiO_2 \leftrightarrow Fe^{2+}{}_3Al_2(SiO_4)_3 + H_2O$

(chlorite + chloritoide + quartz ↔ almandine + water)

This reaction is a sign for the epidote - amphibolite facies a subfacies of the amphibolites facies. This facies is the continuation of the stability fields of the greenschist facies under conditions of

higher p and T. Also remarkable is that this facies is equal to the almandine zone of Barrow (MATTHES & OKRUSCH, 2005). Like in the greenschist facies epidote is stable next to albite. But in contrast to the greenschist facies there is Almandine-rich garnet instead of Fe-rich chlorite.

The chlorite in this "almandine zone" is Mg-rich and coexists with almandine, chloritoide and biotite in dependence of the chemical composition. The area of the facies is given by p-T combinations of 460°C/9kbar, 500°C/3 kbar and 660°C/11,5 kbar (MATTHES & OKRUSCH, 2005).

The almandine can also be generated out of the reaction of staurolite with quartz. Reactants of this reaction will be almandine and andalusite/sillimanite/kyanite. But there is no staurolite detected in the observated samples of the Timeball Hill Shale reasoned in the ratios of Fe_2O_3tot/MgO and Al_2O_3/(CaO+K_2O+Na_2O) which are obviously to low (Fig. 6.18).

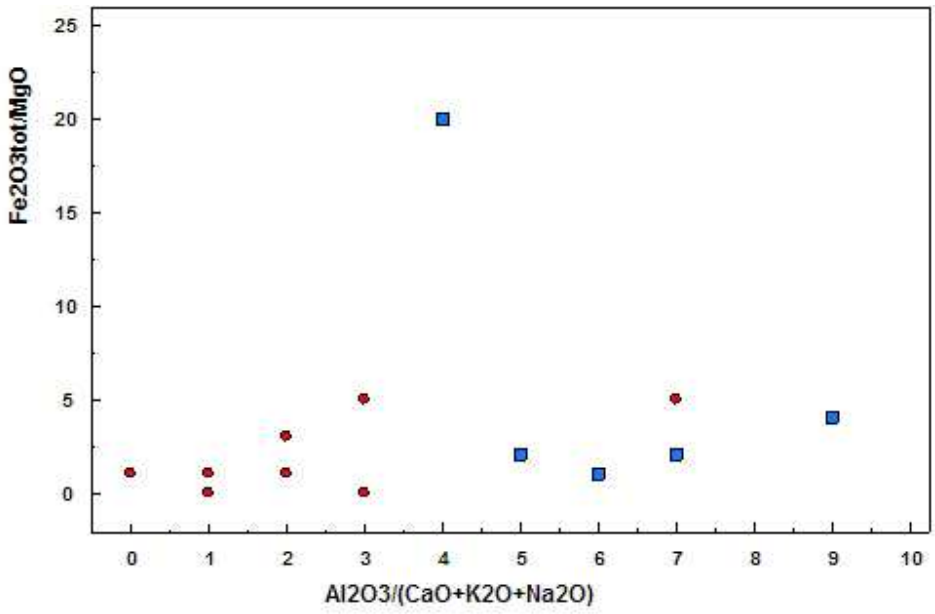

Fig. 6.18: Bivariate plot Fe_2O_3tot/MgO vs. Al_2O_3/(CaO+K_2O+Na_2O – diagram; quadrats = surface samples, spots = borehole samples

That is the reason why the possibility of a creation of almandine out of staurolite is not possible. But beside the reaction (7) given above is the following reaction no. 8):

$KAl_2[(OH,F)_2/AlSi_3O_{10}] + K(MgFe^{2+},Mn^{2+})_3[(OH,F)_2/(Al,Fe^{3+}.Ti^{3+})Si_3O_{10} + SiO_2 \leftrightarrow$
$Fe^{2+}{}_3Al_2(SiO_4)_3 + K(MgFe^{2+},Mn^{2+})_3[(OH,F)_2/(Al,Fe^{3+}.Ti^{3+})Si_3O_{10} + Al_2SiO_5 + KAlSi_3O_8 + H_2O$

(muscovite + biotite$_1$ + quartz ↔ almandine + biotite$_2$ + sillimanite + K-feldspar + water)

Biotite$_1$ and biotite$_2$ are different concerning their Fe/Mg – ratio. The ratio in biotite$_1$ is higher as in biotite$_2$. But this reaction would be end in an increase of the feldspar-mica ratio. The result would be metapelites which are preferential developed as paragneisses (MATTHES & OKRUSCH, 2005).

But the samples cannot be described as paragneisses. The other possibility for the generation of almandine is not probable, because of the metamorphic conditions which were needed were not processed in the Timeball Hill Shales.

So it can be assumed that reaction (7) is the equation which is responsible for the creation of almandine.

It has, however, to be kept in mind that not only the temperature and the pressure are the steering impacts of metamorphic crystallisation. Also the influence of the oxygen fugacity is of an eminent importance for the reactions in the Timeball Hill Shales. Next to f_{O2} the fugacity of hydrogen (f_{H2}) is from minor importance. Water is released by dehydration reactions like the muscovite breakdown. But there are no hints in the samples that this transformation was processed in the distinct distances from the contact which are represented by the samples. An evidence for the impact of the O_2-fugacity is the occurrence of ilmenite (Fig. 6.20) in the samples which can also be seen in Fig. 6.16 the BSE-picture of an almandine in JK – 74. In other places it is visible that the almandine grain is accumulated around a quartz grain which is an evident for the generation of almandine after the equation no. 7. An example for such an assemblage is given in Fig. 6.19.

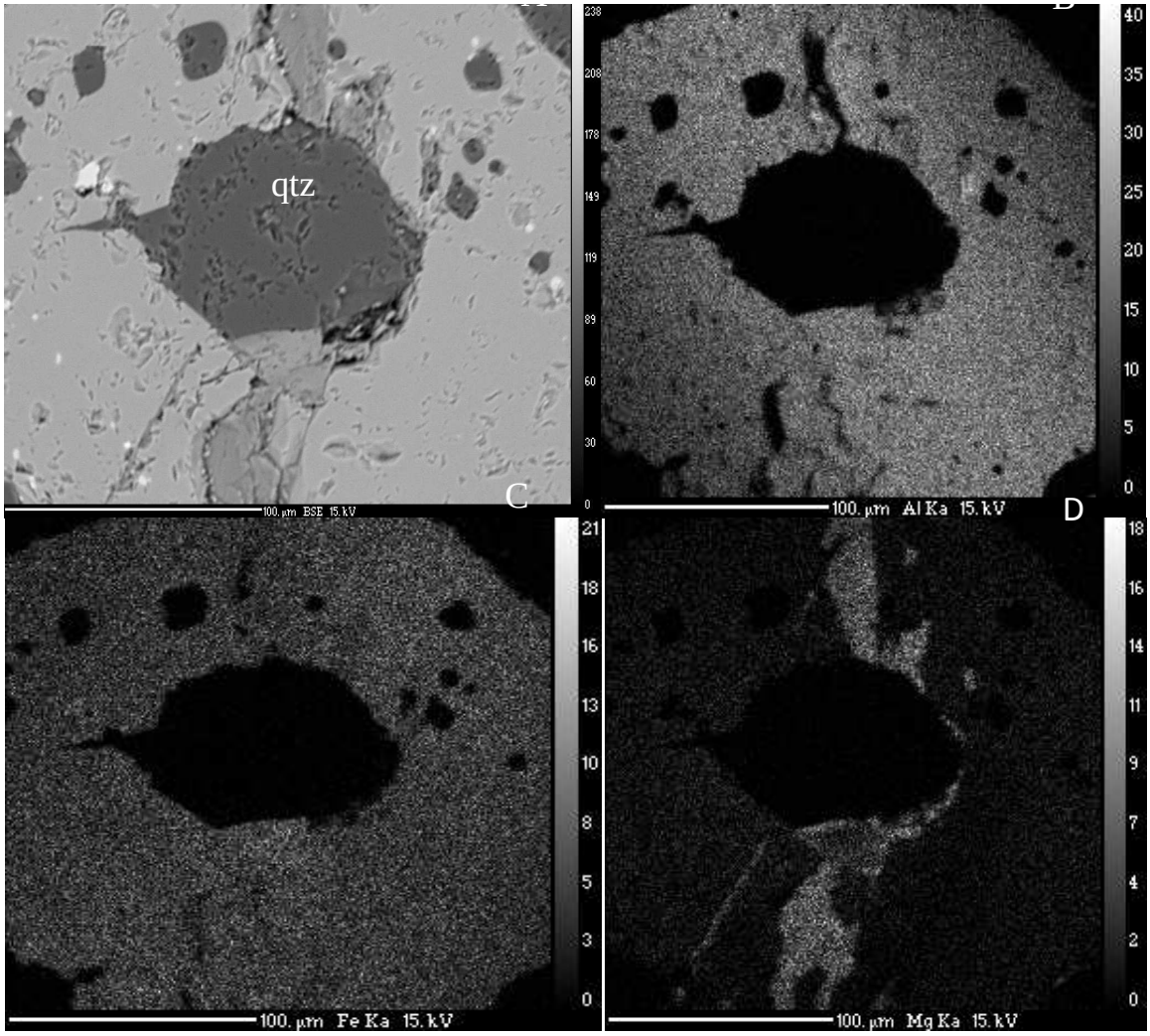

Fig. 6.19: Element mapping of an almandine in JK-74; A) BSE-image of an almandine in JK – 74; grain of quartz in the centre; B) Al-distribution; C) Fe-distribution; D) Mg-distribution

The images above show an almandine-rich garnet with a quartz grain in its center. Fe and Al show the same distribution in the almandine. Mg is concentrated in a vein. The composition in this vein includes the elements Fe, Al and Mg. So it is ascertainable that there is no garnet in this vein but an Mg-Fe-Al mineral, probably a chlorite.

The conclusion of the descriptions is an estimation of the temperature in the Timeball Hill Shales during the emplacement of the Complex. At pressures about 3kbar the almandine is generated at temperatures of ca. 500°C (MATTHES & OKRUSCH, 2005).

The fact that sillimanite can also be found in the observed samples allows two reactions which can create almandine.

Reaction (7) is the reason for the accumulation of almandine without the production of sillimanite. In contrast to this reaction stands the reaction no. (8) which produces sillimanite next to almandine. In the sample JK – 74, where almandine was proved, no sillimanite was detected. That makes it plausible that reaction (7) was responsible for the crystallization of almandine.

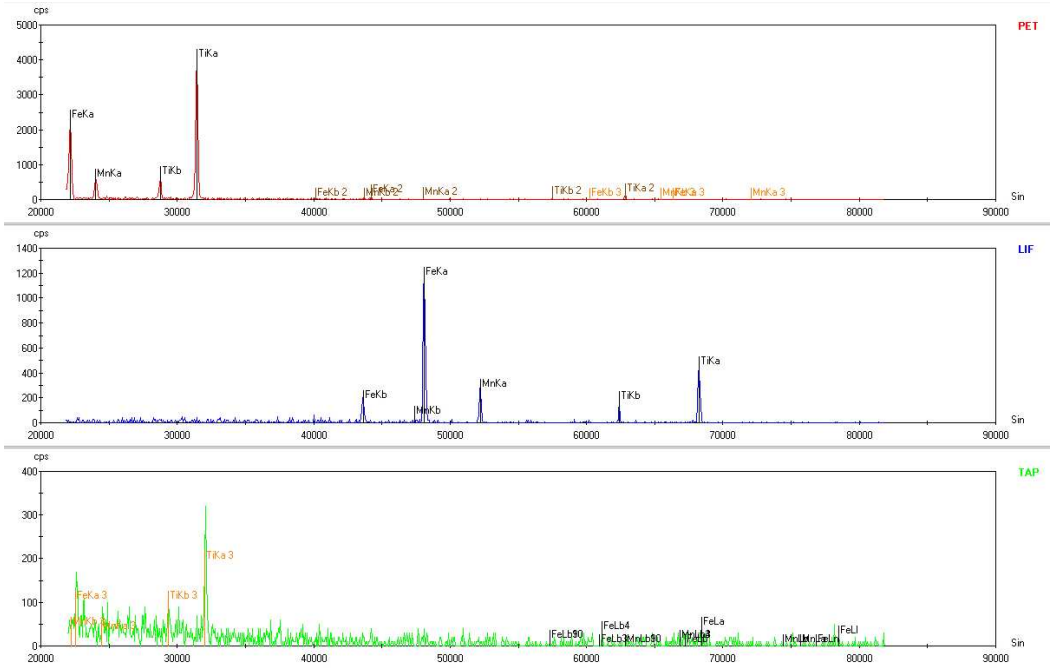

Fig. 6.20: WDS-spectra of the Mn-bearing ilmenite (point 7) in JK-74; Fig. 6.16

The last determined mineral-zone in the Timeball Hill Shale is in a distance from 250 – 300 m the corundum zone [cor]. The educts for the corundum – bearing surface samples were rich in Al_2O_3 and depleted in SiO_2. The corundum is generated in the following way:

9) gibbsite (γ-$Al(OH)_3$) →boehmite (γ-AlO(OH)) → diaspore (α-AlO(OH)) →corundum (Al_2O_3) + water (H_2O)

Explicit the corundum is generated through:

9a) 2(α-AlO(OH)) →Al_2O_3 + H_2O

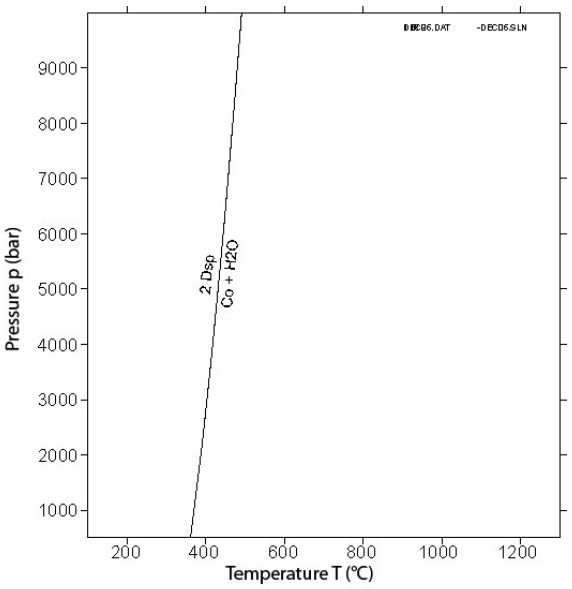

Fig. 6.21: Stability fields for the reaction from diaspore (dsp) to corundum (co) and water; calculated with TWQ (BERMAN 2006)

at the entry of the greenschist facies. The pressure dependence of this reaction is relatively low and can be estimated with an average temperature increase of 5°C/1000 bars (WINKLER, 1965). In the diagram on the left hand side the intersection for one of the first reactions of the greenschist facies: diaspore →corundum (Fig. 6.21). The image shows that the accumulation of corundum is relatively independent from pressure. The generation of corundum starts at approximately 400°C.

6.3 Bevets Conglomerate

The samples of the Bevets Conglomerate are no prior indicators for the reconstruction of the metamorphic conditions. The behaviour under metamorphic and metasomatic impacts is similar to the behaviour of the Malmani Dolomite samples, but in a much smaller scale.
That is why the Conglomerate is omitted at this chapter. The Conglomerate is partly represented, concerning the physicochemical properties, by the Malmani Dolomites.
The chemical composition in form of the XRF-data is given in Appendix I.

6.4 Malmani Dolomite

6.4.1 Chemical composition

Table 6.7: Chemical composition of all samples (surface + boreholes) of the Malmani Dolomite

	average content	Max	Min	standard deviation
	[wt-%]	[wt-%]	[wt-%]	
SiO_2	50.33	92.09	15.86	19.45
Al_2O_3	4.87	28.62	0.05	7.45
Fe_2O_3	7.25	15.91	1.16	5.05
MnO	0.23	0.57	0.02	0.14
MgO	14.30	32.18	1.51	8.24
CaO	21.08	55.91	0.04	15.16
Na_2O	0.47	4.44	0.00	1.12
K_2O	0.39	3.39	0.00	0.90
TiO_2	0.42	2.87	0.00	0.84
P_2O_5	0.09	0.58	0.01	0.15

Table 6.7 shows the average composition of the surface and the borehole samples of the Malmani Dolomite. Especially the values for SiO_2 and CaO vary strongly. These both elementoxides are the main components of the calc-silicate felses which are the main constituents of the Malmani Dolomite. The maximum in quartz-content is shown by the sample JK-78 which is located about 100 m away from the contact. JK-89, a sample from the contact zone, shows the maximum value of CaO-content. With 32.18 wt - % JK-50 has the highest content in MgO. But overall it is visible

that the contents of the different elementoxides are varying in a high degree. Those variations are caused by the different position of the samples in the surrounding of the Uitkomst Complex. Beside they are due to the different susceptibility for metamorphic and metasomatic processes.

6.4.2 Pearson Correlation

Table 6.8: Pearson Correlation – Surface samples Malmani Dolomite; n = 5, green: r ≥ 0.5; red: r ≤ -0.5

		SiO2	Al2O3	Fe2O3	MnO	MgO	CaO	Na2O	K2O	TiO2	P2O5
SiO_2	Pearson Correlation	1	-0.271	-0.491	-0.749	-0.691	-0.706	.939(*)	0.321	-0.201	-0.288
Al_2O_3	Pearson Correlation	-0.271	1	0.802	0.018	0.306	-0.155	0.039	0.637	.995(**)	-0.250
Fe_2O_3	Pearson Correlation	-0.491	0.802	1	0.174	0.537	-0.045	-0.289	0.468	0.812	0.301
MnO	Pearson Correlation	-0.749	0.018	0.174	1	0.047	.970(**)	-0.669	-0.071	-0.063	0.497
MgO	Pearson Correlation	-0.691	0.306	0.537	0.047	1	0.013	-0.721	-0.455	0.292	-0.008
CaO	Pearson Correlation	-0.706	-0.155	-0.045	.970(**)	0.013	1	-0.677	-0.253	-0.243	0.389
Na_2O	Pearson Correlation	.939(*)	0.039	-0.289	-0.669	-0.721	-0.677	1	0.590	0.100	-0.367
K_2O	Pearson Correlation	0.321	0.637	0.468	-0.071	-0.455	-0.253	0.590	1	0.669	0.058
TiO_2	Pearson Correlation	-0.201	.995(**)	0.812	-0.063	0.292	-0.243	0.100	0.669	1	-0.239
P_2O_5	Pearson Correlation	-0.288	-0.250	0.301	0.497	-0.008	0.389	-0.367	0.058	-0.239	1

The Correlation above shows some relations which are not confirming with the real mineral assemblage. The negative correlation of CaO and SiO_2 is in contrast to the occurrence of several Ca-Silicates like in the samples. The reason of this phenomenon is disequilibrium in the mineral assemblage due to metamorphism. The major part of Ca is linked to the calcitic minerals, more explicit calcite, dolomite and ankerite. The positive relation of Fe and Al can be explained with the existence of augite $[Ca_{0.4\text{-}0.9}(Mg,Fe^{2+})_{1.1\text{-}1.6}Si_2O_6]$ which bears Fe and Al. The Al can be inserted in the M2-place that means for Fe or Mg (MATTHES & OKRUSCH, 2005). Another

possibility is the creation of clinoferrisillite [$Fe^{2+}{}_2Si_2AlO_6$] where Al is implemented at the T-position in the general formula of pyroxenes [M1 M2 T_2O_6]. But the existence of clinoferrosillite was not certifiable with the used methods. Also Ti can be a constituent of pyroxenes. The insertion of Ti is a degree for the thermic overprint (MATTHES & OKRUSCH, 2005). The positive correlation between Mg and Fe is based in the common appearance in biotite, hornblendes and diverse pyroxenes.

Table 6.9: Pearson Correlation – Borehols samples Malmani Dolomite; n = 18, green: r ≥ 0,5; red: r ≤ -0,5

		SiO2	Al2O3	Fe2O3	MnO	MgO	CaO	Na2O	K2O	TiO2	P2O5
SiO_2	Pearson Correlation	1	-0.157	-.760(**)	-.739(**)	-0.530	-.673(**)	0.046	0.112	-0.029	0.000
Al_2O_3	Pearson Correlation	-0.157	1	0.328	-0.248	-0.118	-0.496	.738(**)	.748(**)	.595(*)	0.523
Fe_2O_3tot	Pearson Correlation	-.760(**)	0.328	1	0.484	0.193	0.266	0.065	0.120	0.231	0.258
MnO	Pearson Correlation	-.739(**)	-0.248	0.484	1	0.522	.705(**)	-0.297	-0.333	-0.176	-0.149
MgO	Pearson Correlation	-0.530	-0.118	0.193	0.522	1	0.269	-0.400	-0.477	-0.274	-0.292
CaO	Pearson Correlation	-.673(**)	-0.496	0.266	.705(**)	0.269	1	-0.323	-0.454	-0.329	-0.356
Na_2O	Pearson Correlation	0.046	.738(**)	0.065	-0.297	-0.400	-0.323	1	0.515	0.175	0.059
K_2O	Pearson Correlation	0.112	.748(**)	0.120	-0.333	-0.477	-0.454	0.515	1	.913(**)	.841(**)
TiO_2	Pearson Correlation	-0.029	.595(*)	0.231	-0.176	-0.274	-0.329	0.175	.913(**)	1	.950(**)
P_2O_5	Pearson Correlation	0.000	0.523	0.258	-0.149	-0.292	-0.356	0.059	.841(**)	.950(**)	1

Generally the correlation leads to the same results like the correlation of the Malmani Dolomite surface samples. The positive Pearson coefficients for Si and Fe and Si and Mn are due to the common implementation in pyroxenes like augite, hedenbergite or aegirinaugite and all solid solutions. Beside that such positive relations are also based in the association of Fe, Si in amphiboles and chlorites. The positive correlation of Na_2O and K_2O can be explained with a tschermakatic exchange of K^+ and Na^+ in feldspars and amphiboles (NESSE, 2000). The correlations which including Ti can be neglected because of their minor content in all samples.

6.4.3 Geochemical trends and relations in the Malmani Dolomite

Following bivariate plots, Harker diagrams and diverse triangular plot are used to recognize and explain geochemical trends.

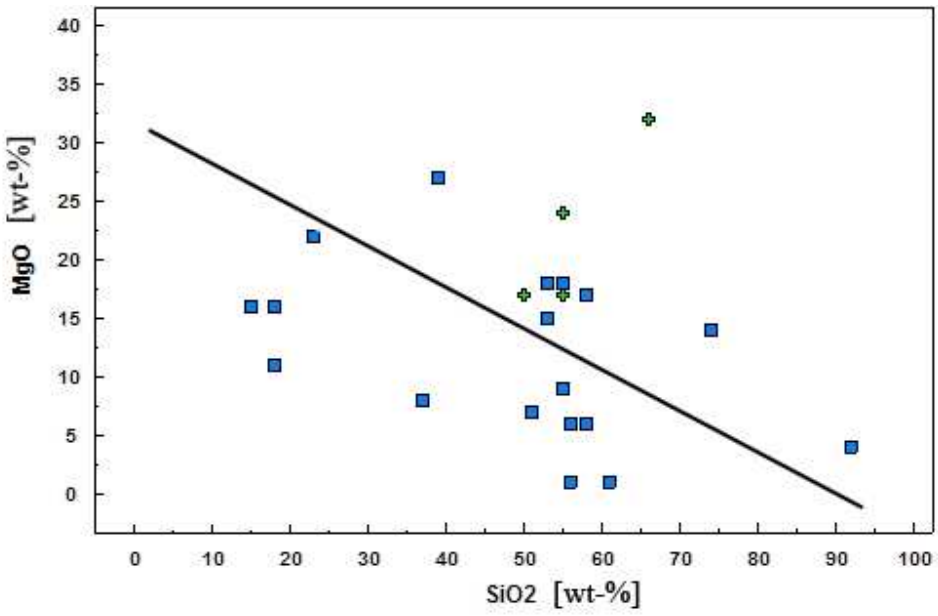

Fig. 6.22: Harker diagram SiO_2 vs. MgO; Malmani Dolomite; crosses = surface samples, quadrats = borehole samples

Fig. 6.22 illustrates two trends of the content in MgO with rising content in SiO_2. It is remarkable that the MgO content is rising if the content in SiO_2 is rising too whereas the value of MgO in the mineral assemblages of the borehole samples shrinks while the SiO_2-content increases. This accounted by the partly different minerals assemblages of both environments.

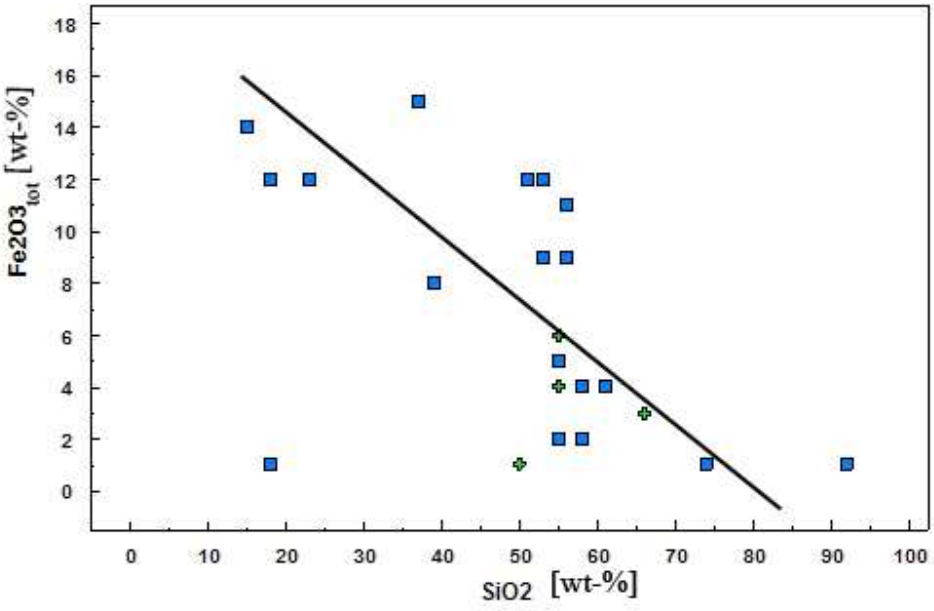

Fig. 6.23: Harker diagram SiO_2 vs. Fe_2O_3tot; Malmani Dolomite; crosses = surface samples, quadrats = borehole samples

The image above (Fig. 6.23) exposes the relation of the both elementoxides SiO_2 and Fe_2O_{3tot}. The behaviour of iron is similar to the behaviour of Mg in this contact metamorphic environment. So it is natural that the trend for Fe and Mg are both negative, at least in the borehole samples. The content of Fe_2O_{3tot} with rising content of SiO_2 in the surface samples is also decreasing contrary to the trend of MgO in Fig. 6.21 in the surface samples.

The surface samples show a higher average content of MgO is higher as in the borehole samples whereas the average content of Fe_2O_{3tot} is higher in the borehole samples. The high Fe-content in the borehole samples are due to the more intensive exposition to the metamorphic processes and the related Fe - metasomatism. The more intense exposition to those processes is founded in the contact nearer positions of the samples. Grab samples from the surface show more MgO in their chemical composition because of the prevalence of Mg-chlorites and Mg-amphiboles in their mineral assemblage whereas the mineralogical composition of the Malmani Dolomite borehole samples is more manifoldly.

Furthermore the elementoxide CaO should be taken in to account. So it is useful to create bivariate plots with relevance to CaO.

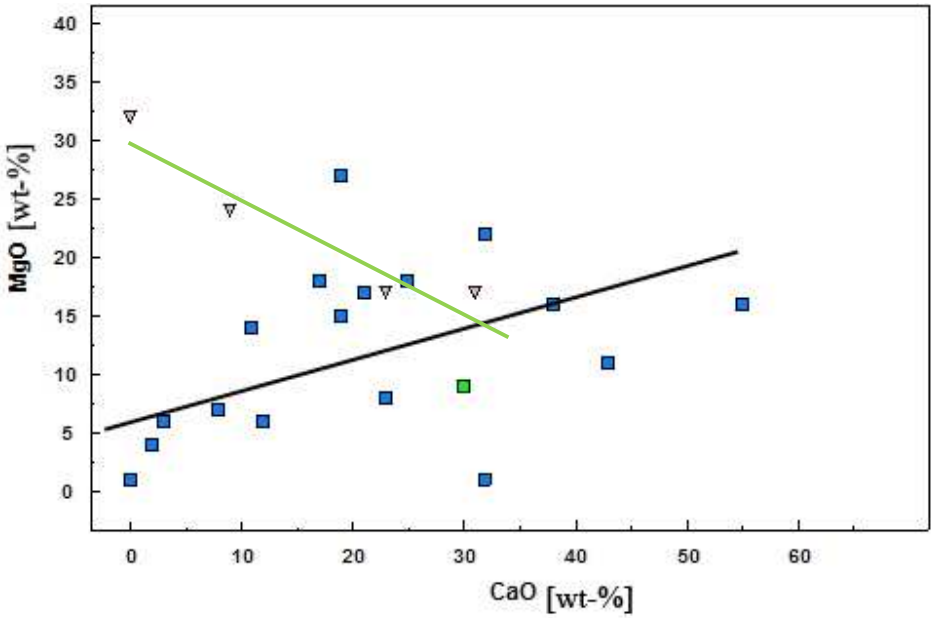

Fig. 6.24: Binary plot of CaO vs. MgO with trend lines (green = surface; black = borehole) for the Malmani Dolomite; triangle = surface sample, quadrat = borehole sample

The binary plot in Fig. 6.24 shows the coherence of CaO and MgO. Again there are different trends remarkable dependent of the environment where the observed sample was taken from. Specimens from the surface show a negative trend for the occurrence of Mgo if the content of CaO increases. In the borehole samples the contents of MgO and CaO are rising simultaneously. The grade of Ca-insertion, especially in the plagioclases, is increasing with a rising grade of metamorphism (WINKLER, 1979).

Next to binary plots it is favourable to create triangular plot for displaying the whole rock geochemistry and metamorphic processes.

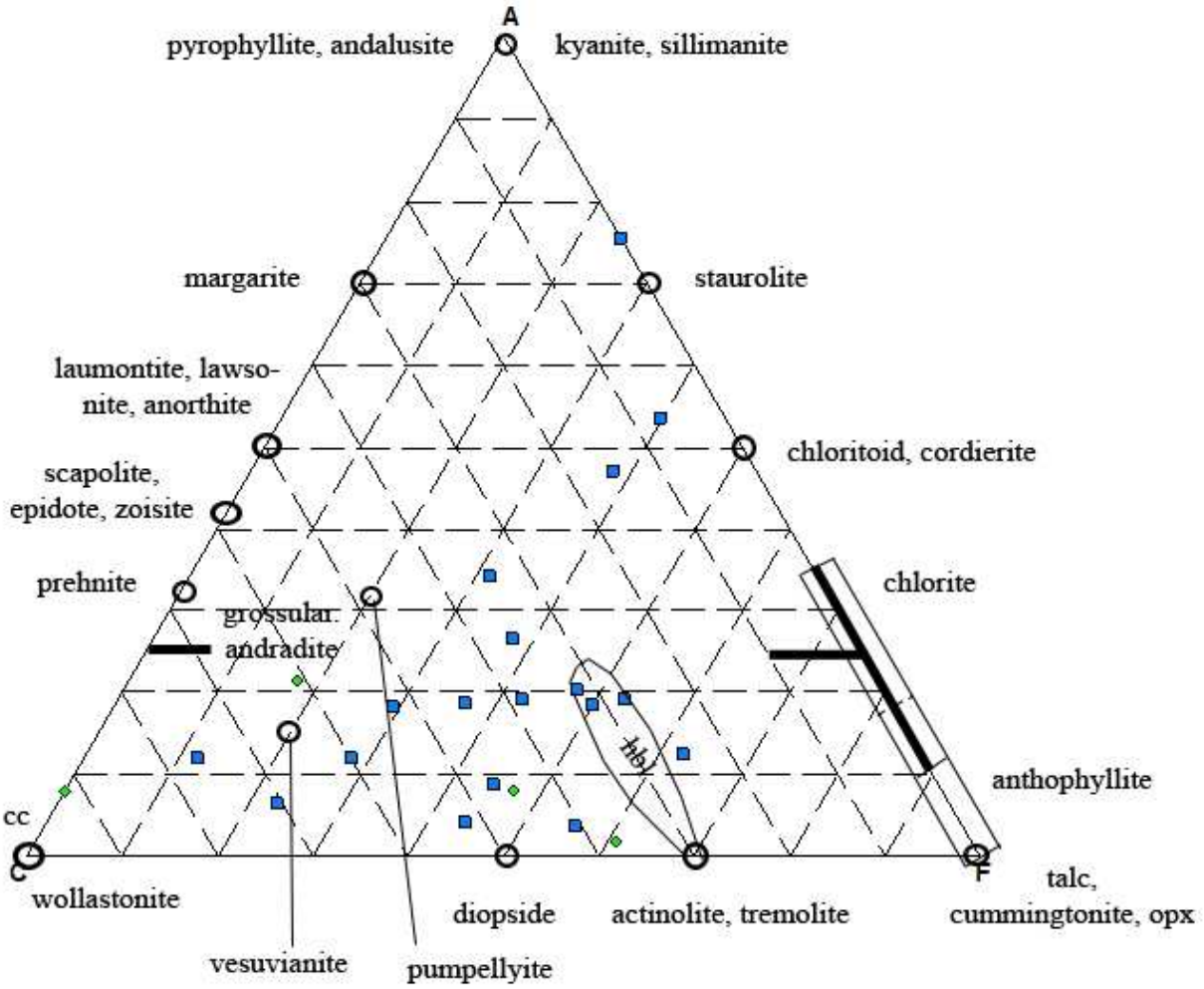

Fig. 6.25: ACF – diagram (after WINKLER 1979) for Malmani Dolomite – samples with mineralogy; quadrats = surface samples, spots = borehole samples

The ACF-projection in Fig. 6.25 shows the manifold appearance of minerals. The projection is based on the determination of the whole rock chemistry. It is visible that the bulk of the samples show assemblages which contain Ca-silicates like diopside next to hornblende, actinolite or tremolite. Some phases show a slightly trend to the A-vertex which is similar to a higher content in Al-bearing minerals like sillimanite. It is conspicuous that the surface samples are built up by phases which have a smaller content of Al-bearing phases. Samples with a high content in CaO contain wollastonite. The samples which are plotted in the middle of the projection with a composition of nearly $A_{20}C_{60}F_{20}$ are hosting andradite- or grossular-rich garnets. Because of the

fact that Si-undersaturated or Si-poor phases cannot be displayed in an ACF-diagram a further triangular plot is presented below (Fig. 6.26).

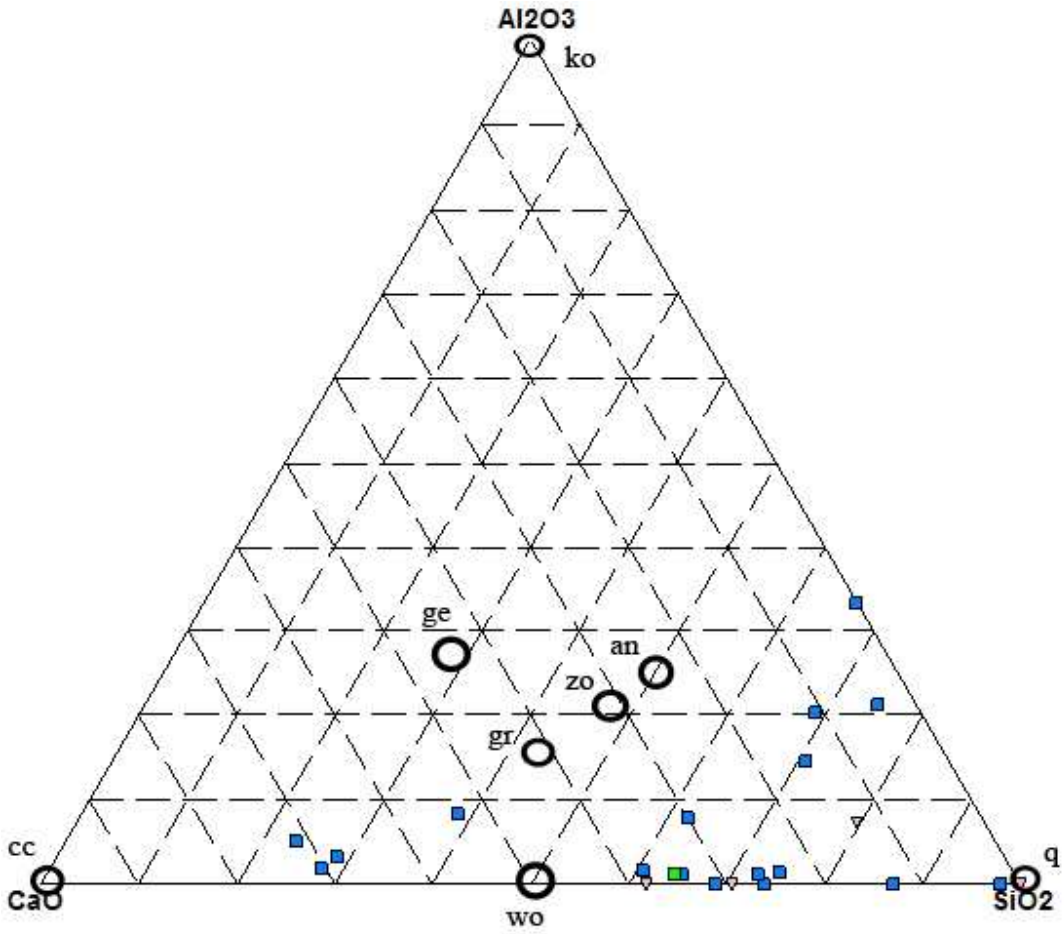

Fig. 6.26: Triangular plot of the system CaO – Al_2O_3 – SiO_2; cc = calcite, q = quartz, ko = corundum, wo = wollastonite, gr = grossular, zo = zoisite, an = anorthite, ge = gehlenite (STORRE, 1970)

The projection above shows the minerals which are probable in the chemical environment of the Malmani Dolomite. Most of the minerals are of calc-silicatic composition and are distributed around a point which displays the composition of a wollastonite. In the area of the SiO_2 – vertex minerals are shown which contain Ca- Al and Si-phases. An example for such a kind of mineral would be the augite.

6.4.3.1 Distance dependent geochemistry

Table 6.10: Average content of the major elementoxides in the Malmani Dolomite

el-oxide [wt-%]	0 - 50 m	50 - 100 m	100 - 150 m	200 - 250 m	250 - 300 m	300 - 500 m	500 - 800 m
SiO2	41,86	55,21	92,09	49,42	53,91	55,37	72,656
Al2O3	5,00	8,84	0,77	1,18	0,44	2,89	0,19
Fe2O3	8,11	10,33	1,58	6,38	12,26	5,36	1,69
MnO	0,27	0,18	0,10	0,28	0,29	0,24	0,11
MgO	13,02	12,04	4,07	15,81	15,69	20,97	15,76
CaO	28,37	10,79	2,95	23,99	19,28	16,43	8,92
Na2O	0,83	0,00	0,13	0,00	0,00	0,08	0,29
K2O	0,17	1,73	0,65	0,11	0,02	0,02	0,01
TiO2	0,51	1,50	0,04	0,04	0,01	0,07	0,02
P2O5	0,09	0,32	0,02	0,04	0,01	0,09	0,01

Table 6.10 shows the average contents in the major elements in the samples of the Malmani Dolomite. These zones are corresponding partly to the several mineral zones which were described in chapter 5. In the following text the diversification of the chemistry dependent on the distance to the contact will be shown.

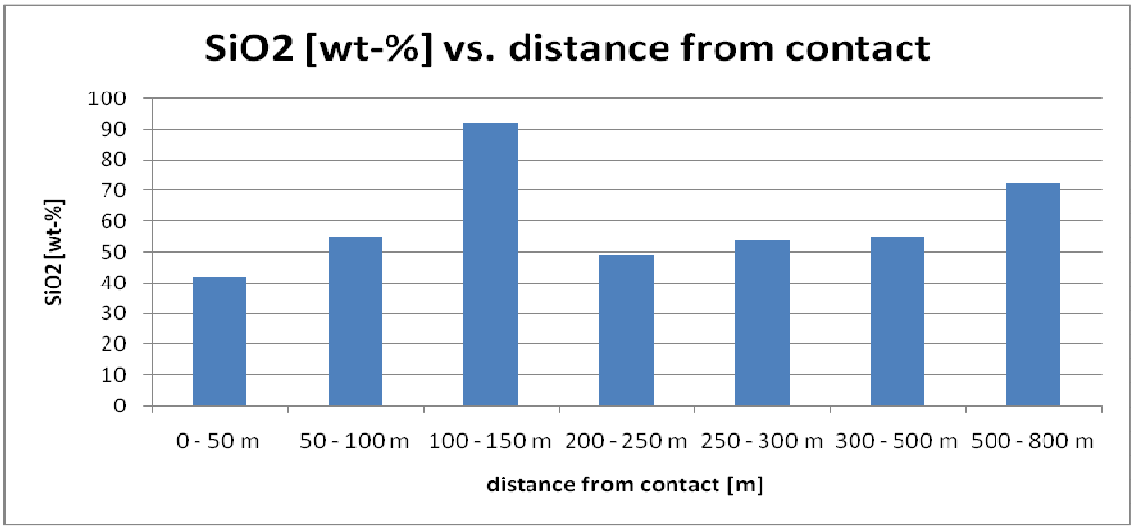

Fig. 6.27: Contents of SiO_2 in the Malmani Dolomite - samples in wt-% in several distances from the contact

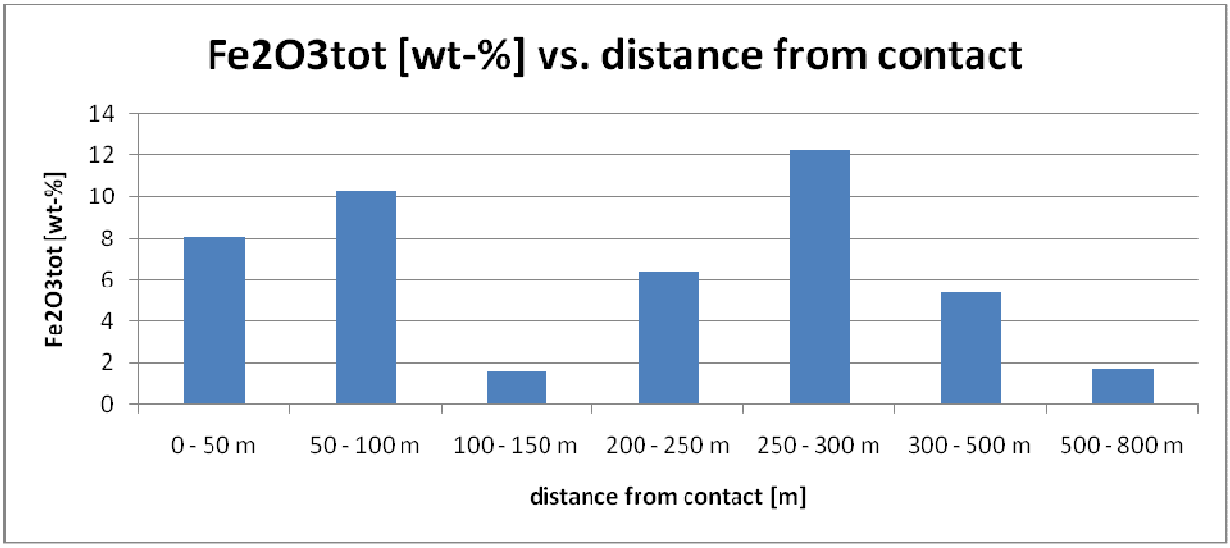

Fig. 6.28: Contents of Fe_2O_{3tot} in the Malmani Dolomite - samples in wt-% in several distances from the contact

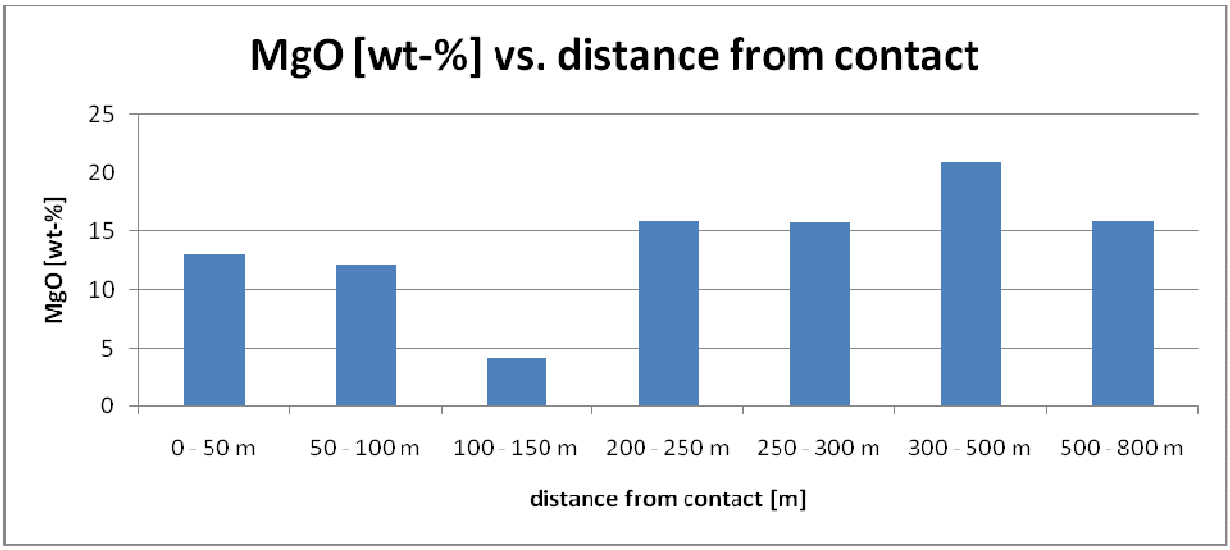

Fig. 6.29: Contents of MgO_t in the Malmani Dolomite - samples in wt-% in several distances to the contact

First of all it has to be mentioned that the content of quartz is rising tendentially with a rising distance to the contact except in the zone of 100 – 150 m away from the contact where the observed specimen are no dolomites in the unit of Malmani Dolomite against first assumptions in the field. But in contrast to the metapelites there is no increase or exceptional high contents in MgO or Fe_2O_{3tot} in the contact near area. This is due to the immunity of the Ca-silicatic minerals to implement Mg^{2+} or Fe^{2+} and Fe^{3+} in the same scale minerals in metapelitic mineral

assemblages do. The low content of iron far away (300 – 800 m) from the contact is founded in the increased occurrence of talc and quartz in the calc-silicates. The zone from 250 – 300 m away from the contact which shows a maximum in the content of Fe_2O_3 combined with a high value for MgO expose magnesiohornblende, tremolite, green hornblende and tschermakitic hornblendes as main constituents. The number of the minerals in the direct contact zone is intrinsic higher so that Fe is relatively depleted in the contact area.

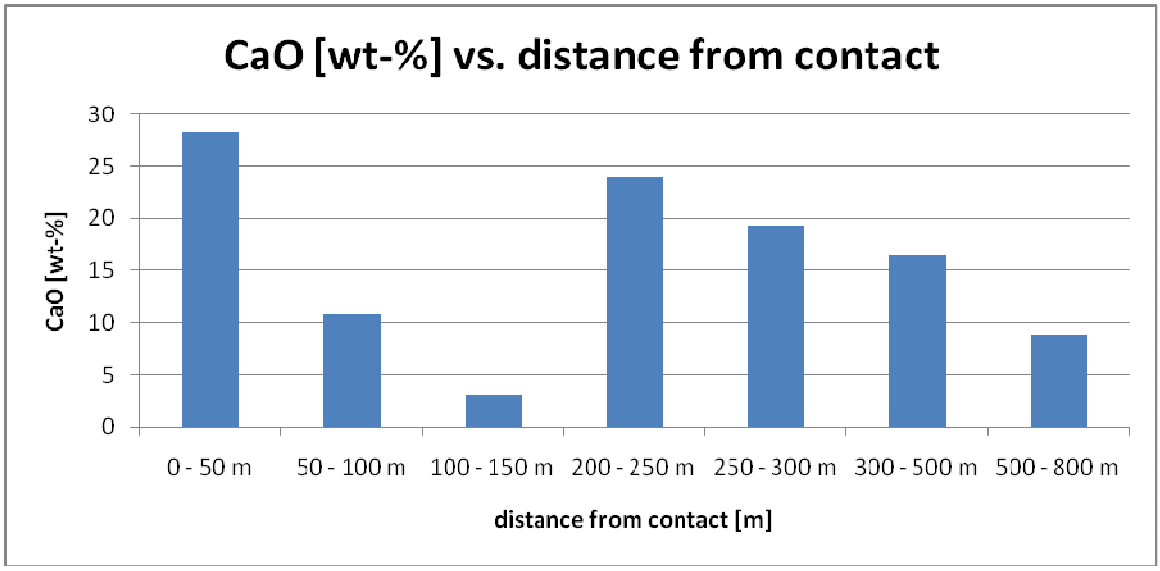

Fig. 6.30: Contents of CaO in the Malmani Dolomite - samples in wt-% in several distances from the contact

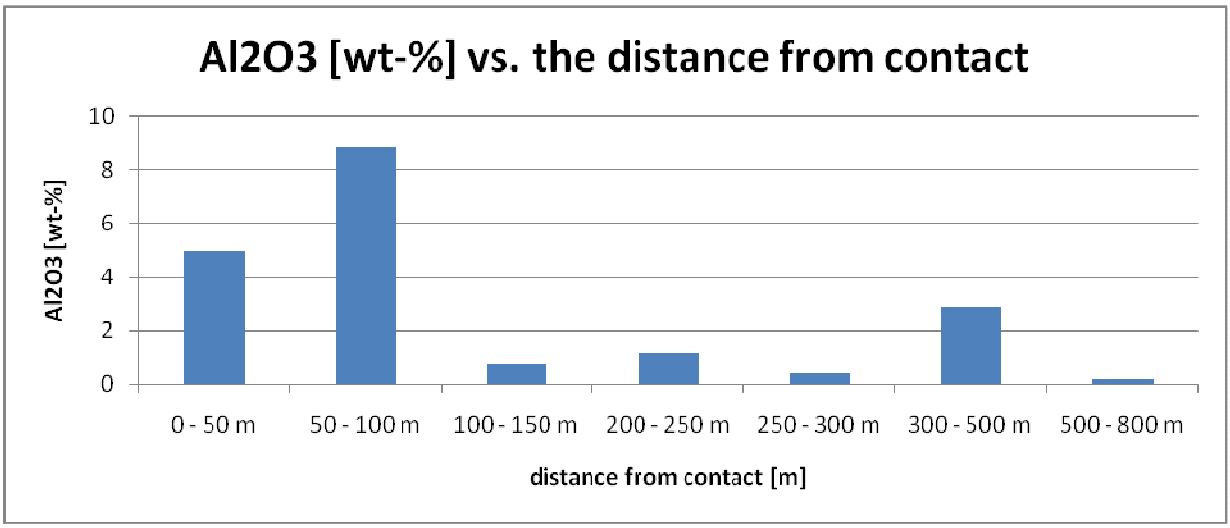

Fig. 6.31: Contents of Al_2O_3 in the Malmani Dolomite - samples in wt-% in several distances from the contact

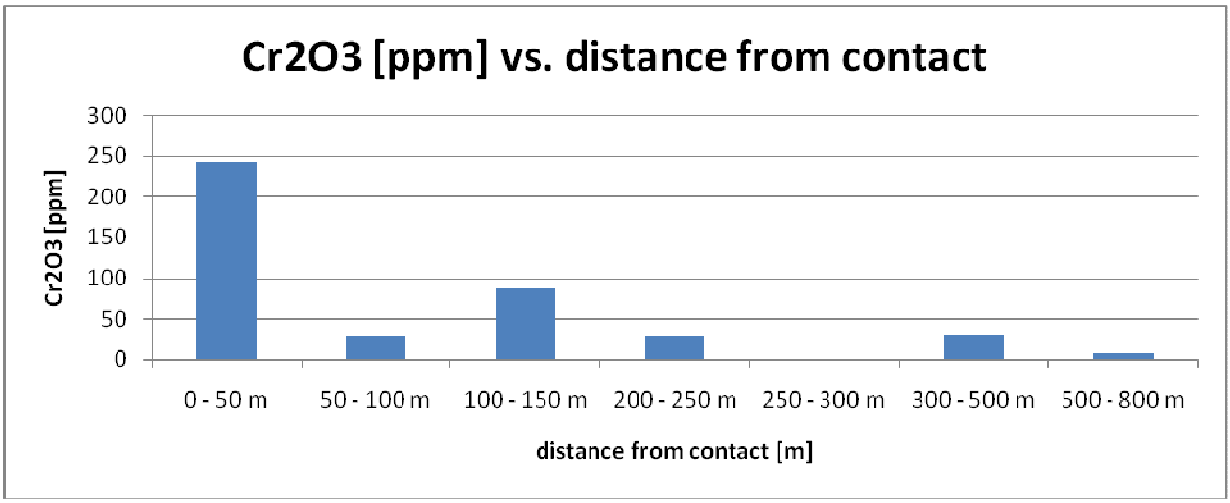

Fig. 6.32: Contents of Cr_2O_3 in the Malmani Dolomite - samples in ppm in several distances from the contact

The exposition of the Cr_2O_3 – content in several distances to the contact shows enrichment in the contact near zone like in the metapelites but in a smaller scale. Represented of the occurrence of Cr_2O_3 is the presence of chromian chlorite which was detected with XRD – analyes. In areas of the Malmani Dolomite in distances of more than 50 m the content of Cr_2O_3 is very low and can be neglected.

Areas close to the contact show maximal values of CaO because of the increased insertion of Ca in minerals in high-temperature environments. The content for Al is relatively high in zones up to 100 m away from the contact reasoned in the enhanced implementation of Al for Si in contact metamorphic scenes.

6.4.4 Phase relations in the Malmani Dolomite

Based on field observations, XRD-analyzes and the chemical analyze of the specimens a reconstruction of the most important mineral reactions and transitions was processed.

The “wollastonite zone” [wo] is characterized by the presence of wollastonite which is the marker for the temperature in this region of the Malmani Dolomite during the emplacement of the Uitkomst Comples.

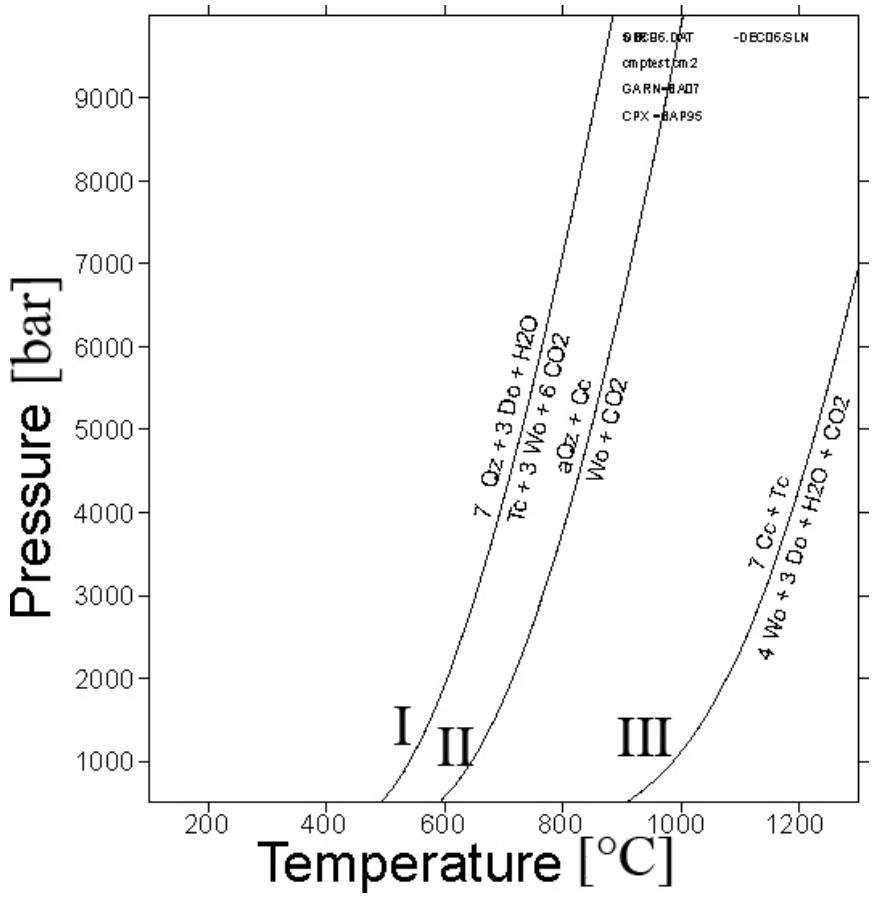

Fig. 6.33: Possible mineral reactions for the generation of wollastonite (wo); qz = quartz, do = dolomite, tc =talc, cc = calcite

Figure 6.33 above presents different possibilities for the generation of wollastonite. Regarding to the short distance to the contact (0-50 m) and the knowledge about the temperature conditions of the sillimanite zone in the metapelites it is assumable that the wollastonite in the contact-near dolomites was created by reaction (III). This predicts a temperature of ca. 1000 – 1100°C and contact metamorphic pressure conditions of 1 – 1.5 kbar. So it can be ascertained that wollastonite is the result of the following reaction:

III) $7\ CaCO_3 + Mg_3Si_4O_{10}(OH)_2 \leftrightarrow 4\ CaSiO_3 + 3\ CaMg(CO_3)_2 + H_2O + CO_2$

(7 calcite + talc ↔ 4 wollastonite + 3 dolomite + water + carbondioxide)

Reactions I and II, also plotted in Fig. 6.33 are also common in zones of mineralisation which are further away from the contact than the wollastonite zone. Reaction II is responsible for the generation of wollastonite in the area 50 – 100 m away from the contact, the so called "diopside – serpentine – hornblende zone" [di-serp-hbl]. Of course there is a transition area in the threshold of these two zones.

II) $CaCO_3 + SiO_2 \leftrightarrow CaSiO_3 + CO_2$

(calcite + quartz ↔ wollastonite + carbondioxide)

In contrast to dolomite and magnesite, calcite as most widespread carbonate is not reacting at low-grade metamorphism if quartz is present. High temperatures are essential to initiate a reaction of calcite and quartz. That is why calcite and quartz are combined in many mineral assemblages from very low to high-grade.

They react if either the CO_2-rich fluid phase is considerably diluted by H_2O or the pressure of the CO_2-rich fluid is low for instance in contact metamorphic geological settings. The given reaction is processed only in the higher temperature ranges of shallow contactmetamoprhism.

In exceptional cases wollastonite can be also produced during regionalmetamorphism if water from the surrounded rocks intrudes in the carbonate layers and dilutes the CO_2-concentration of the fluid phase (WINKLER, 1979).

In the form the reaction is written above the reaction is univariant. But the reaction is bivariant in nature caused by the presence of water in the pore fluids of the rocks. The resulting four phases, quartz, calcite, wollastonite and vapour predict two degrees of freedom. So it is assumable that at any given fluid pressure the equilibrium temperature increases with increasing $x_{CO2.}$

GREENWOOD (1967a) has determined the temperatures for several x_{CO2} at pore fluid pressures of 1 kbar and 2 kbar. The results are given in a diagram (Fig. 6.34).

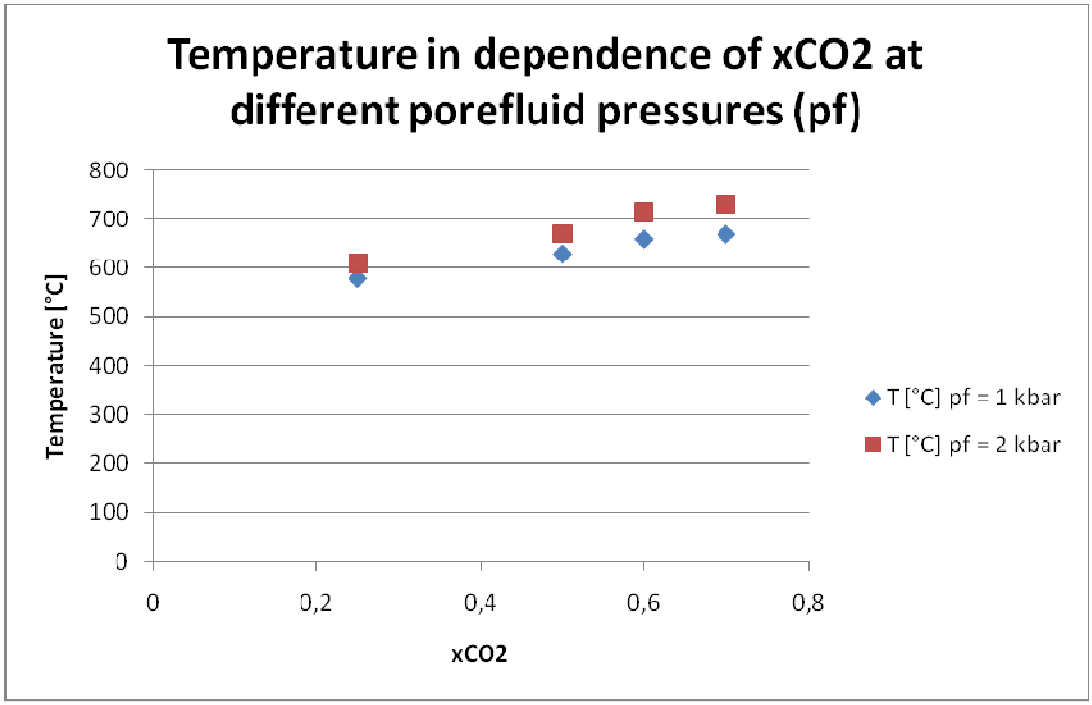

Fig. 6.34: Equilibrium temperature at fluid pressures of 1 and 2 kbar in dependence of different compositions of the fluid phase (x_{CO2}) (GREENWOOD 1967a)

The diagram makes it visible that the formation of wollastonite is not suitable without any knowledge regarding the composition of the fluid phase.

But one can say that wollastonite can never be found in rocks metamorphosed at relatively low temperatures between 400 and 500°C not even in contact metamorphic rocks formed at shallow depths corresponding to pressures of only a few hundred bars. The consequence is the cognition that the x_{CO2} of the fluid present during metamorphism is never very small it is always rather large (WINKLER, 1979).

Nevertheless the presence of wollastonite is a sign for high-grade metamorphism.

In the region 50 m away from the contact andradite is also common, especially in the surface samples inter alia in JK-48. Andradite is a sign for an intensive metasomatic overprint of the carbonates by, Fe-rich, ore-bearing fluids or gas phases. The andradite is generated following the reaction which is mentioned below.

10) $Ca_2(Al,Fe^{3+},Mg)_3(SiO_4)_3OH + SiO_2 \leftrightarrow CaAl_2Si_2O_8 + Ca_3Al_2[SiO_4]_3/Ca_3Fe_2Si_3O_{12} \pm Fe_2O_3 + H_2O$

(epidote + quartz ↔ anorthite + grossularite/andradite ± hematite + water)

In the specific setting of the Uitkomst Complex andradite-rich garnet was evidenced. But it is assumable that the found garnets are solid solutions of grossularite and andradite. The heat the andradite was exposed to can only be estimated. The "skarn-like" environment predicts temperatures of approximately 650°C (MATTHES & OKRUSCH, 2005).

The chemical composition of andradite is given below (table 6.11)

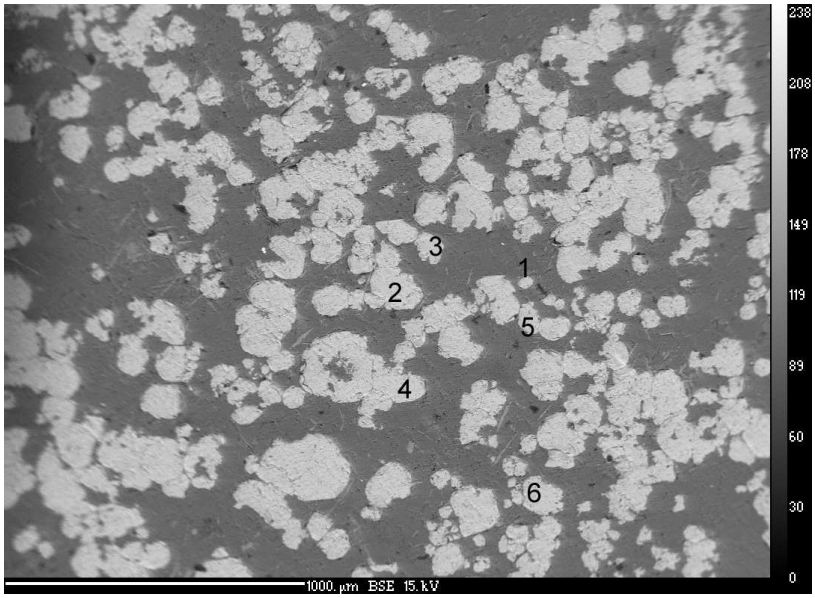

Fig. 6.35: BSE-image of andradite in JK-48; 1-6 points of EMPA measurements

Table 6.11: Chemical compositions of andradite (JK-48)

	Andr.	Andr.	Andr.	Andr.	Andr.	Andr.
el.-oxide	Oxide wt-%	Oxide wt-%	Oxide wt-%	Oxide wt-%	Oxide wt-%	Oxide wt-%
	point 1	point 2	point 3	point4	point 5	point 6
SiO_2	34.70	35.45	35.75	35.45	34.89	35.96
TiO_2	0.33	0.05	0.05	0.05	0.10	0.27
Al_2O_3	0.32	0.49	0.91	0.45	0.96	0.32
Fe_2O_3tot	27.59	28.44	27.50	28.34	26.95	28.13
MnO	0.06	0.04	0.05	0.03	0.03	0.00
MgO	0.18	0.07	0.15	0.05	0.20	0.15
CaO	33.47	32.87	32.83	33.01	33.44	32.49
Na_2O	0.03	0.03	0.05	0.05	0.08	0.04
K_2O	0.00	0.00	0.00	0.00	0.00	0.00
Cr_2O_3	0.00	0.00	0.00	0.03	0.03	0.00
sum	**96.69**	**97.43**	**97.29**	**97.45**	**96.68**	**97.36**

Calculations lead to the following mineral compositions (Tab. 6.12).

Table 6.12: Explicit formulae of the andradites in Malmani Dolomite (JK-48)

Point no.	Formula
1	$Ca_{3.125}Fe_{1.81}(Si_{3.02}O_{12})$
2	$Ca_{3.035}Fe_{1.485}Al_{0.05}(Si_{3.05}O_{12})$
3	$Ca_{3.02}Fe_{1.775}Al_{0.09}(Si_{3.07}O_{12})$
4	$Ca_{3.045}Fe_{1.835}Al_{0.05}(Si_{3.05}O_{12})$
5	$Ca_{3.11}Fe_{1.76}Al_{0.1}(Si_{3.025}O_{12})$
6	$Ca_{2.99}Fe_{1.82}Al_{0.03}(Si_{3.09}O_{12})$

The foregoing table exposes the explicit formulae for the andradites in the Malmani Dolomites. Especially the grade of the insertion of Fe is varying. Over all the constituents of the andradite are varying in a small scale but nearly all of them show a low content of Al. But the points of measuring are optically identic in the BSE-picture.

The sum of the elements differs from 100 % because of the systematic error of the microprobe. That is the reason why other elements with very low contents are neglected.

The so-called “diopside - serpentine – hornblende” zone [di-serp-hbl] is marked by the intensified appearance of diopside which marks the next level of metamorphism in the siliceous carbonates. Diopside is formed by two reactions in our environment dependent from the original composition of the calc-silicatic educts. There are alternative reactions (Fig. 6.36) existent to produce diopside but they are all linked with the production of forsterite which was not detected in the samples of the Malmani Dolomite. The regarding reactions are:

(11) $Ca_2Mg_5[(OH,F)|Si_4O_{11}]_2 + 3\ CaCO_3 + 2\ SiO_2 \leftrightarrow 5\ CaMg[Si_2O_6] + 3\ CO_2 + H_2O$

(tremolite + 3 calcite + 2 quartz ↔ 5 diopside + 3 carbondioxide + water)

(12) $Ca_2Mg_5[(OH,F)|Si_4O_{11}]_2 + 3\ CaCO_3 \leftrightarrow CaMg(CO_3)_2 + 4\ CaMg[Si_2O_6] + CO_2 + H_2O$

(tremolite + 3 calcite ↔ dolomite + 4 diopside + carbondioxide + water)

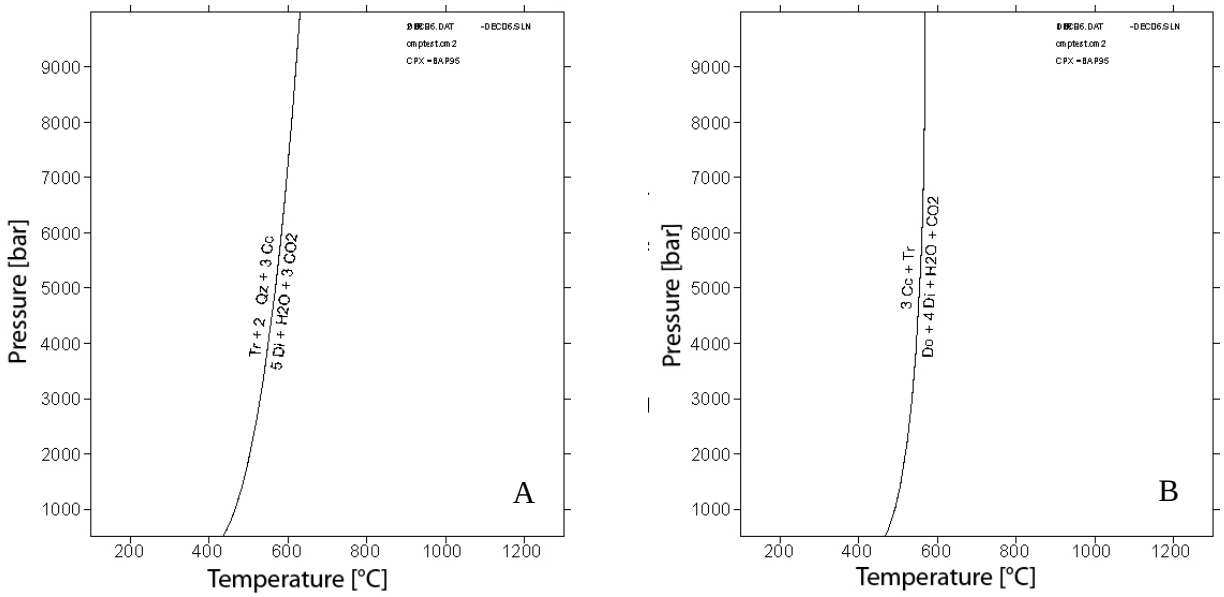

Fig. 6.36: A: Reaction (11) and B: reaction (12) for the creation of diopside in the Malmani Dolomites; calculated with TWQ (BERMAN, 2006)

It is conspicuous that particulary the reaction (12) is nearly independent from the pressure in the metamorphic setting. The diopside is generated under all pressures at ca. 500°C. In the case of a SiO_2 – free or undersaturated mineral assemblage reaction (12) is the common way for the generation of diopside.

The adjoining zone, named as "hornblende zone" [hbl] extents over a distance from 150 to 300 m away from the contact. Different hornblendes are the predominating minerals. The minerals which are common in this zone are given in chapter 5. Based on the observed minerals it is assumable that the metamorphic environment confirms to the threshold of the greenschist to the epidote-amphibolite facies. Under high grade metamorphic conditions a coexistence of calcite + dolomite + chlorite + quartz + epidote ± tremolite/actinolite (MATTHES & OKRUSCH, 2005). Calcite is also able to coexist with quartz under higher temperatures and in the amphibolites

facies. The temperature in this facies is given with ca. 500°C at 3 kbar (MATTHES & OKRUSCH, 2005). Hornblende is generated after the following equation:

13) $Na0,5(Al,Mg)6(Si,Al)8O18(OH)12{\cdot}5(H2O) + Ca_2Mg_5Si_8O_{22}(OH)_2$
$/Ca_2(Mg,Fe^{++})_5Si_8O_{22}(OH)_2 + Ca_2(Fe,Al)Al_2(SiO_4)(Si_2O_7)O(OH) + SiO_2 \leftrightarrow$
$Ca_2\,[Mg_4(Al,Fe^{+++})]Si_7AlO_{22}(OH)_2 + H_2O$

(chlorite + tremolite/actinolite + epidote + quartz ↔ hornblende + water)

Tremolite is generated by the reaction no. 14)

14) $8\ SiO_2 + 5\ CaMg(CO_3)_2 + H_2O \leftrightarrow 3\ CaCO_3 + Ca_2Mg_5Si_8O_{22}(OH)_2 + 7\ CO_2$

(8 quartz + 5 dolomite + water ↔ 3 calcite + tremolite + 7 carbondioxide)

and is illustrated in the plot below:

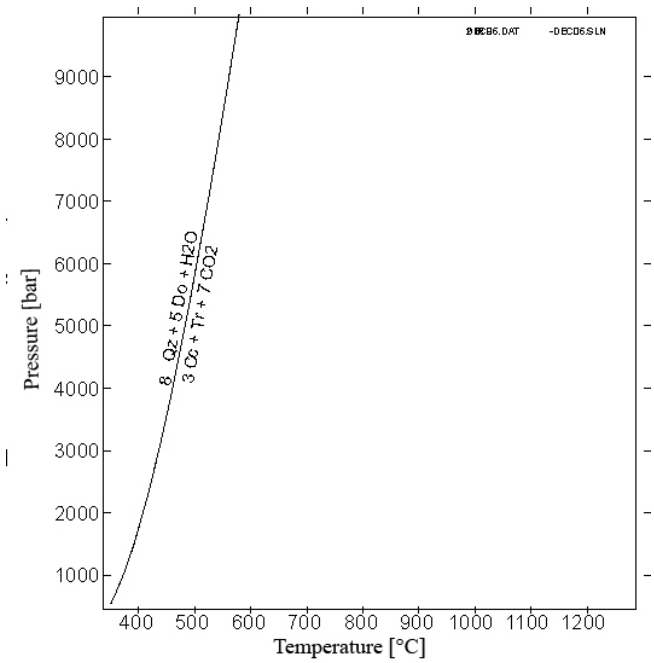

Fig. 6.37: Reaction (14) for the creation of tremolite in the Malmani Dolomite; calculated with TWQ (BERMAN, 2006)

Fig. 6.37 shows that tremolite is produced combined with temperatures of ca. 400°C. So it confirms to the “corundum-zone” in the metapelites.

7. Corundum at the Uitkomst Complex – properties and possible applications

The assessment of the qualities and the properties of corundum is a special part of this thesis and are investigated besides the study of the contact aureole.
Possible applications of corundum are manifold. It can be used as a constituent in cement as a cheap Al-source in high-alumina cement (RÖSLER, 1991). It is a component in concretes which have to be abrasion-resistant. But it is also used for abrasive techniques (RÖSLER, 1991).
But nevertheless there are some modifications, which are coloured red caused by the insertion of Cr and blue by the insertion of Ti and Fe. The red variant is known as ruby the blue one as sapphire. Both are precious, popular gemstones (RÖSLER, 1991).

7.1 Corundum – The mineral

The mineral with the formula α-Al_2O_3 is the second hardest natural mineral (Mohs 9). The physical properties are the reason for the widespread field of applications. Corundum is very stable under the influence of high temperatures. The mineral has a melting point of 2040 °C which makes the mineral interesting for the industry.

7.2 Occurrence

Corundum is a part of the mineral assemblage in rocks which show an undersaturation of SiO_2 and an extreme oversaturation of Al_2O_3, for example in metabauxites or Al-rich clays.
The presence of corundum in the country rocks of the Uitkomst Complex is restricted to the Timeball Hill Shale (Fig. 7.1) in the southeast and the northwest of the intrusion. The mineral can be found in a zone which is named as “corundum hornfels” and in fine-grained metapelites with a high content of Al_2O_3. The zones of corundum are uniting different facts which are necessary to create corundum. The width of this zone is limited to ca. 50 m. But it cannot be excluded that at least in the northwesterrn part of the complex-surrounding country rocks the appearance of corundum is more widespread than in the south.

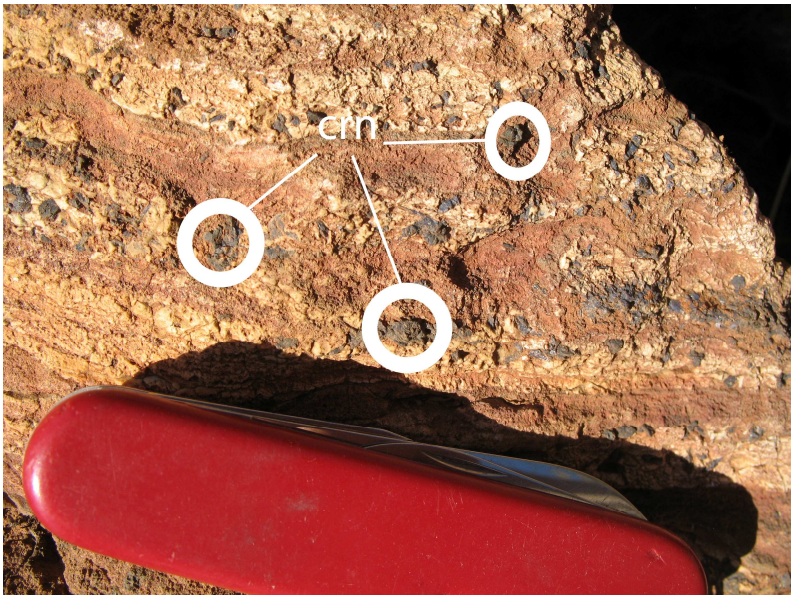

Fig. 7.1: Corundum (crn) in a specimen of the Timeball Hill Shale in the southwest of the Complex

The image above (Fig. 7.1) shows a specimen of Timeball Hill Shale which in enriched in corundum (marked spots).

7.3. The "Uitkomst corundum"

As visible the Uitkomst corundum shows grain sizes up to 5 mm. They are of brown to blue (Fig. 7.2 and 7.3) colour and of ideal shape in several places.
The rocks, which house the corundum are highly weathered and show cavities in places where corundum was situated.
The abundance of corundum is too low for industrial applications. Deposits which are generated as placers are more interesting for the industry. Because of the possibility for the artificial creation of corundum, the importance of natural deposits is decreasing.
But the natural aggregates of corundum keep their importance as gem stones with regard to its application the corundum was investigated during this study.
It was necessary to process measurements with the EMPA to get knowledge of the degree of Ti-, Cr- and Fe-insertion. To estimate the suitability as gem stones the degree of insertion also determines the colour of the corundum. If it is red, the Cr-insertion is evidenced. Blue colour of

the gem stones is caused by Fe- and Ti-insertion. The results of the EMPA-analyses are presented in the following table 7.1.

Table 7.1: Chemical compositions of corundum (southwesterly from the Complex

Elementox.	Crn 1	Crn 2	Crn 3	Crn 4	Crn 5	Crn 6	Crn 7	Crn 8	Crn 9	Crn 10	Crn 11	Crn 12
SiO_2	1.75	1.43	0.71	0.00	0.02	0.00	0.02	0.00	0.06	0.02	0.04	0.06
TiO_2	0.10	0.17	0.02	0.12	0.05	0.07	0.22	0.45	0.28	0.37	0.57	0.45
Al_2O_3	97.25	97.34	97.84	98.78	98.84	99.43	99.16	98.92	98.88	99.01	98.82	98.91
Fe_2O_3tot	0.59	0.71	0.91	0.37	0.37	0.12	0.31	0.40	0.49	0.39	0.31	0.35
MnO	0.00	0.05	0.03	0.00	0.00	0.00	0.00	0.03	0.00	0.03	0.03	0.00
MgO	0.02	0.00	0.02	0.00	0.00	0.00	0.00	0.00	0.00	0.00	0.00	0.00
CaO	0.06	0.01	0.00	0.00	0.00	0.00	0.00	0.00	0.01	0.00	0.00	0.00
Na_2O	0.09	0.11	0.07	0.03	0.03	0.08	0.12	0.08	0.03	0.05	0.05	0.03
K_2O	0.00	0.00	0.00	0.00	0.00	0.00	0.00	0.00	0.00	0.00	0.00	0.00
Cr_2O_3	0.00	0.00	0.00	0.00	0.00	0.00	0.00	0.00	0.00	0.00	0.00	0.00
sum	100.12	100.14	100.24	99.30	99.31	99.70	99.83	99.88	99.75	99.87	99.82	99.80

Table 7.2: Explicit formulae of corundum in the Timeball Hill Shale

Corundum no.	**Formula**	**Corundum no.**	**Formula**
1	$Fe_{0.01}(Al_{1.95},Si_{0.03})O_3$	7	$(Fe_{0.005}Ti_{0.005})Al_{1.99}O_3$
2	$Fe_{0.01}(Al_{1.955,}Si_{0.025})O_3$	8	$(Fe_{0.005}Ti_{0.005})Al_{1.985}O_3$
3	$Fe_{0.01}(Al_{1.97},Si_{0.01})O_3$	9	$(Fe_{0.005}Ti_{0.005})Al_{1.985}O_3$
4	Al_2O_3	10	$(Fe_{0.005}Ti_{0.005})Al_{1.985}O_3$
5	Al_2O_3	11	$(Fe_{0.005}Ti_{0.005})Al_{1.985}O_3$
6	Al_2O_3	12	$(Fe_{0.005}Ti_{0.005})Al_{1.985}O_3$

As visible the corundum of in the country rocks which are located southwesterly from the Complex show contents of Ti and Fe in traces. The lowest limit of detection of the EMPA is 13,598 ppm for TiO_2 and 16,52 ppm for Fe_2O_3tot. So it is evidenced that the “Uitkomst corundum” is developed as sapphire in some places.

For a better appraisal of the gemstone quality the results are compared with results of analyses of other researchers in the following (Table 7.3).

Table 7.3: Corundum compositions from literature

Elementoxide	**1**	**2**	**3**	**4**
SiO_2	0.20 %	0.68 %	0.137 %	0.542 %
TiO_2	0.32 %	-	0.00 %	0.00 %
Al_2O_3	98.84 %	96.72 %	98.8 %	97.61 %
Cr_2O_3	-	0.00 %	0.945 %	1.81 %
Fe_2O_3tot	0.20 %	0.18 %	0.0147 %	0.0252 %
MnO	-	-	0.00 %	0.00 %
MgO	0.04 %	0.96 %	0.02265 %	0.0328 %
CaO	0.34 %	1.16 %	-	-
sum	**99.94 %**	**99.7 %**	**99.92 %**	**100.02 %**

The first composition describes dark blue corundum out of a contact altered marble from the Urals (GAVRUSEVICH, B. A. 1941). Measurement no. 2 illustrates the composition of green corundum which was found in a syenite pegmatite in the Urals (GAVRUSEVICH, 1941). The third measurement shows the chemical composition of a light colour gem ruby (ALEXANDER, 1948) whereas composition no. 4 was measured in a dark coloured natural gem ruby (ALEXANDER, 1948).

It is obviously that the analysis no.1 is similar to the results of the study of the "Uitkomst-corundum".

This fact is supported by images which were made of the corundum and are given in Fig. 7.2. Finally the measurements, the comparison with other data and the pictures show that the corundum occurs in two different ways. They are of a brownish colour, caused by Fe-oxides, or dark blue, caused by the insertion of Fe and Ti. It is ascertainable that there is partly sapphire generated in the Time Ball Hill Shales in the south of the Uitkomst Complex. The area north of the Complex was not investigated concerning the gem stone quality of corundum.

Fig. 7.2: Corundum crystal; south of the Complex

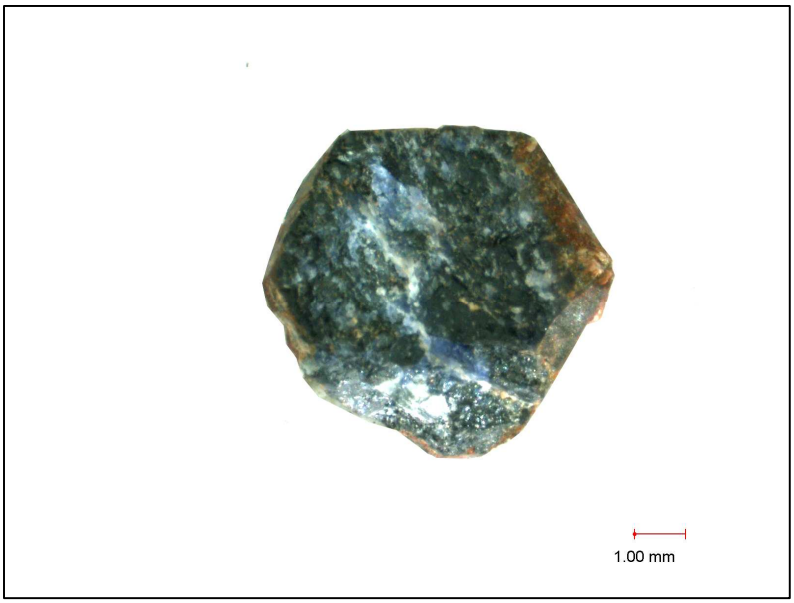

Fig. 7.3: Corundum crystal of almost ideal shape; south of the Complex

As visible in Fig. 7.2 and Fig. 7.3, the corundum crystals are of almost ideal shape. Fig. 7.3 mirrors the hexagonal shape of the corundum.

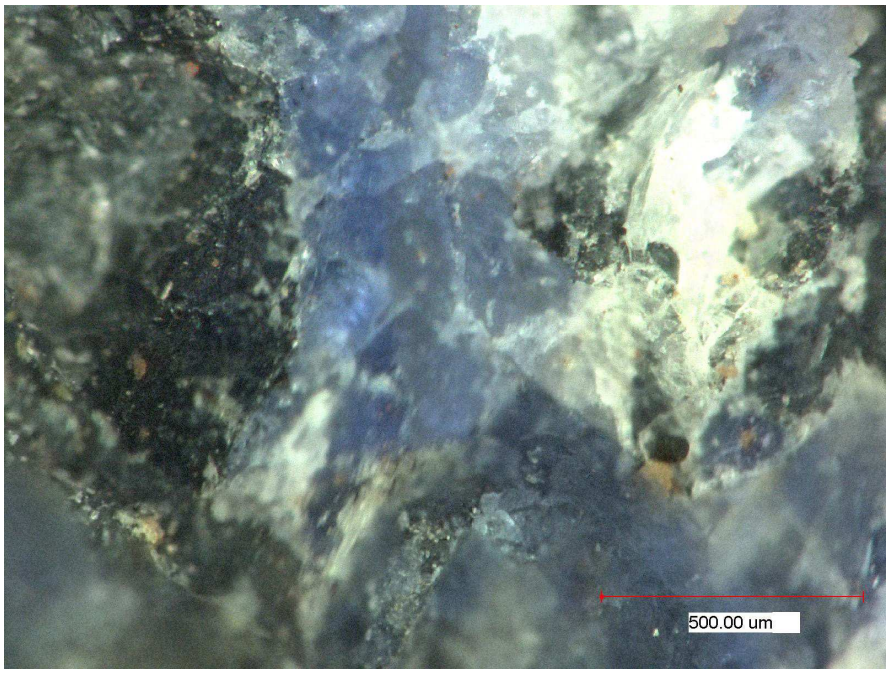

Fig. 7.4: Surface of a corundum crystal in detail with visible blue colour; south of the Complex

7.4 Conclusion

Corundum in the shape and the abundance of the corundum in the county rocks of the Uitkomst Complex is not useable for industrial applications. It is much cheaper to produce corundum artificially (RÖSLER, 1991) for example for creating abrasive materials.

The distribution is limited in the Uitkomst contact aureole. This is mainly due to the dependence on the chemistry of the metapelites. Those are rich in Al_2O_3 (35.77 wt-% in average) and SiO_2-free or SiO_2-undersaturated. Placer deposits are more interesting for the industry. But the blue variety in some locations in the south of the Complex could be interesting as gem stones.

The chance for such an application is given because the occurrence of sapphires in the southern Timeball Hill Shales was evidenced.

8. Discussion

In the past many contact aureoles and also metapelites in contact aureoles were in the spot of scientific efforts. A thesis which is appropriate for a comparison with the setting at the Uitkomst Complex is the work of (SYMNES & FERRY, 1995). They described the "Metamorphism, Fluid Flow and the Partial Melting in Pelitic Rocks from the Onawa Contact Aureole, Central Maine, USA". The Onawa pluton is a composite quartz diorite-granodiorite intrusion which was emplaced into chlorite zone metasediments.
At first it has to be mentioned that they divide 5 different mineral zones in the metapelites:

1) chlorite zone
2) andalusite cordierite zone
3) alkali feldspar zone
4) sillimanite zone
5) leucocratic vein zone

A classification of different zones in the Timeball Hill Shale is possible by the appearance of certain (indicator) minerals. The zones are named after the predominating minerals. "Indicator minerals" means that several minerals predict a certain range of temperature. In the samples of the Timeball Hill Shales can be divided:

1) Sillimanite – zone [sil]
2) Augite – antigorite – zone [aug-atg]
3) Sanidine zone [san]
4) Almandine zone [alm]
5) Corundum zone [cor]

Also in the Malmani Dolomite different mineralization zones were detected. More explicit following zones were determined:

1) Wollastonite zone [wo]
2) Diopside – serpentine –hornblende zone [di-serp-hbl]
3) Hornblende zone [hbl]
4) Quartz – diopside - mica zone [qtz-di-mic]
5) Quartz – hornblende – mica [qtz-hbl-mic]

The main difference between the Contact aureoles of Onawa and Uitkomst is the generation of sillimanite. Sillimanite is generated out of andalusite at the Onawa Contact aureole whereas sillimanite in the metapelites of the Uitkomst Complex was created by the reaction:

Muscovite ($KAl_2[(OH,F)_2/AlSi_3O_{10}]$) + Quartz ($SiO_2$) →K-feldspar ($KAlSi_3O_8$) + Sillimanite ($Al_2SiO_5$)

The common appearance of K-feldspar and sillimanite stands for a high temperature metamorphic environment (MATTHES & OKRUSCH, 2005). Also it is remarkable that the metapelites of the Onawa Contact Aureole host cordierite and andalusite. Those minerals are not detectable in the metapelites of the Uitkomst Complex. The generation of corundum is understood as a further reaction of the Al-hydroxides in the absence of quartz after the following reaction:

Gibbsite (γ-$Al(OH)_3$) →boehmite (γ-AlO(OH)) → diaspore (α-AlO(OH)) →corundum (Al_2O_3) + water (H_2O)

The presence of corundum is restricted to a zone with an undersaturation of SiO_2 and a high content (ca. 36 % in average) Al_2O_3 in the bulk rock chemistry and the right temperature for the creation of corundum of 400°C. The corundum is distributed especially in the southwestern part of the Complex restricted to a zone which extends over ca. 50 m. The grains of the corundum are up to 5 mm in diameter. EMPA and optical analytics suggest a Ti-insertion in the corundum

which means that sapphirine is existent in some areas. Beside Ti only Fe is implemented in the structure of the corundum in small scales. The compositions given in other research papers (GAVRUSEVICH, B. A. 1941; ALEXANDER, 1948) show the constitution of several corundum minerals. It has to be mentioned that the results of the first analyse of a dark blue corundum (GAVRUSEVICH, B. A. 1941) in table 7.2 confirm to the results concerning the composition of the "Uitkomst-corundum". For comparison the compositions of green corundum which was found in a syenite pegmatite in the Urals (GAVRUSEVICH, B. A. 1941) and a light and a dark coloured gem ruby are presented (ALEXANDER 1948). It is conspicuous is that the metapelites around the Uitkomst Complex show no signs for partial melting. In the metapelites of the Onawa Contact Aureole melt is developed after the two following reactions:

1) qtz + alk fsp + plag + biot + sill + H_2O = H_2O-saturated melt + ilm
2) qtz + plag + biot + sill = cord + alk fsp + H_2O-saturated melt and + ilm

(qtz = quartz, alk fsp = alkali feldspar, plag = plagioclase, biot = biotite, sill = sillimanite, cord = cordierite, ilm = ilmenite)

The melt production of the Onawa Contact Aureole is possible through the infiltration of H_2O-rich fluids.

Ilmenite is also present in the Timeball Hill Shales but there occurrence is mainly controlled by the O_2-fugacity.

The generation of almandine is processed which the following reaction:

$Na_{0.5}Al_4Mg_2Si_7AlO_{18}(OH)_{12}\cdot 5(H_2O) + {Fe^{2+}}_{1.2}Mg_{0.6}{Mn^{2+}}_{0.2}Al_4Si_2O_{10}(OH)_4 + SiO_2 \leftrightarrow {Fe^{2+}}_3Al_2(SiO_4)_3 + H_2O$

(chlorite + chloritoide + quartz ↔ almandine + water)

A further work which deals with Contact Aureoles is the thesis of BRÖCKER & FRANZ (2000). In their thesis "The contact aureole on Tinos (Cyclades, Greece): tourmaline-biotite geothermometry and Rb-Sr geochronology" they describe a contact aureole around a monzogranite intrusion.

In contrast to the country rocks of the Uitkomst Complex, the metapelites and dolomites of the contact aureole on Tinos are sparely distributed.

POVODEN, HORACEK & ABART (2002) dealt with the eastern Monzoni contact aureole. The estimated temperatures of maximal 1000°C are similar to the maximal temperatures at the contact of the Uitkomst Comples with nearly 1100°C in the contact area. Unfortunately this assumption isn't supported so far by field investigations of partly molten rocks. Because of that it is essential to take more samples in the conact nearest area and analysing them concerning their amorphous component.

The estimation for the temperature of the gabbroic magma of 1200°C is based on the work of WINKLER (1965).

The Monzoni Contact aureole is developed around a suite of pyroxenites, monzogabbros and monzodiorites.

The intrusion generated a contact aureole which is 860 m wide in the carbonate country rocks, where the contact aureole of the Uitkomst Complex is evidenced in a distance of approximately 800 m in the Malmani Dolomite and minimum 300 m in the Timeball Hill Shale.

The different extension in the two different lithotypes is caused by different petrological conditions. Those are mainly influenced by diverse bulk rock chemical compositions and different sensitivity for external fluids.

Originated by the emplacement of the Complex metasomatic processes took place proved by the enrichment of Mg and Fe in the contact near metapelites and calc-silicates. Beside that a enrichment in Cr_2O_3 is detectable in the contact-nearest Timeball Hill Shales up to a distance of 50 m away from the contact.

The markers for the temperature in the Malmani Dolomite around the Uitkomst Complex are certain mineral accumulations which can be expressed with the following reactions:

1. $3\ CaMg(CO_3)_2 + 4\ SiO_2 + H_2O \leftrightarrow Mg_3Si_4O_{10}(OH)_2 + 3CaCO_3 + 3CO_2$
   (3 dolomite + 4 quartz + water ↔ talc + 3 calcite + 3 carbondioxide)

2. $5\ Mg_3Si_4O_{10}(OH)_2 + 6\ CaCO_3 + 4\ SiO_2 \leftrightarrow 3\ Ca_2Mg_5[(OH,F)|Si_4O_{11}]_2 + 6\ CO_2 + 2H_2O$
   (5 talc + 6 calcite + 4 quartz ↔ 3 tremolite + 6 carbondioxide + 2 water)

3. $2\ Mg_3Si_4O_{10}(OH)_2 + 3\ CaCO_3 \leftrightarrow Ca_2Mg_5[(OH,F)|Si_4O_{11}]_2 + CaMg(CO_3)_2 + CO_2 + H_2O$
   (2 talc + 3 calcite ↔ tremolite + dolomite + carbondioxide + water)

4. $5\ CaMg(CO_3)_2 + 8\ SiO_2 + H_2O \leftrightarrow Ca_2Mg_5[(OH,F)|Si_4O_{11}]_2 + 3\ CaCO_3 + 7\ CO_2$
   (5 dolomite + 8 quartz + water ↔ tremolite + 3 calcite + 7 carbondioxide)

5. $Ca_2Mg_5[(OH,F)|Si_4O_{11}]_2 + 3\ CaCO_3 + 2\ SiO_2 \leftrightarrow 5\ CaMg[Si_2O_6] + 3\ CO_2 + H_2O$
   (tremolite + 3 calcite + 2 quartz ↔ 5 diopside + 3 carbondioxide + water)

6. $Ca_2Mg_5[(OH,F)|Si_4O_{11}]_2 + 3\ CaCO_3 \leftrightarrow CaMg(CO_3)_2 + 4\ CaMg[Si_2O_6] + CO_2 + H_2O$
   (tremolite + 3 calcite ↔ dolomite + 4 diopside + carbondioxide + water)

7. $CaCO_3 + SiO_2 \leftrightarrow CaSiO_3 + CO_2$

   (calcite + quartz ↔ wollastonite + carbondioxide)

8. $7\ CaCO_3 + Mg_3Si_4O_{10}(OH)_2 \leftrightarrow 4\ CaSiO_3 + 3\ CaMg(CO_3)_2 + H_2O + CO_2$

   (7 calcite + talc ↔ 4 wollastonite + 3 dolomite + water + carbondioxide)

The andradite is generated by the following reaction:

9. $Ca_2(Al,Fe^{3+},Mg)_3(SiO_4)_3OH + SiO_2 \leftrightarrow CaAl_2Si_2O_8 + Ca_3Al_2[SiO_4]_3/Ca_3Fe_2Si_3O_{12} \pm Fe_2O_3 + H_2O$
   (epidote + quartz ↔ anorthite + grossularite/andradite ± hematite + water)

The emplacement of the Complex was processed in impulses (LI et al 2002). Also ENGELBRECHT (1988) suggests a multiple emplacement of the Bushveld Complex and an associated refreshment of the Contact aureole. If there is a connection between the Uitkomst Complex and the Bushveld Complex (GAUERT 1998) it would be logical if the contact metamorphism of the Uitkomst Complex was a multiple process. The appearance of signs for overprints, like alteration processes and uncompleted transformation processes support this assumption.

A problem is to estimate the pressure which was existent during the emplacement. It is sure that the pressure was 0.7 kbar at minimum evidenced by the occurrence of epidote (PICHLER & SCHMITT-RIEGRAF, 1993). Minerals like sillimanite predict higher pressures of usually 2 kbar at ca. 600°C (MATTHES & OKRUSCH 2005).

For a better comparison a pressure of 2 kbar was assumed and is the basis for the estimations of the temperature. This pressure is suitable for contactmetamorphic settings (WINKLER 1965).

9. Conclusions

A short list should be given to present the most important results of this thesis:

1) The mineral assemblage and the chemical composition of the different lithotypes, in detail the Timeball Hill Shales and the Malmani Dolomite was object of detailed investigation and ends in the following results:

Table 9.1: Average chemical composition and predominating minerals of the main lithotypes of the country rocks of the Uitkomst Complex

Elementoxide [wt-%]	**Timeball Hill Shale**		**Malmani Dolomite**	
	surface	borehole	surface	borehole
SiO_2	50.39	62.64	56.97	48.86
Al_2O_3	35.57	16.49	1.53	5.61
Fe_2O_3tot	5.80	7.63	3.73	8.03
MnO	0.02	0.22	0.21	0.24
MgO	3.75	4.86	22,92	12.39
CaO	1.02	2.61	16.01	22.21
Na_2O	2.21	0.80	0.06	0.57
K_2O	2.45	4.57	0.01	0.48
TiO_2	0.48	0.92	0.04	0.51
P_2O_5	0.06	0.14	0.05	0.10
predominating minerals	quartz, corundum, biotite, mica	quartz, sillimanite, antigorite,	calcite, dolomite, ankerite,	calcite, dolomite, ankerite, diopside/augite,hornblende, antigorite, tremolite

		augite, chlor. serpentine, sanidine, albite, almandine	wollastonite, diopside, serpentine, hornblende, actinolite, andradite, talc	

2) Critical mineral reactions were calculated with TWQ (BERMAN 2006) and presented in this study.
3) Different zones of mineralisation were defined and they trace the contact aureole of the Uitkomst Complex (Fig. 9.1).

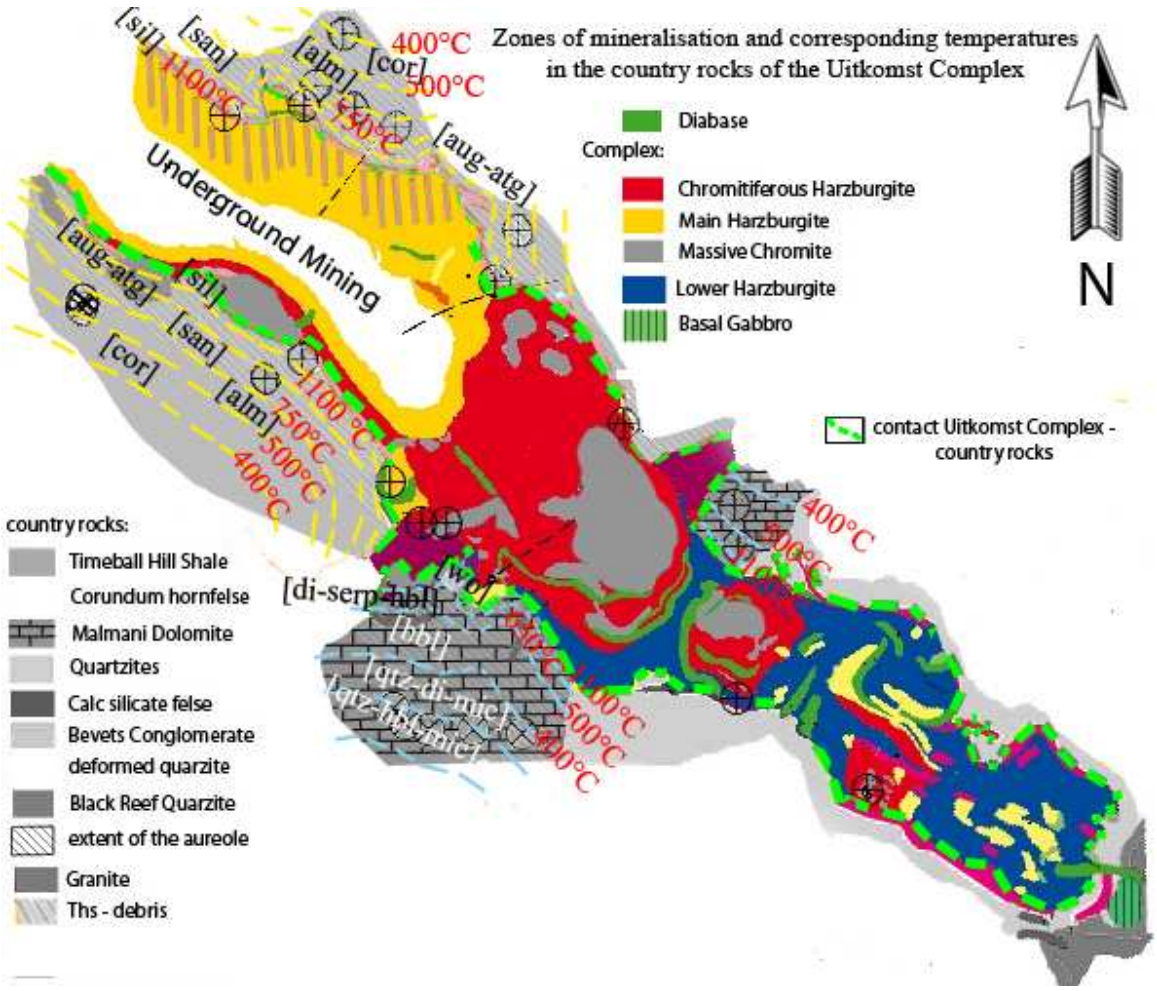

Fig. 9.1: Reconstruction of the different mineral zones linked with related isograde (not to scale)

4) The Construction of isogrades around the Uitkomst Complex (Fig. 9.1).

5) The presence of a Mg/Fe-metasomatism during the emplacement is evidenced by the observation of an extraordinary enrichment of these two elements in the contact near zones of the country rocks and the appearance of andradite in the contact close dolomites and almandine in the metapelites.

6) An intensified occurrence of Cr in the contact near Timeball Hill Shales is evidenced by the appearance of Cr-bearing minerals like chlorite chromian. That makes a "Cr-metasomatism" in the metapelites plausible.

7) The existence of dehydrated chlorites and the generation of wollastonite out of talc + calcite indicate decarbonatization and dehydration processes in the contact near country rocks. The dehydration leads to an increase of the p_{H2O} and causes an increase of the temperature for several critical mineral reactions (e.g. the formation of wollastonite out of the reaction of calcite + quartz).

8) Corundum is most prevalent in the southwestern part of the Timeball Hill Shales and is detectable in the surface samples of the Timeball Hill Shale which are characterized by an undersaturation of SiO_2 and an average content of Al_2O_3 of nearly 36 %. The composition of the corundum was in the focus of the investigation and lead to the assumption that the corundum hosts traces of Ti. This result is supported by optical investigation which shows a blue coloration of some corundum minerals. The rest of the corundum appears in a dirty brownish colour. Because of the small-scale distribution the corundum is not extractable. But the sapphire is maybe useable as gemstone if there are aggregates in an appropriate size.

9.1 Suggestion for further works

It is necessary to refine the reconstruction of the metamorphic conditions by including fluid information into the calculation of the phase equilibria after a copious investigation of fluid inclusions. Beside that it is advantageous to implement analyse data of the underground samples to the study. Both will lead to more detailed information about the contactmetamorphic scenery of the Uitkomst Complex.

Furthermore it is advantageous to collect more samples in smaller areas, especially in the contact closest area to proof the described temperatures in the contact zone which are suggested by the mineral assemblages.

10. References

ALEXANDER, A. E. (1948): Journal Gemn., 1 no. 8: p. 4.

ALLEN, I.V. L. (1990): The geology and geochemistry of the Uitkomst Igneous Complex, eastern Transvaal. B. Sc. (Hons) thesis 47 p. University Witwatersrand, Johannesburg, South Africa.

ANHAEUSSER, C. R., ROBB, L. J. & VILJOEN, M. J. (1981): Provisional geological map of the Barberton Greenstone Belt and surrounding granitic terrane, eastern Transvaal and Swaziland, Geological Society of South Africa, scale 1 : 250000.

ANHAEUSSER, C.R. (2001): The anatomy of an extrusive-intrusive Archaean mafic-ultramafic sequence: the Nelshoogte Schist Belt and Stolzberg Layered Ultramafic Complex, Barberton Greenstone Belt, South Africa, S. Afr. J. Geol., 104: 167 – 204.

ARAMAKI, S. & ROY R. (1963): A new polymorph of Al_2SiO_5 and further studies in the system $Al_2O_3 – SiO_2 – H_2O$, American Mineralogist, 48: 1322 – 1347.

ARTH, J. G. & HANSON, G. N. (1975): Geochemistry and origin of the early Prrecambrian Crust of northeastern Minnesota , Geochim. Cosmochim. Acta, 39: 325 – 362.

BERMAN, R.G., (1988): Internally-consistent thermodynamic data for minerals in the system Na_2O-K_2O-CaO-MgO-FeO-Fe_2O_3-Al_2O_3-SiO_2-TiO_2-H_2O-CO_2, Journal of Petrology, 29, 445-522.

BERMAN R.G., (1991): TWQ version 2.34 (database 2.32. BERMAN & ARANOVICH 2006) Can. Mineralogist, 29: 833-856.

BERMAN, R.G. (2007): Open file 5462, winTWQ (version 2.3) (ed. 2.32): a software package for performing internally-consistent thermobarometric calculations, Geological Survey of Canada, 41p.

BRÖCKER, M. & FRANZ, L. (2000): The contact aureole on Tinos (Cyclades, Greece): tourmaline-biotite geothermometry and Rb-Sr geochchronology. Mineralogy and Petrology, 70: 257-283.

BUCHER K. & FREY M. (2002): Petrogenesis of metamorphic rocks, 7th edition, Berlin, Heidelberg, New York (Springer), 318p.

BUTTON, A. (1976): Stratigraphy and relations of the Bushveld floor in the eastern Transvaal. Trans. Geol. Soc. S. Afr. 79: 3-12.

CLAUSER, C. & HUENGES, E. (1995): Thermal conductivity of rocks and minerals. – American Geophysical Union. 105 – 126.

CLENDENIN, C. W., HENRY G. & CHARLESWORTH, E. G. (1991): Characteristics of and influences on the Black Reef depositional sequence in the eastern Transvaal. South African Journal of Geology, 94: 321 – 327.

CONDIE, K. C. & HUNTER, D. R. (1976): Trace element geochemistry of Archean granitic rocks from the Barberton region, South Africa. Earth and Planetary Science Letters, 29: p. 389.

CONNOLLY, J.A.D (2005): Computation of phase equilibria by linear programming: A tool for geodynamic modeling and its application to subduction zone decarbonation. Earth and Planetary Science Letters, 236: 524 - 541

DE WAAL, S.A., MAIER W., ARMSTRONG R. & GAUERT C.D.K. (2001): Chemical constraints on the differentiation and emplacement of the Uitkomst Complex, Mpumalanga Province, South Africa, Canadian Mineralogist, 39: 557 – 571

EHLERS, E.G. & BLATT, H. (1982): Petrology – Igneous, Sedimentary and Metamorphic, San Francisco (W. H. Freeman and Company)

ENGELBRECHT, J. P. (1988): The metamorphic aureole of the Bushveld Complex in the Marico district, western Transvaal, South Africa, Research Report No. 77, University of Pretoria: 22 p.

ERIKSSON P. G., SCHREIBER U.M. & VAN DER NEUT, M. (1991): A review of the sedimentology of the Early Proterozoic Pretoria Group, Transvaal Sequence, South Africa: implications for tectonic setting. Journal of African Earth Sciences vol. 10: 107 – 119

ERIKSSON P. G., SCHWEITZER, J. K., BOSCH, B. J. A., SCHREIBER, U. M., VAN DEVENTER, J. L. & HATTON, C. J. (1993): The Transvaal Sequence: an overview. Journal of African Earth Sciences Vol. 16: 25 – 51

ERIKSSON P. G., HATTINGH P. J. & ALTERMANN W. (1995): An overview of the geology of the Transvaal Sequence and Bushveld Complex, South Africa. In: Mineralium Deposita 30, 98 – 111. Berlin, Heidelberg, New York (Springer).

FÜCHTBAUER, H. (1988): Sedimente und Sedimentgesteine. 4th edition. Schweizerbart'sche Verlagsbuchhandlung, Stuttgart, 356p.

GAUERT, C. D. K., DE WAAL, S.A. & WALLMACH T. (1995): The Geology of the Uitkomst Complex, Eastern Transvaal – Evidence for a Magma Conduit. In: Extended Abstracts of the Centennial Geocongress: 512-515. Geological Society South Africa, Johannesburg.

GAUERT, C. D. K., DE WAAL, S.A. & WALLMACH T. (1995): Geology of the ultrabasic to basic Uitkomst Complex, eastern Transvaal, South Africa: an overview – Journal of African Earth Sciences, 12: 108 – 126.

GAUERT, C. D. K. (1998): The petrogenesis of the Uitkomst Complex. PhD thesis, unpublished. University of Pretoria, South Africa, 315 p.

GAVRUSEVICH, B. A. (1941): Doklady Acad. Sci. USSR. 31. p. 686.

GREENWOOD, H. J. (1967a): American Mineralogist, 52: 1169 – 1180.

GUIRAUD, M., KIENAST, J.R. & OUZEGANE, K. (1996): Corundum – quartz bearing assemblage in the Ihouhaouene area (In Ouzal, Algeria), Journal of Metamorphic Geology, 14: 754 – 762.

HARLOV. D.E. & MILKE, R. (2002): Stability of corundum + quartz relative to kyanite and sillimanite at high temperature and pressure, American Mineralogist, 87: 424 – 432.

HARTZER F. J. (1995): Transvaal Supergroup inliers: geology, tectonic development and relationship with the Bushveld complex, South Africa. Journal of African Earth Sciences, 21 No. 4: 521-547

HATTON, C. J. & SHARPE, M. R. (1989): Significance and origin of boninite-like rocks associated with the Bushveld Complex. In: Boninites (Edited by CRAWFORD, A. J.): 174 – 208. London. (Unwin Hyman).

HENRY, G., CLENDENIN C. W. & CHARLESWORTH, E. G. (1990): Depositional facies of the Black Reef Quartzite Formation in the eastern Transvaal. Geocongress ’90 (Cape Town, South Africa) Abstract nos. 230 – 233.

HORNSEY, A.E. (1999): The genesis and evolution of Nkomati mine Ni-Sulfide deposit, Mpumalanga Province, South Africa. M.Sc. thesis University of Natal (Durban), 224 pp.

LI, C. & NALDRETT, A.J. (1993): Sulphide capacity of magma: A Quantitative model and its application to the formation of sulphide ores of Sudbury, Ontario. Economic Geology 88: 1253 – 1260.

LI, C., RIPLEY, E.M., MAIER, W.D. & GOMWE, T.F.S. (2002): Olivine and sulfur isotopic compositions of the Uitkomst Ni-Cu sulphide ore-bearing complex, South Africa: evidence for sulfur contamination and multiple magma emplacements, Chemical Geology, 188: 149 – 159.

LIKHANOV, I.I., REVERDATTO, V.V., SHEPLEV, V.S., VERSCHININ, A.E., KOZLOV, P.S. (2000): Contact metamorphism of Fe- and Al-rich graphitic metapelites in the Transangarian region of the Yenisei Ridge, eastern Siberia, Russia, Lithos, 58: 55 – 80.

KERRICK, D. M. (1972): Experimental determination of muscovite + quartz stability with $p_{H2O} < p_{total}$, American Journal of Science 272: 946 – 958.

KENYON, A. K., ATTRIDGE, R.L. & COETZEE, G.L. (1986): The Uitkomst Nickel-Copper Deposit, Eastern Transvaal. In: Mineral Deposits of Southern Africa I (Edited by ANHAEUSSER, C.R. & MASKE S.). 1009 – 1019. Geological Society of South Africa, Johannesburg.

KROGH, E.J. (1977): Origin and metamorphism of iron formation and associated rocks, Lofoten – Vesterålen, N. Norway. I. The Vestpolltind Fe-Mn deposit, Lithos, 10: 243 – 255.

MAIER, W.D., GOMWE, T, BARENS, S.J., LI, C., THEART, H.(2004): Platinum group elements in the Uitkomst Complex, South Africa, Econ. Geol., 99: 499 – 516.

MASON, B. & MOORE,C. B. (1985): Grundzüge der Geochemie. Stuttgart (Enke), 338p.

MATTHES, S. & OKRUSCH, M. (2005): Mineralogie – Eine Einführung in die spezielle Mineralogie, Petrologie und Lagerstättenkunde. 7th edn. Berlin, Heidelberg, New York (Springer), 567p.

MOURI, H., GUIRAUD, M. & OSANAI, Y. (2004): Review on “corundum + quartz assemblage in nature: Possible indicator of ultra-high temperature conditions?, Journal of Mineralogical and Petrological Sciences, 99: 159 – 163.

MYASHIRO, A. (1973): Metamorphism and metamorphic belts, London (Allen & Unwin), 428p.

NESSE, W.D. (2000): Introduction to mineralogy. (Oxford University Press), 297p.

PICHLER, H. & SCHMITT-RIEGRAF, C. (1993): Gesteinsbildende Minerale im Dünnschliff. 2nd edn. Stuttgart (Enke), 233p.

POVODEN E., HORACEK M. & ABART, R. (2002): Contact metamorphism of siliceous dolomite and impure limestones from the Werfen formation in the eastern Monzoni contact aureole. Mineralogy and Petrology, 76: 99 – 120.

ROBB, L. J. & ANHAEUSSER C. R. (1983): Chemical and petrogenetic characteristics of the Archean tonalite-trondhjemite gneiss plutons in the Barberton Mountain Land. In: ANHAEUSSER, C.R. (ed.) Contributions to the Geology of the Barberton Mountain Land. Special Publication of the Geological Society of South Africa, 9: 103-116.

RÖSLER, H. J. (1991): Lehrbuch der Mineralogie. 5th ed. Leipzig (Deutscher Verlag für Grundstoffindustrie), 833p.

SARKAR, A., RIPLEY, E.M., CHUSI, L., MAIER, W.D. (2008): Stable isotope, fluid inclusion and mineral chemistry constraints on contamination and hydrothermal alteration in the Uitkomst Complex, South Africa. Chemical Geology, 257: 129 – 138.

SCHREIBER, U. M. (1990): A palaeoenvironmental study of the Pretoria Group in the eastern Transvaal. PhD thesis, University of Pretoria, South Africa, 308 p.

SCHREIBER, U. M., ERIKSSON, P. G., VAN DER NEUT M., & SNYMAN, C. P (1992): Sedimentary petrography of the Early Proterozoic Pretoria Group, Transvaal Sequence, South Africa: implications for tectonic setting. Sedim. Geol. Vol. 80: 89 – 103.

SHAW, R.K. & ARIMA, M. (1998): A corundum-quartz assemblage from the Eastern Ghats Granulite Belt, India: evidence for high P-T metamorphism?, Journal of Metamorphic Geology, 16: 189 – 196.

STORRE, B. (1970): Stabilitätsbedingungen Grossular – führender Paragenesen im System $CaO – Al_2O_3 – SiO_2 – CO_2 – H_2O$. Contr. Mineral. and Petrol. 29: 145 – 162.

SYMNES G. H. & FERRY, J. M. (1995): Metamorphism, Fluid Flow and Partial Melting in Pelitic Rocks from the Onawa Contact Aureole, Central Maine, USA. Journal of Petrology, 36 No.2: 587 – 612.

TARNEY, J., WEAVER, B. L. & DRURY S. A. (1979): Geochemistry of Archaen trondhjemitic and tonalitic gneisses from Scotland and E. Greenland. In: Barker F. (Ed.) Trondhjemites, Dacites and Related Rocks: 275 – 299. Amsterdam (Elsevier).

WAGNER, P. A. (1929): The Platinum Deposits and Mines of South Africa (1973 edition). Johannesburg (Struik), 247p.

WALRAVEN, F. & MARTINI, J (1995): Zircon Pb-evaporation age determinations of the Oak Tree Formation, Chuniespoort Group, Transvaal Sequence: implications for Transvaal-Griqualand West basin correlations, S. Afr. J. Geol. 98: 58 -67.

WINKLER, H. G. F. (1965): Petrogenesis of Metamorphic Rocks. Berlin, Heidelberg, New York (Springer), 298p.

WINKLER, H. G. F. (1979): Petrogenesis of Metamorphic Rocks. Berlin, Heidelberg, New York (Springer), 348p.

WOOLFE, J. (2006): Nkomati presentation May 2006, unpublished company slideshow, ARM.

VON SCHEIBLER, W. H. T. M. (1991): The genesis of the Uitkomst Igneous Complex. Anglo American Prospecting Services Report (unpublished), including one geological map: 12 p., Verwoerdburg, RSA.

YARDLEY, B. W. D. (1997): Einführung in die Petrologie metamorpher Gesteine. Stuttgart (Enke), 323p.

Interactive data origin:

http://www.nornik.ru/en/our_products/norilsknickelafrica/#2
http://www.cameca.fr/html/epma_technique.html

ACKNOWLEDGEMENTS

I would like to thank my supervisor Prof. Dr. Christoph Gauert for his support, his advice and the fruitful discussions while writing this thesis. Furthermore I want to thank Prof. Dr. Klaus Bente for helping me in questions of mineralogy and thermodynamics and for making the investigations with the electron microprobe possible. Also I am thanking Mark Davidson from Nkomati Nickel for his support and making this project possible. Tebogo Phokanaka, Zongs, Richard Carey, Yvonne Flattery, Grant Halbeck and Neil Hamilton are also thanked for their advice, their ideas and their support while doing the field work at Nkomati Nickel. I am grateful for the assistance of Dr. Hans-Joachim Höbler during the measurements with the EMPA. I wish to thank Dr. Charles Barker for his helpful contributions for the work with ArcGIS. Also I would like to thank Prof. Dr. Willem v. d. Westhuizen for his effort concerning the realization of this study and his great support.

DECLARATION

I, Jens Kirste declare that this thesis is my own, unaided work. It is being submitted for the Degree of Master of Science at the University the Free State, Bloemfontain, South Africa. The thesis has not been submitted before for any degree or examination in any other University.

Leipzig, the 14th May 2009

APPENDIX I – XRF – results

I-Ia Timeball Hill Shale – boreholes

	SiO2	Al2O3	Fe2O3	MnO	MgO	CaO	Na2O	K2O	TiO2	P2O5
	(%)	(%)	(%)	(%)	(%)	(%)	(%)	(%)	(%)	(%)
JK-64	60,15	7,38	11,66	0,09	19,93	0,64	0,84	0,41	0,42	0,13
LLD (ppm)	195,58	63,50	14,05	23,49	63,55	16,52	219,59	12,00	58,76	14,53
JK-65	51,70	32,57	10,63	0,03	1,94	0,57	1,21	2,81	0,80	0,27
LLD (ppm)	196,46	71,25	14,09	23,81	67,18	16,66	215,28	12,75	58,89	14,87
JK-72	65,05	20,27	4,69	0,06	3,21	0,55	1,39	4,89	0,64	0,08
LLD (ppm)	194,89	66,94	13,66	23,38	60,55	16,86	214,36	13,24	59,16	14,65
JK-74	52,77	20,94	14,71	1,28	2,73	0,56	0,37	4,70	2,11	0,13
LLD (ppm)	195,14	67,02	14,59	24,24	60,82	16,84	216,73	13,29	59,19	14,82
JK-79	78,05	13,04	0,66	0,01	0,90	0,11	0,15	8,20	0,48	0,08
LLD (ppm)	193,53	65,60	13,49	23,46	54,11	17,29	212,50	14,09	59,51	14,72
JK-80	66,17	15,28	1,60	0,03	3,03	1,63	0,44	12,22	0,66	0,10
LLD (ppm)	193,62	65,93	13,86	23,94	56,62	18,09	213,38	15,33	60,10	14,66
JK-82	63,39	20,84	7,02	0,04	1,81	0,39	0,28	6,50	0,81	0,09
LLD (ppm)	194,76	67,46	13,96	23,71	59,39	16,97	214,19	13,68	59,24	14,88
JK-83	72,69	3,96	5,62	0,25	3,13	10,96	0,30	1,14	0,09	0,02
LLD (ppm)	192,89	61,69	14,07	24,01	49,16	18,65	214,86	12,29	59,81	14,84
JK-87	53,78	14,11	12,03	0,22	7,06	8,05	2,24	0,31	2,27	0,39
LLD (ppm)	194,74	64,76	14,47	24,15	59,52	18,12	217,73	11,97	59,56	14,86

	Sum	Result type	S	CaO	Sc	TiO2	V	Cr
	of conc.		S	Ca	Sc	Ti	V	Cr
	(%)		(ppm)	(ppm)	(ppm)	(ppm)	(ppm)	(ppm)
JK-64	16,033	Concentration	9,14	5951,39	37,78	4149,48	327,03	3448,81
		LLD (ppm)	1,13	14,68	3,26	13,09	4,68	3,68
JK-65	14,144	Concentration	16,80	5296,45	12,21	7286,40	247,68	279,86
		LLD (ppm)	1,06	14,12	3,32	13,21	4,94	3,56
JK-72	6,011	Concentration	117,44	3988,88	10,52	2818,83	135,70	185,55
		LLD (ppm)	1,13	12,91	3,47	9,95	4,81	3,37
JK-74	17,266	Concentration	12,24	4389,96	21,05	23983,15	207,95	235,57
		LLD (ppm)	1,13	14,28	3,56	14,19	6,84	4,39
JK-79	1,335	Concentration	11,20	836,77	5,19	4741,72	88,57	315,21
		LLD (ppm)	1,09	13,09	3,68	11,71	4,88	3,35
JK-80	3,711	Concentration	326,13	13926,24	11,56	5993,89	111,20	393,99
		LLD (ppm)	1,18	13,03	4,02	11,16	5,70	3,68
JK-82	8,632	Concentration	4720,44	3475,08	15,03	8042,78	573,40	238,38
		LLD (ppm)	1,73	13,40	3,33	12,86	5,11	3,52
JK-83	14,617	Concentration	4328,83	93968,41	10,96	792,56	18,44	40,07
		LLD (ppm)	1,67	16,75	4,04	11,59	4,94	3,57
JK-87	18,867	Concentration	1618,94	34393,58	18,39	2450,33	210,62	30242,42
		LLD (ppm)	1,33	16,59	4,58	13,45	6,07	6,08

	Sum of conc.	Result type	Fe2O3 Fe	Co Co	Ni Ni	Cu Cu	Zn Zn	Ga Ga
	(%)		(ppm)	(ppm)	(ppm)	(ppm)	(ppm)	(ppm)
JK-64	16,033	Concentration	144117,30	75,33	1749,70	303,74	61,08	9,04
		LLD (ppm)	15,43	Not calc.	1,45	1,27	1,33	0,85
JK-65	14,144	Concentration	127070,20	40,86	80,24	23,00	27,79	34,83
		LLD (ppm)	15,02	Not calc.	1,36	1,26	1,30	0,86
JK-72	6,011	Concentration	51156,00	9,62	104,46	17,43	17,21	23,32
		LLD (ppm)	15,94	Not calc.	1,18	0,92	1,16	0,76
JK-74	17,266	Concentration	142115,10	12,82	123,97	29,16	20,11	28,56
		LLD (ppm)	15,42	Not calc.	1,66	1,48	1,56	1,02
JK-79	1,335	Concentration	6494,90	8,40	25,58	43,90	0,00	13,94
		LLD (ppm)	13,42	Not calc.	1,02	1,03	1,07	0,69
JK-80	3,711	Concentration	14961,54	20,09	196,97	89,76	0,00	16,89
		LLD (ppm)	12,96	Not calc.	1,16	1,14	1,18	0,77
JK-82	8,632	Concentration	67026,55	26,56	179,47	91,27	27,30	22,83
		LLD (ppm)	14,98	Not calc.	1,21	1,16	1,20	0,80
JK-83	14,617	Concentration	45712,92	11,55	29,60	310,29	50,30	3,29
		LLD (ppm)	15,10	Not calc.	1,19	1,15	1,21	0,79
JK-87	18,867	Concentration	116531,40	125,52	2354,27	570,04	97,28	7,23
		LLD (ppm)	16,37	Not calc.	1,65	1,48	1,55	0,97

	Sum	Result type	Ge	As	Se	Br	Rb	Sr	Y	Zr	Nb
	of conc.		Ge	As	Se	Br	Rb	Sr	Y	Zr	Nb
	(%)		(ppm)	(ppm)	(ppm)	(ppm)	(ppm)	(ppm)	(ppm)	(ppm)	(ppm)
JK-64	16,033	Concentration	1,78	1,25	0,00	0,27	20,83	6,95	18,02	76,15	7,31
		LLD (ppm)	0,84	7,45	1,19	1,28	0,80	0,57	0,92	0,83	0,81
JK-65	14,144	Concentration	0,48	61,54	0,00	0,90	137,45	118,13	23,69	93,82	11,95
		LLD (ppm)	0,85	7,38	1,18	1,28	0,81	0,57	1,07	0,91	0,81
JK-72	6,011	Concentration	1,13	5,99	1,79	1,31	161,91	76,51	112,15	138,29	15,44
		LLD (ppm)	0,76	6,70	1,06	1,17	0,74	0,52	1,01	0,81	0,75
JK-74	17,266	Concentration	0,77	0,00	0,11	0,80	175,65	30,04	37,20	287,58	21,62
		LLD (ppm)	1,00	8,79	1,41	1,50	0,95	0,67	1,29	0,99	0,94
JK-79	1,335	Concentration	0,70	1,25	0,00	0,85	142,53	26,05	9,29	102,09	6,90
		LLD (ppm)	0,69	5,93	0,94	1,02	0,67	0,48	0,92	0,71	0,69
JK-80	3,711	Concentration	0,00	2,72	0,82	1,18	210,96	47,14	17,43	125,56	9,52
		LLD (ppm)	0,77	6,61	1,05	1,14	0,74	0,53	1,08	0,80	0,75
JK-82	8,632	Concentration	1,25	0,00	4,16	0,97	157,43	18,77	53,58	189,83	15,22
		LLD (ppm)	0,78	6,88	1,09	1,19	0,76	0,54	1,03	0,79	0,77
JK-83	14,617	Concentration	0,22	2,54	3,79	2,95	35,09	74,13	28,73	32,24	2,88
		LLD (ppm)	0,78	6,67	1,06	1,15	0,75	0,53	0,88	0,82	0,76
JK-87	18,867	Concentration	0,00	1,81	3,70	1,00	16,60	29,77	6,03	31,80	2,01
		LLD (ppm)	0,97	8,19	1,31	1,41	0,91	0,64	1,02	0,93	0,90

	Sum of conc. (%)	Result type	Mo Mo (ppm)	Ag Ag (ppm)	Cd Cd (ppm)	Sn Sn (ppm)	Sb Sb (ppm)	Te Te (ppm)	I I (ppm)	Ba Ba (ppm)
JK-64	16,033	Concentration	0,00	0,00	0,02	0,00	0,00	0,01	6,34	61,95
		LLD (ppm)	0,75	6,95	6,88	5,12	7,61	0,02	8,74	Not calc.
JK-65	14,144	Concentration	4,40	5,50	0,27	0,00	0,00	0,00	13,14	634,68
		LLD (ppm)	0,75	6,92	6,84	5,12	7,64	0,02	8,78	Not calc.
JK-72	6,011	Concentration	0,00	7,49	3,69	0,00	3,35	0,02	9,76	935,09
		LLD (ppm)	0,69	6,47	6,40	4,93	7,47	0,02	8,47	Not calc.
JK-74	17,266	Concentration	0,00	1,84	2,45	0,00	0,00	0,01	8,82	1038,30
		LLD (ppm)	0,87	8,30	8,21	6,06	8,95	0,03	10,28	Not calc.
JK-79	1,335	Concentration	0,00	8,81	5,06	0,00	0,00	0,01	7,33	444,87
		LLD (ppm)	0,64	5,25	5,20	4,05	6,19	0,02	7,18	Not calc.
JK-80	3,711	Concentration	0,00	2,55	0,00	0,00	0,35	0,02	10,74	612,04
		LLD (ppm)	0,70	6,25	6,18	4,61	6,85	0,02	8,00	Not calc.
JK-82	8,632	Concentration	19,07	2,30	0,00	0,00	1,20	0,02	14,24	1389,27
		LLD (ppm)	0,71	6,47	6,39	4,78	7,12	0,02	8,31	Not calc.
JK-83	14,617	Concentration	0,30	3,89	0,66	0,00	0,00	0,02	17,93	679,98
		LLD (ppm)	0,70	6,28	6,22	4,68	6,99	0,02	8,10	Not calc.
JK-87	18,867	Concentration	0,00	2,15	0,00	0,00	0,00	0,04	9,96	70,02
		LLD (ppm)	0,82	7,82	7,74	5,60	8,17	0,03	9,47	Not calc.

	Sum	Result type	Yb	Hf	Ta	W	Hg	Tl	Pb	Bi	Th	U
	of conc.		Yb	Hf	Ta	W	Hg	Tl	Pb	Bi	Th	U
	(%)		(ppm)	(ppm)	(ppm)	(ppm)	(ppm)	(ppm)	(ppm)	(ppm)	(ppm)	(ppm)
JK-64	16,033	Concentration	0,00	3,50	0,00	0,80	0,00	0,00	1,71	0,74	15,94	3,82
		LLD (ppm)	8,00	5,26	4,01	2,90	0,02	2,74	2,07	2,99	3,02	1,98
JK-65	14,144	Concentration	0,00	3,84	0,00	3,55	0,00	0,31	1,52	0,00	21,95	4,86
		LLD (ppm)	5,83	5,20	3,67	2,72	0,02	2,71	2,10	2,97	3,05	2,01
JK-72	6,011	Concentration	0,00	3,40	0,59	7,11	0,00	3,99	52,74	0,00	14,88	3,84
		LLD (ppm)	4,08	4,63	3,15	2,35	0,02	2,50	1,96	2,66	2,80	1,90
JK-74	17,266	Concentration	0,00	10,48	1,50	6,41	0,00	1,34	0,00	0,35	19,59	3,57
		LLD (ppm)	7,61	6,16	4,41	3,24	0,03	3,22	2,47	3,55	3,51	2,33
JK-79	1,335	Concentration	0,00	2,28	0,00	5,32	0,00	0,00	2,84	0,51	8,51	2,55
		LLD (ppm)	2,89	4,20	2,76	2,08	0,02	2,21	1,72	2,35	2,56	1,65
JK-80	3,711	Concentration	0,00	4,22	2,57	6,58	0,00	1,85	15,82	1,29	9,13	1,65
		LLD (ppm)	3,77	4,63	3,11	2,32	0,02	2,45	1,92	2,64	2,81	1,84
JK-82	8,632	Concentration	0,00	3,60	2,67	11,63	0,00	0,00	3,54	1,92	24,03	16,13
		LLD (ppm)	4,63	4,83	3,27	2,46	0,02	2,55	1,96	2,73	2,86	1,85
JK-83	14,617	Concentration	0,00	1,64	0,00	19,91	0,00	1,98	5,83	3,24	7,17	2,78
		LLD (ppm)	4,03	4,81	3,27	2,42	0,02	2,48	1,89	2,65	2,84	1,82
JK-87	18,867	Concentration	0,00	0,43	0,00	0,00	0,00	0,57	2,86	4,14	1,15	3,38
		LLD (ppm)	9,35	6,13	4,70	3,39	0,03	3,02	2,28	3,28	3,35	2,19

I-Ib Timball Hill Shale – surface

	Sum	Result type	SiO2	Al2O3	Fe2O3	MnO	MgO	CaO	Na2O	K2O	TiO2	P2O5
	of conc.		(%)	(%)	(%)	(%)	(%)	(%)	(%)	(%)	(%)	(%)
	(%)											
JK-40	100,47	Concentration	39,78	49,30	2,30	0,02	1,50	1,84	2,00	3,30	0,41	0,04
		LLD (ppm)	197,76	73,96	13,40	23,31	75,76	16,98	64,57	12,75	59,00	14,55
JK-41	103,93	Concentration	38,34	47,15	6,46	0,03	2,77	1,58	4,76	2,30	0,46	0,10

		LLD (ppm)	201,32	74,10	13,67	23,25	75,92	16,85	215,30	12,56	58,98	14,52
JK-42	101,87	Concentration	85,90	0,16	1,41	0,04	12,97	1,67	-0,30	0,00	0,02	0,00
		LLD (ppm)	193,95	61,38	13,24	23,06	54,36	16,40	63,83	11,82	58,80	14,66
JK-43	102,76	Concentration	39,17	47,22	7,06	0,02	2,81	0,53	3,09	2,30	0,51	0,05
		LLD (ppm)	198,06	74,72	13,70	23,12	75,32	16,56	65,83	12,51	58,77	14,50
JK-44	100,37	Concentration	44,33	38,51	10,54	0,03	2,11	0,28	1,50	2,48	0,53	0,04
		LLD (ppm)	196,61	71,32	14,03	23,61	70,40	16,46	62,82	12,55	58,90	14,53
JK-45	101,15	Concentration	54,86	31,11	7,05	0,01	0,35	0,21	2,19	4,30	0,94	0,15
		LLD (ppm)	196,10	69,31	13,89	23,54	65,75	16,82	63,85	13,26	59,07	14,53

	Sum of conc.	Result type	S	CaO	Sc	TiO2	V	Cr	Fe2O3	Co	Ni
	(%)		(ppm)	(ppm)	(ppm)	(ppm)	(ppm)	(ppm)	(ppm)	(ppm)	(ppm)
JK-40	5,403	Concentration	328,97	17664,29	8,19	3663,24	542,87	790,84	29325,12	18,03	95,68
		LLD (ppm)	1,33	15,91	3,60	13,61	4,70	3,19	15,53	Not calc.	1,05
JK-41	10,401	Concentration	43,28	14622,88	9,28	4122,40	531,57	682,38	82378,13	28,93	150,25
		LLD (ppm)	1,25	16,35	3,65	13,96	4,88	3,34	16,26	Not calc.	1,25
JK-42	3,743	Concentration	23,54	19326,92	2,51	75,08	2,89	60,33	17852,94	3,29	7,31
		LLD (ppm)	1,26	15,52	3,49	12,35	3,97	2,73	15,32	Not calc.	0,93
JK-43	10,207	Concentration	28,91	4656,50	12,54	4905,87	516,31	611,61	89963,27	24,26	190,87
		LLD (ppm)	1,32	16,46	3,48	13,84	4,79	3,27	18,22	Not calc.	1,22
JK-44	13,46	Concentration	30,62	2473,52	11,61	3965,12	392,71	510,43	125975,60	39,36	204,43
		LLD (ppm)	1,36	15,68	3,74	13,98	5,02	3,51	16,93	Not calc.	1,41
JK-45	9,383	Concentration	151,01	2326,95	22,46	9337,50	221,97	645,32	79177,57	11,71	43,04
		LLD (ppm)	1,30	15,04	3,82	13,85	5,66	3,52	16,87	Not calc.	1,30

	Sum of conc.	Result type	Cu	Zn	Ga	Ge	As	Se	Br	Rb	Sr
	(%)		(ppm)	(ppm)	(ppm)	(ppm)	(ppm)	(ppm)	(ppm)	(ppm)	(ppm)
JK-40	5,403	Concentration	31,71	0,24	50,03	0,43	11,64	0,00	1,26	85,07	385,66
		LLD (ppm)	1,04	0,92	0,67	0,68	6,35	0,96	1,05	0,67	0,47
JK-41	10,401	Concentration	37,84	36,03	57,89	0,00	0,70	0,03	1,28	57,44	442,64
		LLD (ppm)	1,18	1,05	0,76	0,77	7,14	1,08	1,17	0,75	0,52
JK-42	3,743	Concentration	72,70	-0,58	-0,13	0,00	0,00	0,12	1,18	1,07	1,28
		LLD (ppm)	0,94	0,84	0,60	0,61	5,59	0,84	0,92	0,60	0,41
JK-43	10,207	Concentration	47,84	23,69	50,98	1,49	5,35	0,40	2,06	74,95	292,93
		LLD (ppm)	1,16	1,02	0,74	0,74	6,94	1,05	1,14	0,74	0,51

JK-44	13,46	Concentration	88,03	45,43	45,08	0,47	8,46	0,14	1,39	61,94	103,03
		LLD (ppm)	1,30	1,14	0,82	0,83	7,83	1,18	1,29	0,80	0,55
JK-45	9,383	Concentration	48,62	0,00	37,05	1,69	10,73	0,16	2,04	142,38	272,21
		LLD (ppm)	1,24	1,08	0,79	0,80	7,62	1,15	1,25	0,78	0,54

	Sum of conc.	Result type	Y	Zr	Nb	Mo	Ag	Cd	Sn	Sb	Te
	(%)		(ppm)	(ppm)	(ppm)	(ppm)	(ppm)	(ppm)	(ppm)	(ppm)	(ppm)
JK-40	5,403	Concentration	24,09	37,98	4,48	0,00	2,52	2,71	0,00	0,75	0,06
		LLD (ppm)	0,83	0,89	0,70	0,62	5,42	4,97	3,77	5,65	0,03
JK-41	10,401	Concentration	11,54	48,33	4,59	0,00	0,66	0,00	0,00	0,00	0,04
		LLD (ppm)	0,88	1,00	0,77	0,68	6,24	5,72	4,26	6,31	0,03
JK-42	3,743	Concentration	0,74	0,15	0,00	0,00	0,00	1,02	0,00	0,00	0,02
		LLD (ppm)	0,67	0,62	0,65	0,58	4,86	4,46	3,38	5,06	0,03
JK-43	10,207	Concentration	16,20	49,15	5,76	1,68	3,38	1,05	0,00	0,00	0,03
		LLD (ppm)	0,89	0,91	0,76	0,67	6,04	5,53	4,19	6,28	0,03
JK-44	13,46	Concentration	13,58	52,83	5,94	2,70	0,00	0,00	0,00	0,00	0,02
		LLD (ppm)	0,95	0,87	0,82	0,73	7,05	6,46	4,69	6,85	0,04
JK-45	9,383	Concentration	33,89	147,46	17,75	0,65	4,72	5,63	0,00	0,00	0,05
		LLD (ppm)	1,03	0,96	0,80	0,72	6,56	6,01	4,50	6,71	0,04

	Sum of conc.	Result type	I	Ba	Yb	Hf	Ta	W	Hg	Tl	Pb	Bi	Th	U
	(%)		(ppm)	(ppm)	(ppm)	(ppm)	(ppm)	(ppm)	(ppm)	(ppm)	(ppm)	(ppm)	(ppm)	(ppm)
JK-40	5,403	Concentration	19,57	937,19	0,00	0,96	0,00	2,21	0,00	1,32	4,30	0,18	4,89	1,11
		LLD (ppm)	7,16	Not calc.	3,51	4,09	3,19	2,39	0,02	2,54	1,72	2,19	2,62	1,68
JK-41	10,401	Concentration	16,59	783,70	0,00	0,00	0,00	0,00	0,00	1,78	3,07	0,00	7,11	2,69
		LLD (ppm)	7,95	Not calc.	4,86	4,68	3,77	2,82	0,02	2,84	1,90	2,47	2,88	1,86
JK-42	3,743	Concentration	10,92	9,46	0,00	0,00	0,00	0,00	0,00	1,61	0,00	0,50	0,00	0,00
		LLD (ppm)	6,32	Not calc.	2,80	3,70	2,87	2,15	0,01	2,25	1,52	1,90	2,37	1,49
JK-43	10,207	Concentration	20,90	594,42	0,00	2,67	1,25	5,95	0,00	1,81	2,69	0,57	8,80	2,65
		LLD (ppm)	7,82	Not calc.	4,91	4,55	3,64	2,69	0,02	2,76	1,86	2,41	2,82	1,82
JK-44	13,46	Concentration	11,67	656,60	0,00	3,58	0,00	1,34	0,00	0,00	0,27	0,57	9,23	1,22
		LLD (ppm)	8,61	Not calc.	6,14	5,09	4,21	3,10	0,02	3,13	2,08	2,68	3,05	1,99
JK-45	9,383	Concentration	20,12	1150,12	0,00	4,28	1,17	6,72	0,00	-0,90	6,74	-0,05	34,01	8,31
		LLD (ppm)	8,42	Not calc.	4,94	4,90	3,87	2,86	0,02	3,04	2,04	2,63	3,00	1,95

I-II Bevets Conglomerate

	Sum		SiO2	Al2O3	Fe2O3	MnO	MgO	CaO	Na2O	K2O	TiO2	P2O5
	of conc.											
	(%)		(%)	(%)	(%)	(%)	(%)	(%)	(%)	(%)	(%)	(%)
JK-69	102,57	Concentration	98,58	2,30	0,47	0,01	0,17	0,12	0,23	0,60	0,10	0,01
		LLD (ppm)	193,33	63,10	13,14	22,81	46,73	16,12	59,58	11,95	58,70	14,80
JK-70	102,45	Concentration	96,83	2,74	0,87	0,02	0,13	0,19	1,12	0,39	0,15	0,01
		LLD (ppm)	193,59	63,81	13,15	23,10	46,74	16,10	61,59	11,79	58,70	14,72
JK-73	101,53	Concentration	91,44	1,68	2,68	0,08	2,14	3,11	0,30	0,02	0,07	0,01
		LLD (ppm)	193,20	63,24	13,38	23,24	47,02	16,82	60,86	11,70	59,01	14,64
JK-84	102,16	Concentration	99,11	0,70	0,83	0,02	0,28	1,05	0,00	0,15	0,02	0,01
		LLD (ppm)	193,07	62,90	13,22	22,97	45,48	16,15	58,55	11,76	58,72	14,71
JK-88	101,47	Concentration	97,60	1,99	0,74	0,02	0,17	0,27	0,00	0,56	0,12	0,01
		LLD (ppm)	193,15	63,15	13,17	22,98	45,84	16,21	58,72	12,08	58,74	14,73

APENDIX II – XRD - graphs

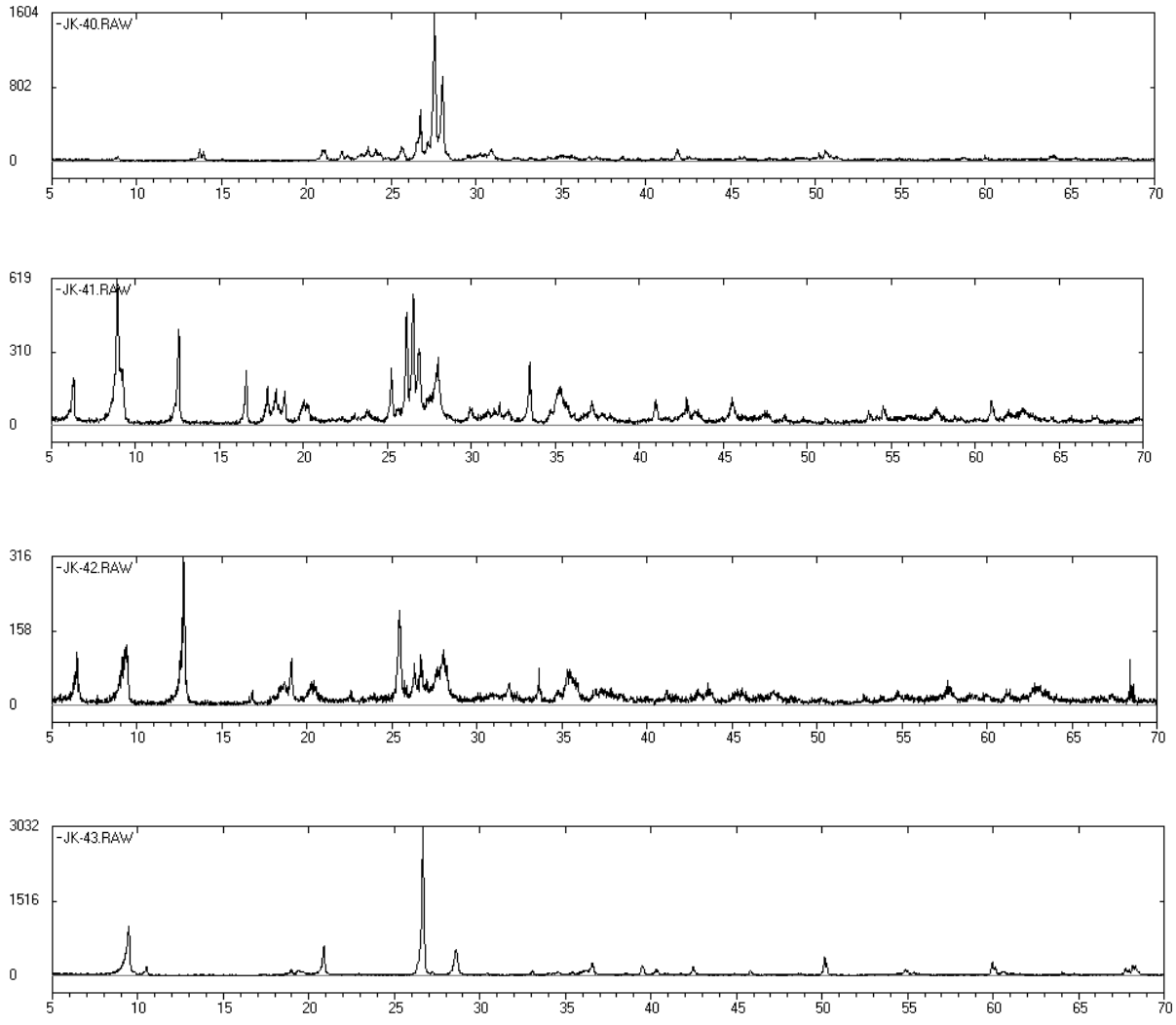

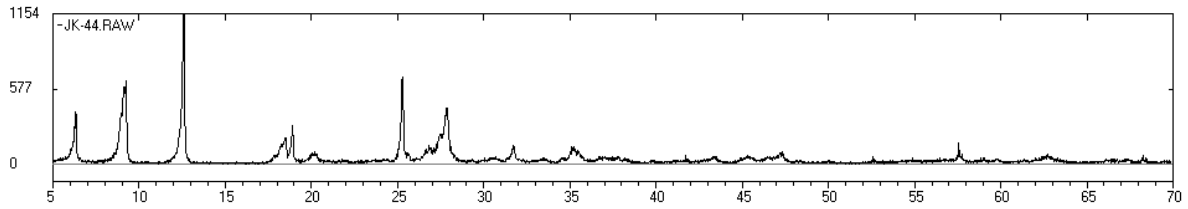
1154
577
0
-JK-44.RAW
5 10 15 20 25 30 35 40 45 50 55 60 65 70

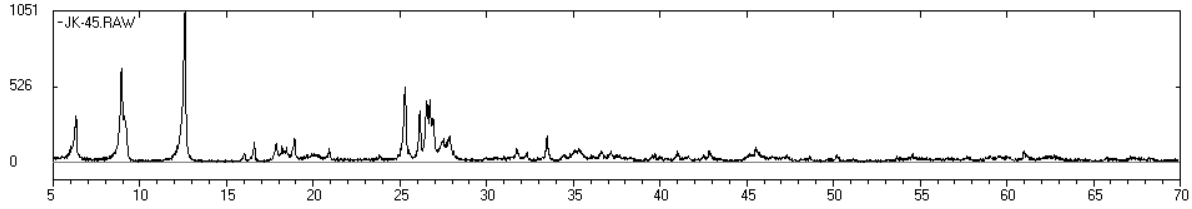
1051
526
0
-JK-45.RAW
5 10 15 20 25 30 35 40 45 50 55 60 65 70

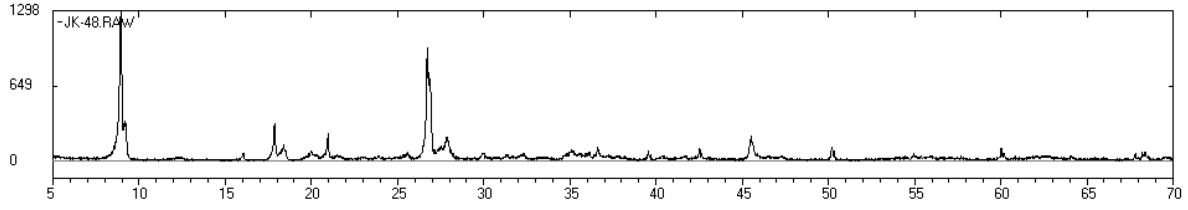
1298
649
0
-JK-48.RAW
5 10 15 20 25 30 35 40 45 50 55 60 65 70

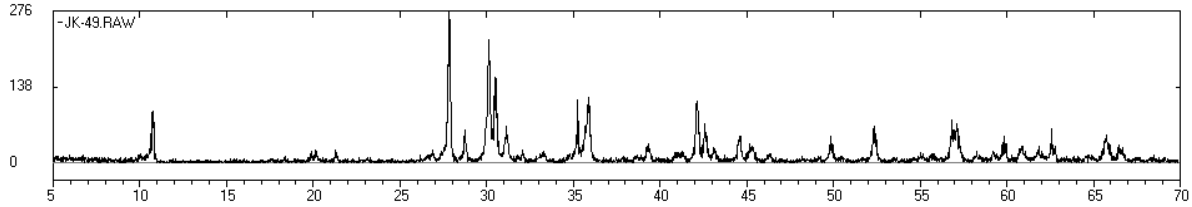
276
138
0
-JK-49.RAW
5 10 15 20 25 30 35 40 45 50 55 60 65 70

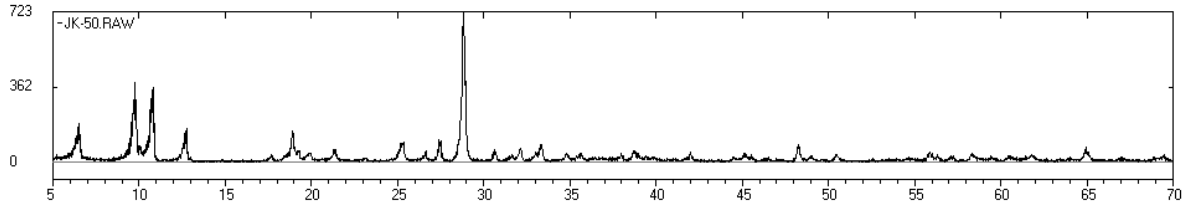
723
362
0
-JK-50.RAW
5 10 15 20 25 30 35 40 45 50 55 60 65 70

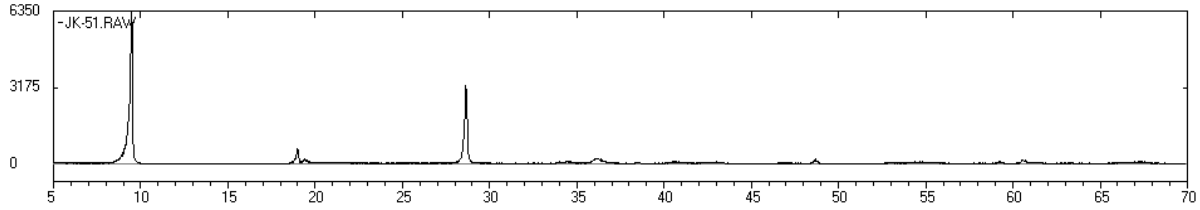
6350
3175
0
-JK-51.RAW
5 10 15 20 25 30 35 40 45 50 55 60 65 70

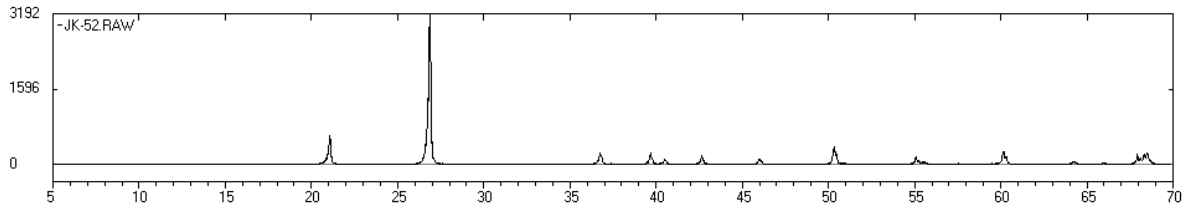
3192
1596
0
-JK-52.RAW
5 10 15 20 25 30 35 40 45 50 55 60 65 70

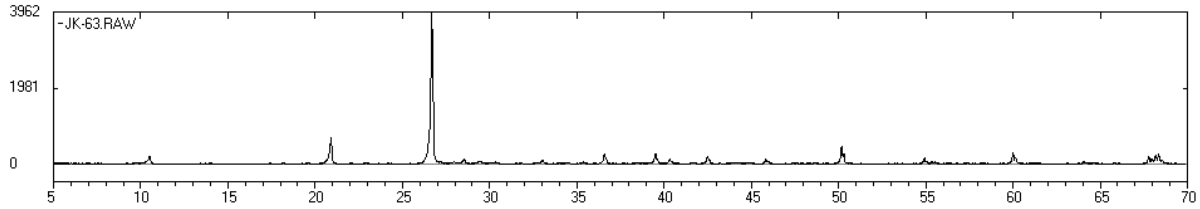
3962
1981
0
-JK-63.RAW
5 10 15 20 25 30 35 40 45 50 55 60 65 70

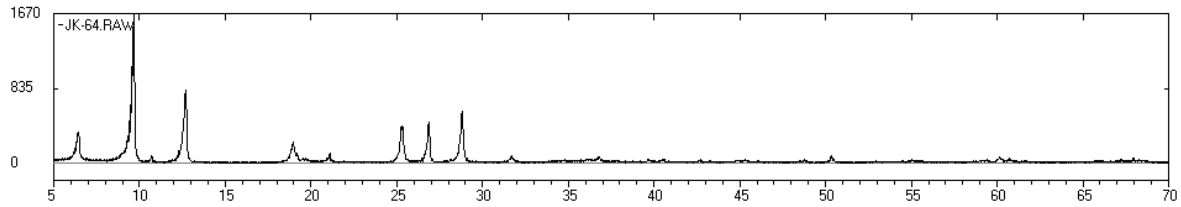
1670
835
0
-JK-64.RAW
5 10 15 20 25 30 35 40 45 50 55 60 65 70

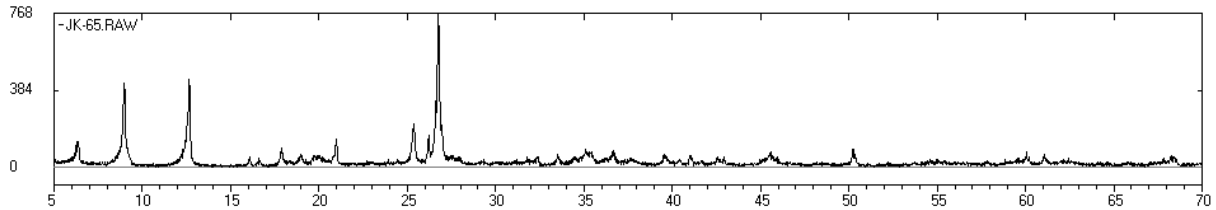
768
384
0
-JK-65.RAW
5 10 15 20 25 30 35 40 45 50 55 60 65 70

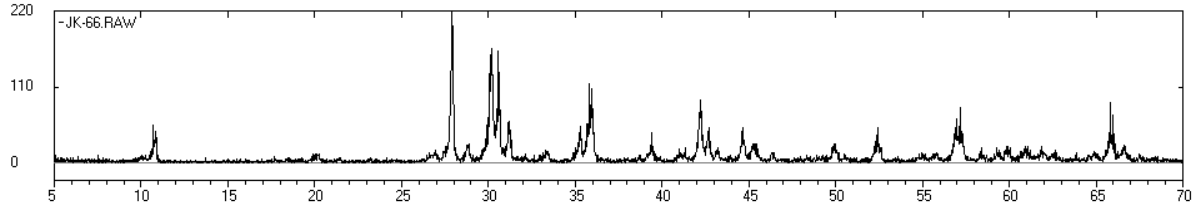
220
110
0
-JK-66.RAW
5 10 15 20 25 30 35 40 45 50 55 60 65 70

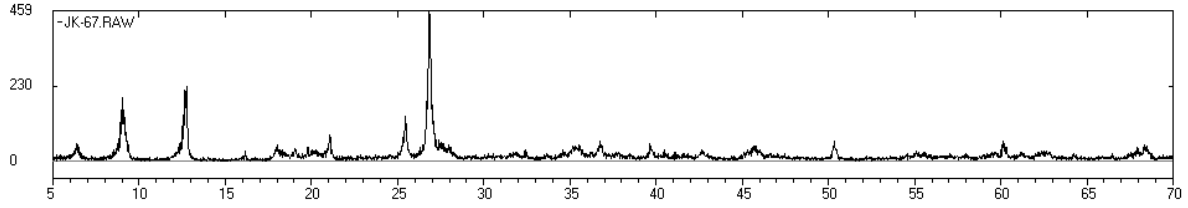
459
230
0
-JK-67.RAW
5 10 15 20 25 30 35 40 45 50 55 60 65 70

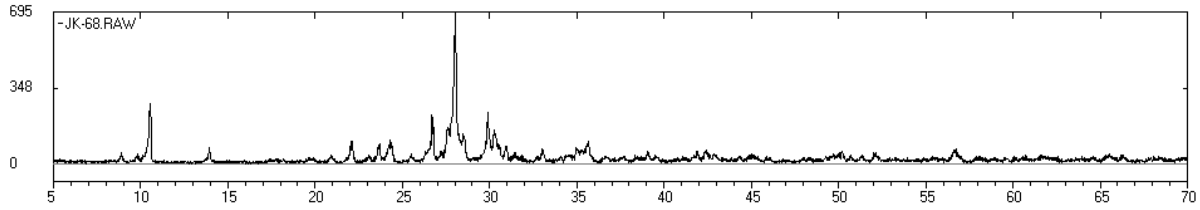
695
348
0
JK-68.RAW
5 10 15 20 25 30 35 40 45 50 55 60 65 70

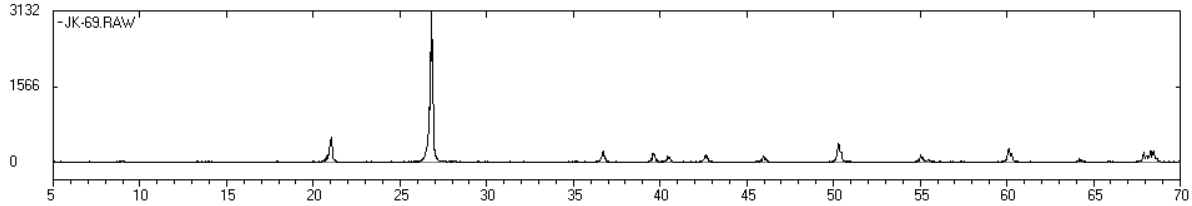
3132
1566
0
JK-69.RAW
5 10 15 20 25 30 35 40 45 50 55 60 65 70

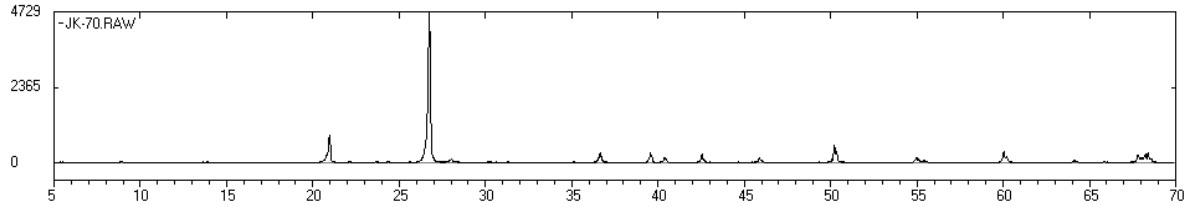
4729
2365
0
JK-70.RAW
5 10 15 20 25 30 35 40 45 50 55 60 65 70

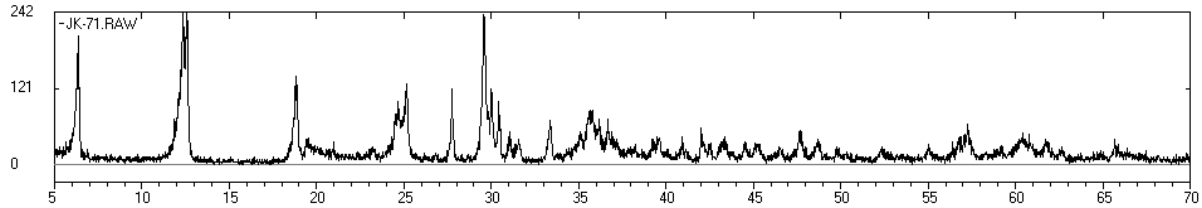
242
121
0
JK-71.RAW
5 10 15 20 25 30 35 40 45 50 55 60 65 70

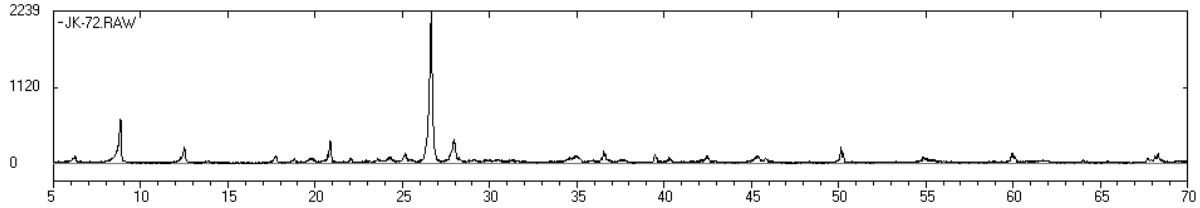
2239
1120
0
JK-72.RAW
5 10 15 20 25 30 35 40 45 50 55 60 65 70

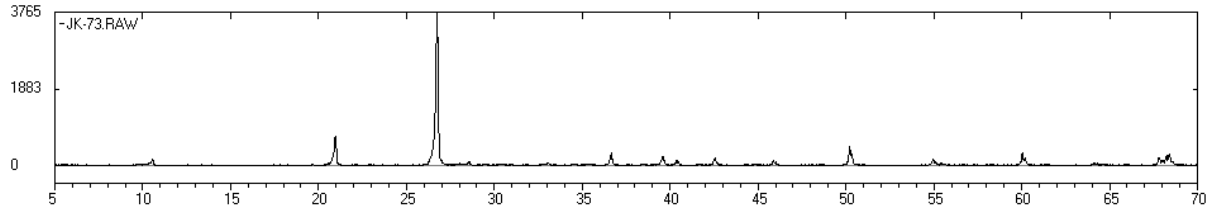
3765
1883
0
JK-73.RAW
5 10 15 20 25 30 35 40 45 50 55 60 65 70

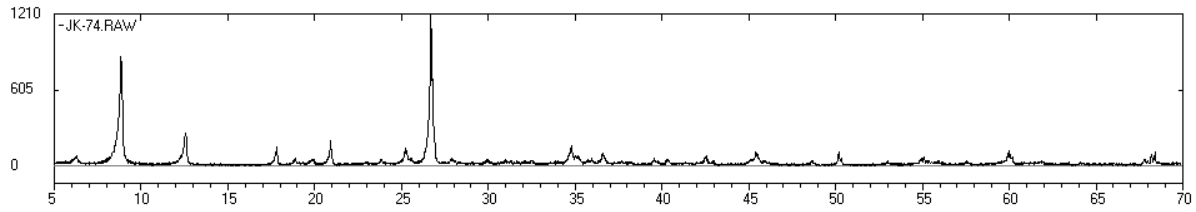
1210
605
0
-JK-74.RAW
5 10 15 20 25 30 35 40 45 50 55 60 65 70

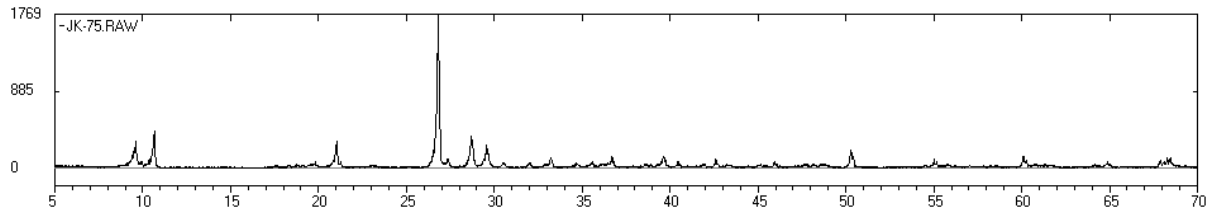
1769
885
0
-JK-75.RAW
5 10 15 20 25 30 35 40 45 50 55 60 65 70

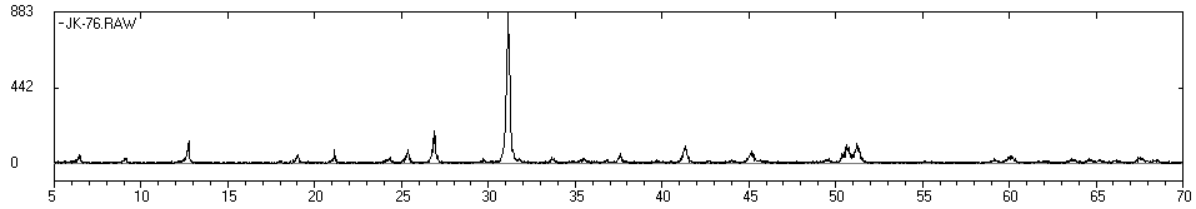
883
442
0
-JK-76.RAW
5 10 15 20 25 30 35 40 45 50 55 60 65 70

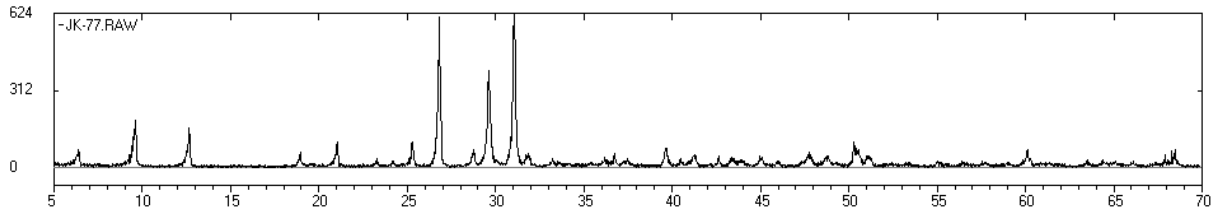
624
312
0
-JK-77.RAW
5 10 15 20 25 30 35 40 45 50 55 60 65 70

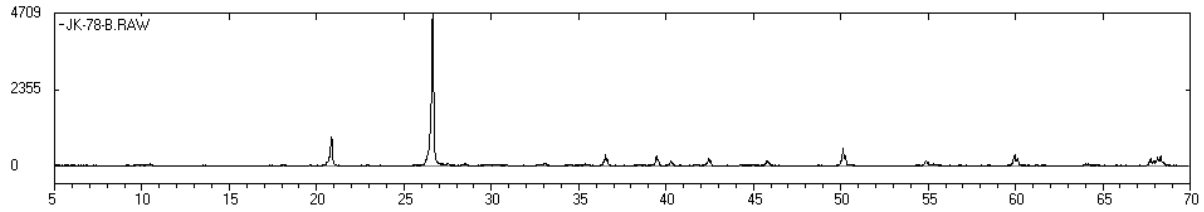
4709
2355
0
-JK-78-B.RAW
5 10 15 20 25 30 35 40 45 50 55 60 65 70

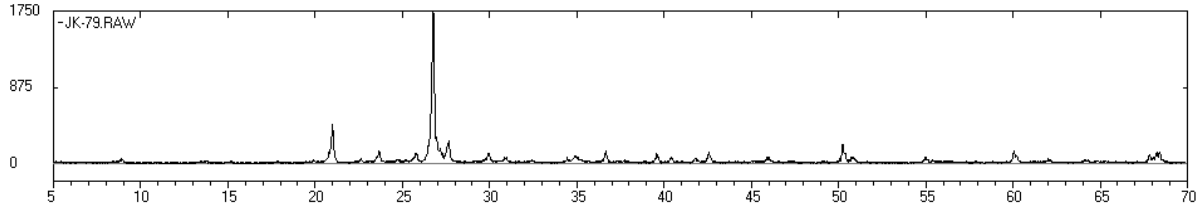
1750
875
0
-JK-79.RAW
5 10 15 20 25 30 35 40 45 50 55 60 65 70

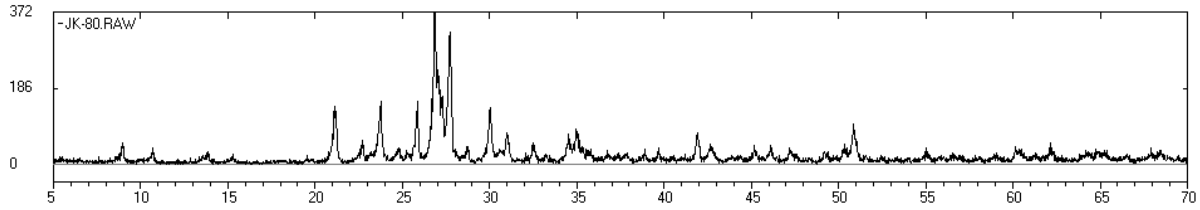
372
186
0
-JK-80.RAW
5 10 15 20 25 30 35 40 45 50 55 60 65 70

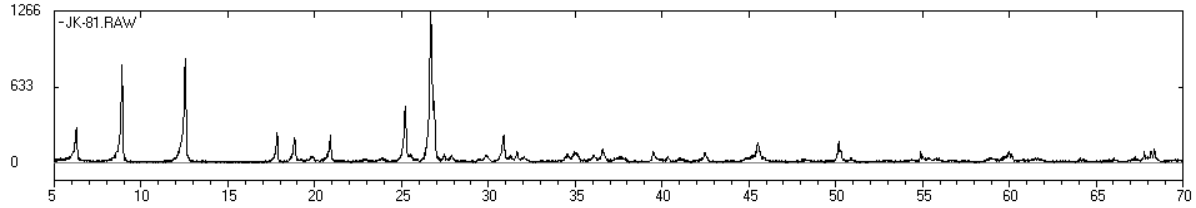
1266
633
0
-JK-81.RAW
5 10 15 20 25 30 35 40 45 50 55 60 65 70

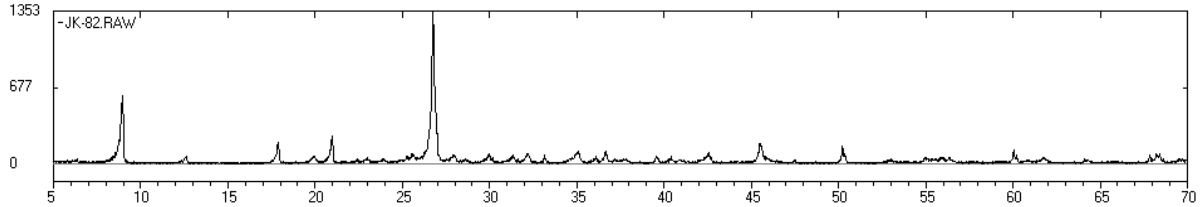
1353
677
0
-JK-82.RAW
5 10 15 20 25 30 35 40 45 50 55 60 65 70

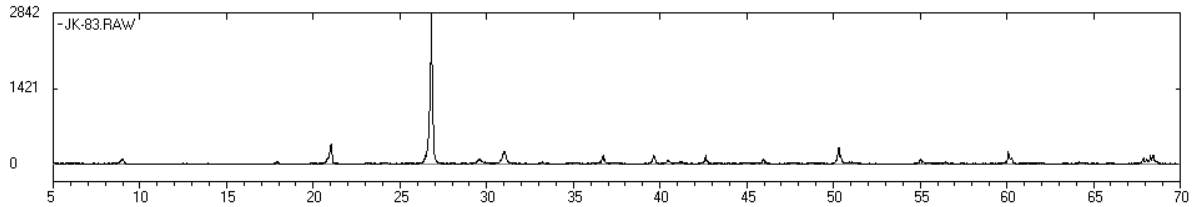
2842
1421
0
-JK-83.RAW
5 10 15 20 25 30 35 40 45 50 55 60 65 70

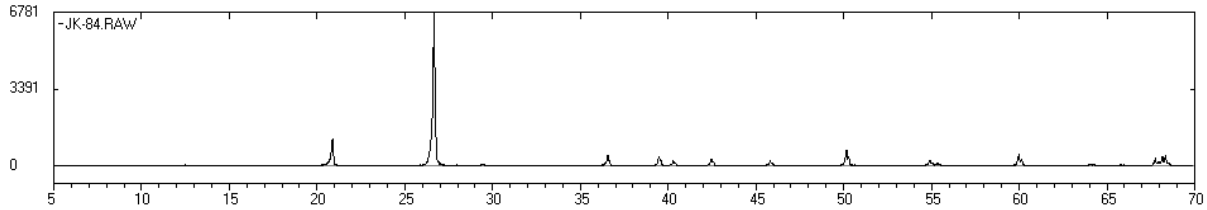
6781
3391
0
-JK-84.RAW
5 10 15 20 25 30 35 40 45 50 55 60 65 70

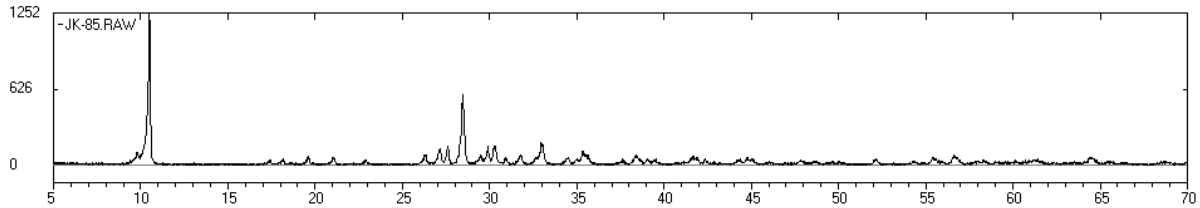
1252
626
0
-JK-85.RAW
5 10 15 20 25 30 35 40 45 50 55 60 65 70

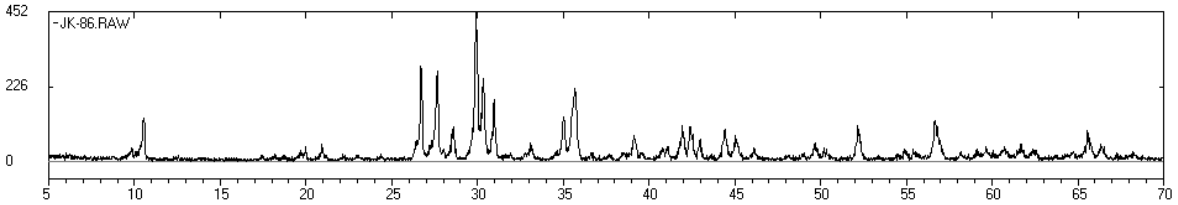
452
226
0
-JK-86.RAW
5 10 15 20 25 30 35 40 45 50 55 60 65 70

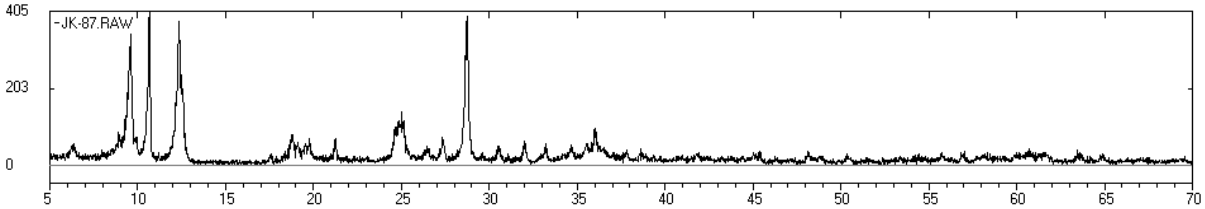
405
203
0
-JK-87.RAW
5 10 15 20 25 30 35 40 45 50 55 60 65 70

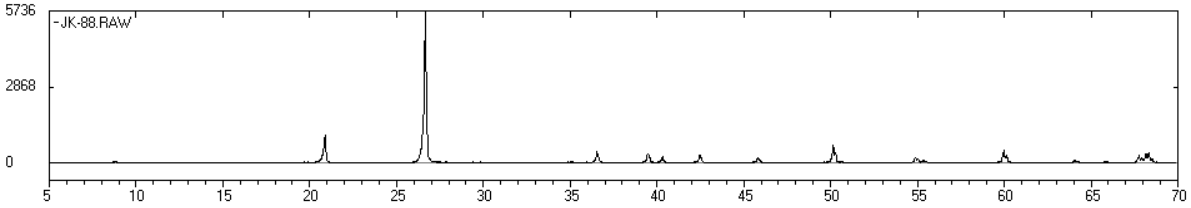
5736
2868
0
-JK-88.RAW
5 10 15 20 25 30 35 40 45 50 55 60 65 70

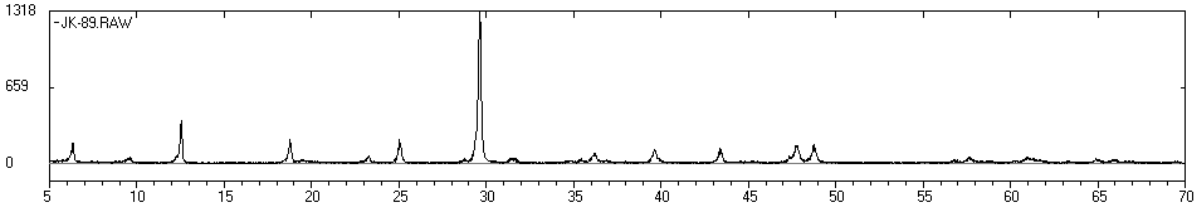
1318
659
0
-JK-89.RAW
5 10 15 20 25 30 35 40 45 50 55 60 65 70

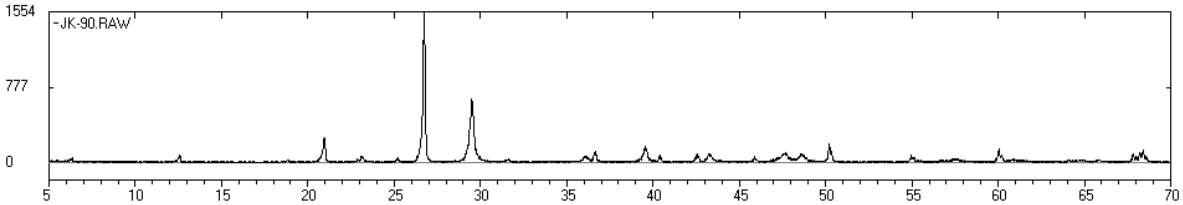
1554
777
0
-JK-90.RAW
5 10 15 20 25 30 35 40 45 50 55 60 65 70

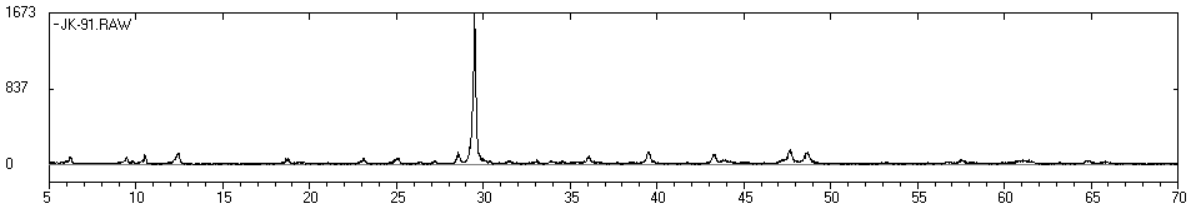
1673
837
0
-JK-91.RAW
5 10 15 20 25 30 35 40 45 50 55 60 65 70

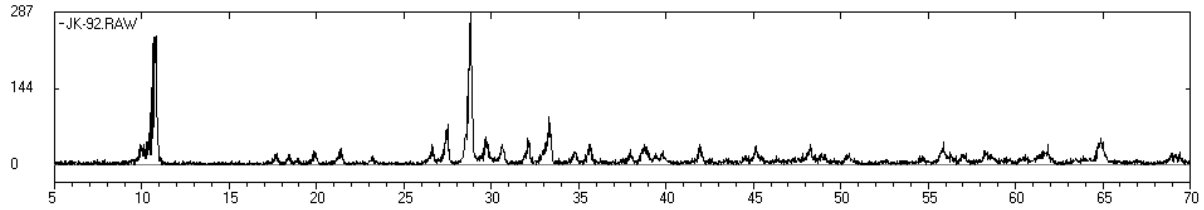
-JK-92.RAW
287
144
0
5
10
15
20
25
30
35
40
45
50
55
60
65
70

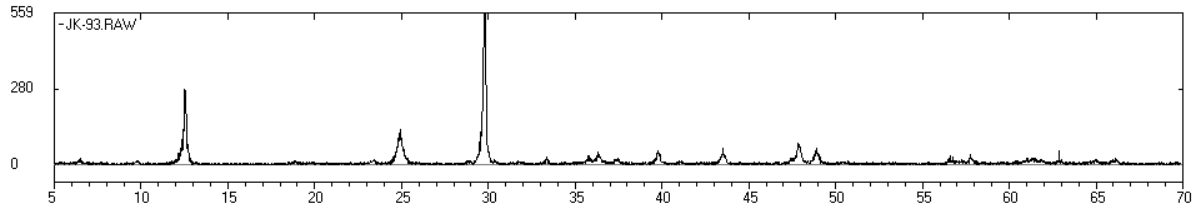
-JK-93.RAW
559
280
0
5
10
15
20
25
30
35
40
45
50
55
60
65
70

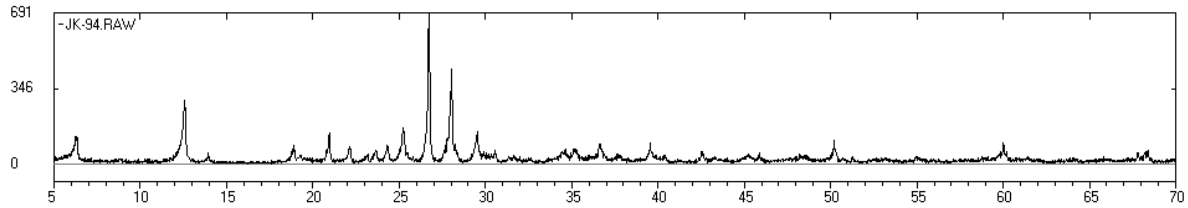
-JK-94.RAW
691
346
0
5
10
15
20
25
30
35
40
45
50
55
60
65
70

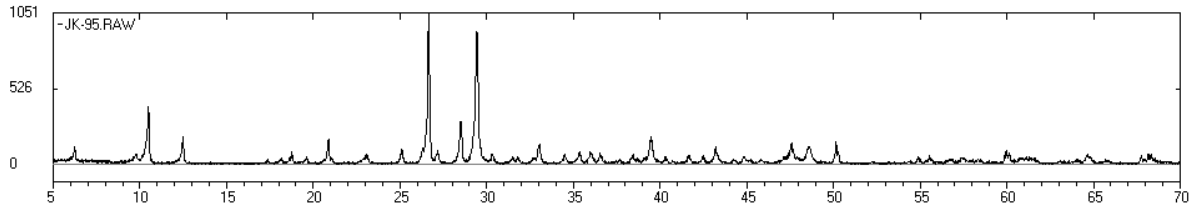
-JK-95.RAW
1051
526
0
5
10
15
20
25
30
35
40
45
50
55
60
65
70

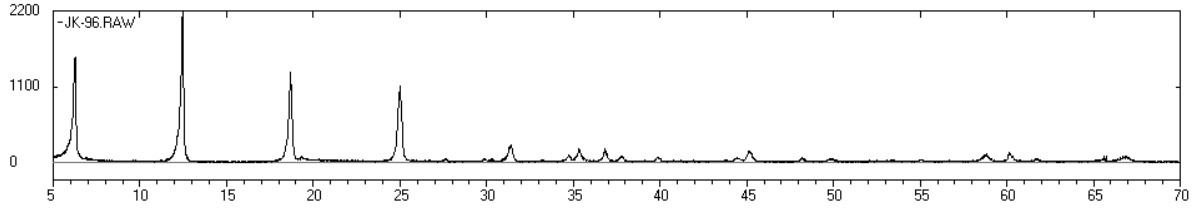
-JK-96.RAW
2200
1100
0
5
10
15
20
25
30
35
40
45
50
55
60
65
70

APPENDIX III – Boreholes – stratigraphy

AH 114

From(m)	To	ROCKTYPE ALTERATION	STRAT
0	15,05	OVB HI_WEAT	UIT
15,05	20.18	OVB HI_WEAT	UIT
20.18	26.97	DIAB HI_WEAT	UIT
26.97	29.97	OVB HI_WEAT	UIT
29.97	46.65	DIAB	UIT
33.96	34.29	DOLE	UIT
46.65	49.95	DOLM QCV CARB	MAL
49.95	52.27	SCHI QCV TALC	UIT
50.95	51.26	QCV QCV	UIT
52.27	69.94	DIAB CARB	UIT
68.9	69.19	PEGM	UIT
69.94	78.29	PRD SERP TALC	UIT
76.49	76.79	MCHR	UIT
78.29	92.3	DOLM	MAL
81.66	82	PRD SERP	UIT
89.42	92.16	DOLM	MAL
92.3	114.2	DIAB	UIT
108.29	108.9	FRACT QCV	UIT
114.23	116.7	DOLM CARB	MAL
116.77	117.2	PRD	UIT
117.28	117.5	DOLM	MAL
117.54	118.0	PXT	UIT
118.06	124.1	SHZO QCV	MAL
124.19	175.0	DIAB QCV CARB	UIT
142.86	143.5	QCV QCV	UIT
146	146.3	DOLE	UIT
175.06	176.9	PXT CARB	UIT
176.9	177.4	DOLM CARB	UIT
177.4	178.9	PRD CARB	UIT

178.93	179.3	DOLM	UIT
179.31	179.7	PEGM	UIT
179.7	181	AMPH	UIT
181	184.3	GAB	UIT
184.39	185.9	AMPH CARB AMPH	MAL
185.9	187.9	QTZ	MAL
187.95	188.4	SHZO TALC	MAL

AH 116

From(m)	To	ROCKTYPE	ALTERATION	STRAT
0	4,98	OVB OXID	HI_WEAT	MAL
4,98	9,33	OVB OXID	HI_WEAT	MAL
9,33	18.56	PRD OXID	HI_WEAT	UIT
18.56	29.83	DOLM OXID	HI_WEAT	MAL
29.83	60.75	DIAB OXID	HI_WEAT	MAL
60.75	77.4	DOLM	SERP	MAL
68.14	69.08	SCHI	TALC CARB	MAL
74.56	77.05	SHZO	SERP CARB	MAL
77.4	84	DIAB		MAL
84	84.7	PEGM	SILIC SERP	UIT
84.7	99.4	DOLM	SERP SILI	MAL
99.4	101.5	PEGM	SILIC	UIT
101.58	104.2	DOLM	SILIC SERP	MAL
102.93	103.1	PXT	SERP AMPH	UIT
104.1	104.2	PEGM	SILIC	UIT
104.23	106.7	CHERT META	AMPHI	MAL
105.19	105.5	PEGM	SILIC	UIT
106.1	106.2	AMPH	SILIC	UIT
106.7	110.1	DOLM	AMPHI SERP	MAL
108.35	108.9	SERP		MAL
110.12	112.0	SERP		MAL
112.04	123.7	HORN	AMPHI SILI	MAL
123.75	126.7	DOLM	SERP	MAL
126.76	148.9	DIAB		MAL
148.94	153.6	DOLM	AMPHI SERP	MAL
150.63	151.4	SHZO	AMPHI SERP	MAL

151.43	152.2	SCHI TALC	MAL
153.67	163.7	FRACT TALC CARB	MAL
163.79	164.8	SHZO TALC SERP	UIT
164.8	167.6	PXT TALC SERP	UIT
167.61	172.2	PRD SERP CARB	UIT
172.27	174.3	PXT SERP TALC	UIT
174.32	176.0	DOLE CARB	UIT
176.03	176.7	PXT AMPHI SERP	UIT
176.77	177.0	SHZO SERP AMPH	UIT
177.04	177.6	PXT AMPHI SILI	UIT
177.64	179.8	DOLM SILIC AMPH	MAL
179.81	181.0	DIAB CARB CHLO	MAL
181.09	184.0	DOLM OXID SERP	MAL
184.08	186.0	QTZ SERIC	BRQ
186.09	193.9	GRAN SL_OXID	NELS

AH 117

From(m)	To	ROCKTYPE ALTERATION	STRAT
0	13	SHLE HI_WEAT OXID	TBH
13	21.77	PCR HI_WEAT OXID	UIT
21.77	21.93	SCHI HI_WEAT TALC	UIT
21.93	22.18	QCV CARB SILIC	UIT
22.18	22.64	SCHI TALC SILIC	UIT
22.64	22.87	QCV CARB SILIC	UIT
22.87	23.45	SCHI TALC SILIC	UIT
23.45	37.28	DIAB SAUSS CARB	UIT
37.28	59.38	DOLM EPIDO META	MAL
37.78	41.5	DOLM SERP SILIC	MAL
52.5	52.6	DOLM SERP SILIC	MAL
52.74	52.99	SHZO SERP CARB	MAL
52.99	53.22	SERP SERP CARB	MAL
56.88	57.33	PXT SAUSS AMPHI	UIT
59.38	67.44	QTZ CARB SILIC	MAL
61.87	62.2	PEGM SAUSS AMPHI	UIT
62.2	63.25	PXT SAUSS AMPHI	UIT
67.44	68.84	PEGM SAUSS AMPHI	UIT
68.84	73.82	GAB AMPHI SAUSS	UIT
73.82	76.34	PXT SERP AMPHI	UIT
75.61	75.88	PEGM AMPHI SAUSS	UIT

76.34	85.37	PRD SERP AMPHI	UIT
85.37	85.97	SCHI SERP CARB	UIT
85.97	86.15	SHZO SILIC CARB	UIT
86.15	86.42	QCV CARB SILIC	UIT
86.42	86.59	SHZO SILIC CARB	UIT
86.59	88.43	SCHI TALC CARB	UIT
88.43	89.26	PRD SERP	UIT
89.26	90.4	GAB SAUSS AMPHI	UIT
90.4	91	PXT CARB AMPHI	UIT
91	98.64	GAB AMPHI SAUSS	UIT
98.64	101.5	QTZ SILIC META	MAL
101.58	102.4	SHZO SILIC SERP	UIT
102.49	127.4	DIAB SAUSS AMPHI	MAL
102.57	103.6	QCV CARB SILIC	MAL
127.4	129.9	DOLM META EPIDO	MAL
129.94	131.4	QTZ SILIC META	BRQ
131.48	134.1	GRAN SERIC SILIC	NELS

AH 53

From(m)	To	ROCKTYPE ALTERATION	STRAT
0	3,03	QTZ SILIC CARB	MAL
3,03	17,09	QTZ SILIC CARB	MAL
17,09	23	DOLM SILIC CARB	MAL
23	27,12	DOLM SILIC CARB	MAL
27,12	27.82	DOLM SILIC CARB	MAL
27.82	28.38	SHLE SILIC META	MAL
28.38	28.69	DOLM SERP META	MAL
28.69	29,06	SHLE SILIC META	MAL
29,06	31.58	DOLM SERP META	MAL
31.58	34.07	QTZ META CHLO	MAL
34.07	35.03	DOLM SILIC	MAL
35.03	36.26	CHERT SILIC CARB	MAL
36.26	36.69	DOLM SILIC META	MAL
36.69	37.07	CHERT SILIC CARB	MAL
37.07	37.52	DOLM SILIC CARB	MAL
37.52	41.54	QTZ CARB SILI	MAL
38.37	39.14	PXT AMPHI SAUS	UIT

41.54	44.45	DOLM SILIC META	MAL
44.06	44.18	QTZ CARB META	MAL
44.35	44.45	QTZ CARB META	MAL
44.45	50.04	QTZ CARB META	MAL
45.69	46.03	DOLM SILIC META	MAL
47.58	47.65	PXT SAUSS AMPH	UIT
47.87	47.95	PXT AMPHI SAUS	UIT
48.19	48.37	PXT SAUSS AMPH	UIT
48.37	48.8	PRD SERP AMPH	UIT
48.91	49.22	PXT AMPHI SAUS	UIT
49.22	49.44	PRD AMPHI SERP	UIT
50.04	50.56	PXT AMPHI SAUS	UIT
50.56	50.73	PXT AMPHI	UIT
50.73	50.9	GAB SAUSS AMPH	UIT
50.9	51.07	PXT AMPHI SAUS	UIT
51.07	52.24	PRD SERP AMPH	UIT
52.24	62.23	GAB SAUSS CARB	UIT
52.26	53.88	GAB SAUSS AMPH	UIT
62.23	66.24	QTZ CARB SILI	MAL
66.24	66.92	SHLE SILIC AMPH	MAL
66.92	68.42	DOLM SILIC META	MAL
68.42	69.02	QTZ CHLOR SILI	BRQ
69.02	71.56	QTZ CHLOR SILI	BRQ
71.56	79.25	GRAN SERIC SILI	NELS

AH 66

From(m)	To	ROCKTYPE ALTERATION	STRAT
0	20.76	CORELOSS	UIT
20.76	25.26	SHLE HI_WEAT	TBH
25.26	46.2	DIAB HI_WEAT QCV	UIT
46.2	57.56	PXT QCV SERP	UIT
51.25	51.32	QCV QCV SL_ALT	UIT
57.56	129.93	DIAB QCV SL_WEAT	UIT
129.93	135.17	DIAB SL_ALT QCV	UIT
135.17	137.74	DOLM SERP TALC	MAL
135.27	135.77	DOLM SERP TALC	MAL

137.74	160.92	DIAB QCV SL_ALT	UIT
160.92	224.84	DOLM SILIC CARB	MAL
187.78	188.92	DOLE QCV SL_ALT	UIT
194.94	195.61	DOLE QCV SL_ALT	UIT
207.27	224.8	DIAB QCV CARB	UIT
224.84	256.61	GRAN SL_ALT SILIC	NELS
243.65	244.06	DOLE QCV SL_ALT	UIT
244.06	245.88	QTZ SILIC CARB	NELS

AH 76

From(m)	To	ROCKTYPE ALTERATION	STRAT
0	2,85	MCHR HI_WEAT OXID	UIT
2,85	4,07	PCR HI_WEAT OXID	UIT
4,07	9,18	MCHR HI_WEAT OXID	UIT
9,18	19,05	PCR HI_WEAT OXID	UIT
19,05	27.86	PXT HI_WEAT OXID	UIT
27.86	29.94	PXT SERP SAUSS	UIT
29.94	32.24	QTZ CHLOR META	UIT
32.24	32.48	PXT SERP SAUSS	UIT
32.48	32.74	PRD SERP AMPHI	UIT
32.74	33.01	QTZ CHLOR META	UIT
33.01	40.21	PRD SERP AMPHI	UIT
40.21	40.78	PXT SERP SAUSS	UIT
40.42	40.66	AMPH AMPHI SAUSS	UIT
40.78	43.16	GAB AMPHI SAUSS	UIT
43.16	47.81	QTZ META SILIC	MAL
47.81	49.76	DOLM SILIC META	MAL
49.76	51.1	QTZ SILIC CHLOR	BRQ
51.1	56.78	GRAN SILIC SERIC	NELS

AH 94

From(m)	To	ROCKTYPE ALTERATION	STRAT
0	8,27	OVB HI_WEAT	UIT
8,27	14	PRD HI_WEAT	UIT
14	32.87	PRD HI_WEAT	UIT
27.69	30.38	PRD SERP	UIT
32.87	67.79	PRD SERP	UIT
33.81	35.98	PRD SL_WEAT	UIT
47.8	48.5	PRD SERP	UIT
49.6	50.22	PRD SERP	UIT
67.79	70.99	DIAB	UIT
70.99	97.54	PRD SERP	UIT
76.56	76.59	MCHR	UIT
86.66	86.68	SERP	UIT
97.54	113.6	DIAB	UIT
113.6	113.6	PRD SERP	UIT
113.6	167.5	PRD SERP	UIT
118.06	118.1	MCHR	UIT
121.04	121.1	MCHR	UIT
124	124.7	PRD SERP	UIT
151.53	152.2	PRD SERP	UIT
154.07	156.6	PXT SERP	UIT
160.6	160.7	PRD SERP	UIT
167.56	168.7	SCHI TALC CARB	UIT
168.77	171	DOLE QCV	UIT
171	173.3	PRD TALC QCV	UIT
172.4	172.5	QCV QCV	UIT
173.3	174.9	PRD SERP	UIT
174.97	196.7	PRD SERP	UIT
177.11	177.1	MCHR	UIT

177.17	177.2	SERP SERP	UIT
182.3	182.4	MCHR	UIT
182.44	183.4	PRD SERP	UIT
189.57	189.7	MCHR	UIT
193.52	194.7	PRD SERP	UIT
196.78	202.2	DIAB	UIT
202.22	208.4	PRD SERP	UIT
208.4	231.4	DIAB	UIT
231.46	233.4	PRD SERP TALC	UIT
233.46	235.6	PRD SERP	UIT
235.62	235.7	SHZO QCV	UIT
235.71	236.5	MCHR	UIT
236.59	236.7	SHZO QCV	UIT
236.74	237.4	PRD TALC	UIT
237.47	242.3	MCHR	UIT
238.45	238.5	PXT SERP TALC	UIT
240.16	240.2	PXT SERP TALC	UIT
240.55	240.6	PXT SERP TALC	UIT
242.37	242.4	SHZO QCV	UIT
242.44	245.6	PCR TALC SERP	UIT
245.63	246.3	MCHR	UIT
246.35	246.8	PCR TALC SERP	UIT
246.87	247.8	PCR TALC SERP	UIT
247.83	252.2	PCR TALC	UIT
248.36	249.1	MCHR	UIT
249.33	249.6	MCHR	UIT
252.27	261.0	PCR TALC	UIT
261.09	265.5	DIAB	UIT
265.52	269.6	PCR TALC	UIT
268.48	268.8	PCR TALC	UIT
269.66	269.9	PXT TALC	UIT
269.92	270.9	PCR TALC	UIT
270.97	276.5	PCR TALC	UIT
276.5	278.1	PCR TALC	UIT
276.85	276.9	PCR TALC	UIT
278.11	286.3	PCR TALC	UIT
286.31	294.7	PCR TALC	UIT
294.26	294.2	QCV	UIT
294.78	300.1	PXT SERP TALC	UIT
296.23	296.3	SERP	UIT
300.12	300.5	SHZO QCV	UIT

300.5	300.7	PXT	UIT
300.75	300.9	DOLE	UIT
300.94	301.1	QCV QCV	UIT
301.15	301.6	DOLE	UIT
301.63	301.9	QCV QCV	UIT
301.96	305.2	PXT	UIT
303.85	304.5	DOLM	UIT
304.66	304.9	DOLM	UIT
305.24	330.0	DIAB QCV	UIT
330.09	333.2	PXT SERP	UIT
331.25	331.2	SHZO QCV	UIT
333.2	334.2	SHZO QCV	UIT
334.29	344.1	DOLM	MAL
344.1	349.1	GAB	UIT
349.17	350.2	PXT	UIT
350.23	351.4	AMPH AMPHI	UIT
351.47	356.3	GAB	UIT
351.48	352.3	GAB	UIT
353.33	354.0	GAB	UIT
356.31	373.2	DOLM	MAL
357.96	360.9	QTZ	MAL
370.82	371.1	SHZO QCV	MAL
373.2	387.0	GRAN	NELS
382	383.7	GRAN	NELS

UD 100

From(m)	To	ROCKTYPE ALTERATION	STRAT
0	4,52	CORELOSS	UIT
4,52	54.5	OVB HI_WEAT	UIT
54.5	59.22	DIAB HI_WEAT SL_ALT	UIT
59.22	64.47	PRD HI_WEAT TALC	UIT
64.47	67.27	PXT HI_WEAT SERP	UIT
67.27	73.81	HORN SL_WEAT META	TBH
73.81	74.26	DIAB SL_ALT QCV	UIT
74.26	107.0	SHLE META QCV	TBH
89.37	89.83	DOLM CARB SILIC	TBH

107.03	124.2	DIAB QCV SL_ALT	UIT
124.23	166.0	SHLE META	TBH
166.04	171.0	DIAB SL_ALT	UIT
171.04	176.2	SHLE META QCV	TBH
176.2	197.8	DIAB QCV	UIT
176.55	177.4	QTZ SILIC SL_ALT	TBH
197.86	203.5	HORN SILIC META	TBH
203.57	204.7	SHLE SILIC META	TBH
204.71	214.1	SHLE META SL_ALT	TBH
214.1	233.7	DIAB CARB SILIC	UIT
220.57	221.0	QV CARB SILIC	UIT
233.76	242.7	SHLE META QCV	TBH
237.41	237.6	SHZO CARB SILIC	UIT
238.8	239.0	SHZO CARB SILIC	UIT
242.76	249.7	DIAB SL_ALT QCV	UIT
249.76	249.9	QTZ CARB SILIC	TBH
249.93	255.1	CONG META SILIC	RHF

UD 106

From(m)	To	ROCKTYPE ALTERATION	STRAT
0	25	OVB HI_WEAT	UIT
25	37	PRD HI_WEAT	UIT
37	66.5	DIAB	UIT
54.72	64.91	FRACT	UIT
66.5	101.37	PRD SERP	UIT
69.11	69.17	MCHR	UIT
84.3	85.78	PXT SERP	UIT
92	92.31	PRD QCV	UIT
95.68	95.76	MCHR	UIT
100.88	100.99	DOLE	UIT
101.37	106.77	DIAB	UIT
106.77	117.5	PRD SERP	UIT
117.5	119.98	PRD SERP	UIT
119.98	129.07	PRD TALC	UIT
129.07	156.58	DIAB QCV	UIT
131.86	132.17	DOLE	UIT

134.78	135.79	DIAB	UIT
141.32	142.14	DIAB	UIT
156.58	163.02	PXT CARB QCV	UIT
156.77	156.85	QCV QCV	UIT
157	158.92	SHZO QCV	UIT
160.5	160.64	PXT	UIT
161.47	161.72	PXT	UIT
163.02	178.45	DIAB QCV	UIT
167.48	171.83	DOLE QCV	UIT
172.5	173.5	DIAB QCV	UIT
178.45	182.93	PXT QCV CARB	UIT
180.82	182.22	SHZO QCV	UIT
182.93	186.94	GAB CARB	UIT
186.94	195.3	DIAB	UIT
195.3	196.61	DIAB CARB	UIT
196.5	196.61	DOLE	UIT
196.61	199.67	DOLE	UIT
199.67	209.62	SHLE	TBH
209.62	212.1	SHLE	TBH
212.1	213.28	SHLE	TBH
213.28	214.5	CONG	RHF

UD 109

From(m)	To	ROCKTYPE ALTERATION	STRAT
0	36	OVB HI_WEAT	UIT
36	55	DOLE	UIT
55	64.5	PRD SERP	UIT
64.5	70.08	PRD QCV SERP	UIT
70.08	83.68	PRD SERP QCV	UIT
74.13	74.73	PRD	UIT
76.59	76.75	PRD	UIT
83.08	83.22	PRD	UIT
83.68	89.86	DIAB	UIT
89.86	99.9	PRD SERP	UIT
99.9	103.9	PRD SERP	UIT
103.71	103.9	PRD SERP	UIT
103.91	105.2	SHLE SILIC	TBH

105.23	106.8	DIAB	UIT
106.8	110.2	PEGM	UIT
106.91	107.3	PRD	UIT
110.25	130.5	DIAB	UIT
115.01	119.1	DIAB	UIT
130.5	151.2	DIAB CARB	UIT
151.2	164.0	SHLE CARB SILI	TBH
153.43	155.1	SHZO QCV	UIT
156.7	159.0	SHLE	TBH
160.29	160.6	DOLE	UIT
164.04	166.5	CONG SILIC	RHF
164.26	166.2	QTZ SILIC	RHF
166.55	170.5	CONG SILIC	RHF
168.92	169.9	DOLE CARB	UIT
170.5	192.5	DIAB CARB	UIT
192.54	199.4	CONG SILIC	RHF
199.44	201.9	QTZ	MAL
201.97	202.3	DOLM	MAL
202.35	208.8	DOLM	MAL

UD 110

From(m)	To	ROCKTYPE ALTERATION	
0	7,58	OVB HI_WEAT	UIT
7,58	8,03	PCR HI_WEAT	UIT
8,03	10,94	MCHR QCV	UIT
10,94	42.29	DIAB HI_WEAT	UIT
42.29	43	PRD HI_WEAT	UIT
43	46.68	PRD SERP	UIT
46.68	51.4	DIAB	UIT
51.4	53.14	PRD SERP	UIT
53.14	54.06	PXT	UIT
54.06	55.57	DOLM	MAL
55.57	55.86	PXT	UIT
55.86	59.3	PRD CARB	UIT
57.31	57.39	QTZ	UIT
59.3	64.94	DOLM	MAL

UD 39

From(m)	To	ROCKTYPE ALTERATION1	STRAT
0	24.71	CORELOSS	UIT
24.71	31.95	PCR HI_WEAT OXID	UIT
31.95	37.55	DIAB HI_WEAT OXID	UIT
37.55	52.62	DIAB SL_WEAT	UIT
52.62	52.77	DIAB SL_OXID	UIT
52.77	54.51	PCR TALC CARB	UIT
54.51	58.93	DIAB	UIT
58.93	60.29	PCR TALC	UIT
60.29	61.9	PCR TALC	UIT
61.9	63	MCHR TALC	UIT
63	64.52	PXT TALC	UIT
64.52	68.66	PCR TALC	UIT
68.66	87.07	DIAB SL_ALT AMPH	UIT
87.07	89.8	PCR TALC CARB	UIT
89.8	90.35	DOLE SL_ALT CHLO	UIT
90.35	92.5	PRD SERP TALC	UIT
92.5	95.64	PCR TALC	UIT
95.64	99.44	PRD SERP	UIT
97.49	98.1	PCR TALC	UIT
99.44	101.8	PCR TALC	UIT
101.84	102.8	PRD SERP TALC	UIT
102.86	106.2	PCR TALC SERP	UIT
104.65	105.5	PRD SERP	UIT
106.2	113.0	PCR TALC	UIT
107.62	108.1	MCHR	UIT
113.06	121.1	DIAB CHLOR CARB	UIT

121.02	121.1	QCV	UIT
121.17	121.7	PCR CARB SILI	UIT
121.76	123.6	DOLE CARB CHLO	UIT
123.66	127.7	PCR TALC SILI	UIT
126.4	127.0	QV	UIT
127.75	129.3	PCR TALC	UIT
129.3	131.3	PXT SILIC CARB	UIT
131.32	139.5	SCHI TALC SERP	UIT
136.96	137.1	QCV TALC	UIT
139.51	141.0	QCV SERIC	UIT
141.08	144.1	SCHI TALC	UIT
144.15	146.0	DOLM AMPHI SILI	UIT
144.25	144.8	PXT AMPHI SILI	UIT
145.25	145.5	PXT AMPHI SILI	UIT
146.03	154.6	DIAB SL_ALT CARB	UIT
154.61	154.9	SHZO CARB TALC	UIT
154.96	155.0	QTZ AMPHI	MAL
155.07	183.4	DIAB SL_ALT CARB	UIT
183.42	184.5	PXT AMPHI SERP	UIT
184.52	186.7	GAB AMPHI	UIT
186.71	192.4	QTZ AMPHI CARB	MAL
186.93	188.4	AMPH CARB	MAL
188.96	189.2	AMPH CARB	MAL
189.48	189.7	AMPH CARB	MAL
190.49	191.3	AMPH CARB	MAL
192.47	194.3	SHZO TALC CARB	MAL

UD 72

From(m)	To	ROCKTYPE ALTERATION	STRAT
0	5,37	OVB HI_WEAT	UIT
5,37	10,36	PRD HI_WEAT TALC	UIT

10,36	14,04	GAB OXID CHLOR	UIT
14,04	15.45	QTZ OXID CARB	MAL
15.45	16.21	DOLM OXID TALC	MAL

UD 75

From(m)	To	ROCKTYPE ALTERATION	STRAT
0	36	CORELOSS	UIT
36	40.1	PRD HI_WEAT	UIT
40.1	59.1	PRD SL_WEAT	UIT
59.1	76.01	DIAB CARB	UIT
76.01	102.68	PRD SERP	UIT
86.8	87.25	SERP QCV	UIT
88.17	88.2	MCHR	UIT
102.68	107.39	DIAB CARB	UIT
107.39	109.58	PRD SERP TALC	UIT
109.58	118.69	PRD SERP	UIT
116.17	116.44	PRD SERP	UIT
117.56	117.86	MCHR	UIT
118.69	123.29	DIAB	UIT
123.29	135.17	PRD SERP	UIT
128.03	128.13	MCHR	UIT
128.88	129	MCHR	UIT
135.17	140.39	DIAB	UIT
140.39	146.59	PRD SERP	UIT
146.59	147.84	MCHR SERP TALC	UIT
147.84	150.1	PCR TALC	UIT
150.1	154.86	PXT TALC	UIT
150.11	150.95	PXT TALC	UIT
154.86	158.26	DIAB QCV	UIT
158.26	163.76	PXT TALC	UIT
163.76	165.27	DIAB	UIT

165.27	166.86	PXT	UIT
166.86	180.67	CONG	RHF
172.95	173.87	PXT	UIT
175.41	176.62	PXT	UIT
180.67	181.15	QTZ	RHF
181.15	181.27	DOLE	UIT
181.27	182.48	PXT	UIT
182.27	182.43	DOLE	UIT
182.48	202.58	DIAB QCV	UIT
202.58	243.56	DOLM	MAL
205.29	205.96	SERP	MAL
212.14	236.9	DIAB QCV	UIT
243.56	355.66	DOLM	MAL
297.41	297.63	SERP SERP	MAL
351.21	352.07	DOLM	MAL
355.29	355.58	PXT SERP CHLO	UIT
355.66	366.69	GAB	UIT
356.38	356.48	QTZ	MAL
360.09	360.77	DOLM	MAL
361.14	361.48	PXT	UIT
361.69	361.91	PXT	UIT
362.12	362.5	PXT	UIT
362.5	362.67	DOLM	MAL
362.88	363.25	PXT	UIT

UD 77

From(m)	To	ROCKTYPE ALTERATION	STRAT
0	11	CORELOSS SL_ALT CHLOR	MAL
11	20.54	QTZ SL_ALT CHLOR	MAL
20.54	29.97	DIAB AMPHI SAUSS	MAL
29.97	33.65	DOLM SILIC META	MAL
33.65	35.04	SHLE CARB	MAL
33.9	34.06	DOLM SILIC SL_ALT	MAL
35.04	53.34	QTZ SILIC CHLOR	MAL
36.41	36.56	QTZ OXID CHLOR	MAL
37.21	38.8	DOLM SILIC CARB	MAL

41.79	42.93	DOLM SILIC TALC	MAL
42.95	43.65	CHERT SILIC CARB	MAL
43.7	45.45	QTZ SL_ALT SILIC	MAL
45.5	48.03	QTZ OXID SL_ALT	MAL
48.04	48.11	QTZ SILIC CARB	MAL
48.11	48.58	CHERT SILIC	MAL
48.6	48.79	DOLE AMPHI SAUSS	MAL
48.8	49.69	QTZ OXID CHLOR	MAL
49.7	51.2	DOLM SILIC CHLOR	MAL
51.25	52.43	QTZ OXID SL_ALT	MAL
52.5	52.75	GAB AMPHI SAUSS	UIT
52.75	53.33	QTZ CHLOR OXID	MAL
53.34	59.5	PXT AMPHI SAUSS	UIT
53.4	53.72	GAB AMPHI SAUSS	UIT
53.75	54.48	QTZ CHLOR SL_ALT	UIT
54.5	55.27	GAB AMPHI SAUSS	UIT
55.3	56.07	QTZ OXID CHLOR	UIT
56.1	58.57	GAB AMPHI SAUSS	UIT
58.57	58.82	PXT AMPHI SERP	UIT
58.82	59.5	AMPH AMPHI SERP	UIT
59.5	61.23	GAB AMPHI SAUSS	UIT
59.5	67.86	GAB SAUSS AMPHI	UIT
67.14	67.84	GAB AMPHI SAUSS	UIT
67.86	71.49	QTZ CHLOR OXID	UIT
69.1	69.22	GAB CHLOR AMPHI	MAL
69.41	69.56	QTZ CHLOR AMPHI	MAL
69.79	70.09	DOLE AMPHI SAUSS	MAL
71.49	73.72	DOLM CARB META	MAL
73.72	76.88	QTZ CHLOR SILIC	BRQ
76.88	79.31	GRAN SERIC SILIC	NELS

UD 88

From(m)	To	ROCKTYPE ALTERATION	STRAT
0	43.68	OVB SILIC HI_WEAT	TBH
43.68	50.6	DIAB HI_WEAT CARB	UIT
46.47	48.85	DIAB HI_WEAT	UIT

50.6	51.66	SHLE SILIC	TBH
51.3	51.41	DIAB	UIT
51.66	77.54	DIAB QCV CARB	UIT
77.54	79.43	SHLE SILIC	TBH
79.43	85.21	CONG	RHF
85.21	88.61	QTZ SILIC	MAL
88.61	100.4	3 DOLM	MAL

UD 95

From(m)	To	ROCKTYPE ALTERATION	STRAT
0	13.25	OVB HI_WEAT	UIT
13.25	40.25	PRD HI_WEAT	UIT
40.25	49.25	CORELOSS	UIT
49.25	52.25	PRD SERP	UIT
52.25	68.69	DIAB	UIT
68.69	91.58	PRD SERP	UIT
75.41	75.6	FRACT SERP	UIT
78.31	78.4	MCHR	UIT
78.4	80.56	PRD SERP	UIT
91.58	96.27	DIAB	UIT
96.27	138.7	PRD SERP	UIT
112.66	112.7	DOLE	UIT
113.45	116.7	PXT	UIT
127.68	127.9	MCHR	UIT
129.69	130.1	MCHR	UIT
136.01	138.7	PRD SERP	UIT
138.7	143.8	DIAB	UIT
143.82	146.9	PRD SERP	UIT
146.95	152.0	DIAB	UIT
152.08	157.1	PRD SERP	UIT
157.19	160.3	DIAB	UIT
160.3	166.3	PRD SERP TALC	UIT
166.3	172	PCR TALC	UIT
172	176.8	PRD TALC SERP	UIT

176.8	191.5	DIAB QCV	UIT
191.51	193.1	PXT QCV	UIT
193.11	213.3	DIAB QCV	UIT
213.36	215.6	PRD SERP	UIT
215.65	218.9	PXT	UIT
218.93	225.3	PEGM	UIT
225.33	228.3	CONG	RHF

UD 98

From(m)	To	ROCKTYPE ALTERATION	STRAT
0	7,02	OVB SL_WEAT	UIT
7,02	36.3	PXT	UIT
13.52	13.81	QTZ	TBH
13.92	17.55	QTZ	TBH
36.3	41.49	SHLE QCV	TBH
38.44	40.82	SHZO QCV	TBH
41.49	42.36	DOLE QCV	UIT
42.36	45.98	SHLE QCV	TBH
42.41	44.66	SHZO QCV	TBH
45.05	45.23	DOLE	UIT
45.98	51.93	DIAB QCV	UIT
51.93	56.29	SHLE QCV	TBH
51.94	52.03	QCV QCV	TBH
54.52	54.62	QV	TBH
54.84	55	QCV QCV	TBH
56.29	61.14	DIAB QCV	UIT
61.14	67.48	SHLE QCV	TBH
62.87	63.22	PXT	UIT
67.48	89.57	CONG	RHF
89.57	96.72	DIAB QCV	UIT
90.53	90.73	CONG	RHF
94.48	94.67	QTZ	RHF
96.72	96.78	SHZO QCV	MAL

96.78	136.9	DOLM CHLOR EPID	MAL
136.95	164.4	DIAB CARB	UIT
149.37	149.8	FRACT	UIT
164.44	203.3	DOLM QCV EPID	MAL
203.37	211.1	DIAB QCV	UIT
211.19	223.4	DOLM	MAL
211.33	211.4	SHZO QCV CHLO	MAL
220.48	221.8	DOLM	MAL
223.43	246.6	DIAB	UIT
228.54	229.7	DIAB	UIT
246.63	298.4	DOLM	MAL
280.07	280.3	DOLM	MAL
295.92	296.8	DOLE QCV	UIT
298.48	303.5	DIAB QCV	UIT
303.58	310.1	QTZ	MAL
310.14	322.1	DIAB CARB QCV	UIT
313.6	317	DOLE QCV	UIT
322.17	325.4	QTZ	MAL
325.48	329.1	SCHI TALC QCV	MAL
329.1	330.3	QTZ	BRQ
330.34	343.4	GRAN QCV SAUS	NELS

UD 99

From(m)	To	ROCKTYPE ALTERATION	STRAT
0	18.85	CORELOSS	UIT
18.85	34	SHLE HI_WEAT	TBH
34	43	SHLE HI_WEAT	TBH
43	45.72	SHLE SL_ALT SL_WEAT Cp	TBH
45.72	47.64	QTZ CARB SILIC	TBH
47.64	74.1	DOLE SL_ALT SL_WEAT	UIT
74.1	80.66	SHLE QCV SL_ALT Py	TBH
74.52	74.71	SHZO QCV SILIC Cp	TBH
76.46	76.57	QV QCV SILIC Cp	TBH
80.66	86.18	DIAB SL_ALT	UIT
86.18	91	SHLE SL_ALT QCV Cp	TBH
88	89	SHLE QCV SILIC Py	TBH

91	95.96	SHLE QCV SILIC Py	TBH
95.96	101.5	DIAB SL_ALT	UIT
101.51	102.0	DIAB SL_ALT SILIC	UIT
102.02	106.1	CONG SILIC SL_ALT Py	RHE
106.13	112.8	CONG SILIC SL_ALT	RHE
112.84	135.8	DOLM SILIC CARB	MAL
115.42	115.6	SHLE SL_ALT Cp	MAL
118.46	118.5	QV SILIC CARB	MAL
128.63	128.8	DOLE QCV SL_ALT	UIT
135.8	163.8	DIAB QCV SL_ALT	UIT
163.85	169.6	DOLM SILIC CARB	MAL
164.21	164.2	MAG CARB SL_ALT	MAL
166.49	166.5	MAG CARB SL_ALT	MAL
166.64	166.7	MAG CARB SILIC	MAL
167.43	167.5	MAG CARB SILIC	MAL
167.78	167.8	MAG CARB SILIC	MAL
168.27	168.3	MAG CARB SILIC	MAL

APPENDIX IV – XRF-standards - composition

Table : standards program sodium only

Standard	DT-N	G2	GA	GH	GS-N	GSP-1	JG-1	SY-2
Total (%)	100,061	99,694	99,999	100,027	100,069	100,111	100,005	100,01
Na2O (%)	0,04	4,06	3,58	3,87	3,81	2,81	3,4	4,32
Al2O3 (%)	60,29	15,39	14,64	12,55	14,83	15,14	14,26	12,08
As (ppm)	0,2	0,25	1,7	0,4	1,6	0,1	0,36	17,3
Ba (ppm)	130	1882	840	20	1400	1310	462	460
CaO (%)	0,04	2	2,47	0,69	2,53	2,08	2,19	7,99
Ce (ppm)	134	160	76	60	135	399	45,9	175
CeO2 (ppm)	134	160	/	60	/	399	/	/
Co (ppm)	15	4,6	5	0,3	65	6,6	4	8,6
Cr (%)	260	8	12	3	55	13	64,6	9,5
Cr2O3 (%)	0,0379	0,0008	0,0017	0,0004	0,008	0,0018	0,009	0,0013
Cu (ppm)	7	11	16	3	20	33	1,5	5,2
F (ppm)	40	1260	500	3500	1050	3630	496	5030

Fe2O3 (%)	1	3	3	1	4	4	2	6
Hf (ppm)	10	7,9	4	6,6	6,2	15,5	3,79	7,7
HfO2 (ppm)	10	7,9	/	6,6	/	15,5	/	/
K20 (%)	0,12	4,48	4,07	4,78	4,68	5,52	3,99	4,47
La (ppm)	21,5	89	89	40	75	75	22,4	75
La2O3 (ppm)	90	89	/	25	/	184	/	/
MgO (%)	0,04	0,75	0,96	0,03	2,33	0,96	0,74	2,7
MnO (%)	0,01	0,034	0,09	0,05	0,06	0,04	0,06	0,32
Sc (ppm)	2,10	3,50	7,00	0,80	7,30	6,20	6,54	7,00
Ti (ppm)	/	0,91	/	1,80	/	/	1,00	1,50
SO3 (ppm)	/	100	/	70	/	320	/	/
Cd (ppm)	/	0,01	/	/	/	0,06	/	/
Ge (ppm)	4,90	1,14	1,70	2,00	1,30	1,36	1,70	/
Ag (ppm)	/	40,00	/	/	/	/	/	/
Bi (ppm)	/	43,00	/	/	0,18	/	/	/
Cs (ppm)	/	1,40	/	/	/	/	/	/
Sm (ppm)	/	7,20	/	/	/	/	/	/
Ta (ppm)	/	0,80	/	4,80	2,60	/	/	2,00
Te (ppm)	/	/	/	/	/	/	0,02	/
W (ppm)	120,00	0,10	1,50	1,60	450,00	0,30	/	/
Standard	DT-N	G2	GA	GH	GS-N	GSP-1	JG-1	SY-2
Yb (ppm)	/	0,86	/	/	/	/	/	/
Mo (ppm)	0,50	1,10	0,50	2,00	1,20	0,80	1,46	1,80
Nb (ppm)	34,00	12,00	12,00	85,00	21,00	27,90	12,60	29,00
Nd (ppm)	52,00	58,00	27,00	29,00	49,00	196,00	19,50	73,00
Ni (ppm)	14,00	5,00	7,00	3,00	34,00	8,80	6,00	9,90
P205 (%)	0,09	0,13	0,12	0,01	0,28	0,28	0,10	0,43

Pb (ppm)	25	30	30	45	53	55	26,2	85
Rb (ppm)	6	170	175	390	185	254	181	217
Sb (ppm)	0,25	0,06	0,2	/	0,7	3,2	0,35	/
SiO2 (%)	37,1	69,22	70,56	76,12	66,53	67,4	72,6	60,32
Sn (ppm)	2,2	1,4	2,7	10	3	6,6	4,1	5,7
Sr (ppm)	30	478	310	10	570	234	184	271
Th (ppm)	2	24,7	17	87	41	106	13,5	379
TiO2 (%)	1,43	0	0,38	0,08	0,69	0,65	0,26	0,15
U (ppm)	2,3	2,07	5	18	7,5	2,54	3,3	284
V (ppm)	150	36	38	5	65	53	25	50
Y (ppm)	6,6	11	21	75	16	26	28,5	128
Zn (ppm)	28	86	80	55	48	104	41,5	248
Zr (ppm)	370	309	150	150	235	530	114	280
Cl (ppm)	/	66	250	100	450	330	60	140
S (ppm)	/	100	80	70	140	320	11,3	160
Ga (ppm)	30	23	16	23	22	23	17	29

Table: standards program major elements

Standard	AC-E	AGV-1	AL-1	AN-G	ASK-1	ASK-2	BCR-1	BE-N	BHVO-1	BR	BX-N	DR-N	DT-N	DTS-1	FK-N	G-1	G-2
Total (%)	100	100	100	100	106,9	110,3	100	100,1	100	100,1	99,95	100	100,1	100,6	100	100	100,0
SiO_2 (%)	70,65	59,83	69,86	46,6	68,83	66,5	54,3	39,33	49,5	39,29	8,4	53,91	37,12	40,43	65,4	72,52	69,4
Al_2O_3 (%)	14,76	17,44	18,73	30	21,52	23,07	13,69	10,37	13,7	10,49	61,52	17,87	60,29	0,19	18,72	14,23	15,4
Fe_2O_3 (%)	3	6,86	0,08	3,38	5	7	13,51	13,21	12,3	13	26,29	9,9	1	8,78	0	1,94	2,7
MnO (%)	0,06	0,09	0	0,04	0,16	0,05	0,18	0,21	0,17	0,21	0,06	0,22	0,01	0,12	0,01	0,03	0,03
MgO (%)	0,03	1,56	0,04	1,81	1,27	2,45	3,49	13,54	7,17	13,66	0,12	4,49	0,04	49,62	0,01	0,36	0,75
CaO (%)	0,34	5,02	0,39	16	3,2	0,75	6,97	14,28	11,3	14,2	0,19	7,19	0,04	0,17	0,11	1,37	1,97
Na_2O (%)	6,57	4,33	10,67	1,64	0,93	0,02	3,28	3,27	2,24	3,14	0,05	3,05	0,04	0,02	2,6	3,33	4,1
K_2O (%)	4,51	2,97	0,14	0,13	4,86	6,5	1,7	1,43	0,52	1,44	0,06	1,73	0,12	0	12,88	5,51	4,5
TiO_2 (%)	0,11	1,07	0,01	0,22	1,06	0,92	2,25	2,69	2,69	2,67	2,69	1,11	1,43	0,01	0,02	0,27	0,48
P_2O_5 (%)	0,01	0,5	0,04	0,01	0	0	0,36	1,08	0,27	1,07	0,15	0,26	0,09	0	0,02	0,08	0,14
Ag (ppm)	0	0	0	/	/	/	/	/	/	/	/	/	/	/	/	/	/
As (ppm)	2,3	0,88	0,8	0,2	1	25	0,65	1,8	0,4	2	115	3	0,2	0,034	0,3	0,7	0,25
Ba (ppm)	55	1226	85	34	1100	8000	681	1025	139	1050	30	385	130	1,7	200	1080	1882
Bi (ppm)	0,4	0	/	/	/	/	/	/	/	/	/	/	/	/	/	/	/
Cd (ppm)	0	0	/	/	/	/	/	/	/	/	/	/	/	/	/	/	/
Ce (ppm)	154	67	21	4,7	260	90	53,7	152	39	151	520	46	134	0,072	1	173	160
Cl (ppm)	180	119	110	300	100	15	59	200	92	350	30	400	/	10,5	20	40	70
Co (ppm)	0,2	15,3	0,2	25	6	27	37	60	45	52	30	35	15	137	14	2,3	4,6

Cr (ppm)	3,4	10,1	2	50	50	90	16	360	289	380	280	40	260	3990	5	20	8,7
Cs (ppm)	0	/	/	/	/	/	/	/	/	/	/	/	/	/	/	/	/
Cu (ppm)	4	60	3	19	7	124	19	72	136	72	18	50	7	7,1	2	12	11
F (ppm)	2100	425	45	120	1050	1300	490	1000	385	1000	900	500	40	13	30	680	1280
Ga (ppm)	39	/	/	18	30	24	/	17	21	20	/	/	30	/	23	/	/
Ge (ppm)	2,3	/	/	/	2	1	/	1,2		1,2	/	/	4,9	/	2,5	/	/
Hg (ppm)	0	/	/	/	/	/	/	/	/	/	/	/	/	/	/	/	/
La (ppm)	59	38	9,7	2,2	125	46	24,9	82	15,8	82	35		21,5	90	0,029	0,95	105
Mo (ppm)	2,5	2,7	0,1	0,2	5	60	1,6	2,8	1,02	2,4	8,3	0,9	0,5	0,14	0,25	6,8	1,1
Nb (ppm)	110	15	1,6	0,7	60	30	14	105	19	98	52	7	34	2,2	0,3	22,6	12
Nd (ppm)	92	33	10,4	2,4	95	30	28,8	67	25,2	65	163	23,5	52	0,029	0,3	57	55
Ni (ppm)	1,5	16	2	5	120	150	13	267	121	260	180	15	14	2360	1,5	3,4	5
Pb (ppm)	39	36	4,5	2	6	40	13,6	4	2,6	5	135	55	25	12	240	46	30
Rb (ppm)	152	67,3	5,8	1	85	160	47,2	47	11	47	3,6	73	6	0,058	860	214	170
S (ppm)	70	26	85	140	400	20000	410	300	102	390	/	350	/	12	60	130	100
Sb (ppm)	0,4	4,3	0,2	0,1	0,03	5	0,62	0,26	0,16	0,2	8	0,4	0,25	0,05	0,45	0,3	0,07
Sc (ppm)	0,11	12,2	1,75	10	7	17,5	32,6	22	31,8	25	/	/	2,1	3,5	0,05	2,8	3,5
Sn (ppm)	13	4,2	0,4	1,4	3	3	2,7	2	2,1	2	13,4	2	2,2	0,55	0,3	3,2	1,8
Sr (ppm)	3	662	80	76	680	100	330	1370	403	1320	110	400	30	0,32	39	248	478

Standard	GL-O	GR	GS-N	GSP-1	IF-G	JA-1	JA-2	JA-3	JB-1	JB-1A	JB-2	JB-3	JCH-1	JDO-1	JF-1	JF-2	JG-1	JG-1A	JG-2
Total (%)	100	100	100	100	100,07	100	100	100	100	100	100	100	100	99,98	100	100	100	100	100

SiO_2 (%)	55,33	66,45	67	67	40,86	65	57	62	52,7	53	53	50,7	98,5	0,38	67	65,6	73	73	77
Al_2O_3 (%)	8,21	14,87	15	15	0,15	15	16	16	14,7	15	15	16,8	0,72	0,02	18,1	18,5	14	14	12
Fe_2O_3 (%)	21,31	4,08	4	4	55,39	7	6,3	6,6	9	9,2	14	12	0,38	0,04	0,08	0,06	2	2,1	1
MnO (%)	0,01	0,06	0,1	0	0,04	0,2	0,1	0,1	0,16	0,2	0,2	0,16	0,02	0,01	0	0	0,1	0,1	0
MgO (%)	4,85	2,42	2,3	1	1,87	1,6	7,9	3,7	7,81	7,8	4,6	5,17	0,08	34,83	0,01	0	0,7	0,7	0
CaO (%)	1,04	2,52	2,5	2,1	1,54	5,7	6,6	6,3	9,29	9,3	9,9	9,9	0,04	64,59	0,92	0,09	2,2	2,2	0,8
Na_2O(%)	0,04	3,83	3,8	2,8	0,03	3,9	3,2	3,2	2,82	2,8	2	2,8	0,03	0,02	3,56	2,47	3,4	3,4	3,6
K_2O (%)	8,64	4,54	4,7	5,5	0,01	0,8	1,8	1,4	1,45	1,4	0,4	0,78	0,22	0	10,1	13,2	4	4	4,7
TiO_2(%)	0,08	0,66	0,7	0,7	0,01	0,9	0,7	0,7	1,35	1,3	1,2	1,44	0,03	0	0,01	0	0,3	0,3	0
P_2O_5 (%)	0,4	0,28	0,3	0,3	0,06	0,2	0,2	0,1	0,26	0,3	0,1	0,29	0,01	0,06	0,01	0	0,1	0,1	0
Ag (ppm)	/	/	/	/	/	/	/	/	/	/	/	/	/	/	/	/	/	/	/
As (ppm)	10,5		1,6	0,1	1,5	2,9	0,8	4,5	2,48	2,3	3	1,66	0,4	0,11	0,96	0,28	0,4	0,4	0,8
Ba (ppm)	6	1050	1400	1310	1,5	307	317	318	490	497	208	251	/	/	1680	320	462	458	67
Bi (ppm)	/	/	0,2	/	/	/	/	/	/	/	/	/	/	/	/	/	/	/	/
Cd (ppm)	/	/	/	0,1	/	/	/	/	/	/	/	/	/	/	/	/	/	/	/
Ce (ppm)	54	/	135	399	4	14	33	23	66,7	66	6,8	21,5	4,72	2,54	4,11	1,2	46	45	50
Cl (ppm)	/	/	450	330	25	35	/	/	172	170	240	260	/	/	/	/	60	/	/
Co (ppm)	14	10	65	6,6	29	12	30	21	38,7	40	40	36,3	15	/	0,2	0,4	4	5,7	4,3
Cr (ppm)	140	110	55	13	4	7,3	465	68	469	415	27	60,4	9	7	5,8	4	65	19	7,6
Cs (ppm)	/	/	/	/	/	/	/	/	/	/	/	/	/	/	/	/	/	/	/
Cu (ppm)	3,5	345	20	33	13	42	29	45	56,3	56	227	198	15,5	1,4	0,2	0,3	1,5	1,3	0,4
F (ppm)	/	/	1050	3630	50	180	485	280	393	385	101	295	/	/	/	4	496	450	960
Ga (ppm)	/	/	22	23	/	17	16	/	18,1	18	/	20,7	/	/	/	/	17	/	19
Ge (ppm)	/	/	1,3	1,4	/	/	/	/	1,2	/	/		/	/	/	/	1,7	/	/
Hg (ppm)	/	/	/	/	/	/	/	/	/	/	/	/	/	/	/	/	/	/	/
La (ppm)	25	20	75	75	184	2,8	0,5	0,3	0,32	38	0,3	0,39	1,5	7,87	0,05	0,01	22	22	20
Mo (ppm)	0,03	18	1,2	0,8	0,7	2	0,5	1,6	34	1,4	1,1	1,1	/	/	0,04	0,3	1,5	0,7	0,2
Nb (ppm)	3,7	/	21	28	0,1	1,7	9,8	3	34,5	27	0,8	2,3	/	/	0,5		13	2	15
Nd (ppm)	27	/	49	196	0,8	11	14	12	29,7	5,5	6,7	15,4	/	/	1,44	0,3	20	21	26

Ni (ppm)	36	55	34	8,8	22,5	1,8	142	36	139	140	14	38,8	7,5	2,9	0,4	0,4	6	6,4	2,1
Pb (ppm)	3	32	53	55	4	5,8	19	6,7	7,1	7,2	5,4	5,5	2	1	33,4	47,9	26	27	33
Rb (ppm)	238	175	185	254	0,4	12	68	36	41,2	41	6,2	13	8,5	/	264	222	181	180	297
S (ppm)	/	/	140	320	700	23	8	228	17,9	9	19	8	4	86	/	/	11	10	9
Sb (ppm)	0,3	/	0,7	3,2	0,63	0,3	0,1	0,3	0,08	0,3	0,3	0,15	/	/	0,06	0,04	0,4	/	/
Sc (ppm)	8	/	7,3	6,2	0,3	28	20	22	27,5	28	54	33,3	0,85	0,14	0,22	0,09	6,5	6,3	2,5
Sn (ppm)	2	10	3	6,6	0,3	0,8	1,5	0,9	1,8	2	0,6	0,86	/	/	0,3	0,1	4,1	4,2	2,5
Sr (ppm)	19,3	550	570	234	3	266	252	294	435	443	178	395	4,6	119	163	193	184	185	16
Standard	GL-O	GR	GS-N	GSP-1	IF-G	JA-1	JA-2	JA-3	JB-1	JB-1A	JB-2	JB-3	JCH-1	JDO-1	JF-1	JF-2	JG-1	JG-1A	JG-2
Ta (ppm)	/	/	2,6	/	/	/	/	/	2,7	/	/	/	/	/	/	/	/	/	/
Th (ppm)	3,4	/	41	106	0,1	0,8	4,7	3,4	9,2	8,8	0,3	1,3	/	/	1,3	1	14	12	30
Tl (ppm)	/	/	/	/	/	/	/	/	0,11	0,1	/	/	/	/	/	/	1	/	/
U (ppm)	0,8	/	7,5	2,5	0,02	0,3	2,4	1,4	1,7	1,6	0,2	0,46	/	/	0,33	0,2	3,3	4,7	13
V (ppm)	5	65	65	53	2	105	130	172	212	220	578	383	6	/	3	0,7	25	23	3
W (ppm)	/	/	450	0,3	/	3,9	/	/	20	/	/	/	/	/	/	/	/	/	/
Y (ppm)	65	19	16	26	2	31	18	21	24,4	24	25	27	1,84	11,2	2,99		29	32	88
Zn (ppm)	38	60	48	104	20	91	63	68	83	82	110	106	9,1	34,4	3,2	0,8	42	39	13
Zr (ppm)	36	180	235	530	1	88	119	119	143	146	51	98,3	11,7	/	39,1	6,6	114	121	101
Hf (ppm)	1,1	/	6,2	16	0,04	2,4	2,9	3,4	3,4	3,5	1,4	2,68	0,2	0,1	1,22	0,19	3,8	3,8	5,4
Li (ppm)	/	/	/	/	/	/	/	/	/	/	/	/	/	/	/	/	/	/	/
CeO_2(ppm)	/	/	/	399	/	/	/	/	/	/	/	/	/	/	/	/	/	/	/
HfO_2 (ppm)	/	/	/	16	/	/	/	/	/	/	/	/	/	/	/	/	/	/	/
La_2O_3(ppm)	/	/	/	184	/	/	/	/	/	/	/	/	/	/	/	/	/	/	/
SO_3 (ppm)	/	/	/	320	/	/	/	/	/	/	/	/	/	/	/	/	/	/	/
Cr_2O_3 (%)	0,02	0,016	0	0	0,0006	0	0,1	0	0,07	0,1	0	0,01	0	0,001	0	0	0	0	0
Se (ppm)	/	/	/	/	/	/	/	/	0,03	/	/	0,08	/	/	/	/	/	/	/
Te (ppm)	/	/	/	0	/	/	/	/	/	/	/	/	/	/	/	/	/	/	/
Yb (ppm)	/	/	/	/	/	/	/	/	/	/	/	/	/	/	/	/	/	/	/

Standard	JG-3	JGB-1	JGB-2	JH-1	JLK-1	JLS-1	JP-1	JR-1	JR-2	JR-3	JSD-1	JSD-2	JSI-1	JSI-2	Kim?	MA-N	MAG-1	MICA-FE	MICA-MG
Total (%)	99,998	100,2	100,1	100,2	100	100	100	100	100	100	100	101	100	100	0	99,5	103	99,95	99,98
SiO_2 (%)	67,5	43,64	47,12	49,05	64,7	0,2	43,6	76	77	73,3	68,5	63,1	63,2	63	/	67,6	58,07	34,65	38,68
Al_2O_3 (%)	15,61	17,74	23,54	5,63	19,1	0	0,64	13	13	12,2	15,1	13,1	18,8	19	/	17,9	18,88	19,64	15,35
Fe_2O_3 (%)	3,76	15,23	6,91	10,46	7,75	0	9	1	1	4,81	5,27	12,1	7,28	7,1	/	0	7,95	26	9,55
MnO (%)	0,07	0,17	0,13	0,19	0,31	0	0,12	0,1	0,1	0,09	0,1	0,13	0,07	0,1	/	0,04	0,11	0,35	0,26
MgO (%)	1,8	7,87	6,3	17,32	1,99	1,1	45,9	0,1	0,1	0,05	1,91	2,94	2,64	2,6	/	0,04	3,46	4,58	20,6
CaO (%)	3,78	12,04	14,33	15,2	0,77	99	0,58	0,6	0,5	0,09	3,17	3,8	1,52	2,1	/	0,6	1,58	0,43	0,08
Na_2O(%)	4,05	1,24	0,93	0,73	1,19	0	0,02	4,1	4,1	4,73	2,82	2,59	2,34	1,5	/	5,93	4,42	0,3	0,12
K_2O (%)	2,65	0,24	0,06	0,53	3,14	0	0	4,5	4,5	4,38	2,26	1,2	3,03	3,1	/	3,23	4,09	8,81	10,1
TiO_2(%)	0,48	1,63	0,59	0,68	0,76	0	0	0,1	0,1	0,21	0,67	0,66	0,78	0,8	/	0,01	0,87	2,52	1,65
P_2O_5 (%)	0,12	0,05	0,01	0,11	0,24	0,1	0	0	0	0,01	0,12	0,08	0,2	0,2	/	1,41	0,19	0,45	0,01
Ag (ppm)	/	/	/	/	/	/	/	/	/	/	/	/	/	/	/	/	/	/	/
As (ppm)	0,37	1,11	1,06	1,12	27,7	0,2	0,34	16	20	0,72	2,36	39,4	15,6	12	/	13	9,2	3	/
Ba (ppm)	453	63	/	/	/	/	17	40	39	/	/	/	/	/	/	42	479	150	4000
Bi (ppm)	/	/	/	/	/	/	/	/	/	/	/	/	/	/	/	/	/	1,9	/
Standard	JG-3	JGB-1	JGB-2	JH-1	JLK-1	JLS-1	JP-1	JR-1	JR-2	JR-3	JSD-1	JSD-2	JSI-1	JSI-2	Kim?	MA-N	MAG-1	MICA-FE	MICA-MG
Cd (ppm)	/	/	/	/	/	/	/	/	/	/	/	/	/	/	/	/	/	/	/
Ce (ppm)	40,1	7,86	/	/	89,1	0,9	0,2	47	39	/	35,4	20,7	60,5	71	/	0,9	88	420	0,35
Cl (ppm)	/	/	/	/	/	/	50	920	730	/	/	/	/	/	/	140	31000	500	800
Co (ppm)	11,4	61,6	28	53	18,1	/	116	0,7	0	1	10,9	48	14,7	15	/	0,5	20,4	23	24
Cr (ppm)	23,6	59,3	130	630	69	3	2970	2,3	2,6	2,5	22	104	58	64	/	3	97	90	100
Cs (ppm)	/	/	/	/	/	/	/	/	/	/	/	/	/	/	/	/	/	/	/
Cu (ppm)	6	86,8	11	9	59,8	/	5,7	1,4	0,4	2,1	22,2	1114	40	41	/	140	30	5	5

F (ppm)	335	150	/	/	/	/	10	942	1087	/	/	/	/	/	/	17000	770	16000	28500
Ga (ppm)	17	/	/	/	/	/	0,5	18	18	/	/	/	/	/	/	59	/	95	21
Ge (ppm)	/	/	/	/	/	/	/	/	2,4	/	/	/	/	/	/	3,5	/	3,2	1,55
Hg (ppm)	/	/	/	/	/	/	/	/	/	/	/	/	/	/	/	/	/	/	/
La (ppm)	20,7	3,74	/	/	41,3	0,2	0,1	0,7	0,9	/	18,6	12,3	29,9	33	/	0,5	43	200	0,32
Mo (ppm)	0,44	0,45	/	/	/	/	/	3,2	2,9	/	/	/	/	/	/	0,3	1,6	1,2	0,25
Nb (ppm)	5,6	2,8	/	/	/	/	1,2	16	19	/	/	/	/	/	/	173	12	270	116
Nd (ppm)	16,8	5,65	/	/	/	/	0,07	24	21	/	/	/	/	/	/	0,4	38	180	0,08
Ni (ppm)	13	25,4	13,8	56	36,9	0,3	2460	0,7	0,8	1,1	6,9	94	38,5	39	/	53	3	35	110
Pb (ppm)	12,3	1,9	/	/	45	/	0,11	19	22	34,5	14	151	18	21	/	29	24	13	9
Rb (ppm)	66	4	/	12	144	/	/	257	297	458	65	27	285	116	/	3600	149	2200	1300
S (ppm)	45	1950	707	650	1130	135	30	9	6	39	68	13300	1633	588	/	100	100	70	125
Sb (ppm)	/	0,11	/	/	/	/	/	1,4	1,8	/	/	/	/	/	/	1,7	0,96	/	/
Sc (ppm)	8,93	36,6	/	/	16	0	7,07	5,2	5,6	/	11,4	16,8	16,6	17	/	0,2	17,2	14,8	1,2
Sn (ppm)	1	0,36	/	/	/	/	0,05	2,7	3,2	/	/	/	/	/	/	900	3,6	70	5
Sr (ppm)	372	321	435	155	69	296		30	8	9	323	202	192	231	/	84	146	5	27
Ta (ppm)	/	/	/	/	/	/	/	/	/	/	/	/	/	/	/	290	/	35	4,4
Th (ppm)	8	0,53	/	/	/	/	0,18	27	32	/	/	/	/	/	/	1,4	11,9	150	0,1
Tl (ppm)	/	/	/	/	/	/		1,6	/	/	/	/	/	/	/	15	/	16	/
U (ppm)	2	0,15	/	/	/	/	0,05	9	11	/	/	/	/	/	/	12,5	2,7	80	0,15
V (ppm)	73	640	175	231	16	/	29		/	/	81	124	135	127	/	0,2	140	135	90
W (ppm)	/	/	/	/	/	/	/	1,9	/	/	/	/	/	/	/	70	/	/	90
Y (ppm)	17,2	10,75	/	/	40,8	/	/	45	51	/	15,7	17	30,3	31	/	0,2	28	48	0,04
Zn (ppm)	44,8	111	48	62	151	2,9	29,5	30	27	204	99	2070	112	107	/	220	130	1300	290
Zr (ppm)	143	33,5	/	/	146	/	6,3	101	97	/	134	108	167	194	/	25	126	800	16
Hf (ppm)	4,29	0,88	/	/	3,93	0,1	0,21	4,7	5,2	/	3,4	2,8	3,2	5	/	5,8	3,7	4,5	26
Li (ppm)	/	/	/	/	/	/	/	/	/	/	/	/	/	/	/	/	/	/	/
CeO_2(ppm)	/	/	/	/	/	/	/	/	/	/	/	/	/	/	/	/	/	420	/
HfO_2 (ppm)	/	/	/	/	/	/	/	/	/	/	/	/	/	/	/	/	/	26	/

La_2O_3(ppm)	/	/	/	/	/	/	/	/	/	/	/	/	/	/	/	/	/	200	/
SO_3 (ppm)	/	/	/	/	/	/	/	/	/	/	/	/	/	/	/	/	/	70	/
Standard	JG-3	JGB-1	JGB-2	JH-1	JLK-1	JLS-1	JP-1	JR-1	JR-2	JR-3	JSD-1	JSD-2	JSI-1	JSI-2	Kim?	MA-N	MAG-1	MICA-FE	MICA-MG
Cr_2O_3 (%)	0,0038	0,009	0,019	0,092	0,01	0	0,43	0	0	0	0	0,02	0,01	0	/	0	0,014	0,013	0,015
Se (ppm)	/	/	/	/	/	/	/	/	/	/	/	/	/	/	/	/	/	/	/
Te (ppm)	/	/	/	/	/	/	/	/	/	/	/	/	/	/	/	/	/	/	/
Yb (ppm)	/	/	/	/	/	/	/	/	/	/	/	/	/	/	/	/	/	/	/

Standard	NIM-D	NIM-G	NIM-L	NIM-N	NIM-P	NIM-S	PCC-1	SARM-39	SARM-40	SARM-41	SARM-42	SARM-43	SARM-44	SARM-45	SARM-46	SARM-47	S
Total (%)	100	100	99,927	100,01	103,49	99,997	100,39	100,26	99,895	100,14	100,61	100,03	100,08	100,09	99,902	100,21	9
SiO_2 (%)	38,6	75,9	53,94	52,5	51,37	63,76	43,73	37,86	5,08	65,02	79,47	11,66	35,43	50,18	44,97	43,04	
Al_2O_3 (%)	0,3	12,1	14,04	16,45	4,2	17,37	0,71	4,86	0,68	15,49	10,76	0,12	59,8	26,52	8,41	1,29	
Fe_2O_3 (%)	16,8	2	10,29	8,89	12,86	1,41	9	10,51	4,55	4,86	5,02	0,51	2,1	12,75	35,28	4,91	
MnO (%)	0,22	0,02	0,79	0,18	0,22	0,01	0,13	0,19	0,3	0,07	0,11	0,02	0,03	0,1	1,43	0,07	
MgO (%)	43,1	0,06	0,29	7,48	25,46	0,46	45,53	29,71	3,25	9,29	2,06	85,9	0,1	3,43	3,96	49,91	
CaO (%)	0,28	0,78	3,31	11,47	2,67	0,68	0,55	10,97	82,15	1,72	0,95	1,46	0,14	0,79	1,65	0,12	
Na_2O(%)	0,04	3,37	8,62	2,45	0,37	0,43	0,03	0,57	0,08	1,07	0,16	0,1	0,05	0,85	0,35	0,06	
K_2O (%)	0,01	5	5,67	0,25	0,09	15,38	0,01	1,18	0,05	1,59	0,48	0,08	0,18	3,22	0,44	0,02	
TiO_2(%)	0,02	0,09	0,49	0,2	0,2	0,04	0,01	1,79	0,08	0,63	0,39	0,02	1,86	1,84	0,75	0,01	
P_2O_5 (%)	0,01	0,01	0,06	0,03	0,02	0,12	0	1,65	3,38	0,06	0,04	0,04	0,1	0,08	0,14	0,02	
Ag (ppm)	/	/	/	/	/	/	/	/	/	/	/	/	/	/	/	/	
As (ppm)	/	15	/	/	/	/	0,056	/	/	/	/	/	/	/	/	/	
Ba (ppm)	10	120	450	100	46	2400	1,2	1700	310	820	250	25	50	900	180	75	
Bi (ppm)	/	/	/	/	/	/	/	/	/	/	/	/	/	/	/	/	
Cd (ppm)	/	/	/	/	/	/	/	/	/	/	/	/	/	/	/	/	
Ce (ppm)	/	195	240	6	/	12	0,1	85	160	60	30	20	210	100	110	20	
Cl (ppm)	400	170	1200	100	100	80	71	/	/	/	/	/	/	/	/	/	

Co (ppm)	210	4	8	58	110	3	112	77	20	15	35	4	8	41	56	79	
Cr (ppm)	2900	12	0	30	24000	12	2730	1300	35	123	4310	195	384	256	559	1984	
Cs (ppm)	/	/	/	/	/	/	/	/	/	/	/	/	/	/	/	/	
Cu (ppm)	10	12	13	14	18	19	10	58	10	53	17	5	0	1	566	5	
F (ppm)	/	4200	4400	/	/	120	12	/	/	/	/	/	/	/	/	/	
Ga (ppm)	/	27	54	16	8	11	/	/	/	/	10	/	50	/	/	/	
Ge (ppm)	/	/	/	/	/	/	/	/	/	/	/	/	/	/	/	/	
Hg (ppm)	/	/	/	/	/	/	/	/	/	/	/	/	/	/	/	/	
La (ppm)	0,2	109	250	3	2	5	0,052	/	/	/	/	/	/	/	/	/	
Mo (ppm)	4	3	4	/	/	/	2	5	10	5	5	/	15	/	10	/	
Nb (ppm)	/	53	960	/	/	4	/	110	10	/	8	/	96	27	/	/	
Nd (ppm)	/	72	48	3	/	6	0,042	/	/	/	/	/	/	/	/	/	
Ni (ppm)	2050	8	1	120	560	7	2380	994	25	122	125	252	15	80	125	2221	
Standard	NIM-D	NIM-G	NIM-L	NIM-N	NIM-P	NIM-S	PCC-1	SARM-39	SARM-40	SARM-41	SARM-42	SARM-43	SARM-44	SARM-45	SARM-46	SARM-47	S
Pb (ppm)	/	40	43	7	6	5	10	25	20	30	10	/	30	20	13000	60	
Rb (ppm)	8,5	320	190	6	5	530	0,066	52	10	59	22	/	13	142	20		
S (ppm)	/	/	/	/	/	/	20	1500	500	1500	200	400	300	500	1700	200	
Sb (ppm)	/	0,6	/	/	/	0,6	1,28	/	/	/	/	/	/	/	/	/	
Sc (ppm)	7	1	0,3	38	29	4	8,4	/	/	/	/	/	/	/	/	/	
Sn (ppm)	2	4	/	/	2	/	1,6	/	/	/	/	/	/	/	/	/	
Sr (ppm)	3	10	4600	260	2	62	0,04	1400	1600	4	37	8	5	92	25	3	
Ta (ppm)	/	4,5	22	/	/	/	/	/	/	/	/	/	/	/	/	/	
Th (ppm)	0,8	51	66	0,6	1	1	0,013	10	12	12	5	/	50	21	/	/	
Tl (ppm)	/	/	/	/	/	/	/	/	/	/	/	/	/	/	/	/	
U (ppm)	/	15	14	0,6	0,4	0,6	0,005	/	/	/	/	/	/	/	/	/	
V (ppm)	40	2	81	220	230	10	31	109	27	139	94	/	395	266	225	16	
W (ppm)	/	/	/	/	/	/	/	/	/	/	/	/	/	/	/	/	
Y (ppm)	/	143	22	7	5	20	0,1	17	33	17	11	/	84	63	20	5	

Zn (ppm)	90	50	400	68	100	10	42	70	25	76	44	10	271	74	5900	45	
Zr (ppm)	20	300	11000	23	30	33	10	239	87	146	192	/	406	322	101	/	
Hf (ppm)	3,76	12	190	/	/	/	0,04	/	/	/	/	/	/	/	/	/	
Li (ppm)	/	/	/	/	/	/	/	/	/	/	/	/	/	/	/	/	
CeO_2(ppm)	/	/	/	/	/	/	/	/	/	/	/	/	/	/	110	/	
HfO_2 (ppm)	/	/	/	/	/	/	/	/	/	/	/	/	/	/	/	/	
La_2O_3(ppm)	/	/	/	/	/	/	/	/	/	/	/	/	/	/	/	/	
SO_3 (ppm)	/	/	/	/	/	/	/	/	/	/	/	/	/	/	1700	/	
Cr_2O_3 (%)	0,42	0	0,0015	0,0044	3,5078	0,0018	0,3959	0,1898	0,0051	0,018	0,625	0,0283	0,0557	0,0371	0,0811	0,2897	0
Se (ppm)	/	/	/	/	/	/	/	/	/	/	/	/	/	/	/	/	
Te (ppm)	/	/	/	/	/	/	/	/	/	/	/	/	/	/	/	/	
Yb (ppm)	/	14,2	/	/	/	/	/	/	/	/	/	/	/	/	/	/	

Standard	SARM-51	SARM-52	SY-2	SY-3	UB-N
Total (%)	99,901	100,165	100,01	100,045	100,069
SiO_2 (%)	49,44	64	60,32	59,77	44,79
Al_2O_3 (%)	17,36	10,38	12,08	11,78	3,29

Fe_2O_3 (%)	26,85	21,82	6	7	9,47
MnO (%)	0,31	0,3	0,32	0,32	0,14
MgO (%)	1,35	0,66	2,7	2,67	40
CaO (%)	1,26	0,41	7,99	8,26	1,36
Na_2O(%)	0,1	0,11	4,32	4,13	0,11
K_2O (%)	0,48	0,28	4,47	4,24	0,02
TiO_2(%)	1,2	1,44	0,15	0,15	0,12
P_2O_5 (%)	0,31	0,1	0,43	0,54	0,05
Ag (ppm)	/	/	/	/	/
As (ppm)	/	/	17,3	18,8	10
Ba (ppm)	410	460	450	27	
Bi (ppm)	/	/	/	/	
Cd (ppm)	/	/	/	/	
Ce (ppm)	210	175	2230	0,8	
Cl (ppm)	/	140	150	800	
Co (ppm)	81	8,6	8,8	100	
Cr (ppm)	1300	9,5	11	2300	
Cs (ppm)	/	/	/	/	
Cu (ppm)	219	5,2	17	28	
F (ppm)	/	5030	6960	95	
Ga (ppm)	/	15	29	27	/
Ge (ppm)	/	/	/	1,4	/
Hg (ppm)	/	/	/	/	/
La (ppm)	/	/	75	1340	0,35
Mo (ppm)	/	/	1,8	1	0,55
Nb (ppm)		11	29	148	0,05
Nd (ppm)	/	/	73	670	0,6
Standard	SARM-51	SARM-52	SY-2	SY-3	UB-N

Ni (ppm)	178	182	9,9	11	75
Pb (ppm)	5200	1200	85	133	13
Rb (ppm)	37	20	217	206	4
S (ppm)	2400	200	160	510	200
Sb (ppm)	/	/	/	/	0,3
Sc (ppm)	/	/	7	6,8	/
Sn (ppm)	/	/	5,7	6,5	/
Sr (ppm)	44	25	271	302	9
Ta (ppm)	/	/	2	30	/
Th (ppm)	10	11	379	1003	0,07
Tl (ppm)	/	/	1,5	1,5	/
U (ppm)	/	/	284	650	0,07
V (ppm)	181	346	50	50	75
W (ppm)	/	/	/	1,1	/
Y (ppm)	21	20	128	718	2,5
Zn (ppm)	2200	264	248	244	85
Zr (ppm)	121	250	280	320	4
Hf (ppm)	/	/	7,7	9,7	0,1
Li (ppm)	/	/	/	/	/
CeO_2(ppm)	/	/	/	/	/
HfO_2 (ppm)	/	/	/	/	/
La_2O_3(ppm)	/	/	/	/	/
SO_3 (ppm)	/	/	/	/	/
Cr_2O_3 (%)	0,0738	0,1885	0,0013	0,0016	0,3358
Se (ppm)	/	/	/	/	/
Te (ppm)	/	/	/	/	/
Yb (ppm)	/	/	/	/	/

Table: standards for program vms trace 3

Standard		AC-E	AN-G	ASK-1	ASK-2	ASK-3	BE-N	BHVO-1	BR	DT-N	FK-N	GA	GH	G
Total	(%)	100	100,02	106,915	110,262	35,04	100,102	100,084	100,084	100,06	100,02	99,999	100,027	10
S	(ppm)	70	140	400	20000	/	300	102	390	/	60	80	70	
CaO	(ppm)	3400	160200	32000	7500	/	142800	113000	142000	400	1100	24700	6900	2
Sc	(ppm)	0,11	10	7	17,5	/	22	31,8	25	2,1	0,05	7	0,8	
TiO_2	(ppm)	1100	2200	10600	9180	60	26900	26900	26700	14300	200	3800	800	6
V	(ppm)	3	70	45	200	/	235	317	235	150	0,5	38	5	
Cr	(ppm)	3,4	50	50	90	/	360	289	380	260	5	12	3	
Fe_2O_3	(ppm)	25400	33800	46000	69000	350000	132100	122500	132500	6700	900	28500	13500	3
Co	(ppm)	0,2	25	6	27	/	60	45	52	15	14	5	0,3	
Ni	(ppm)	1,5	5	120	150	/	267	121	260	14	1,5	7	3	
Cu	(ppm)	4	19	7	124	/	72	136	72	7	2	16	3	

Zn	(ppm)	224	20	96	160	/	120	105	160	28	10	80	55	
Ga	(ppm)	39	18	30	24	6	17	21	20	30	23	16	23	
Ge	(ppm)	2,3	/	2	1	/	1,2		1,2	4,9	2,5	1,7	2	
As	(ppm)	2,3	0,2	1	25	/	1,8	0,4	2	0,2	0,3	1,7	0,4	
Se	(ppm)	/	0,06	0,07	3	17	/	/	/	/	/	/	/	
Br	(ppm)	/	/	/	/	/	/	/	/	/	/	/	/	
Rb	(ppm)	152	1	85	160	/	47	11	47	6	860	175	390	
Sr	(ppm)	3	76	680	100	/	1370	403	1320	30	39	310	10	
Y	(ppm)	184	7,5	/	/	/	30	27,6	30	6,6	0,5	21	75	
Zr	(ppm)	780	11	400	170	/	260	179	260	370	0,7	150	150	
Nb	(ppm)	110	0,7	60	30	/	105	19	98	34	0,3	12	85	
Mo	(ppm)	2,5	0,2	5	60	/	2,8	1,02	2,4	0,5	0,25	0,5	2	
Ag	(ppm)	0	/	/	/	/	/	/	/	/	/	/	/	
Cd	(ppm)	0	/	/	/	310	/	/	/	/	/	/	/	
Sn	(ppm)	13	1,4	3	3	/	2	2,1	2	2,2	0,3	2,7	10	
Sb	(ppm)	0,4	0,1	0,03	5	/	0,26	0,16	0,2	0,25	0,45	0,2	/	
Te	(ppm)	/	/	/	/	/	/	/	/	/	/	/	/	
I	(ppm)	/	/	/	/	/	/	/	/	/	/	/	/	
Ba	(ppm)	55	34	1100	8000	/	1025	139	1050	130	200	840	20	1
Yb	(ppm)	/	/	/	/	/	/	/	/	/	/	/	/	
Standard		AC-E	AN-G	ASK-1	ASK-2	ASK-3	BE-N	BHVO-1	BR	DT-N	FK-N	GA	GH	G
Hf	(ppm)	27,9	0,38	10	/	/	5,6	4,38	5,6	10	0,04	4	6,6	
Ta	(ppm)	6,4	/	8	7	/	5,7	/	6,2	/	/	/	4,8	
W	(ppm)	0	105	/	/	/	29	/	1,3	120	120	1,5	1,6	
Hg	(ppm)	0	/	/	/	8	/	/	/	/	/	/	/	
Tl	(ppm)	0,9	/	/	/	/	0,04	/	/	/	/	/	1,8	
Pb	(ppm)	39	2	6	40	/	4	2,6	5	25	240	30	45	
Bi	(ppm)	0,4	/	/	/	32	/	/	/	/	/	/	/	
Th	(ppm)	18,5	0,04	16	13	/	10,4	1,08	11	2	0,15	17	87	

U	(ppm)	4,6	0,12	5	22	/	2,4	0,42	2,5	2,3	0,15	5	18	
Al_2O_3	(ppm)	1E+05	300200	215200	230700	/	103700	136800	104900	602900	187200	146400	125500	14
SiO_2	(ppm)	7E+05	466400	688300	665000	/	393300	495000	392900	371200	654000	705600	761200	66
Sm	(ppm)	/	/	/	/	/	/	/	/	/	/	/	/	
Ce	(ppm)	154	4,7	260	90	/	152	39	151	134	1	76	60	
La	(ppm)	59	2,2	125	46	/	82	15,8	82	21,5	0,029	89	40	
MnO	(%)	0,06	0,04	0,16	0,05	/	0,21	0,17	0,21	0,01	0,01	0,09	0,05	0
Nd	(ppm)	92	2,4	95	30	/	67	25,2	65	52	0,3	27	29	
Cs	(ppm)	0	/	/	/	/	/	/	/	/	/	/	/	
C	(%)	/	/	/	/	/	/	/	/	/	/	/	/	
ZnO	(%)	/	/	/	/	/	/	/	/	/	/	/	/	
Cl	(ppm)	180	300	100	15	/	200	92	350	/	20	250	100	
Cr_2O_3	(%)	5E-04	0,0073	0,0073	0,0131	/	0,0526	0,0422	0,0555	0,0379	0,0007	0,0017	0,0004	0
F	(ppm)	2100	120	1050	1300	/	1000	385	1000	40	30	500	3500	1
K_2O	(%)	4,51	0,13	4,86	6,5	/	1,43	0,52	1,44	0,12	12,88	4,07	4,78	
MgO	(%)	0,03	1,81	1,27	2,45	/	13,54	7,17	13,66	0,04	0,01	0,96	0,03	
Na_2O	(%)	6,57	1,64	0,93	0,02	/	3,27	2,24	3,14	0,04	2,6	3,58	3,87	
P_2O_5	(%)	0,01	0,01	0	0	/	1,08	0,27	1,07	0,09	0,02	0,12	0,01	0
CeO_2	(ppm)	/	/	/	/	/	152	/	/	134	/	/	60	
HfO_2	(ppm)	/	/	/	/	/	5,6	/	/	10	/	/	6,6	
La_2O_3	(ppm)	/	/	/	/	/	82	/	/	90	/	/	25	
SO_3	(ppm)	/	/	/	/	/	300	/	/		/	/	70	
Li	(ppm)	93	/	/	/	/	/	/	/	/	/	/	/	

Standard		JA-2	JB-1	JB-1A	JB-3	JG-1	JG-2	JG-3	JP-1	JR-2	MA-N	MICA-FE	MICA-I
Total	(%)	100,053	99,966	100,058	100,077	100,005	99,99	99,998	100,427	100,005	99,529	99,947	99,98
S	(ppm)	8	17,9	9	8	11,3	9	45	30	6	100	70	125
CaO	(ppm)	66199,99	92900	93300	98600	21900	8000	37800	5800	4600	6000	4300	800

Sc	(ppm)	19,6	27,5	27,9	33,3	6,54	2,47	8,93	7,07	5,57	0,2	14,8	1,2
TiO_2	(ppm)	6800	13500	13100	14400	2600	400	4800	0	900	100	25200	1650
V	(ppm)	130	212	220	383	25	3	73	29	/	0,2	135	90
Cr	(ppm)	465	469	415	60,4	64,6	7,6	23,6	2970	2,6	3	90	100
Fe_2O_3	(ppm)	62700	90400	92000	118100	22100	9400	37600	85700	8700	4800	258400	9550
Co	(ppm)	30	38,7	39,5	36,3	4	4,3	11,4	116	0,04	0,5	23	24
Ni	(ppm)	142	139	140	38,8	6	2,1	13	2460	0,84	53	35	110
Cu	(ppm)	28,6	56,3	55,5	198	1,5	0,4	6	5,7	0,4	140	5	5
Zn	(ppm)	62,7	83	82	106	41,5	12,7	44,8	29,5	27,2	220	1300	290
Ga	(ppm)	16,4	18,1	18	20,7	17	19	17	0,5	18,2	59	95	21
Ge	(ppm)	/	1,2	/	/	1,7	/	/	/	2,4	3,5	3,2	1,55
As	(ppm)	0,77	2,48	2,34	1,66	0,36	0,8	0,37	0,34	19,5	13	3	/
Se	(ppm)	/	0,026		0,08	/	/	/	/	/	/	/	/
Br	(ppm)	/	/	/	/	/	/	/	/	/	/	/	/
Rb	(ppm)	68	41,2	41	13	181	297	66	/	297	3600	2200	1300
Sr	(ppm)	252	435	443	395	184	16	372	/	8	84	5	27
Y	(ppm)	18,1	24,4	24	27	28,5	88,2	17,2	/	51,3	0,2	48	0,04
Zr	(ppm)	119	143	146	98,3	114	101	143	6,3	97,2	25	800	16
Nb	(ppm)	9,8	34,5	27	2,3	12,6	15	5,6	1,2	19,2	173	270	116
Mo	(ppm)	0,54	34	1,4	1,1	1,46	0,23	0,44		2,9	0,3	1,2	0,25
Ag	(ppm)	/	/	/	/	/	/	/	/	/	/	/	/
Cd	(ppm)	/	/	/	/	/	/	/	/	/	/	/	/
Sn	(ppm)	1,5	1,8	2	0,86	4,1	2,5	1	0,05	3,2	900	70	5
Sb	(ppm)	0,13	0,08	0,28	0,15	0,35	/	/	/	1,83	1,7	/	/
Te	(ppm)	/	/	/	/	/	/	/	/	/	/	/	/
I	(ppm)	/	/	/	/	/	/	/	/	/	/	/	/
Ba	(ppm)	317	490	497	251	462	67	453	17	39	42	150	4000
Yb	(ppm)	/	/	/	/	/	/	/	/	/	/	/	/
Hf	(ppm)	2,89	3,4	3,48	2,68	3,79	5,36	4,29	0,21	5,23	5,8	4,5	26

Ta	(ppm)	/	2,7	/	/	/	/	/	/	/	290	35	4,4
Standard		JA-2	JB-1	JB-1A	JB-3	JG-1	JG-2	JG-3	JP-1	JR-2	MA-N	MICA-FE	MICA-I
W	(ppm)	/	20	/	/	/	/	/	/	/	70	/	90
Hg	(ppm)	/	/	/	/	/	/	/	/	/	/	/	/
Tl	(ppm)	/	0,11	0,11	/	1	/	/	/	/	15	16	/
Pb	(ppm)	19,3	7,1	7,2	5,5	26,2	32,8	12,3	0,114	21,9	29	13	9
Bi	(ppm)	/	/	/	/	/	/	/	/	/	/	1,9	/
Th	(ppm)	4,7	9,2	8,8	1,3	13,5	29,7	8	0,18	32,2	1,4	150	0,1
U	(ppm)	2,4	1,7	1,6	0,46	3,3	12,5	2	0,05	10,5	12,5	80	0,15
Al_2O_3	(ppm)	156600	146900	146700	167900	142600	124500	156100	6400	129800	178900	196400	1535(
SiO_2	(ppm)	574300	527300	527400	507400	726000	772200	675000	435500	765899,9	676000	346500	3868(
Sm	(ppm)	/	/	/	/	/	/	/	/	/	/	/	/
Ce	(ppm)	32,7	66,7	66,1	21,5	45,9	49,5	40,1	0,2	38,8	0,9	420	0,35
La	(ppm)	0,47	0,32	37,9	0,39	22,4	20,1	20,7	0,1	0,9	0,5	200	0,32
MnO	(%)	0,11	0,16	0,15	0,16	0,06	0,02	0,07	0,12	0,11	0,04	0,35	0,26
Nd	(ppm)	13,8	29,7	5,5	15,4	19,5	25,8	16,8	0,07	21,1	0,4	180	0,08
Cs	(ppm)	/	/	/	/	/	/	/	/	/	/	/	/
C	(%)	/	/	/	/	/	/	/	/	/	/	/	/
ZnO	(%)	/	/	/	/	/	/	/	/	/	/	/	/
Cl	(ppm)	/	172	170	260	60	/	/	50	730	140	500	800
Cr_2O_3	(%)	0,0679	0,068	0,0602	0,0088	0,009	0,0011	0,0038	0,434	0,0003	0,0004	0,0131	0,014
F	(ppm)	485	393	385	295	496	960	335	10	1087	17000	16000	2850
K_2O	(%)	1,84	1,45	1,44	0,78	3,99	4,74	2,65	0	4,51	3,23	8,81	10,1
MgO	(%)	7,85	7,81	7,84	5,17	0,74	0,04	1,8	45,94	0,05	0,04	4,58	20,6
Na_2O	(%)	3,15	2,82	2,77	2,8	3,4	3,56	4,05	0,02	4,08	5,93	0,3	0,12
P_2O_5	(%)	0,15	0,26	0,26	0,29	0,1	0	0,12	0	0,01	1,41	0,45	0,01
CeO_2	(ppm)	/	/	/	/	/	/	/	/	/	/	420	/
HfO_2	(ppm)	/	/	/	/	/	/	/	/	/	/	26	/
La_2O_3	(ppm)	/	/	/	/	/	/	/	/	/	/	200	/

SO_3	(ppm)	/	/	/	/	/	/	/	/	/	/	70	/

Standard		NIM-L	NIM-N	NIM-P	NIM-S	SARM39	SARM46	SARM48	SARM51	SY-2	SY-3	TR-1	TR-1
Total	(%)	99,927	100,012	103,493	99,997	87,08	77,13	95,6	67,46	100,01	100,045	100,206	100,53
S	(ppm)	/	/	/	/	/	/	/	/	160	510	/	/
CaO	(ppm)	33100	114700	26700	6800	96900	13200	89000	8600	79900	82600	/	/
Sc	(ppm)	0,3	38	29	4	/	/	/	/	7	6,8	746	/
TiO2	(ppm)	4900	2000	2000	400	/	/	/	8200	1500	1500	/	/
V	(ppm)	81	220	230	10	/	/	/	/	50	50	/	/
Cr	(ppm)	0	30	24000	12	/	/	/	/	9,5	11	/	/
Fe_2O_3	(ppm)	102900	88900	128600	14100	92900	281600	5800	183600	64100	65600	100000	10000
Co	(ppm)	8	58	110	3	/	/	/	/	8,6	8,8	/	/
Ni	(ppm)	1	120	560	7	/	/	/	/	9,9	11	/	/
Cu	(ppm)	13	14	18	19	/	/	/	/	5,2	17	/	1119
Zn	(ppm)	400	68	100	10	/	/	/	/	248	244	498	/
Ga	(ppm)	54	16	8	11	/	/	/	/	29	27	/	/
Ge	(ppm)	/	/	/	/	/	/	/	/	/	1,4	/	/
As	(ppm)	/	/	/	/	/	/	/	/	17,3	18,8	/	1028
Se	(ppm)	/	/	/	/	/	/	/	/	/	/	/	/
Br	(ppm)	/	/	/	/	/	/	/	/	/	/	/	/
Rb	(ppm)	190	6	5	530	/	/	/	/	217	206	/	980
Sr	(ppm)	4600	260	2	62	/	/	/	/	271	302	/	/
Y	(ppm)	22	7	5	20	/	/	/	/	128	718	/	/
Zr	(ppm)	11000	23	30	33	/	/	/	/	280	320	/	/

Nb	(ppm)	960	/	/	4	/	/	/	/	29	148	/	134
Mo	(ppm)	4	/	/	/	/	/	/	/	1,8	1	/	/
Ag	(ppm)	/	/	/	/	/	/	/	/	/	/	/	/
Cd	(ppm)	/	/	/	/	/	/	/	/	/	/	318	/
Sn	(ppm)	/	/	2	/	/	/	/	/	5,7	6,5	/	/
Sb	(ppm)	/	/	/	0,6	/	/	/	/	/	/	/	/
Te	(ppm)	/	/	/	/	/	/	/	/	/	/	/	/
I	(ppm)	/	/	/	/	/	/	/	/	/	/	/	/
Ba	(ppm)	450	100	46	2400	/	/	/	/	460	450	/	/
Yb	(ppm)	/	/	/	/	/	/	/	/	/	/	/	/
Hf	(ppm)	190	/	/	/	/	/	/	/	7,7	9,7	/	/
Standard		NIM-L	NIM-N	NIM-P	NIM-S	SARM39	SARM46	SARM48	SARM51	SY-2	SY-3	TR-1	TR-1
Ta	(ppm)	22	/	/	/	/	/	/	/	2	30	/	/
W	(ppm)	/	/	/	/	/	/	/	/	/	1,1	/	/
Hg	(ppm)	/	/	/	/	/	/	/	/	/	/	/	/
Tl	(ppm)	/	/	/	/	/	/	/	/	1,5	1,5	/	/
Pb	(ppm)	43	7	6	5	/	/	/	/	85	133	/	/
Bi	(ppm)	/	/	/	/	/	/	/	/	/	/	/	2072
Th	(ppm)	66	0,6	1	1	/	/	/	/	379	1003	/	/
U	(ppm)	14	0,6	0,4	0,6	/	/	/	/	284	650	/	/
Al_2O_3	(ppm)	140400	164500	42000	173700	42900	67100	112400	118700	120800	117800	200000	20000
SiO_2	(ppm)	539400	525000	513700	637600	344000	359000	671100	338100	603200	597700	700000	70000
Sm	(ppm)	/	/	/	/	/	/	/	/	/	/	497	/
Ce	(ppm)	240	6	/	12	/	/	/	/	175	2230	/	/
La	(ppm)	250	3	2	5	/	/	/	/	75	1340	/	/
MnO	(%)	0,79	0,18	0,22	0,01	0,17	1,14	0,02	0,21	0,32	0,32	/	/
Nd	(ppm)	48	3	/	6	/	/	/	/	73	670	/	/
Cs	(ppm)	/	/	/	/	/	/	/	/	/	/	/	/
C	(%)	/	/	/	/	/	/	/	/	/	/	/	/

ZnO	(%)	/	/	/	/	/	/	/	/	/	/	/	/
Cl	(ppm)	1200	100	100	80	/	/	/	/	140	150	/	/
Cr_2O_3	(%)	0,0015	0,0044	3,5078	0,0018	/	/	/	/	0,0013	0,0016	/	/
F	(ppm)	4400	/	/	120	/	/	/	/	5030	6960	/	/
K_2O	(%)	5,67	0,25	0,09	15,38	1,04	0,35	4,26	0,33	4,47	4,24	/	/
MgO	(%)	0,29	7,48	25,46	0,46	26,24	3,16	0,18	0,92	2,7	2,67	/	/
Na_2O	(%)	8,62	2,45	0,37	0,43	0,5	0,28	3,22	0,07	4,32	4,13	/	/
P_2O_5	(%)	0,06	0,03	0,02	0,12	1,46	0,11	0,09	0,21	0,43	0,54	/	/
CeO_2	(ppm)	/	/	/	/	/	/	/	/	/	/	/	/
HfO_2	(ppm)	/	/	/	/	/	/	/	/	/	/	/	/
La_2O_3	(ppm)	/	/	/	/	/	/	/	/	/	/	/	/
SO_3	(ppm)	/	/	/	/	/	/	/	/	/	/	/	/
Li	(ppm)	/	/	/	/	/	/	/	/	/	/	/	/

Standard		TR-12	TR-13	TR-14	TR-2	TR-3	TR-4	TR-5	TR-6	TR-7	TR-8	TR-9	TRMAC-
Total	(%)	100,433	100,965	100,819	100,287	100,231	100,355	100,234	100,623	100,368	100,528	100,77	100
S	(ppm)	/	/	/	/	/	/	/	/	/	/	/	/
CaO	(ppm)	/	/	/	/	/	/	/	/	/	/	/	/
Sc	(ppm)	/	/	/	/	/	/	/	/	/	1624	/	/
TiO2	(ppm)	/	/	/	/	/	/	/	/	/	/	2523	/
V	(ppm)	/	/	/	/	/	/	/	/	/	/	/	/
Cr	(ppm)	/	/	/	/	/	/	/	/	/	/	/	/
Fe_2O_3	(ppm)	100000	100000	100000	100000	100000	100000	100000	100000	100000	100000	100000	/
Co	(ppm)	/	850	/	/	/	/	/	933	/	/	/	/
Ni	(ppm)	/	/	/	/	/	/	/	/	/	/	991	/
Cu	(ppm)	/	/	/	/	/	/	/	/	/	/	/	/
Zn	(ppm)	/	/	/	/	/	/	/	/	/	1050	/	/

Ga	(ppm)	/	895	/	/	/	/	/	439	/	/	/	/
Ge	(ppm)	/	/	/	/	/	569	/	/	/	/	/	/
As	(ppm)	/	/	/	/	493	/	/	/	/	/	/	/
Se	(ppm)	/	/	1003	/	/	/	/	/	406	/	/	/
Br	(ppm)	/	/	/	/	/	746	/	/	/	/	/	/
Rb	(ppm)	/	/	/	/	700	/	/	/	/	/	/	/
Sr	(ppm)	2248	/	/	/	/	/	838	/	/	/	/	/
Y	(ppm)	/	/	/	/	/	/	/	/	/	/	/	/
Zr	(ppm)	/	/	/	/	/	671	/	/	/	/	/	/
Nb	(ppm)	/	/	/	/	600	/	/	/	/	/	/	/
Mo	(ppm)	/	/	/	844	/	/	/	/	/	/	1360	/
Ag	(ppm)	/	/	1015	/	/		/	/	503	/	/	/
Cd	(ppm)	/	/	/	/	/	/	/	/	/	419	/	/
Sn	(ppm)	/	/	/	/	/	980	/	/	/	/	/	/
Sb	(ppm)	/	/	/	680	/	/	/	/	/	/	1119	/
Te	(ppm)	/	/	/	/	/	/	/	/	/	/	/	/
I	(ppm)	/	1181	/	/	/	/	/	933	/	/	/	/
Ba	(ppm)	2085	/	/	/	/	/	1499	/	/	/	/	/
Yb	(ppm)	/	/	1133	/	/	/	/	/	536	/	/	/
Hf	(ppm)	/	/	1704	/	/	/	/	/	534	/	/	/
Ta	(ppm)	/	1114		/	/	/	/	590	/	/	/	/
Standard		TR-12	TR-13	TR-14	TR-2	TR-3	TR-4	TR-5	TR-6	TR-7	TR-8	TR-9	TRMAC-
W	(ppm)	/	/	1023	/	/	/	/		523	/	/	/
Hg	(ppm)	/	/	/	/	/	/	/	/	/	/	/	/
Tl	(ppm)	/	1421	/	/	/	/	/	1003	/	/	/	/
Pb	(ppm)	/	/	/	400	/	/	/	/	/	/	671	/
Bi	(ppm)	/	/	/	/	520	/	/	/	/	/	/	/
Th	(ppm)	/	/	1050	/	/	/	/	/	660	/	/	/
U	(ppm)	/	/	/	450	/	/	/	/	/	/	1040	/

Al_2O_3	(ppm)	200000	200000	200000	200000	200000	200000	200000	200000	200000	200000	200000	/
SiO_2	(ppm)	700000	700000	700000	700000	700000	700000	700000	700000	700000	700000	700000	500000
Sm	(ppm)	/	/	/	/	/	/	/	/	/	1094	/	/
Ce	(ppm)	/	/	/	497	/	/	/	/	/	1094	/	/
La	(ppm)	/	/	/	/	/	588	/	/	/	/	/	/
MnO	(%)	/	0,259	/	/	/	/	/	0,146	/	/	/	/
Nd	(ppm)	/	1595	/	/	/	/	/	874	/	/	/	/
Cs	(ppm)	/	/	1263	/	/	/	/	/	521	/	/	/
C	(%)	/	/	/	/	/	/	/	/	/	/	/	50
ZnO	(%)	/	/	/	/	/	/	/	/	/	/	/	/
Cl	(ppm)	/	/	/	/	/	/	/	/	/	/	/	/
Cr_2O_3	(%)	/	/	/	/	/	/	/	/	/	/	/	/
F	(ppm)	/	/	/	/	/	/	/	/	/	/	/	/
K_2O	(%)	/	/	/	/	/	/	/	/	/	/	/	/
MgO	(%)	/	/	/	/	/	/	/	/	/	/	/	/
Na_2O	(%)	/	/	/	/	/	/	/	/	/	/	/	/
P_2O_5	(%)	/	/	/	/	/	/	/	/	/	/	/	/
CeO_2	(ppm)	/	/	/	/	/	/	/	/	/	/	/	/
HfO_2	(ppm)	/	/	/	/	/	/	/	/	/	/	/	/
La_2O_3	(ppm)	/	/	/	/	/	/	/	/	/	/	/	/
SO_3	(ppm)	/	/	/	/	/	/	/	/	/	/	/	/
Li	(ppm)	/	/	/	/	/	/	/	/	/	/	/	/

Standard		TRMAC-3	TRMAC-4	TRMAC-5	TRMAC-6	UREM10	UREM11	UREM4	UREM9	VS-N
Total	(%)	100	100	100	100	0,124	0,007	0,01	0,026	99,04
S	(ppm)	/	/	/	/	/	/	/	/	/
CaO	(ppm)	/	/	/	/	/	/	/	/	45300
Sc	(ppm)	/	/	/	/	/	/	/	/	300

TiO2	(ppm)	/	1000000	/	/	/	/	/	/	10800
V	(ppm)	/	/	/	/	/	/	/	/	600
Cr	(ppm)	/	/	/	/	/	/	/	/	700
Fe_2O_3	(ppm)	250000	/	1000000	/	/	/	/	/	41400
Co	(ppm)	/	/	/	/	/	/	/	/	700
Ni	(ppm)	/	/	/	/	/	/	/	/	800
Cu	(ppm)	/	/	/	/	/	/	/	/	800
Zn	(ppm)	/	/	/	/	/	/	/	/	800
Ga	(ppm)	/	/	/	/	/	/	/	/	400
Ge	(ppm)	/	/	/	/	/	/	/	/	/
As	(ppm)	/	/	/	/	/	/	/	/	/
Se	(ppm)	/	/	/	/	/	/	/	/	/
Br	(ppm)	/	/	/	/	/	/	/	/	/
Rb	(ppm)	/	/	/	/	/	/	/	/	800
Sr	(ppm)	/	/	/	/	/	/	/	/	700
Y	(ppm)	/	/	/	/	/	/	/	/	/
Zr	(ppm)	/	/	/	/	/	/	/	/	700
Nb	(ppm)	/	/	/	/	/	/	/	/	/
Mo	(ppm)	/	/	/	/	/	/	/	/	700
Ag	(ppm)	/	/	/	/	/	/	/	/	/
Cd	(ppm)	/	/	/	/	/	/	/	/	900
Sn	(ppm)	/	/	/	/	/	/	/	/	800
Sb	(ppm)	/	/	/	/	/	/	/	/	800
Te	(ppm)	/	/	/	/	/	/	/	/	/
I	(ppm)	/	/	/	/	/	/	/	/	/
Ba	(ppm)	/	/	/	/	/	/	/	/	1000
Yb	(ppm)	/	/	/	/	/	/	/	/	900
Hf	(ppm)	/	/	/	/	/	/	/	/	/
Ta	(ppm)	/	/	/	/	/	/	/	/	/

Standard		TRMAC-3	TRMAC-4	TRMAC-5	TRMAC-6	UREM10	UREM11	UREM4	UREM9	VS-N
W	(ppm)	/	/	/	/	/	/	/	/	/
Hg	(ppm)	/	/	/	/	/	/	/	/	/
Tl	(ppm)	/	/	/	/	/	/	/	/	/
Pb	(ppm)	/	/	/	/	/	/	/	/	1000
Bi	(ppm)	/	/	/	/	/	/	/	/	1000
Th	(ppm)	/	/	/	/	/	/	/	/	/
U	(ppm)	/	/	/	/	1241	69,5	100,8	258	/
Al_2O_3	(ppm)	/	/	/	/	/	/	/	/	134400
SiO_2	(ppm)	750000	/	/	/	/	/	/	/	555700
Sm	(ppm)	/	/	/	/	/	/	/	/	/
Ce	(ppm)	/	/	/	/	/	/	/	/	/
La	(ppm)	/	/	/	/	/	/	/	/	/
MnO	(%)	/	/	/	/	/	/	/	/	0,1
Nd	(ppm)	/	/	/	/	/	/	/	/	/
Cs	(ppm)	/	/	/	/	/	/	/	/	900
C	(%)	/	/	/	/	/	/	/	/	/
ZnO	(%)	/	/	/	100	/	/	/	/	/
Cl	(ppm)	/	/	/	/	/	/	/	/	/
Cr_2O_3	(%)	/	/	/	/	/	/	/	/	0,07
F	(ppm)	/	/	/	/	/	/	/	/	/
K_2O	(%)	/	/	/	/	/	/	/	/	8,12
MgO	(%)	/	/	/	/	/	/	/	/	4,51
Na_2O	(%)	/	/	/	/	/	/	/	/	5,95
P_2O_5	(%)	/	/	/	/	/	/	/	/	/
CeO_2	(ppm)	/	/	/	/	/	/	/	/	/
HfO_2	(ppm)	/	/	/	/	/	/	/	/	/
La_2O_3	(ppm)	/	/	/	/	/	/	/	/	/
SO_3	(ppm)	/	/	/	/	/	/	/	/	/

Li	(ppm)	/	/	/	/	/	/	/	/	/